STRUCTURAL AND HYDRODYNAMIC ANALYSIS OF A GAS-FILLED MEMBRANE STRUCTURE SUBMERGED IN WATER

A Thesis Submitted for the Degree of

Doctor of Philosophy

to

Council for National Academic Awards

by

Tabassom Malek, B.Sc., M.Sc.

This Work was Carried out at Middlesex Polytechnic
in Collaboration with The Queen's University of Belfast.

March 1984

To My Beloved Husband
for his kind encouragement and assistance .

ACKNOWLEDGEMENTS

I wish to thank my supervisors, Dr. H.C. Chan, formerly of the School of Civil Engineering, Middlesex Polytechnic, and Dr. E.M. Elsawy of the Department of Civil Engineering, The Queen's University of Belfast, for their guidance throughout this research. My sincere and grateful thanks are due to Mr. R.A. Smith of the School of Civil Engineering, Middlesex Polytechnic, to whom I am indebted for his unfailing patience and valuable assistance during this study.

I wish to express my gratitudes to the technical staff of the Middlesex Polytechnic especially Messrs. P. Lister and C. Willgress, and the technical staff of the Queen's University of Belfast. I wish to express my gratitude and admiration to Mrs. K. Scales for her elegant typing of this thesis.

I would like to acknowledge the financial support and the general assistance given by the Middlesex Polytechnic throughout this work.

Finally, I would like to extend my deepest gratitudes to my parents to whom I shall always be indebted for their support and encouragement throughout my education.

ABSTRACT

In the last two decades there has been an increasing interest in the development of inflatable structures on account of their potential applications in the erection of space and under-water structures. The stability of inflatable structures for use in the fluid environment is founded on such advantages as light weight, ability to carry the environmental forces efficiently by direct tensile stress and ability to utilize the water pressure to counterbalance the gas pressure. The extensive possible applications of inflatable structures in ocean technology have emphasized the demand for investigations aimed at better understanding of the structural and hydraulic behaviour of these structures.

The present study is concerned with the structural and hydraulic analysis of a gas-inflated membrane structure fully submerged in water. The structural analysis of such a structure involves the determination of the profile shape and the tension in the membrane for given inflation and load conditions. This is carried out by the numerical solution of the differential equations of equilibrium of the membrane. The results have been confirmed by an experimental investigation. The incorporation of a two-way set of reinforcing cables has also been considered. The effect of the spacing of the reinforcing cables for various membrane geometries is studied. Also, the effect of partially drawing-off the internal gas of the inflated structure as a result of which, water enters the container, is examined.

The hydraulic aspect of this study is mostly concentrated on the investigation of the effect of waves and currents on the proposed structure. Models of the proposed structure have been tested using wind tunnel and wave flume. The results show the effects of currents and waves on the pressure distributions around the models and on the inertia forces. The changes in the shape of the structure and the tension in the membrane due to the effect of a uniform current are assessed. The scouring action of the current has also been investigated experimentally and qualitative results have been obtained.

A general computer program has been developed which can handle structures with up to 300 joints and can be used efficiently for the analysis of many types of cable and suspended structures under different loading conditions. Numerical results are generated for the proposed inflated cable-reinforced structure.

Finally, the application of such structures for the storage of hydrogen produced from the electrolysis of water using surplus electricity and the storage of associated gas from offshore oil wells is considered.

The work carried out in this thesis shows that the proposed structure is feasible and the results presented may be used as a guideline in the design. However, more investigation is required before a final design can be attained.

CONTENTS

CHAPTER ONE

INTRODUCTION AND LITERATURE SURVEY

1.1 Introduction.

In recent years inflatable structures have gained much prominence because of such properties as light weight, compactability, low cost and ability to withstand the environmental forces by direct tensile stress only. The idea of using the principle of inflated membrane in the construction of buildings and structures originates from the English engineer F.W. Lanchester who in 1918 obtained a patent on it. However, it was only after the World War II that the use of inflatable structures started to accelerate. Some examples of these structures are given in section 1.2.1. In section 1.2.2. the advantages and the disadvantages of inflatable structures are discussed. One of the problems associated with inflatable structures is the development of suitable membrane materials that can sustain high tensile forces. In order to reduce the forces in the membrane, a set of reinforcing cables can be incorporated in the membrane. The use of cable reinforcement is especially useful in the construction of low profile or long span inflatable structures.

A few applications of membrane structures for use in the fluid environment are outlined in section 1.3 followed by the general description of a proposed inflatable structure in section 1.4. The proposed membrane structure can be used for the storage of gas underwater. It utilizes the water pressure to counterbalance the gas pressure thus the gas containing structure is subjected to very much lower pressure loading. The structural and hydraulic analysis of the proposed structure are investigated in the next two chapters. Two possible applications of the proposed structure in the industry are discussed in section 1.4.1. Some of the major practical problems which have to be thoroughly investigated before the actual construction of the proposed structure are outlined in section 1.4.2. These include the choice of a suitable material for the membrane cover and the reinforcement and the choice of an anchorage system. The construction, installation and the maintenance of the proposed structure should also be considered in the design of the structure. The feasibility of the proposed method of gas storage should be assessed from the economics point of view.

1.2 Inflatable Structures.

An inflatable structure consists of a space-enclosing flexible membrane anchored to the ground and kept in tension by internal gas pressure such that it can carry applied loads. The flexible membrane which is only capable of supporting tension, is stressed by the differential pressure of the gas and is deformed in the direction of the medium at least pressure until its surface is stable in both position and form. The conditions for the stability of inflatable structures are given by Price [55] as: (a) The membrane has to remain in tension at all times in at least one direction, and this implies that the internal pressure has to be greater than the applied external pressure, (b) The membrane itself and the joints in the material have to withstand, within a specified design life, the estimated membrane tensions with an acceptable factor of safety depending on use, and (c) The base anchorage of the membrane has to cater adequately for maximum membrane forces at the perimeter. By far the largest amount of architectural design studies of air-structures has been made by Frei Otto. These structures are based on a physical principle that is frequently found in nature, both organic and inorganic and has been applied in the field of technology for centuries.

In recent years there has been an increasing interest in the development of inflatable structures on account of their attractive properties such as low cost, speed of erection, transportability, and efficiency in carrying environmental loads by direct tensile stress without bending. These attractions are however counteracted by some disadvantages such as possibility of large deflections and stress concentrations and instability due to dynamic overpressures. Nevertheless, inflatable structures have been widely used for civil, aeronautical, military and marine applications.

Due to the high flexibility of the inflatable structures, their equilibrium shape and associated external loading can be found only by considering the interaction between the structure and the loads. A specialized theory for inflatable shells has been reported by Leonard [38,39] and methods of solution for pressurized shells of revolution based on this theory have been presented for the static and dynamic behaviour during the pressurization and in-service phases. The basis

of the derivation of this theory is that the known geometry coincides with the inflated shape. Oden[50] and Hart-Smith[25] have conducted studies on inflatables assuming a given initial state and nonlinear material behaviour. Avula and Ural[4] have developed a method of solution for the deformation of a closed axisymmetric membrane which is simultaneously inflated by a gas and a liquid, from the viewpoint of large elastic deformation theory. The behaviour of some inflatable structures in water has been studied by Leonard[41], Itokawa et.al.[33] and Misra[46].

In order to provide additional strength in inflatable structures, a system of reinforcing cables can be incorporated in the membrane. The behaviour of cable reinforced membranes has been studied by Vinogradov et.al.[65], Cowan[14], Verma[64] and many others.

The strength of inflatable structures largely depends on the proper selection of materials and correctly made seams and joints. Other major parameters which have to be considered in the design of these structures are the anchorage, stabilization measures, transport, erection, safety and maintenance. Inflatable structures offer enormous possibilities in shape and colour with a great new design potential and with relatively little cost.

1.2.1. History of Inflatable Structures.

Since Roman times inflated animal skins have been used as buoyancy bags for crossing rivers. Rafts and bridges have been built with numerous inflated bags. Although the skins were kept wet to prevent air escape, it was nevertheless necessary to inflate them afresh every day. In the eighteenth century, the first hot air balloon was sent 200 feet up into the air by the Brazilian cleric, Bartholomew Lourence de Gusmao. Later, Jacques Alexandre César Charles sent up the first hydrogen balloon.

The idea of using the pneumatic principle in buildings originates from the English engineer Frederick William Lanchester[36] who in 1918 obtained a patent on "An Improved Construction of Tent for Field Hospitals, Depots and the Like Purposes". However, Lanchester did not see any of his designs realised mainly due to unavailability of suitable membrane

material. The use of inflatable structures started to increase more rapidly since shortly after World War II when an inflated radome was successfully developed for the United States Military. In 1956 the first air supported warehouse was erected. The first fabridams were constructed in 1957. Fabridams are not only cheaper to manufacture than the conventional dams, but have a further advantage of being able to react quickly to tidal waves by lowering the overflow height simply through discharge. A life span of about 20 years can be anticipated for fabridams if they are regularly given a new protective surface coat. In 1958 Pentadome was constructed as an exhibition area for the U.S. Army. It consisted of five large domes and covered a total area of 4650 m^2 (Herzog[26]). The use of cable reinforcements in inflatable structures was studied by Frei Otto[51] before 1962 and in 1962 he published his first book on pneumatic structures. In 1967 the First International Colloquium on Pneumatic Structures was organized in Stuttgart by the International Assoc. for Shell Structures[31]. Soon after that there were countless experiments within and on the periphery of the subject, especially in England, the Netherlands, Austria and the Western United States. The motive behind them was less that of scientifically orientated interest than of pleasure in the possibility of personally creating environments with a minimum of material expenditure in a short period of time. The pneumatic buildings at World Exhibition 1970 in Osaka represented a temporary high point in the history of air structures. With the development of low profile structures, such as the United States Pavilion at Expo'70 and the roof of the Pontiac Stadium, Michigan the incorporation of a set of reinforcing cables was seen. Such reinforcement has also been used in inflatable greenhouses and similar structures for agricultural and industrial uses.

In the recent years inflatable structures have become increasingly common in civil, marine and aeronautical applications.

1.2.2. Advantages and Disadvantages of Inflatable Structures.

Inflatable structures have recently become increasingly common in many parts of the world especially in the North of America where there are now few North American cities that do not include an air-supported enclosure for either atheletic facilities, temporary exhibition halls or even office spaces.

The main advantages of inflatable structures are speed and ease of erection and removal, portability, relatively low capital cost and large span capabilities. Also, the use of flexible material in inflatable structures avoids occurrence of bending moment and this allows the material to be efficiently utilized by resisting membrane forces. These attractions of inflatable structures have made them suitable for various applications. They are commonly used as warehouses for storage of industrial and agricultural products, as exhibition buildings and construction shelters. Air structures are successfully used as radomes because the coated fabric causes minimum interference to electrical signals. They are also used for other military purposes such as stores, shelters and temporary hospital units. The very favourable weight to strength ratio and packaged volume to expanded volume ratio in addition to their ease of erection has made inflated structures a prime choice for permanent and semi-permanent lunar structures. If an inflated structure is used in the underwater environment it will be subjected to a much reduced pressure loading since the water pressure counterbalances the internal gas pressure. The use of inflatable dams provides a cheaper and more flexible alternative to the use of moveable gates. They can be inflated to various heights by air or water pressure. The membrane forces in inflated structures can be reduced by using a system of cable reinforcement. The reinforcement gives these structures a potentially efficient and attractive architectural form as well as providing additional strength.

The main disadvantages of inflatable structures are the requirement of inflation equipment and emergency back-up power, possibility of large deflections and instabilities occurring in high winds and accidental deflation due to power or mechanical failure. Other drawbacks of these

structures are the requirement of a suitable anchorage and their limited life expectancy. A recent survey of failures of air supported structures in Canada by Shrivastava et.al.[61] indicates that the most common causes are the tearing of the fabric and inadequate anchorage details in conjunction with high wind speeds.

1.2.3. Cable-Reinforced Inflatable Structures.

The need for greater stability and the capacity to carry concentrated loads in inflatable structures has necessitated the use of such composite structures as cable-reinforced membrane structures. Since most membrane materials are not suitable for sustaining high tensile forces, the use of inflatable structures is limited to small spans and small radii of curvature. The tensile forces in the membrane increase as the radii of curvature increase such as in low-profile inflatables. However, low-profile structures offer greater stability in high winds. If a membrane is connected to a cable net, the membrane distributes the load locally to the cables which transfer the loads to the base anchorage. The membrane can thus be made to have a small radius of curvature between the cables. This is necessary for low-profile or long-span structures so as to reduce membrane forces to a practical level. It is also used with low strength membranes on small spans.

Cable-reinforced membranes are potentially efficient and can be used for designing attractive architectural forms. The cable-reinforcement provides additional strength and allows flexibility in the form. It also improves the internal acoustics of membrane structures and can be useful in the design of inflatable halls. Some examples of cable-reinforced inflatable structures are the United States Pavilion at Expo'70 with a span of 80 meters, the roof of Pontiac Stadium in Michigan with a span of 168 meters and a multi-purpose hall on the English South Coast. Several greenhouses and fieldhouses have also seen the incorporation of reinforcing cables. For most cable networks, spiral strands are used. Steel cables have large elastic modulus, are insensible to environmental forces if properly coated and have high heat resistance properties. On the

other hand,cables woven from aramid fibres such as Kevlar are potentially attractive from the point of view of strength to weight ratio and stiffness to weight ratio. For protection against weather, the cables are drawn in on the inside envelope of the membrane with which they are connected under the same tension. When tensions are minimal the cables can be replaced by sewn-on strips of material because mounting of cables in sewn-on loops is very time consuming. One of the problems associated with the construction of structures utilizing cable networks has been the costly procedure of fabricating the covering material and water-proofing it. Not only must it be waterproof at joints, but these joints must allow sufficient movement to accommodate motions produced by loading and temperature deflections.

The interaction of cables and membranes makes the analysis of inflatable cable-reinforced structures complex. However, it may be greatly simplified if the structure is modelled by a cable network, with the action of the membrane neglected except for transmitting the pressure load to the cable. The actual cable line must fulfil the equilibirum and compatability conditions. In the underformed state that is only possible for a definite load usually dead weight and internal pressure and a geometry selected specifically for it. In all other load conditions, large displacements occur until the cable line which results from the changed geometry can take up the deflection forces from the membrane. Verma and Leonard[64] have investigated large displacement, large strain behaviour of hyperelastic membranes reinforced with cables, using a finite element formulation. In the use of cables care has to be taken so that the tensile forces of the membrane on both sides are applied at equal tangential angles if possible. For the most efficient use of cables, it is desirable that each is stressed equally and uniformly under all loading conditions. It is unlikely that this objective is achieved mainly due to considerable shape changes that may occur under extreme loadings. Nevertheless, as is demonstrated by Malcolm[43], almost constant tension along each cable can be achieved by adopting a system of cables following lines of initial geodesic curvature. This cable configuration has the added superiority under wind loading over cables following lines of principal curvature in minimizing cable

forces and deflections. Vinogradov et.al.[65] have developed a numerical method for the nonlinear static and small forced oscillation analysis of arbitrary cable reinforced air-supported structures. It is shown that the dynamic characteristics of these structures are strongly dependent on internal pressure and static loads, including equivalent static wind pressure. For the relatively small static loads, the changes in natural frequencies can be considered as proportional to the square root of the internal pressure. The influence of an idealized static wind type load is to decrease the fundamental frequency of the structure.

Research in the field of cable-reinforced membranes is continually increasing due to their wide range of applications.

1.3 Offshore Applications of Inflatable Structures.

The use of inflatable membrane structures as temporary or permanent enclosures is a promising technique in the underwater construction technology. The main advantages of these structures for use in the fluid environment are that (a) the environmental loads are efficiently carried by direct tensile stress without any bending moment, (b) the primary load carrying mechanism is part of the habitable environment itself, that is, the internal pressurized gas, (c) they are light in weight and collapsible implying ease in transportation and erection, (d) the leakage of gas through puncture provides early warning of collapse and repairs can be easily made by patching and (e) if they are used as fully submerged structures, the water pressure counterbalances some of the internal gas pressure, thus the structure is subjected to very much lower pressure loading.

The most common application of inflatable membrane in the fluid environment is in the construction of inflatable dams. An inflatable dam consists of a flexible tube, fixed along its base across the river. It can be inflated to the required height by air or water pressure or both, and deflated when not required. It is used as a cheap method of water storage or control. The behaviour of inflatable dams has been widely studied by Anwar[2], Binnie[7], Harrison[24], Parbery[52] and many others.

Inflatable structures can be used for the construction of domed villages on the ocean floor and of decompression stations anchored at various depths below the surface (Leonard[40]). They can also be used for the construction of rescue platforms, building of domes for hydroponic cultivation around the floating cities and for the design of components of buoyancy controlled lift devices (Avula[3]). Neutrally buoyant inflated structures have been proposed for a variety of missions like submarine detection, oceanographic survey and lifting surfaces of hydrofoil type vehicles. Itokawa et.al.[33] have designed a series of flexible undersea storage containers of flying saucer type and have studied them experimentally. These flexible containers can be used for the storage of the imported crude oil under water in the absence of a suitable on-shore site. In the present study, it is proposed to consider the application of inflatable structures for the storage of gas under water.

1.4 The Proposed Structure.

The numerous advantages of inflatable structures have brought forward the idea of employing these structures for the storage of gas in the underwater environment. In addition to the main advantage of inflatable structures, namely, their ability to sustain all applied loads by direct tensile stresses only, the use of inflatable structures in the underwater environment offers a further important advantage of counterbalancing the internal gas pressure of the structure by the external water pressure. The resultant load on the membrane will thus be considerably reduced and the membrane is used in the most efficient way.

It is therefore decided to investigate the feasibility of using an inflatable structure for the storage of gas underwater. The structure is assumed to be of long cylindrical shape . The profile of its cross-section has to be determined analytically by considering the magnitude and the distribution of the resultant load on the membrane together with the characteristics of the membrane material. A structural analysis has been carried out on the proposed structure in section 2.2. Membrane analysis is used in this study to determine the cross-sectional profiles that lead to optimum designs with regards to the strength of the membrane material or the total length of material needed for constructing the structure.

Since the strength of the material usually poses a more difficult problem compared to the amount of material needed, it is decided to conduct the optimization on the basis of obtaining minimum tension in the membrane. However, in spite of using this criteria in the optimization, the tension produced in the membrane may still be quite high. It is therefore decided to use longitudinal and circumferential cables on the membrane. The spacing of the cables has to be determined on the basis of the tensile strength of the cables and the size of the structure. The effect of incorporating a system of reinforcing cables into the membrane is analysed in section 2.4.

The maximum admissible pressure of the gas which is to be stored depends on the depth of submergence of the structure. It is observed that the internal gas pressure of the structure can be increased without any increase in the tensile stress of the membrane or the cables, if the structure is located in deeper water. A suitable outlet has to be designed on the top of the structure so that the stored gas can be easily drawn off whenever required. The drawing off of the stored gas will reduce the internal pressure of the structure. In order that the reduction of the internal pressure does not disturb the equilibrium of the structure, it is decided to replace the removed gas by an equivalent amount of water so that the gas pressure remains unaltered. This may be facilitated by allowing enough water to get into the structure through an inlet fitted on the bottom of the structure. The stored gas must definitely be separated from the sea water. This can be achieved by fitting a suitable separating rubberized diaphragm similar to the one described by Baffico et.al.[5]. When the gas pressure inside the structure is at its maximum level, the diaphragm will adhere to the lower internal surface of the structure. When the stored gas is being gradually drawn off, the rubberized diaphragm moves up, thus letting sea water fill the lower volume of the structure. The behaviour of the structure during the process of drawing off of gas has been discussed in section 2.5.

Since the allowable internal gas pressure of the proposed structure can be increased by increasing the depth of submergence of the structure, it is evident that the proposed structure can be used more efficiently if it is sited in deeper waters. Moreover, the forces induced by the wind and the sea waves and currents are less pronounced on structures if they are located further down from the

sea water surface. The proposed structure is therefore designed for water depths of 100 metres or more. The effects of the major environmental elements which might affect the design of the proposed structure are outlined in chapter three. In that chapter, the behaviour of the structure under the action of currents and waves have been examined mostly by model experiments. The main forces due to waves and currents on the proposed structure are those caused by drag. The changes in the cross-sectional profile of the structure due to the action of currents are found to be insignificant. The effect of other environmental factors such as earthquakes, temperature changes, impact from falling objects, diffusion of the stored gas and the reactive forces of the foundation medium have to be carefully studied.

The proposed structure has useful applications mainly in temporary storage of different gases for later recovery (Chan[12]). It is thought that this structure will be cheaper and easier from the construction point of view, as compared to its existing substitutes. However, the present study provides only the very basic elements of the design of that structure and a more comprehensive research is evidently required before a prototype can be fully developed. Two possible applications of the proposed structure are pointed out in the next section followed by some major practical problems which have to be investigated in detail, before any attempt to the construction of the prototype.

1.4.1. Possible Applications of the Proposed Structure.

There are various uses for the inflatable structures in the underwater environment. The proposed structure is especially useful for the storage of pressurized gas underwater though it can also be used as temporary or permanent protection underwater for interconnected domed villages on the ocean floor. In this section two possible applications of the proposed structure as gas storage containers are outlined.

(a) Storage of Hydrogen Gas.

In most industrialized countries, there is an increasing need for finding efficient and inexpensive methods of storing energy, particularly the storage of hydrogen produced from the electrolysis of water using surplus

electricity generated by nuclear power stations during off-peak periods. One of the many schemes which have been studied is the electrolysis of water in order to produce hydrogen, which can be stored and later used to generate electricity through H_2/O_2 fuel cells during periods of high demand. The major obstacle to this attractive concept of hydrogen economy is the high cost of the construction of suitable pressure vessels for the storage of the hydrogen gas. Since nuclear power stations are generally sited near the sea to ensure plentiful supplies of cooling water, it is proposed to store the hydrogen gas produced by electrolysis, under the sea, in flexible containers. To illustrate the size of the problem, a 1000 Megawatt nuclear power station is used as an example. Assuming that eight hours of off-peak electricity is available per day to supply a highly efficient electrolyser operating at 1.8 volts and 1.0 A/cm^2, the volume of the hydrogen gas produced will be 14.8×10^5 m^3 at NTP. This volume can be reduced considerably if the gas is stored under high pressure. For example if the flexible structure is sited in 100 metres of water, the volume of this hydrogen gas will be reduced to a more manageable level of 1.3×10^5 m^3. This volume of hydrogen gas can be easily stored in the proposed container without having to construct an expensive pressure vessel.

(b) Storage of Associated Gas from Offshore Oil Wells.

In many offshore oil fields the associated gas from the oil wells is flared and wasted. The major reason for flaring gas at oil producing fields is that the cost of laying pipelines for transporting the petroleum waste gas to a suitable treatment plant is higher than the value of the gas itself and therefore it is not economical to process the gas for use as a fuel. As an example of the amount of gas which is being flared in offshore oil fields, it is reported by the Department of Energy[17] that during 1982, in the oil fields in the United Kingdom, an average of 11.09×10^6 m^3 of gas was flared each day. However, measures are being taken to reduce flaring at most oil fields. In some fields, gas is re-injected into the reservoir for later recovery. It is thought that the proposed inflatable structure might provide an economical means of storing the gas instead of flaring it. Depending on the amount of gas available, a number of these membrane containers can be constructed in the vicinity of the oil field so that the associated

gas can be temporarily stored. When required, a suitable barge-mounted gas liquifaction and storage plant similar to that designed by Howard and Andersen[30] is towed to the site where the gas storage containers are located and the stored gas is drawn up to the plant. After pre-treatment and liquifaction, the liquified gas is stored in the storage compartment of the plant. The plant barge then returns ashore carrying the gas with it.

It is well understood that much has to be done before this idea can be put into practice. In the next section some of the major practical problems involved in the development of this storage system, will be discussed.

1.4.2. Major Practical Problems.

The present study of the proposed inflatable structure is limited to its structural and hydraulic analysis only. In order that the proposed structure can be actually constructed and put into operation, many other important factors have to be considered and carefully investigated. In this section, some of these factors are set out and briefly discussed.

1.4.2.1. Material.

One of the major elements to be considered in the design of the proposed structure is the selection of a suitable membrane material. The most important criterion in the selection of a material is its mechanical strength and elasticity. In addition to being able to resist the action of the applied static loads, the chosen material should be able to withstand impact forces from falling objects and cyclic loads due to the action of waves and currents. These cyclic loads may result in fatigue strength becoming a critical concern for many offshore structures. Another important criterion in the selection of a material suitable for the proposed structure is its resistance to marine fouling, the sea water and the stored gas. In addition, the membrane material should be

sufficiently impermeable and resistant to the loss of gas through diffusion under high pressure. Since the chosen material for the proposed gas storage system would be in contact with sea water on the outside and the stored gas on the inside, its thermal stress characteristics must be carefully studied with regards to the environmental thermal conditions at the proposed site as well as the thermal expansion characteristics of the gas and the sea water especially in the loading and the unloading phase. In the selection of materials, consideration must be given not only to the physical and chemical properties of materials but also to costs, fabrication, erection and transportation facilities, maintenance and their life span in the marine environment.

One of the membrane materials which is thought to be suitable for the purpose of the proposed structure is nylon-reinforced butyl rubber. Butyl rubber which is normally used in the tyre industry has low gas permeability and excellent resistance to corrosive chemicals. It has excellent heat resistance properties. With regards to its tensile strength properties, it has been quoted by one of the companies (Butyl Products Limited) which manufactures different types of butyl rubber that 1.5 mm thick nylon-reinforced butyl rubber sheet can be produced with a strength of the order of 120 kN/m but for higher strengths, the thickness has to be increased. Although this material seems suitable for the construction of the proposed structure, its permeability properties under high pressure and its resistance against sea water and the stored gas has to be experimentally determined before it can be used confidently. The use of suitable protective coatings should also be investigated.

If the proposed structure is to be used in its reinforced form, the strength of the membrane need not be as high but all the other essential properties mentioned above are still required. The reinforcing cables should also possess the above mentioned characteristics in addition to being able to resist the required tensile

load without undergoing large extensions. A few firms have been consulted and finally it has been suggested that Kevlar PRD.49 III which is a Kevlar organic polyamid fibre is the most suitable material. One of the firms which produces this material is 'Hawkins and Tipsons Limited'. Kevlar is already being used in the construction of pressure vessels, missile cases and radomes. An important point which has to be investigated if reinforcing cables are to be used is the method of joining the cables to each other and to the membrane material. The strength and the efficiency of the joints should be carefully examined.

As mentioned in section 1.4 a rubberized diaphragm has to be fitted inside the proposed container to prevent any contact and mixing between the sea water and the stored gas. This separation diaphragm must therefore be impermeable to both gas and water. It should also have good resistance against the stored gas and the sea water. Protective coatings may be used for this purpose. The required strength of the membrane diaphragm is determined by the pressure distribution on each side of it. The resultant pressure distribution on the diaphragm is therefore significant. In this case, however, there will be little pressure difference across the diaphragm since the gas pressure on one side of it counterbalances the water pressure on the other side. The method of fitting the diaphragm inside the container in such a way that it can move according to changes in the gas-water levels must be carefully studied.

1.4.2.2. Anchorage.

In the design of most offshore structures it is necessary to select a suitable anchorage system. The proposed inflatable structure has a particular need for an uplift resisting anchorage system. Other qualities considered in the selection of the anchor are efficiency, reliability, cost, simplicity in handling, its operative life and ease of installation and maintenance. It is also important that the condition of the sea bed

is carefully studied and all the forces that are likely to act upon the anchor are accounted for. If the structure is designed for deep water, the importance of rapid installation time becomes a prominant factor.

A simple method of anchoring the proposed structure is by dead weight. The principal advantages of deadweight anchors are explained by McCormic[44] and are as follows:

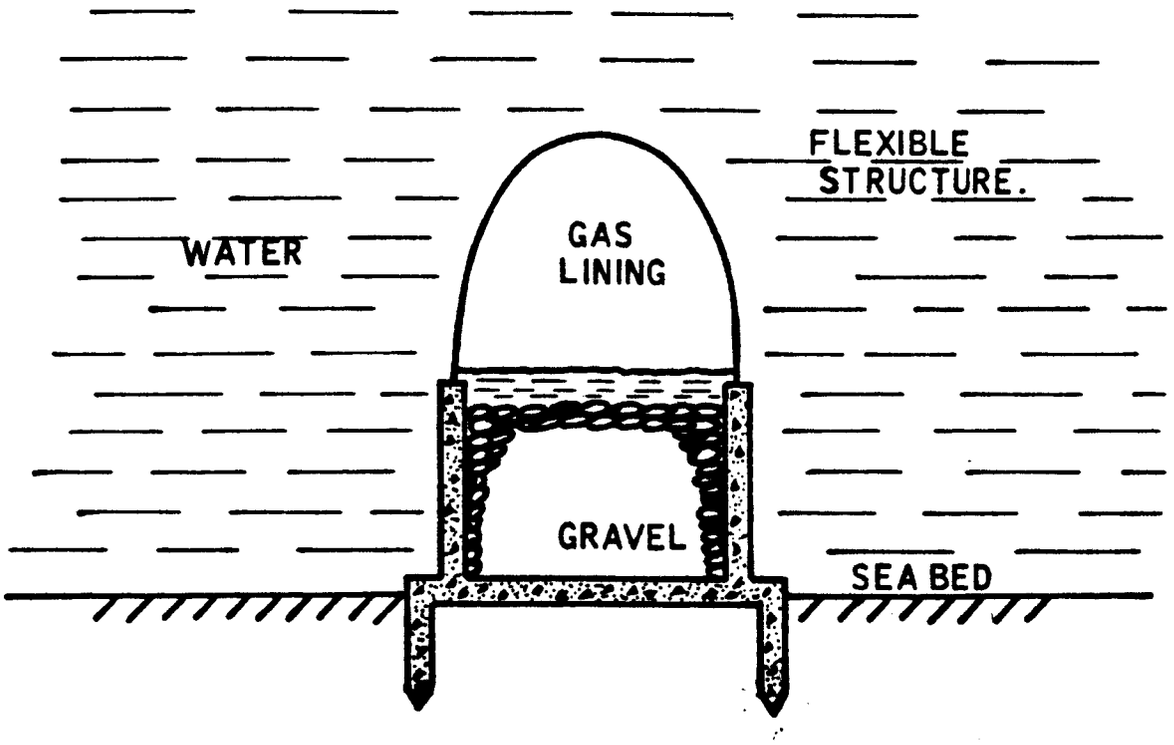

Figure 1.1 Schematic diagram of anchoring system.

1. They are simple to construct, economical and readily available. 2. Their application is independent of most seafloor conditions, excluding steep sloping bottoms. 3. Their uplift resistance is precisely predictable. 4. Their installation procedures are relatively simple and the installation

equipment required is minimal. The main disadvantage of dead weight anchors is that they have undesirably low holding capacity to weight ratio. One scheme in using a dead-weight anchor for the proposed structure is to construct reinforced concrete vessels with sections as shown in Figure 1.1. The vessels are then towed to the correct location. In order to reduce the amount of work done by the divers in deep water, the flexible container can be connected to the anchoring vessels and inflated with air before infilling the vessels with gravel or water and lowering down to the sea bed by crane barges.

Other types of anchoring systems which might be suitable for the proposed structure are suction anchors (Wilson[67]) or pile anchors such as QMC anchors[56]. The feasibility and the economics of all these systems in applying to the proposed flexible container must be studied before the different systems can be compared with each other. It is also essential to investigate the need for the installation of an auxilliary anchorage system.

1.4.2.3. Some Other Practical Problems.

Many of the practical problems which should be considered in the design of the proposed structure are equally important in the design of any offshore structure and are adequately treated in the available literature; others are strongly dependent on conditions at the local area, application for which the structure is to be used and the economical factors involved. The latter can be discussed only in general terms.

Among the most important practical problems are construction, towing and installation procedures of the structure. The additional forces involved in these operations should be accounted for in the design of the structure. The economy of these operations should also be considered. Work done beneath the water surface is expensive and time consuming. Therefore, a structure requiring the minimum amount of this type of work is

the most desirable structure. The construction technique of using buoyant reinforced precast concrete structures with the membrane sheet prefixed just before sinking down to the sea bed is thought to be much more economical than building the conventional highly pressurized vessels. The towing and installation procedures have to be analysed theoretically and also by means of model tests in order to ensure the stability of the structure during all these phases of the design. Also the behaviour of the structure during loading and unloading operations must be investigated. The apparatus required for the operative control of the storage process must be chosen with care and the space they occupy should be examined. The charging and discharging processes of the storage system should be tested under design conditions. In some cases the amount of gas to be stored may exceed the capacity of one container and a number of these containers will have to be used. The effect of shielding by neighbouring structures on each of these containers has to be investigated by model tests and the best arrangement for the structures has to be found.

The other important factors which have to be considered in the design of the proposed structure are maintenance, operative life, anti-pollution and reliability requirements. As regards the maintenance of the operative apparatus and other parts of the underwater structure, an efficient and safe connection with the sea surface may be provided similar to that designed by Bozzo[9] for the transfer of men, devices and equipment. An important part of the maintenance operations is the removal of the sediments which become deposited on the inner and the outer surfaces of the membrane cover of the structure and on both sides of the seperating diaphragm. Regular maintenance of the structure would guarantee its operative life. A determinant factor in ensuring the required operative life of the structure is the proper choice of material and its protective coatings with regards to the design load and operative conditions. As mentioned in section

1.4.2.1. the diffusion of the stored gas through the membrane as well as through the separating diaphragm must be prevented as much as possible since a significant gas diffusion might cause water pollution and the loss of the stored gas. For the same reasons, appropriate devices must be provided for early detection of any gas leakage through weak joints or malfittings or any damaged part of the membrane.

Finally, the feasibility of using the proposed structure as a gas storage container cannot be determined until a comparative cost analysis is carried out on the proposed method of storing gas in relation to the alternative methods which are already in operation. The cost of materials, anchorage, construction, installation, operation and all the other costs involved has to be assessed with regards to the monetary value of the stored gas and the results have to be compared with the existing methods.

1.5 Conclusion.

A thorough literature survey has been carried out on inflatable structures, their history, their advantages and disadvantages and their various applications. It has been shown that inflatable structures can be easily erected and seem more economical. It is therefore proposed to examine the feasibility of using an inflatable structure for the storage of gas. This storage method has the advantage of utilizing the water pressure to counterbalance the gas pressure so that the membrane is subjected to a considerably lower pressure loading. The proposed method has useful applications in the storage of associated gas from offshore oil wells. It can also be used for the storage of hydrogen produced by electrolysis of water using surplus electricity during off-peak periods. For the complete development of the proposed structure, practical problems such as the method of anchorage, construction and installation procedures, maintenance and the operative life of the structure have to be carefully investigated.

CHAPTER TWO

STRUCTURAL ANALYSIS

List of Notations in Chapter Two.

B	base width
d_{il}	length of member i-l before deformation
E	Young's modulus
$E(k,\phi)$	elliptic integral of second type
f	extension ratio
$F(k,\phi)$	elliptic integral of first type
h	height of water in the container
H	total height of the structure
K_{il}	elasticity of member i-l
L	unstretched length of the membrane
L^*	stretched length of the membrane
M	total number of joints
N	total number of unrestrained joints
N^*_{il}	initial force in member i-l
p	resultant pressure
P_i	pressure at i
Q_{il}	generalized force in member i-l
s	distance along unstretched perimeter
t	thickness of the membrane
t_{il}	unit vector along member i-l before deformation
T	tensile force per unit length
T_o	initial tension per unit length
${}_k u_i$	displacement of joint i in direction k

x	co-ordinate
X_l	external force acting on joint l
y	co-ordinate
z	co-ordinate
γ	specific weight of water
δ_{il}	Kronecker's delta
ϵ_{il}	generalized elongation of members i-l
ϕ	inclination to horizontal
ϕ_o	inclination to horizontal at upstream toe
ω	weight per unit area of the membrane.

2.1 Introduction.

The use of inflatable membrane structures is a promising technique for the storage of pressurized gas in deep water. In spite of their numerous advantages, inflatable underwater structures have not been used extensively because of the difficulties involved in the prediction of their complex behaviour. In section 1.4 it has been proposed to use an inflatable structure for the storage of gas underwater. In this chapter, methods of solution are suggested for the structural analysis of that structure in the underwater environment. The primary environmental loads on such structures are hydrostatic in nature especially when the size of the structure is small compared to the depth of the water (Selna[59]). Therefore in this chapter the structure has been theoretically analysed for the hydrostatic condition.

The proposed structure consists of a long cylindrical flexible membrane which is fixed at its base. The structural analysis requires the determination of its equilibrium shape and the computation of the associated tension in the membrane. In section 2.2, the differential equations of equilibrium of the proposed structure are solved by a theoretical method. The results indicate that many configurations are possible for a particular cross-sectional area of the structure, by varying the size of the base width. An optimum configuration which produces minimum tension in the membrane is found in section 2.3. The shapes of the profiles obtained in the theoretical analysis are compared with the results of an experimental investigation in section 2.2.5. The close agreement between the two results confirm the validity of the theory.

In view of the high tensile forces that the membrane material has to sustain, it is beneficial to study the effect of incorporation of a system of two-way reinforcing cables in the membrane. In section 2.4, a three-dimensional analysis of the cable-reinforced inflatable structure under a uniformly varying pressure loading has been carried out based on the assumption that only the cables contribute towards the structural integrity. A general computer program has been developed for the nonlinear analysis of space structures. In section 2.4.3., numerical results have been generated for a number of different shapes of cable-reinforced inflated structures under hydrostatic loading condition.

As mentioned in section 1.4, the stored gas inside the proposed structure is drawn off through an outlet whenever required. The equilibrium of the structure is then restored by replacing the removed gas by an equivalent amount of water so that the internal gas pressure remains unaltered.

In section 2.5, the changes in the shape of the profile and the changes in the tension of the membrane or the reinforcing cables due to partially drawing off the internal gas of the structure are investigated.

2.2 The Membrane.

The proposed inflatable structure in this study is considered to be of long cylindrical shape made of a thin flexible membrane fixed along its base and inflated to the required pressure by gas or by a combination of gas and water. The membrane is assumed to be isotropic and to have a self-weight of ω per unit area and to obey a relation between stress σ and strain ϵ of the form $\epsilon = g(\sigma)$. It is obvious that the shape of a section through an inflatable membrane is not definable in the absence of the applied loads and will change considerably with every variation of gas pressure or water level changes that may occur. Of more significance is the fact that the components of the applied loads caused by gas and water pressures will themselves be a function of the shape of the membrane. The main problem therefore consists of finding the shape of the profile for the given load and inflation conditions and of determining the tension in the membrane under those conditions. The membrane itself is defined by the base length and the unstretched curved perimeter (or the cross-sectional area) together with its thickness and elastic modulus.

2.2.1. Structural Analysis of the Membrane.

In most forms of structural analysis, a basic assumption is to consider that the shape of the structure is not grossly distorted by the loads acting on it, in other words the unloaded and the loaded shapes of the structure are effectively the same. In the case of an inflatable structure, the shape

of the membrane is unpredictable in the absence of the loads and therefore normal linear-elastic structural analysis is not applicable.

The solution method adopted in the present study is based on the work for inflatable dams by R.D. Parbery [52, 53]. It is assumed that the behaviour of the three dimensional structure can be represented reasonably by the behaviour of a two dimensional transverse section of unit length. The analysis involves the determination of the shape of the profile and the tension along the perimeter depending on the resultant pressure acting on the membrane. In considering the differential pressure across the membrane, the gas pressure inside the container is taken as uniform and equal to the maximum hydrostatic pressure at the bottom of the structure. The resultant pressure distribution on the membrane is illustrated in figure 2.1 below. It is comprised of the uniform internal pressure plus the hydrostatic external pressure. The co-ordinate system adopted is shown on the same figure.

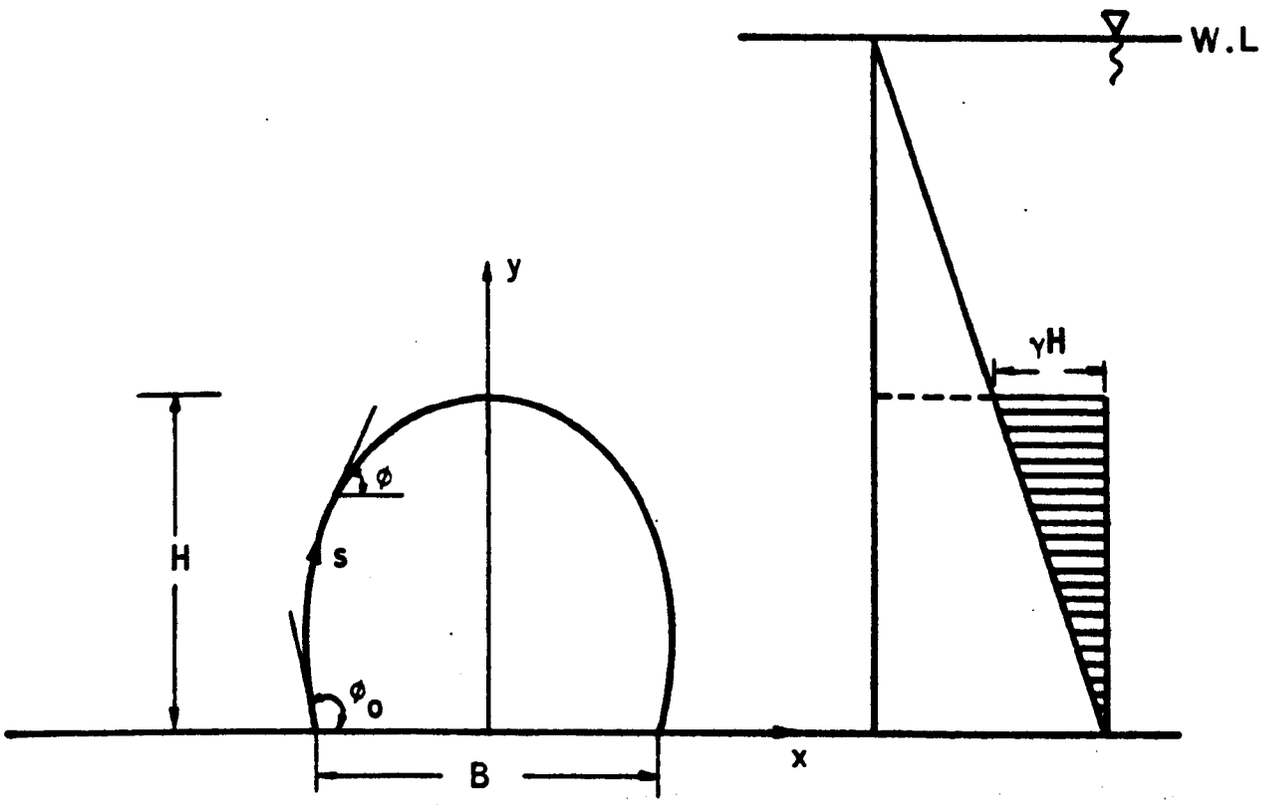

Figure 2.1. Hydrostatic pressure distribution on a cross-section of the proposed structure.

Equilibrium conditions are applied to an element of the perimeter and the differential equations of equilibrium are derived. The derivation of the equilibrium equations using curvilinear co-ordinates is shown in Appendix I. The resulting differential equations of equilibrium are:

$$\frac{d\varphi}{ds} = -\frac{f}{T_o + \omega y}(p - \omega \cos\phi) \qquad (2.1)$$

$$\frac{dx}{ds} = f \cos\phi \qquad (2.2)$$

$$\frac{dy}{ds} = f \sin\phi \qquad (2.3)$$

with the boundary conditions

$$x(0) = -\frac{B}{2}, \quad y(0) = 0 \qquad (2.4)$$

and $$x(L) = \frac{B}{2}, \quad y(L) = 0 \qquad (2.5)$$

where ϕ is the inclination of the tangent in the s direction to the horizontal, s is the length along the unstretched perimeter, f is the extension ratio of the membrane under load, T_o is the initial tension per unit length, ω is the membrane weight per unit area and p is the resultant internal pressure. By solving the differential equations of equilibrium 2.1, 2.2 and 2.3 with the boundary conditions 2.4 and 2.5, the shape of the profile of the membrane and the tension in the membrane can be obtained for the known values of the unstretched length of the membrane L and the base length B.

2.2.2. Computation Technique.

The shape of the membrane profile and the tension in the membrane can be obtained by solving the differential equations of equilibrium (equations 2.1 to 2.3) which are given in section 2.2.1. Because of the nonlinear nature of these equations in their present form, an iterative method of solution is required. Parbery[52] has suggested a numerical method of solution in which these equations are integrated using a fourth order Runge-Kutta method with estimates of $\phi(0)$ and T_o which are then refined by the Newton-Raphson method.

Parbery [53] has later investigated the effects of the various load and design variables. In view of the results of his investigation, it is concluded that for practical values of the membrane self-weight and extensibility, the effect of the self-weight of the membrane is negligible and can therefore be neglected in which case the effect of membrane elasticity may be decoupled from the differential equations of equilibrium. A theoretical method is then developed for the solution of these equations. The method is explained fully in Appendix I. The results are as follows:

$$s = \frac{2}{a}\left[F(k,\frac{\phi_o}{2}) - F(k,\frac{\phi}{2})\right] \qquad (2.6)$$

$$x = \frac{2}{ak^2}\left\{2\left[E(k,\frac{\phi_o}{2}) - E(k,\frac{\phi}{2})\right] + (k^2-2)\left[F(k,\frac{\phi_o}{2}) - F(k,\frac{\phi}{2})\right]\right\} - \frac{B}{2} \qquad (2.7)$$

$$y = \sqrt{2T(\cos\phi - \cos\phi_o)/\gamma} \qquad (2.8)$$

$$T = \frac{\gamma H^2}{2(1-\cos\phi_o)} \qquad (2.9)$$

where E and F are elliptic integrals of the second and first order respectively, γ is the specific weight of water, H is the height of the structure,

$$a^2 = \frac{2\gamma}{T}(1-\cos\phi_o) \qquad (2.10)$$

and $$k^2 = \frac{4\gamma}{a^2 T} \qquad (2.11)$$

Equations 2.6 and 2.7 and 2.8 define the shape of the membrane profile for given values of initial angle ϕ_o and tension T. For practical problems ϕ_o and T have to be found to satisfy the physical restrictions of the base and unstretched perimeter lengths given by the boundary conditions 2.4 and 2.5. This is achieved by using a combination of the Newton-Raphson method and the rule of false position with the aid of a computer program. The cross-sectional area and thus the volume can be calculated by numerical integration using Simpson's rule. The tension in the membrane is obtained from 2.9. If the elasticity of the membrane is to be considered in the calculations, the value of the stretched perimeter L*

given by equation 2.12 has to be accomodated in the iteration process.

$$L^* = L\left(1 + \frac{T}{Et}\right). \qquad (2.12)$$

(Et is the product of Youngs modulus and the thickness of the membrane).

A computer program based on equations 2.6 - 2.12 is developed and the effect of variation of the different parameters in these equations is examined in order to find an optimum configuration for the inflatable underwater structure. The flow chart of the computer program is given in Appendix I.

2.2.3. Theoretical Results.

Numerical results have been generated with the aid of the computer in order to investigate the effects that different factors have on the shape of the profile and the tension in the membrane. These investigations are divided into three groups.

Group One - In group one the variation of area (A), perimeter (S) and the tension in the membrane (T), with the inclination angle at toe (ϕ_o) are studied for different base widths (B). The results are plotted in graphs 2.1, 2.2 and 2.3 respectively. It is observed that in all the three graphs, the curves are smooth and are asymptotic to the line $\phi_o = 130°$. It is therefore concluded that a physical configuration is not possible for base angles greater than 130 degrees. The graphs also indicate that many configurations are possible for a certain area or perimeter with different base widths which in turn produce different tensions in the membrane and different base angles. The values of the area, perimeter and the tension in the membrane increase by increasing the base angle for a fixed base width or by increasing the base width for a fixed base angle.

Group Two - In group two, the variation of perimeter (S) and the tension in the membrane (T) with the base width (B) are studied for different areas (A). The results are plotted separately in graphs 2.4 and 2.5 respectively and then are superimposed in graph 2.6. The curves obtained in these graphs are all concave and each pass through a minimum. The

region around the minimum of each perimeter curve shows a small variation of perimeter with base. On the other hand, the tension curve increases rapidly after the minimum tension. From graph 2.6 in which the two sets of results are superimposed, it is observed that for a fixed area, the minimum of the tension curve does not coincide with the minimum of the perimeter curve. The economics of the structure with regards to the tension and the perimeter dictates that the structure should have a base width which lies somewhere between the minimum tension and the minimum perimeter but a final decision cannot be made unless the strength and the cost of the material is readily available so that they can be compared simultaneously.

Group Three - In group three, the profiles for minimum tension and minimum perimeter for different areas are obtained. These profiles are shown in figures 2.2 and 2.3 respectively. It can be observed from these figures that as a general rule, the profiles for minimum perimeter have a smaller maximum height and a wider base width compared to the profiles for minimum tension. In the case of the profiles for minimum tension, the areas have been recomputed by taking into account the elasticity of the membrane. The results show that the maximum difference in the value of the area with or without considering the membrane elasticity is 1.5%. It is therefore concluded that for commercially available membranes, the effect of elasticity is insignificant. This confirms the findings of Parbery[53].

2.2.4. Experimental Approach.

Experiments designed to check the theoretical results of section 2.2.3. have been conducted for a number of different profiles of the membrane structure. Since the theoretical analysis of the inflatable membrane is based on the resultant pressure distribution on the membrane, it is appropriate to carry out the model investigation on the basis of the same resultant pressure and measure the profile that the membrane takes up under that pressure.

The resultant pressure distribution on which the structural analysis is based, is shown in figure 2.1. It can be seen that this is in fact the distribution of water pressure inside a container of the same height but in an upside down position. Experimentally, it is much easier to measure the profile if a larger model is used and the measurements are taken outside water. It is therefore decided to carry out the experiment on a model which is positioned upside down compared to the prototype and fill the model with water so that the model is exposed to exactly the same pressure distribution as that considered in the theoretical analysis. In this way the membrane profile can be easily measured from the outside of the model.

The flexible material used for the construction of the model is a PVC coated polyester with a thickness of 0.55 mm and an average yield load of 43 kN/m. The strain of the membrane under incremental load is measured and the result is plotted in graph 2.7. The gradient of the curve obtained in this graph gives the value of the product of Youngs Modulus and the thickness of the material. This value is found to be 180 kN/m. The longitudinal dimension of the flexible model is chosen to be long enough to render the end effects insignificant. The end panels of the model are cut from the same material as the main body of the model and are glued to it by Bartol S241 Adhesive glue. The model is supported on a frame. The base width of the model can be fixed using timber strut and ties. The position of the timber struts and the ties are illustrated in figure 2.4.

The measurements of the profile are taken at the cross-section midway along the model. The points on the profile are measured from a fixed vertical line at known vertical distances from the top of the model. A spirit level is used to ensure vertical and horizontal distances. The measurements are taken to an accuracy of 0.5 mm which is sufficient, considering that the overall dimensions of the model is comparatively large.

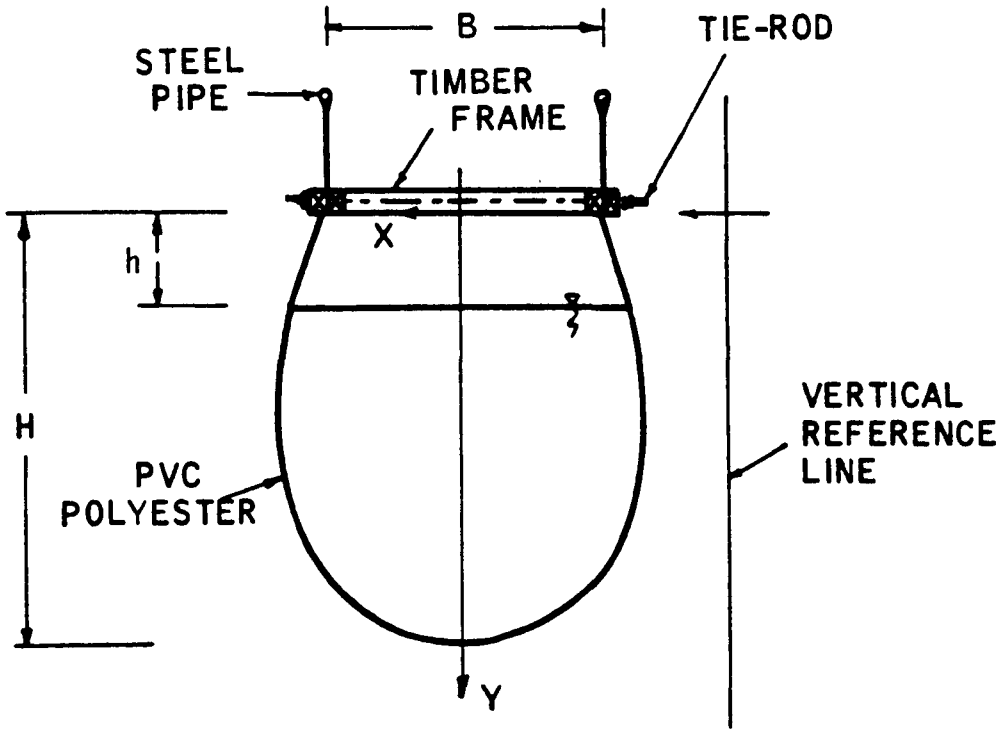

Figure 2.4. Cross-section of model.

The profiles obtained in the experiment can be divided into three types according to whether the base angle is greater than, equal to or smaller than 90°. The results are plotted in figures 2.5, 2.6 and 2.7 respectively. In the cases of base angles greater than and equal to 90°, the experiment is carried out on models with the same unstretched perimeter but with different base widths. In the case of the model with base angle less than 90° a different length of unstretched perimeter is used. The results of these experiments are compared with the theoretical results in section 2.2.5.

2.2.5. Comparison of Experimental and Theoretical Results.

The shape of the flexible membrane which is theoretically calculated in section 2.2.2. is compared with the results of the model investigation of section 2.2.4. Three different model profiles are chosen, one with a base angle greater than 90°, one with a base angle of 90° and

the last one with a base angle smaller than 90°. The base widths of the three models are 0.495, 0.703 and 0.623 m respectively. The unstretched perimeter of each of the first two models is 1.545 m and that of the third model is 0.980 m. Each profile is found by measuring the co-ordinates of at least twenty points along its periphery. The results are shown in figures 2.5, 2.6 and 2.7. The stretched perimeter is also measured on each profile. The area of each profile is calculated by Simpson's rule using the measured co-ordinates.

The tested value of the product of Young's Modulus and the thickness of the membrane material is found to be 180 kN/m. This value is used in the theoretical computation of the profile shapes for the base widths and the unstretched perimeters upon which the experimental investigation is based. Each of the theoretical profiles hence obtained is superimposed on its corresponding experimental result (figures 2.5, 2.6 and 2.7). It can be seen that the calculated shapes are in good agreement with the measured profiles.

The stretched perimeters and the areas of the three models are also compared with the corresponding theoretical values. Table 2.1 shows a summary of these results. It is observed that the percentage differences are very small and on average come to about 1.2% and 0.4% for the area and the stretched perimeter respectively.

From the computed theoretical results of tension based on experimental values of base widths and unstretched perimeters, it is found that the tension per metre width of the membrane is approximately 2 kN/m. The results of the tests on the strength of the membrane sheets used in making the models, show that this material can withstand this tension. This is confirmed in the experiment since the models fully sustain the specified loading condition.

The experiment on each model is followed by further tests in order to investigate the phenomena of partially drawing off of gas in the prototype which is represented by changing the water level inside the model. These

Approx. Base Angle (degrees)	Base Width (m)	Unstretched Perimeter (m)	Theoretical		Experimental (Averaged)		Percentage difference	
			Area (m^2)	Stretched Perimeter (m)	Area (m^2)	Stretched Perimeter (m)	Area (%)	Stretched Perimeter (%)
90	0.703	1.545	0.3504	1.5599	0.3462	1.558	1.21	0.12
103	0.495	1.545	0.3059	1.5584	0 3015	1.553	1.46	0.35
72	0.623	0.980	0.1512	0.9843	0.1528	0.992	1.04	0.78

Table 2.1 - Summary of the Theoretical and the Experimental Results.

experiments are dealt with in Section 2.5.

2.3 Optimum Configuration for the Structure.

The results of the theoretical analyses of a gas-filled membrane structure submerged in water, are shown in Section 2.2.3. From these results, it is evident that many configurations are possible for a particular area by varying the base width. Each of these configurations produces a different tension in the membrane and requires a different length of membrane material for its profile shape. The graphs of tension against base width and unstretched perimeter against base width have been plotted in graphs 2.4 and 2.5 respectively. The curves obtained are parabolic and each passes through a minimum at a certain value of the base width. The curves in graphs 2.4 and 2.5 are superimposed in graph 2.6. It can be seen that the base width for which minimum tension occurs does not coincide with the base width for which minimum unstretched perimeter occurs. The choice of an optimum configuration would therefore depend on the strength and the cost of the membrane material available. Nevertheless, due to the small gradient of the unstretched perimeter curve in the region of its minimum value, the base width for minimum tension corresponds to an unstretched perimeter which does not differ greatly from the minimum value of the perimeter. Therefore, in the absence of any details regarding the cost and strength of the membrane material, it is reasonable to consider the configuration which produces the minimum tension, to be a suitable optimized profile for the inflated underwater structure.

As a practical size for the prototype structure, a cross-sectional area of approximately 40 m^2 is chosen. The base width for minimum tension is 7.5 m which produces 201.0 kN tension per unit length of the membrane. The base angle for this structure is found to be 90.67^0. The stretched and unstretched perimeters of this profile is 16.67 and 16.51 m respectively. The scaled shape of this profile is shown in figure 2.8.

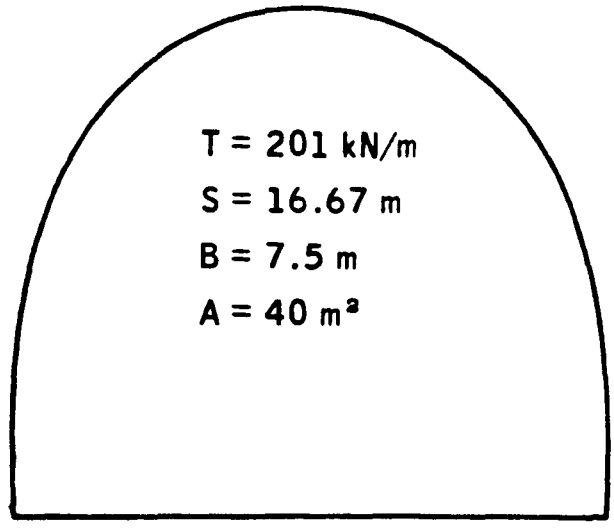

Figure 2.8. Minimum Tension Profile.

In the following sections of this study, the analyses are based on the above profile shape and size.

2.4 Cable-Reinforcement of the Membrane.

In Section 2.2 a gas-filled membrane structure submerged in water has been analysed. The results of the analysis show that in structures of practical size, the tension in the membrane is rather high and increases by increasing the cross-sectional area of the structure. This is well-observed in figure 2.2. In spite of the fact that the profiles in this figure have been designed to produce minimum tension for each particular cross-sectional area, the values of the tension in the membrane are as high as 201.1 and 251.4 kN/m for areas of 40 and 50 m^2 respectively. Although it is possible to obtain suitable membrane materials which can sustain such high tensile forces, it is advantageous to incorporate a system of cable reinforcement in these structures. The reinforcement can serve a dual purpose of allowing extra flexibility in the form of the structure, and of providing additional strength in the structure, thereby making the construction of structures with larger cross-sectional areas, lower profiles and longer spans possible.

In this section the effect of the presence and spacing of reinforcing cables is studied for various geometries of inflatable underwater structures. All the geometries considered, are based on the result of the optimum profile shape obtained in Section 2.3. The cable configuration adopted in this study consists of a set of orthogonal cables, initially running parallel to the longitudinal and circumferential directions of the structure. A three dimensional non-linear analysis of the cable reinforced membrane is presented herein and the method is applied to a number of different structures. The results are discussed in Section 2.4.4.

2.4.1. Structural Analysis of Cable-Reinforced Membrane.

In order to increase the ability of inflatable membrane structures to sustain higher tensile forces, the membranes can be stiffened by a system of reinforcing cables. In this section, a three dimensional analysis of the cable-reinforced membrane structure under hydrostatic loading condition is carried out based on the method suggested by M. Epstein and Y. Tene[20] for the non-linear analysis of space trusses.

The analysis of cable-reinforced membrane structures is a complex problem due to the interaction of cables and the membrane. It can however be greatly simplified if its is assumed that the action of the membrane is neglected except for transmitting the pressure load to the cables. This is not only a conservative assumption, but permits the consideration of the cables in isolation. The pressure load is considered to be distributed along cable elements while all other loads are concentrated at nodes. The pressure loading on the structure is considered to comprise of a uniform internal pressure, together with a uniformly varying external hydrostatic pressure as shown in figure 2.1. It is assumed that the pressure on the area enclosed by cable elements is equal to the average of the pressures on the nodes surrounding that area. The force due to the pressure on this area is then divided equally between those nodes. The force at each node is the sum of the forces from all the surrounding areas. The cables are considered as elastic elements which initially undergo large displacements up to the point of equilibrium. After the equilibrium is reached, the extensibility of the cables is assumed to be small.

The displacement of the cable nodes influences the magnitude of the resultant pressure at the nodes. The spacing of the reinforcing cables is small enough so that the length of each cable element can be approximated by the length of a straight line joining the nodes at the two ends of the cable. The weights of the cables are taken to be small and are therefore neglected. However, they can be considered in the analysis in which case they are added to the external forces at the corresponding nodes, accordingly.

The method of solution herein is based on a general approach for solving nonlinear problems in structural mechanics as presented by Budiansky[10]. This method provides exact equilibrium equations valid for arbitrarily large strains and displacements. It makes use of exact kinematic equations (strain-displacement relations) and a general non-linear stress-strain relation approximated by polynomials. The non-linear equations are written using the known initial geometry, material constants and the loading data of the structure plus a set of imposed initial displacements. The equations allow for the existence of prestress in the initial state of equilibrium. The resulting non-linear equations are polynomials in the unknowns 'displacements of joints' and can be solved by the Newton-Raphson method which converges rapidly to a solution with a specified degree of accuracy. A detailed account of the derivation of the equilibrium equations is given in Appendix II. In cases where the relation between the generalized force Q_{ij} and the generalized elongation ϵ_{ij} can be approximated by a linear function of the form

$$Q_{il} = K_{il}\,\epsilon_{il} \qquad (2.13)$$

in which K_{il} is a constant for each cable element, the equilibrium equation in the h direction for any joint l is

$$\sum_{\substack{i=1\\ i\neq l}}^{M}\left[{}_h t_{il} + \frac{1}{d_{il}}\left({}_h u_l - {}_h u_i\right)\right]\left\{N^*_{il} + K_{il}\left[\sum_{k=1}^{3}\left[{}_k t_{il} + \frac{1}{2d_{il}}\left({}_k u_l - {}_k u_i\right)\right]\right.\right.$$

$$\left.\left.\left({}_k u_l - {}_k u_i\right)\right]\right\} = {}_h X_l \qquad \begin{matrix} h = 1,2,3 \\ l = 1,\ldots,N \end{matrix} \Bigg\} \ldots (2.14)$$

where d_{il} and t_{il} are the length of cable i-l and the unit vector along cable i-l respectively before deformation, N^*_{il} is the prestress force,

u_l and X_l are the displacement and the external force at node l respectively and M and N are the total number of nodes and the number of unrestrained nodes respectively. Equation 2.14 constitutes a system of 3N equations which are polynomials of the third degree in the unknowns ${}_j u_i$. This form of equation is specially suited for using the Newton-Raphson method. The method of solution is explained in the next section.

2.4.2. Method of Solution.

In order to solve the system of equations 2.14, the Newton-Raphson algorithm is used. The system of equations 2.14 can be defined by the functions

$$ {}_h F_l ({}_p u_q) = \sum_{\substack{i=1 \\ i\neq l}}^{M} \left[{}_h t_{il} + \frac{1}{d_{il}} ({}_h u_l - {}_h u_i) \right] \left\{ N^*_{il} + K_{il} \left[\sum_{k=1}^{3} \left[{}_k t_{il} + \frac{1}{2d_{il}} \right. \right. \right. $$

$$ \left. \left. \left. ({}_k u_l - {}_k u_i) \right] ({}_k u_l - {}_k u_i) \right] \right\} - {}_h X_l \quad \ldots\ldots\ldots (2.15) $$

The general term of the Jacobian matrix of the functions 2.15 is given by

$$ \frac{\partial_h F_l}{\partial_p u_q} = \sum_{\substack{i=1 \\ i\neq l}}^{M} \frac{1}{d_{il}} \delta_{hp} (\delta_{lq} - \delta_{iq}) \left[N^*_{il} + K_{il} \left\{ \sum_{k=1}^{3} \left[{}_k t_{il} + \frac{1}{2d_{il}} \right. \right. \right. $$

$$ \left. \left. \left. ({}_k u_l - {}_k u_i) \right] ({}_k u_l - {}_k u_i) \right\} \right] + \sum_{\substack{i=1 \\ i\neq l}}^{M} \left[{}_h t_{il} + \frac{1}{d_{il}} ({}_h u_l - {}_h u_i) \right] $$

$$ K_{il} (\delta_{lq} - \delta_{iq}) \left[{}_p t_{il} + \frac{1}{d_{il}} ({}_p u_l - {}_p u_i) \right] - \frac{\partial_h X_l}{\partial_p u_q} \qquad (2.16) $$

in which δ_{hn} is the Kronecker delta (= 1 if h = n, but = 0 if h ≠ n). Newton-Raphson technique requires an initial displaced shape for the structure. A set of initial values is imposed for the 3N solution vector

$$\{{}_p u_q^o\} \quad \begin{matrix} q = 1, \ldots, N \\ p = 1, 2, 3 \end{matrix} \qquad (2.17a)$$

The residual vector is given by

$$\{{}_h R_l^o\} = {}_h F_l(\{{}_p u_q^o\}) \quad \begin{matrix} l, q = 1, \ldots, N \\ h, p = 1, 2, 3 \end{matrix} \qquad (2.17b)$$

The corrected approximation will be $\{{}_p u_q'\}$ given by

$$\{{}_p u_q'\} = \{{}_p u_q^o\} + \{\Delta_p u_q^o\} \qquad (2.18)$$

in which $\{\Delta_p u_q^o\}$ is obtained from the solution of the following system of linear equations

$$\left[\frac{\partial_h F_l}{\partial_p u_q}\right]_{\{{}_p u_q^o\}} \cdot \{\Delta_p u_q^o\} = -\{{}_h R_l^o\} \qquad (2.19)$$

The main feature of this system is that the matrix $\left[\frac{\partial_h F_l}{\partial_p u_q}\right]_{\{{}_p u_q^o\}}$ is

a square and symmetrical matrix which has usually a large number of zero elements in structures with too many nodes and therefore can be easily solved by Gaussian elimination method. From the solution of the system of linear equations 2.19, the corrected approximation for the set of displacement vector $\{{}_p u_q\}$ is obtained from equation 2.18. The unbalanced force in every unrestrained node of the structure is calculated from equation 2.15 using the corrected approximation of the displacement vector. The unbalanced forces are then checked against the set tolerance and if every single one of them satisfies the specified tolerance, the analysis of the structure is considered to be complete; otherwise the terms of the Jacobian Matrix (2.16) have to be recalculated using the corrected approximation of the displacement and a new solution has to be found to the system of linear equations 2.19 so that the displacement vector $\{{}_p u_q\}$ can be recorrected.

Some difficulties may encounter in the incorporation of structures with tension-only members in the numerical solution. In imposing the initial set of displacement values for such structures, slow convergence can be

avoided if it is ensured that all members are initially in tension. This can be achieved by imposing initial displacements that are proportional to a uniform pressure loading. Nevertheless it is found that for most structures any set of displacements including all zero ones will eventually lead to convergence. Another difficulty in dealing with tension-only members occurs when one or more members experience a negative strain from the previous iteration. If the stiffnesses of such members are given zero values, the properties of the Jacobian Matrix change abruptly and thus convergence cannot be reached. To overcome this problem, whenever negative strain is detected, the stiffness of that member is reduced by a factor of 0.3 and if ever that same member returns to the tensile state, its stiffness is increased by the reciprocal of the same factor. In this way, no members are calculated to have zero forces, but after several iterations all compressive forces will be negligibly small compared to the tensile forces.

It can be seen from the system of equilibrium equations 2.14 that the analysis includes the case where there exists a known state of prestress in the initial geometry of the structure when it is in equilibrium. The pretension N^*_{il} can be the same or different in each cable. The value of K_{il}, the product of the Young's modulus and the cross-sectional area of each cable can also be different in different cables. The method of solution herein thus provides exact solutions to the problem of pin-jointed structures including suspended roofs and many types of cable-reinforced membranes and shells, having arbitrary initial geometry and structure properties with various methods of prestress and under arbitrary loadings including non-uniform pressure loading. The non-linear static analysis presented here is capable of leading to exact solutions even for the case of large displacements and strains. It has the added advantage over the previous methods of being able to handle the case of external loadings which are dependent on the displacements of the structure joints. This feature of the method is especially useful in the analysis of cable-reinforced inflatable structures under non-uniform pressure loading as happens for gas-filled membrane structures which are submerged in water. In these situations, since the pressure at each node depends on its

dimensional position, any change in the displacement of the node results in a change in the value and the direction of the pressure force at that node.

A general computer program has been developed for the non-linear static analysis of pin-jointed structures. It is based on the above presented method of solution. The Flow Chart of the program is shown in Appendix II. The program is quite flexible and includes several subroutines, two of which have to be altered for analyzing different structures. One is SUBROUTINE DATA which comprises the data on all the geometric and material properties of the structure such as the cartesian coordinates of each node, the number of degrees of freedom of each node, the position of all the members and the elasticity of each member. This subroutine should also generate an initial set of displacement values for the unrestrained nodes. The second subroutine which has to be developed differently for individual structures is SUBROUTINE FORCE. As the name applies, this subroutine deals with the loading condition of the structure. In contrast to SUBROUTINE DATA which is only used once during the analysis of a structure, this subroutine is called several times in the course of the analysis. In the case of structures with point loads or other types of fixed loads, SUBROUTINE FORCE simply contains the value and the direction of the external force at each node. In the case of uniform or non-uniform pressure loading, the force at each node due to the pressure has to be calculated seperately. These forces can then be stored in a memory for use in different rounds of iteration. Alternatively, memory blocks can be saved if the force at every node is re-calculated each time the iteration process is repeated. The second option is especially useful in the case where the pressure force at each node is dependent on the displacement of the node as well as its original position. In such cases at every iteration and for each set of corrected approximation of displacement, a new set of pressure forces is calculated.

The computer program has been developed such that the iterations continue until either the assigned maximum number of iterations is reached or when the unbalanced force at every node is less than 0.002 percent of the average force at the nodes. It then computes and prints the forces at all the nodes and in all the members of the structure, on the basis of the last set of displacement values found during the computation. It also prints the final values of the displacement for all the unrestrained nodes and finally draws a three-dimensional view of the structure.

The program is checked against known solution of the three dimensional truss structure of Epstein and Tene[20] and a cable-reinforced membrane spherical cap of Malcolm[43]. The results are shown in figures 2.9 and 2.10. They are almost the same as the published results. It is found that the present computer program can analyse structures using less execution time than the computer program developed by Malcolm[43] In the case of the membrane spherical cap of Malcolm[43], the effect of displacements of the nodes in changing the pressure force at the nodes has been considered in every iteration.

After the correctness of the computer program is established by comparison with known solutions, the program is used for the analysis of the submerged gas-filled cable reinforced membrane structure suggested in section 2.2. The membrane of this structure has already been analysed in the case where no reinforcements are used and the results are shown in section 2.2.3. The optimum configuration of the membrane which yields to minimum tension in the membrane has been discussed in section 2.3. In the next section, the proposed structure with the chosen configuration is further analysed by considering the incorporation of a two-way set of longitudinal and circumferential cable network. Also the effect of spacing of the reinforcement is studied for various structures of the same configuration. The results are discussed in section 2.4.4.

2.4.3. Theoretical Results for Various Structure Shapes.

The computer program developed in section 2.4.2 is used for the analysis of a number gas-filled reinforced membrane structures submerged in water. The common characteristics and properties of these structures are as follows:

(a) The profiles of the main cross-sectional area of all these structures are the same as that obtained in section 2.3. for minimum tension in the membrane (figure 2. 8).

(b) The reinforcing cables run in the circumferential and the longitudinal directions and are usually equally spaced in both directions thus forming a square mesh. In the case of the three-dimensional structures, the longitudinal cables follow the profile of the membrane at the two ends.

(c) The product of Young's modulus and cross-sectional area of the cables is the same for all cables and is taken to be 15000 N.

(d) The prestressed force is taken as zero in all cables.

Moreover,all the assumptions used in the derivation of the equilibrium equations (2.14) for the non-linear analysis of space trusses, apply to all these structures.

The three different types of structures studied are as follows:

(1) The first type of structure analysed is a cylindrically shaped structure with two flat ends (figure 2.11). The effect of changing the length of the structure in the range of 8 meters to 32 meters is examined. Also different cable spacings of approximately 1.0 m and 2.0 m are studied.

(2) The second type of structure investigated is also cylindrically shaped but the two ends are not flat. Instead the two ends are in the form of the shape generated by rotating the main cross-sectional profile about its axis of symmetry. The longitudinal cable reinforcements

follow complete loops around the structure. The circumferential cables on the end caps continue to be parallel to the ones on the main body of the structure. The positions of the circumferential cables of each end cap are such that the top points of these cables intersect the outermost line of the cap at exactly the same point as the longitudinal cables do. If the horizontal distance between any two adjacent circumferential cables of the caps is less than 0.4 times the spacing of the cables of the main body, the outer circumferential cable will be omitted. An example of this type of structure and the arrangement of the reinforcing cables on it is illustrated in figure 2.12. A number of different structures of the cap ended type are analysed. The length of the cylindrical part of these structures are varied between 8 m and 32 m and the spacing of the cables in the main body of the structure is given values of 1 m and 2m. The effect of changing the length of the main body of the structure and the spacing of the cables is investigated.

(3) The third type of structure is a special case of the second type in which a zero value has been given to the length of the main body of the second type structure. In other words it is obtained by connecting the two end caps of the second type structure. An example of this type of structure is shown in figure 2.13. The effect of cable spacing in the range of 0.6 m to 2 m is studied in this structure.

Some of the numerical results generated by the computer are shown on figures 2.14 to 2.24. For each type of structure the effects that the structure's length and the cable spacing have on the displacements of the nodes and the forces in the cables have been investigated. For a few of the structures, the consequences of using all zero values or using any set of arbitrary values for the initial displacement have been examined. It is found that convergence can be reached to exactly the same solution regardless of the initial displacement values but the number of iterations needed to reach convergence is different in each case. In general with a

suitable set of initial displacements,convergence to within the specified accuracy is obtained within eleven iterations for a structure of about 220 unrestrained nodes and 470 cable elements. The execution time for the same structure is in the order of 45 seconds per iteration. For a smaller structure which has 49 unrestrained nodes and 108 members, the execution time is just over 2 seconds per iterations compared to 20 seconds per iteration quoted by Malcolm and Glockner[43] for a similar sized structure.

The results of the cable forces and the displacements in each structure will be discussed in the next section.

2.4.4. Discussion of Results.

As mentioned in section 2.4.3., three different types of cable reinforced membrane structures have been analysed with the aid of the computer program developed in section 2.4.2.

Due to the symmetry of these structures with respect to X-Y plane and the Y-Z plane, the tension forces in the cables of only one quarter of each structure have been shown on the corresponding cables. The magnitudes of these forces have been rounded off to whole numbers. In the case of the first and the second type structures, it is observed that the X and Y co-ordinates of the nodes which are on the same longitudinal cable in a structure are almost equal. It is therefore decided to take only the center circumferential cable in each structure and to draw that section of the structure in the X-Y plane. In the case of the second and third type structure, the nodes on the outermost loop of the caps are plotted in the Y-Z plane. Also, in these two types of structures the nodes on the last circumferential cables are plotted in the X-Y plane simultaneously with the nodes of the middle circumferential cables.

The results of each type of structure are individually discussed in this section.

Type 1 - Fixed-ended structures. Four different structures have been analysed in this group. The cable-spacing in the first three of these structures are approximately 2.0 m . The total length of these structures are 32.0, 16.0 and 8.0 m respectively. The fourth structure in this group has a total length of 8.0 m and its cable spacing is about one meter. The results of the analyses of the structures in this group are shown in figures 2.14 to 2.17. It is observed that in each of these structures, the forces in the longitudinal cables are generally lower, nearer the base of the structure. On the other hand, the forces in the circumferential cables are generally higher towards the base and nearer the flat ends of the structure. In all these structures, the forces in the circumferential cables are considerably higher than the forces in the longitudinal cables. The effect of increasing the longitudinal dimension of the structure can be studied by comparing the results of the analyses of the first three structures (figures 2.14a1, 2.15 a1, and 2.16 a1). The comparison of the forces in the circumferential cables of the first three structures shows that the values of the cable forces are usually smaller in longer structures, the maximum difference between the circumferential cable forces in the 32.0 m long structure and in the 16.0 m long structure is less than 1%, but the corresponding difference with the 8.0 m long structure is as high as 5% as compared to the two longer structures. The percentage difference in the circumferential cable forces gets higher nearer the ends of the structures. The forces in the longitudinal cables greatly decrease as the length of the structure increases.

The computer results have shown that the equilibrium profiles of these structures are the same, irrespective of their lengths.
Therefore only one cross-section has been drawn and this is shown in figure 2.14b. The maximum difference in the cross-section of these structures is in the order of 0.4 percent which is insignificant.

The effect of cable spacing can be studied by comparison of figures 2.16 and 2.17 for 2.0 m and 1.0 m cable spacings respectively in the 8.0 m long structure. The comparison of these figures shows that

the structure with 1.0 m cable spacing takes up a generally lower equilibrium position as compared to the structure with 2.0 m cable spacing. In regards to the tension forces in the cables, it is evident that by reducing the spacing of the cables, the forces in the cables will also be reduced. In the case of the forces in the circumferential cables, it is observed that these forces are approximately halved as the spacings of the cables are halved. The forces in the longitudinal cables are greatly reduced as the spacing of the cables is reduced.

Type 2 - Cap-ended structures. Four different structures have been analysed in this group. The cable spacings in the first three of these structures are approximately 2.0 m. The total length of these structures are taken to be 39.5 m, 23.5 m and 15.5 m respectively. The fourth structure in this group has a total length of 15.5 m but its cable spacing is about 1.0 m. The results of the analyses of the structures in this group are shown in figures 2.18 to 2.21. It is observed that the forces in the circumferential cables are at their maximum midway along the length of the structure. These forces get smaller towards the ends of the structure. However, the forces in the longitudinal cables are larger towards the ends of these structures. In all these structures the forces in the circumferential cables are higher than the forces in the longitudinal cables. From the results of the first three structures,the effect of increasing the size of the structure in the longitudinal direction can be studied. The computer results have shown that the profiles of the cross-sections of these structures are almost the same in all these structures irrespective of their lengths. Therefore only one cross-section profile in the X-Y plane and one profile of the end cap in the Y-Z plane have been plotted (figures 2.18b and c). The comparison of the forces in the cables on the cap-ends of these structures shows that these forces are generally smaller in longer structures. The forces in the longitudinal cables on the cylindrical part of these structures are also smaller in longer structures.

The comparison of the results of the 15.5 m long structure with 2.0 m and 1.0 m cable spacings (figures 2.20 and 2.21

respectively), shows that the latter structure takes up a lower equilibrium position compared to the former. The forces in the cables of the structure with a shorter cable spacing are considerably smaller than those in the cables of the structure with a longer cable spacing, as would be expected.

The comparison of the forces in the structures of type 2 with those of type 1 shows that the forces in the circumferential cables of the structures in type 2 are generally smaller as compared to the corresponding ones in type 1. On the other hand, the forces in the longitudinal cables of the structures in type 2 are larger than the corresponding ones in type 1. However, in all these structures the forces in the longitudinal cables are always smaller than the forces in the circumferential cables. Therefore in order to get minimum tension force in the cables, it is advisable to choose a type 2 structure unless different cable materials are to be used for circumferential and longitudinal reinforcing cables.

Type 3 - Dome-shape structures. Three similar sized structures have been analysed in this group. The only difference between these structures is their cable spacings which are approximately 2.0 m, 1.0 m and 0.6 m respectively. The results are shown in figures 2.22, 2.23 and 2.24 respectively. It is observed that the structure takes up a lower equilibrium position as the spacing of the cables is reduced. As in the other two types of structures, the forces in the horizontal cables are smaller than the forces in the other cables. The forces in the cables are smaller in structures with shorter cable spacings. In the two structures with cable spacings of 1.0 m and 0.6 m, a couple of cable elements have been found in which the forces are almost zero. These cable elements are redundant and can therefore be omitted from these structures.

2.5 Partially Drawing-off of Gas.

In the previous sections of this chapter the analysis of an inflatable membrane structure submerged in water has been carried out. It has been assumed that the container is completely filled with a gas of constant pressure and that the value of this pressure is equal to the hydrostatic pressure at the base of the structure. The resultant static pressure distribution on the membrane is thus of the form shown in figure 2.1. Since the main application of such a structure is for storage of gas, it is inevitable that the stored gas will have to be drawn out of the membrane container regularly and therefore the pressure of the internal gas of the structure will alter from the designed value. In order that the equilibrium of the membrane is retained, the structure has to be designed such that as the stored gas is drawn off, enough water enters the membrane to maintain equilibrium. A rubberized diaphragm of the type designed by Baffico et.al[5] can be used to separate the remaining gas from water so that water pollution and any absorption of gas by water is avoided. The rubberized diaphragm itself has to be resistant against both water and the gas and should sustain the applied stresses during loading and unloading procedures. The method of anchoring the diaphragm to the membrane is quite complicated but it is not an impossible task.

In its extreme position, the diaphragm adheres to the base of the structure in which case the structure is full of gas and the static pressure distribution is as shown in figure 2.1. When some of the internal gas has been drawn off, water enters the structure and the profile of the membrane will be changed to a shape similar to that shown in figure 2.25. There will also be some pressure changes involved and these are also shown in the same figure.

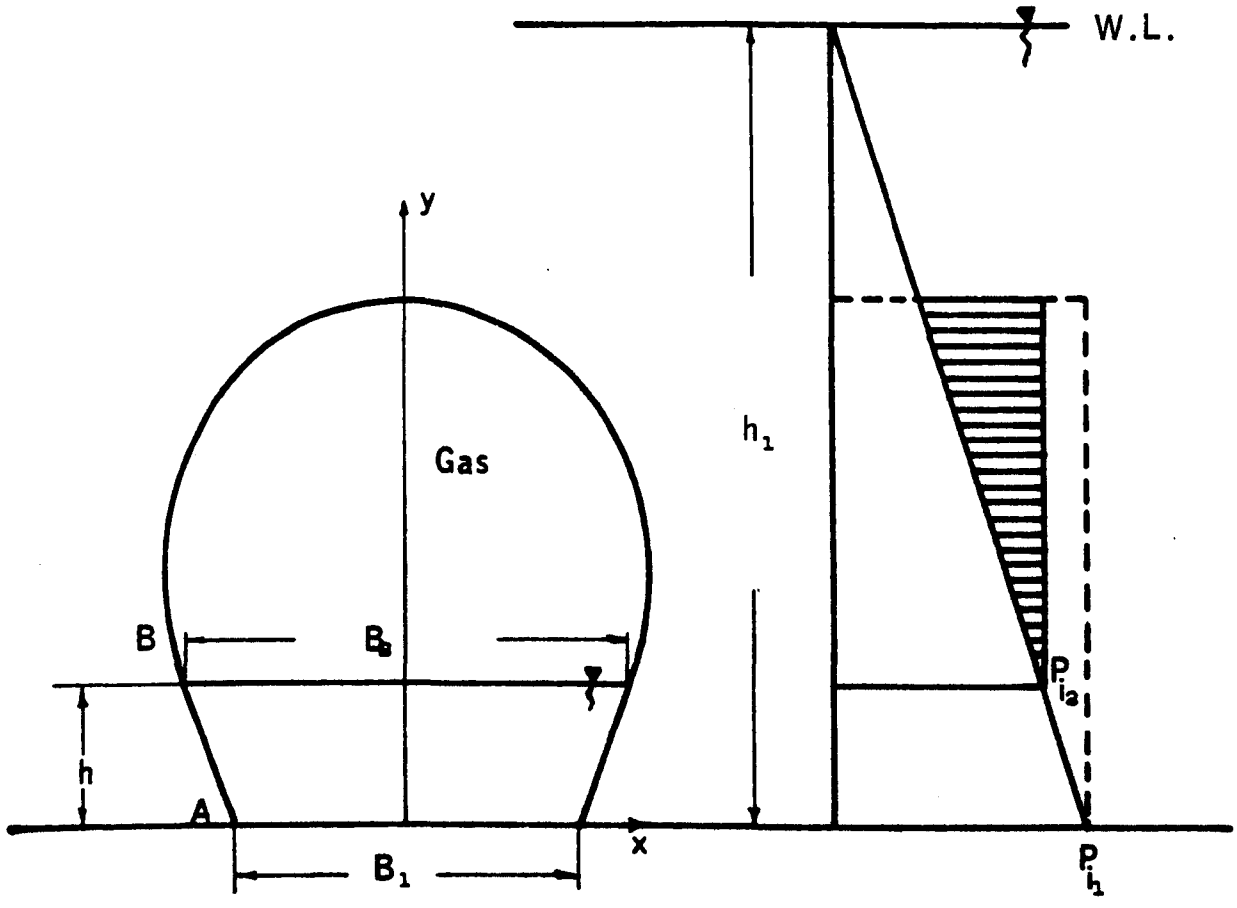

Figure 2.25 - Partially Drawing-off of Gas.

The relation between the level of the water in the structure (h) and the change of the internal gas pressure (ΔP_i) can be found from:

$$\Delta P_i = P_{i_1} - P_{i_2} = \gamma_w h_1 - \gamma_w (h_1 - h) = \gamma_w h \qquad (2.20)$$

which gives

$$h = \frac{\Delta P_i}{\gamma_w} \qquad (2.21)$$

It should be noted that the base angle and the height of the structure will change. Also that part of the membrane which is filled with water, will be exposed to equal pressures on either side and will therefore follow a straight line (line AB in figure 2.25). The problem is therefore the same as the previous case but the length of the unstretched perimeter should be reduced by

2 x the length of AB and the base width should be re-calculated from:

$$B_2 = B_1 + 2h \cot \phi_o \qquad (2.22)$$

The new profile of the membrane can then be calculated using the new values of base width and perimeter length.

The computer program for both reinforced and non-reinforced membrane structures are extended to accommodate the phenomena of partially drawing-off of gas. In each case, new profiles are calculated for the structures at different internal water levels. The results are shown in the next two sections.

2.5.1. Drawing-off of Gas in Non-Reinforced Membrane Structures.

The phenomena of partially drawing-off of gas has been studied for the minimum tension profile obtained in section 2.3. Two different water levels of 3 m and 5 m have been considered. The results are shown together in figure 2.26. It is observed that the height of the membrane increases and the profile narrows by increasing the water level inside the structure; at the same time the tension in the membrane decreases. It is therefore concluded that the maximum tension in the membrane occurs when the structure is entirely filled with gas.

In order to confirm the theoretical results, the model investigations carried out for the membrane profile in section 2.2.4. have been further extended and the case of drawing-off different amounts of gas has been considered by filling the model with different amounts of water. The amount of water in the model is determined by the fact that the level of water in the prototype should be equal to the depth of the empty part of the model. The measured profiles are plotted in figures 2.5, 2.6 and 2.7 and are compared with the theoretical results for the model profiles at the experimental water levels. Close agreement is obtained as can be observed in figures 2.5, 2.6 and 2.7.

From the experimental procedure for modelling the case of drawing-off of gas, it is evident that the tension in the membrane is maximum when

the prototype is filled with gas in which case the model is fully filled with water as compared to the drawing-off phenomena represented by only partially filling the model with water.

2.5.2. Drawing-off of Gas in Reinforced Membrane Structures.

The computer program for the analysis of the reinforced membrane structure submerged in water, has been extended in the following manner in order to include the case of drawing off of gas: After the analysis of the fully gas-filled structure is complete, it is assumed that some of the internal gas of the structure is drawn off gradually and the reduced internal gas pressure is compensated by introducing a quantity of water so that the equilibrium of the membrane structure is restored at all times. For simplicity of calculations, the structure is only analysed at instances when the water level inside the membrane coincides with the level of one of the longitudinal reinforcing cables. In this way, it will not be necessary to calculate the co-ordinates of a new set of points along the membrane at the level of the water inside the structure. The structure is thus analysed for different water levels according to the different levels of its longitudinal cables. At each stage, the water-pressure on the outside and the inside of that portion of the membrane which is filled with water is equal. The final results for the displacements of the nodes in the case of fully gas-filled structures are taken as the initial values in the analysis of the first stage of drawing-off of gas, in which the water level coincides with the first row of longitudinal cables. The final values of the displacements obtained at the end of the analysis of the first stage, are in turn used as the initial displacement values for the second stage and so on. It should be noted that the nodes at or below the internal water level are not assumed as fixed nodes except for the supporting nodes which are originally taken to be fixed. Therefore, the total number of unrestrained nodes of the structure does not change due to drawing-off of gas.

The three types of structures analysed in section 2.4.3. are further analysed here for the case of partially drawing-off of gas. Some of the results

are shown in figures 2.14 to 2.24. The results are similar to those of non-reinforced membrane structures of section 2.5.1.; it is observed that as the water level inside the structure increases, the cross-section of the structure narrows and its height increases while the tensions in the cables reduce. In cases when the water level rises above the first row of the longitudinal cables, some of the cable elements below the water level begin to become slack. This slackness is undesirable from the dynamics point of view.

The results obtained for a flat-ended structure with 1 m cable spacing and with internal water level of approximately 3 m is compared with the results of an identical non-reinforced membrane structure. The resulting cross-sections of the two structures are superimposed in figure 2.27. It can be seen that the cross-section of the reinforced structure does not narrow as much as the cross-section of the non-reinforced structure but its maximum height is higher than that of the non-reinforced one. The comparison of the tension in the structure shows that the maximum force in the circumferential reinforcing cable is 87.7 kN which slightly exceeds the tension in the membrane of the non-reinforced structure which is 86.80 kN. This excess force is mainly due to the larger cross-sectional area acquired in the case of the reinforced structure.

In the light of the results obtained for partially drawing-off the internal gas of the different structures, it is concluded that this phenomenon does not violate the safety of these structures from the statical analysis point of view.

2.6 Conclusion:

In the light of the numerous advantages of inflatable structures, their applications in the construction of enclosures have considerably accelerated in recent years. One potential area of application of inflatable structures is as gas storage container in the fluid environment. The greatest advantage of this method of storing

gas is that the external water pressure counterbalances the internal gas pressure, so the loading on the structure is considerably lowered. This method of storing gas is therefore most suitable for the storage of large quantities of gas in deep waters. The primary environmental loads on such structures are hydrostatic in nature.

In order to explore the feasibility of using flexible structures for the storage of gas underwater, a long cylindrical membrane structure has been analysed. The structural analysis of this structure involves the solution of the differential equations of equilibrium. A theoretical solution has been obtained for the case of idealized weightless membrane. Numerical results have been generated with the aid of the computer and the effect of different design parameters on the membrane profile and tension have been investigated. An optimum configuration for the structure has been obtained based on the profile which produces minimum tension in the membrane.

The validity of the theoretical analysis has been investigated through model experiments. Membrane models are constructed and then exposed to the same resultant pressure distribution as the prototype by hanging them in an upside down position and filling them with water. The shapes that the membrane models take up in that position are found to be in close agreement with the results of the theoretical analysis.

Since the tensile forces in the membrane increase as the radii of curvature and the length of the span increase, it becomes more difficult to find a suitable membrane which can sustain such high tensile forces. However, this can be overcome by incorporation of a two-way set of reinforcing cables in the membrane. In order to simplify the complex interaction of cables and membrane in the analysis of such structures, the action of the membrane is neglected except for transmitting the pressure load to the cables. The cable-reinforced membrane structure has thus been analysed by solving the exact equilibrium equations of the structure by Newton-Raphson technique. A general computer program has been developed for the analysis of truss structures and cable networks. Three different types of gas filled cable-reinforced membrane structures submerged in water have been analysed by the computer. The first two types are both cylindrical

and their cross-sections are the same as the optimum profile obtained in the membrane analysis. The first type has flat ends and the second type has curved cap ends. The third type of structure analysed is in the form of a dome whose shape is obtained by connecting the two cap ends of the second type structure. The effect of the spacing of the cables on the structure profile and on the tension in the cables has been studied in all the three types of structures. It has been observed that in each structure, the tension forces in the circumferential cables reduce by approximately the same ratio as the shortening of the cable spacing but the relative force reduction in the longitudinal cables is considerably more. In all the structures analysed, it has been found that the forces in the circumferential cables are always higher than those in the longitudinal cables. The effect of changing the overall length of the structure is studied in the first two types of structure. It is found that the change in the cross-sectional profile of the structure is insignificant. The changes observed in the forces of the circumferential cables are also very small. However, there is some reduction in both the circumferential and the longitudinal cable forces as the length of the structure is increased. An important conclusion which is drawn from the comparison of the results of the first two types of structures is that the circumferential cable forces in the second type of structure is of the same order of magnitude as those in the first type in spite of the fact that its internal volume is considerably larger. This suggests that the second type of structure is more economical than the first type.

Finally, the effect of drawing-off the internal gas of the structure has been studied. This is necessary because if the proposed flexible structure is used for the storage of gas, during its operative life, it will be filled and emptied regularly. As a result of the drawing-off of gas, some water enters the structure in order to retain its equilibrium. This phenomenon has been accommodated in the computer program for both reinforced and non-reinforced membrane structures. The computer results have shown that as water enters into the structure, the profile of the cross-section of the structure narrows and its height increases but the tension forces decrease. It is therefore concluded that from the static analysis point of view when the structure is filled with gas, it experiences its maximum tensile forces and therefore the drawing-off of gas does not endanger its safety. However, from the dynamic point of view the safety of

the structure may be violated when its internal gas is drawn off. This is due to the slackness which may be induced in some cable elements. In the case of non-reinforced membrane structures, the theoretical results have been confirmed by experimental investigations.

The structural analysis of reinforced and non-reinforced gas-filled membrane structures submerged in water has been successfully completed in this section. It is concluded that in most cases, the values of the maximum tensile forces in the membrane and the cables are in the range that they can be manufactured and therefore this method of gas storage appears to be both feasible and economical.

Figures of Chapter Two

Figure 2.2 - Profiles for Minimum Tension.

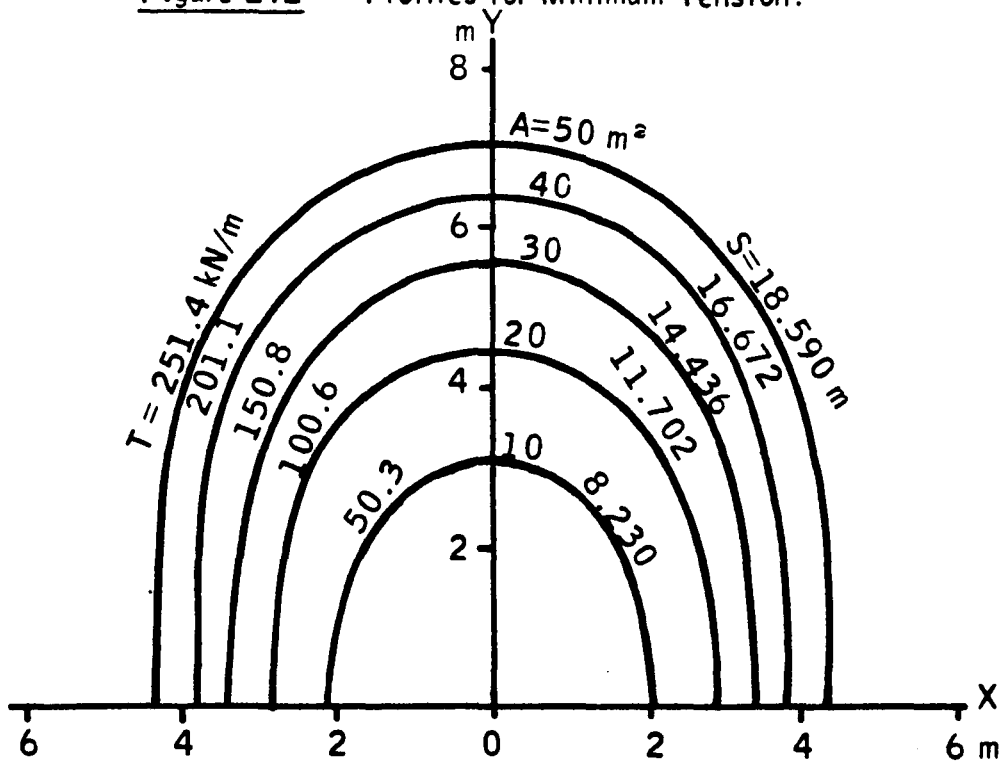

Figure 2.3 - Profiles for Minimum Perimeter.

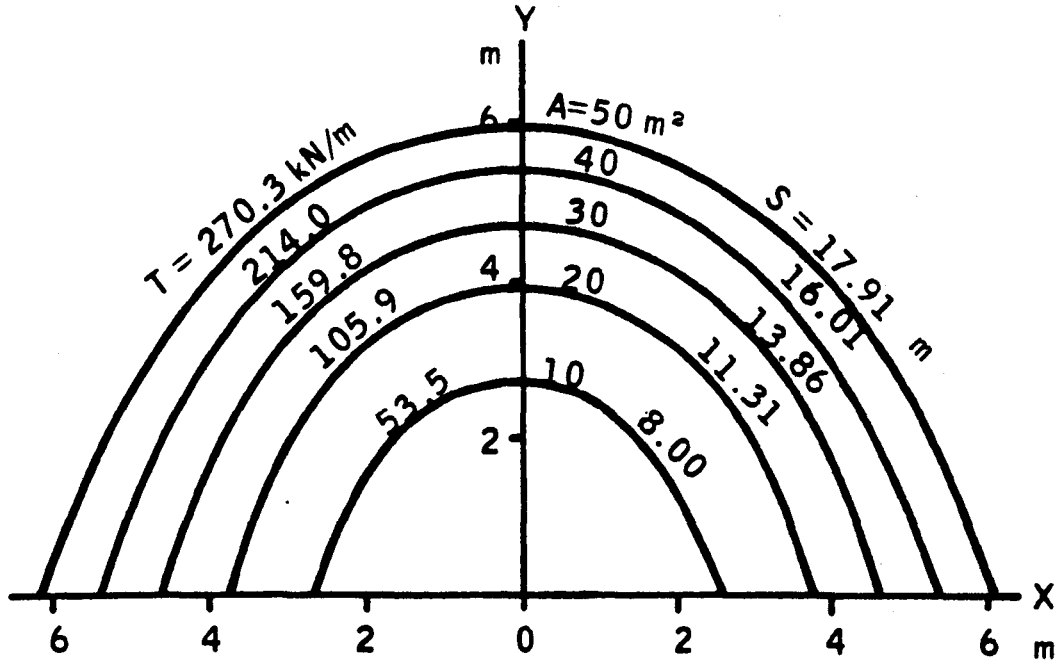

Figure 2.5 - Profiles for the Model at Different Water Levels (Base Width B = 495.5 mm).

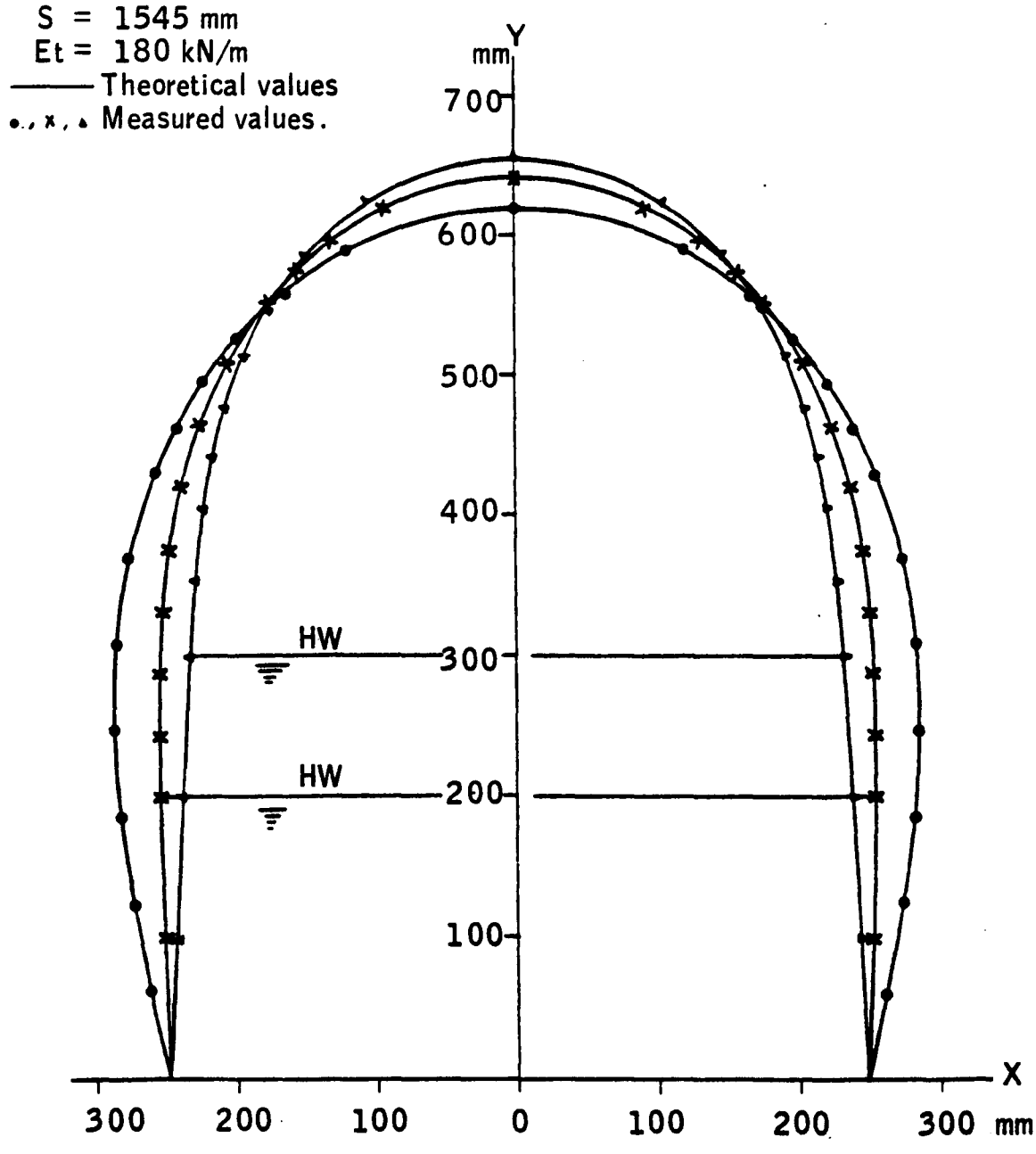

Figure 2.6 - Profiles for the Model at Different Water Levels.
(Base Width B = 703 mm).

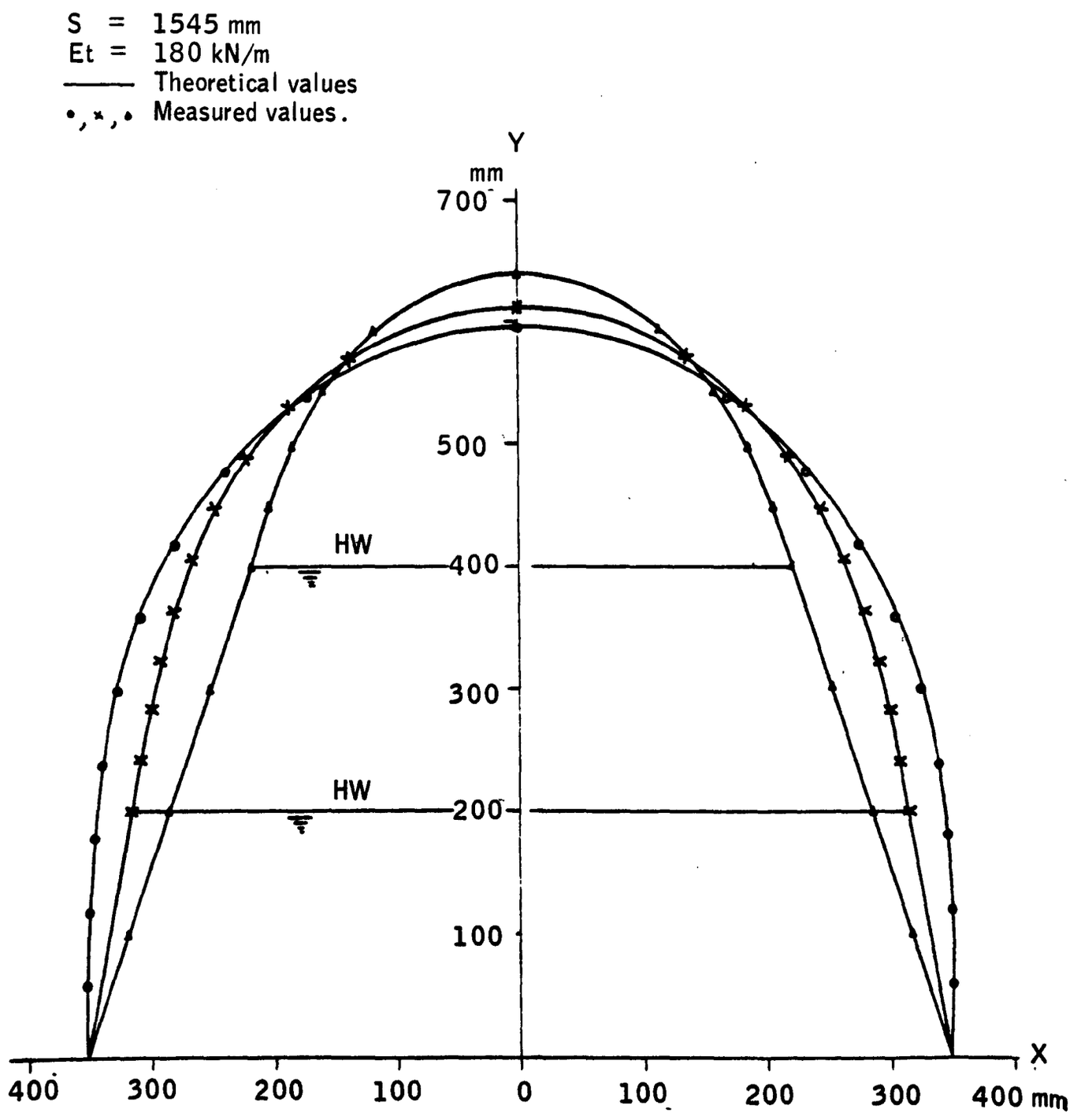

Figure 2.7 - Profiles for the Model at Different Water Levels.
(Base Width B = 623 mm).

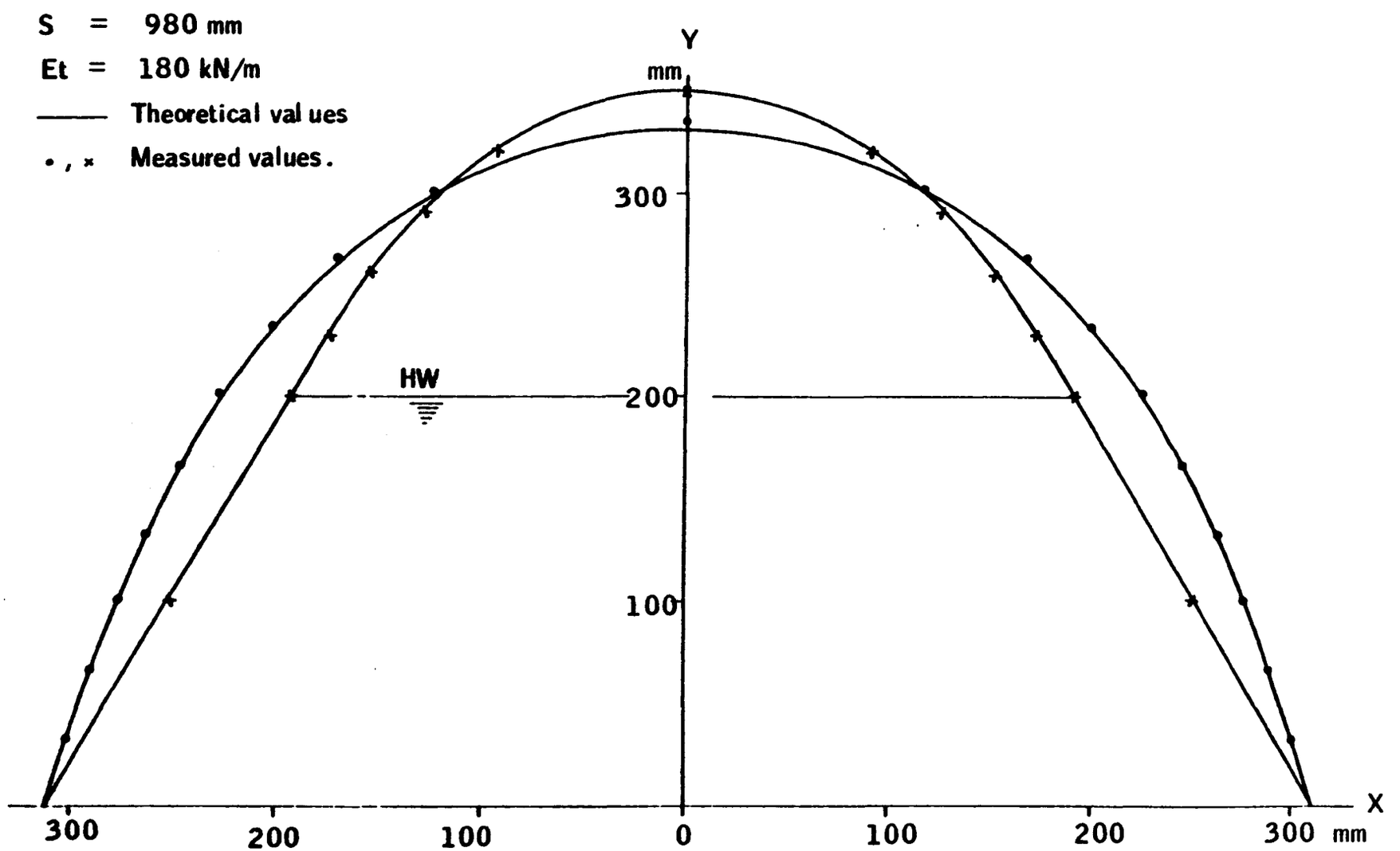

Figure 2.9 - Truss Structure of Epstein and Yene[20]

Horizontal component of prestress : 12.0 kg

Cable Young's Modulus : 2.1×10^6 kg/cm^2

Cross-sectional area of cables : 0.196 cm^2

Forces in cables : in kg

a = 82 cm

f = 56.5 cm

P= 16.6 kg

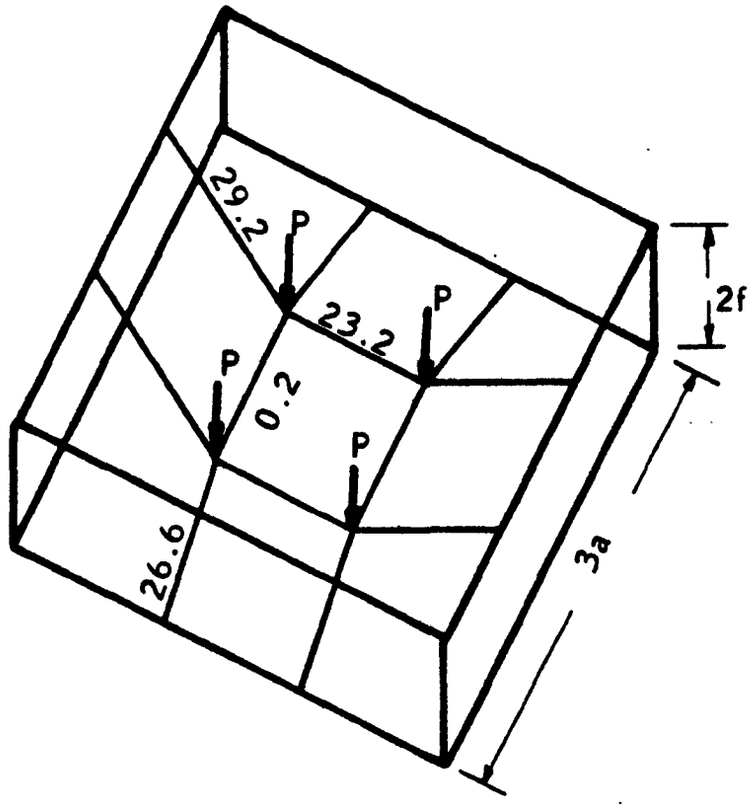

Figure 2.10 - Spherical cap of Malcolm and Glockner[43].

Height of the structure : 12.2 m.

Radius of the Base : 15.2 m.

Loading : uniform, P = 96.Pa

Cable Elasticity : 133×10^6 N

Forces in Cables : in kN.

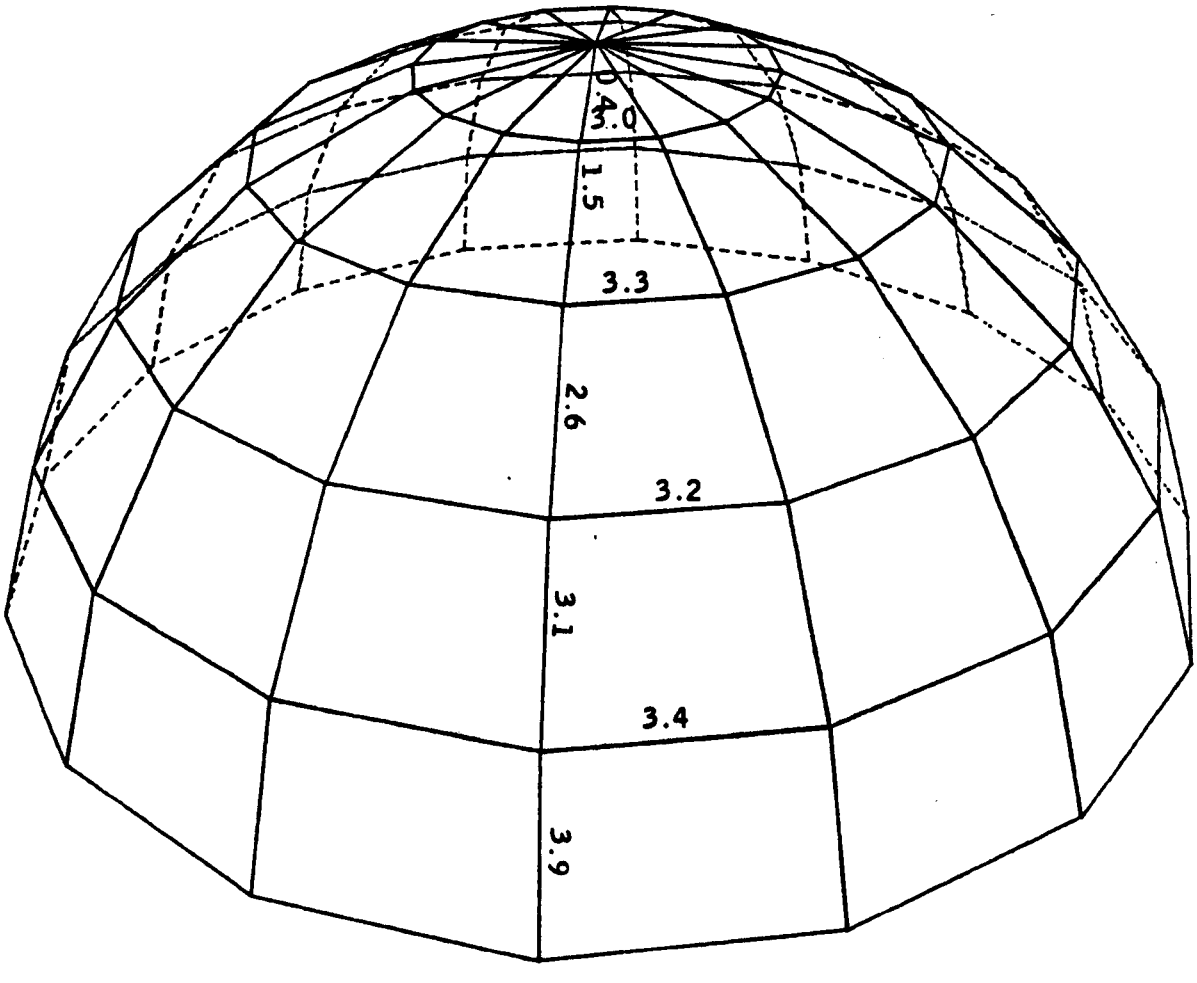

Figure 2.11 : An example of Type 1 Structure.

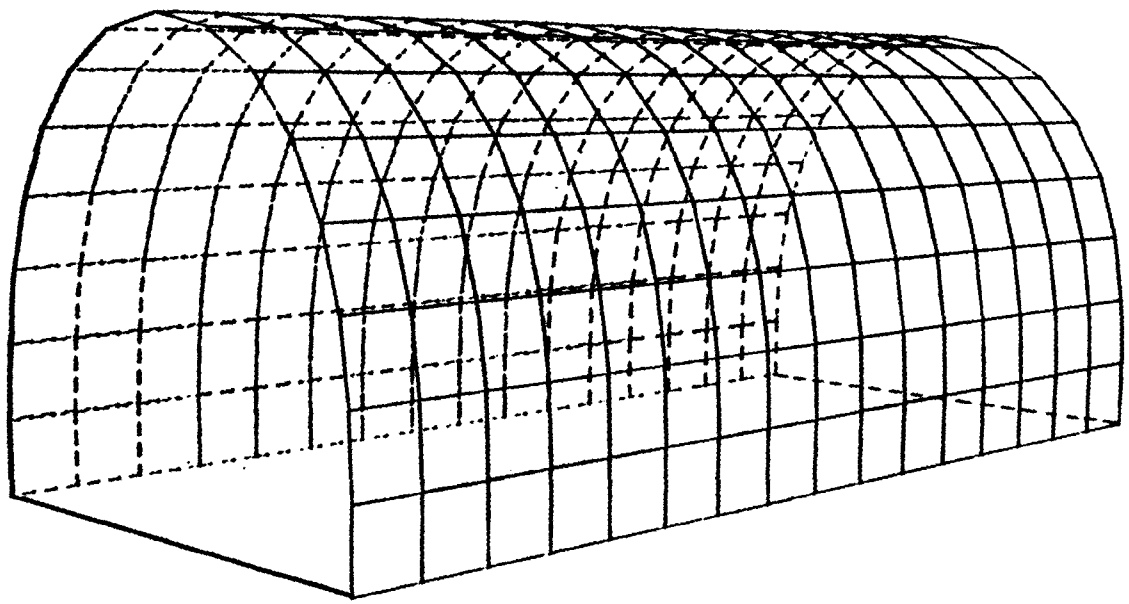

Figure 2.12 : An Example of Type 2 Structure.

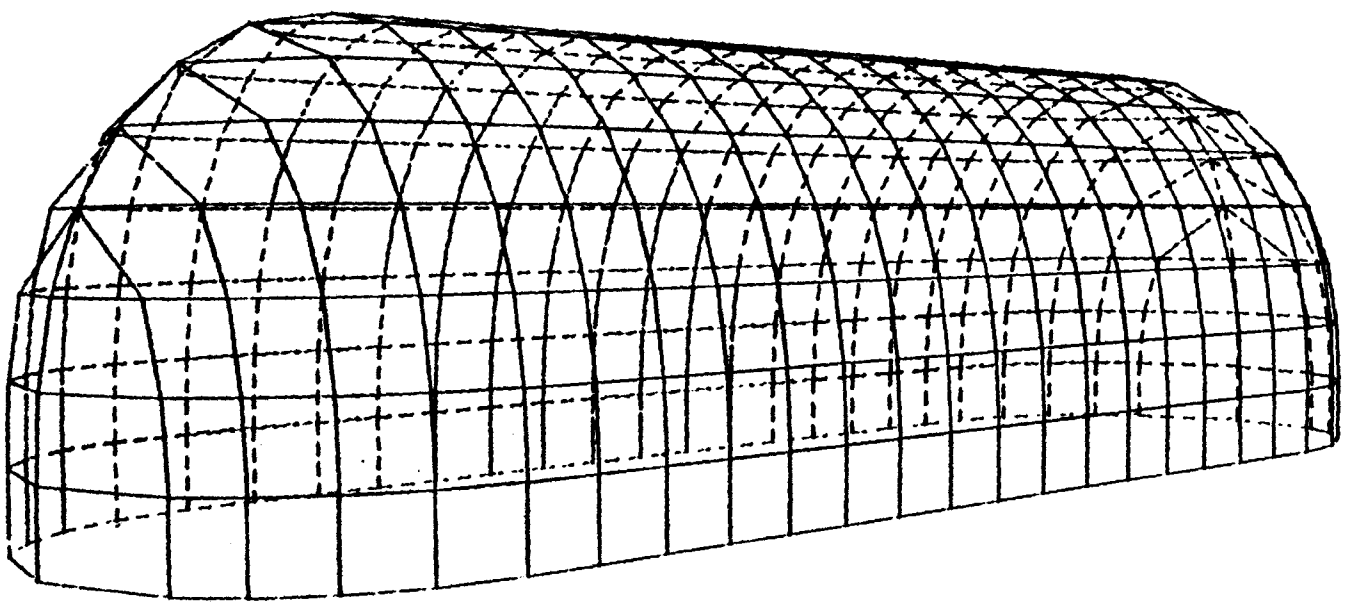

Figure 2.13 : An Example of Type 3 Structure.

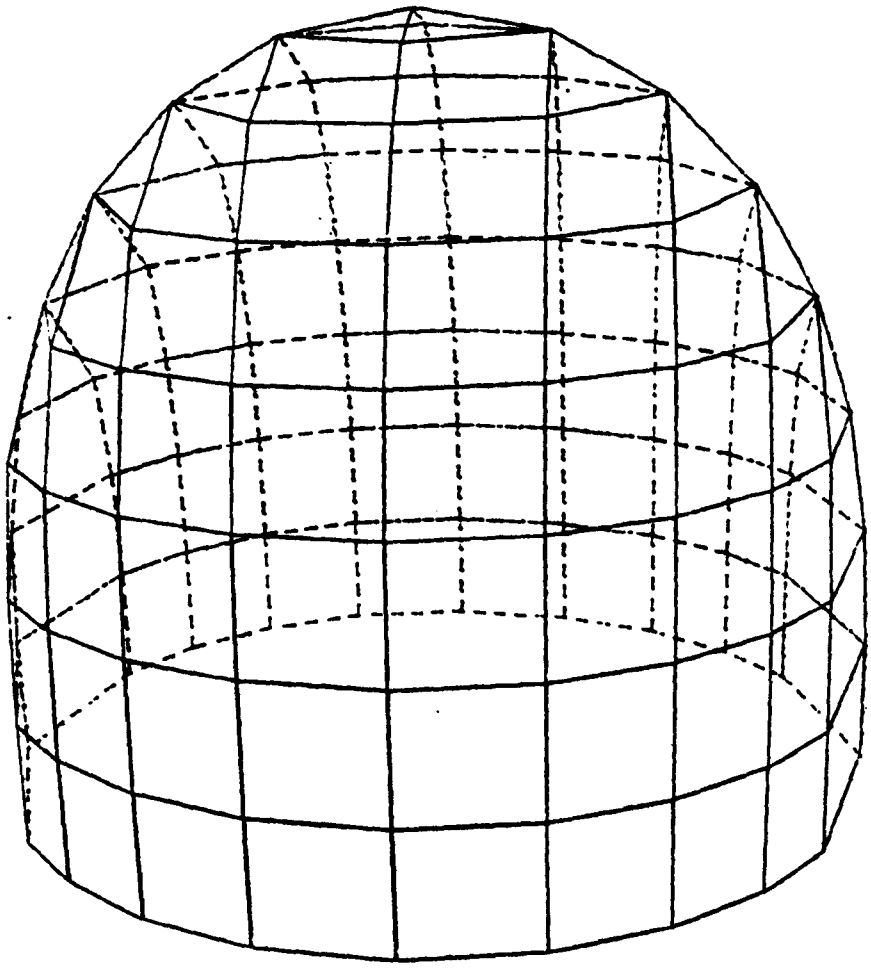

Fig. 2.14 a1 - Tension forces in the cables (in kN).

Structure : Type 1 (32 m long)
Cable Spacing : 2 m
Height of water in the structure = 0.0 m.

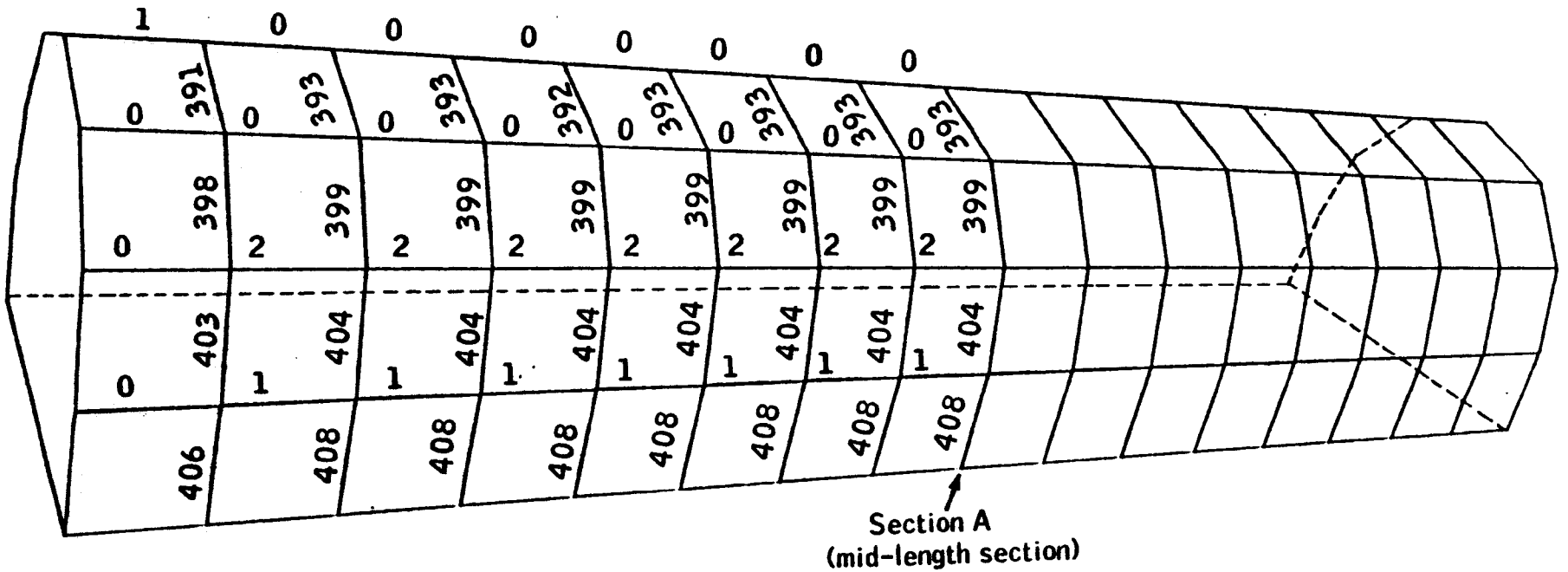

Figure 2.14 a2 - Tension forces in the cables (in kN).

Structure : Type 1 (32 m long)
Cable Spacing : 2 m
Height of water in the structure : 4 m.

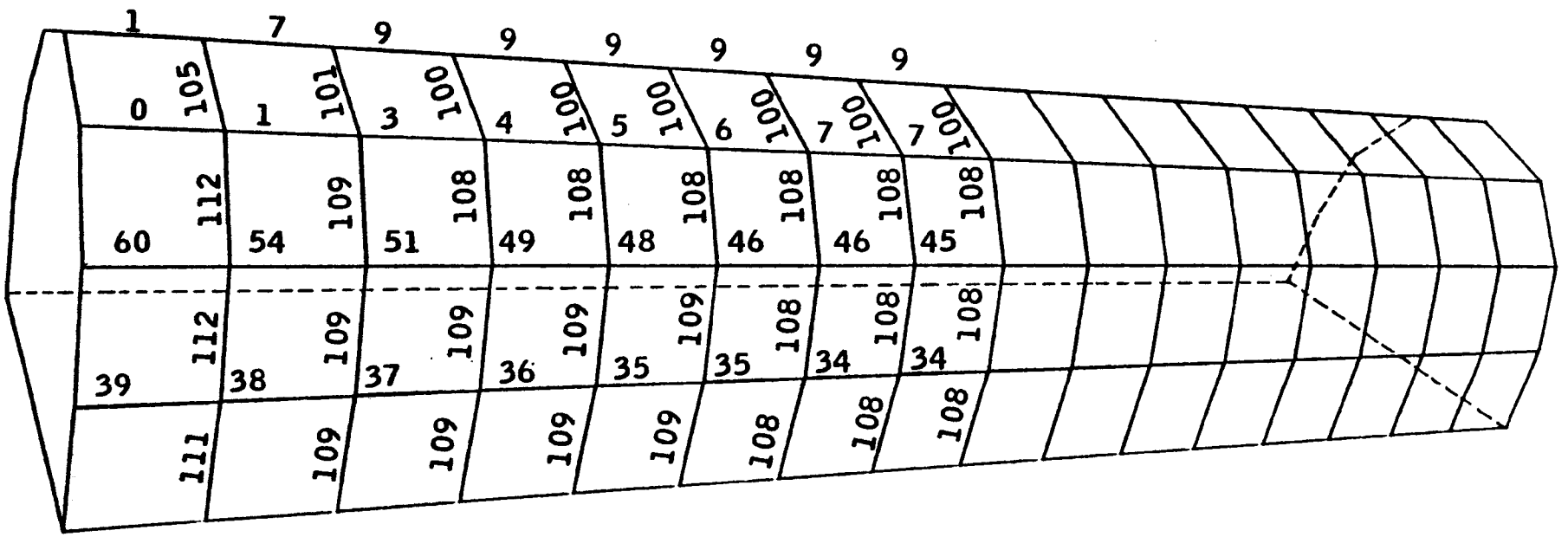

Figure 2.14 b - Cross Section A in the X-Y plane.

Structure : Type 1
Cable Spacing : 2.0 m

—×—×—×— : structure full of gas

—▲—▲—▲— : height of water in the structure = 2.0 m

—◇—◇—◇— : height of water in the structure = 4.0 m
(16 m and 32 m long structures)

—□—□—□— : height of water in the structure = 4.0 m
(8 m long structure).

Scale : 1 : 50.

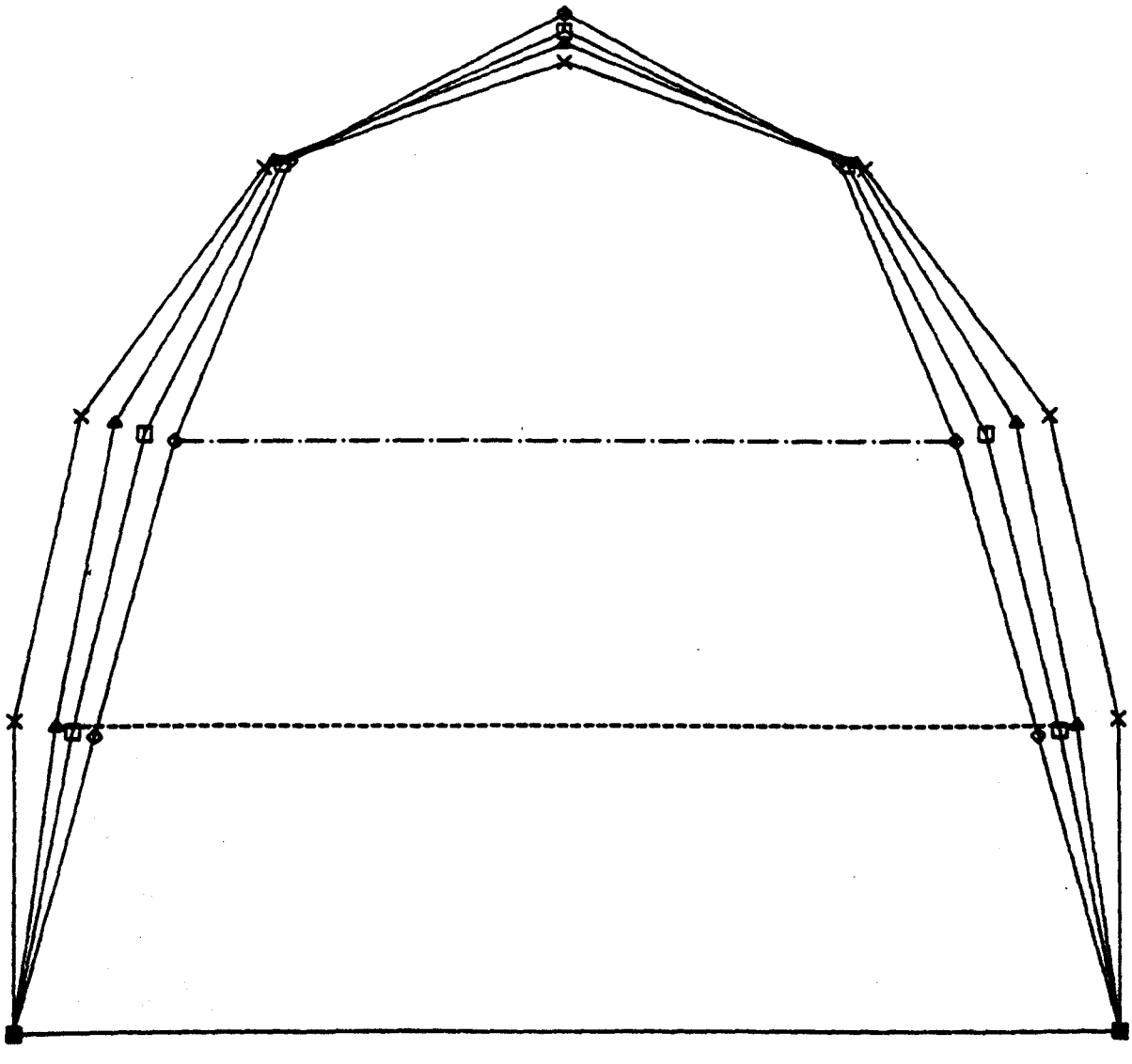

Figure 2.15 a1 : Tension forces in the cables (in kN)

Structure : Type 1 (16 m long)
Cable Spacing : 2 m
Height of water in the structure : 0.0 m.

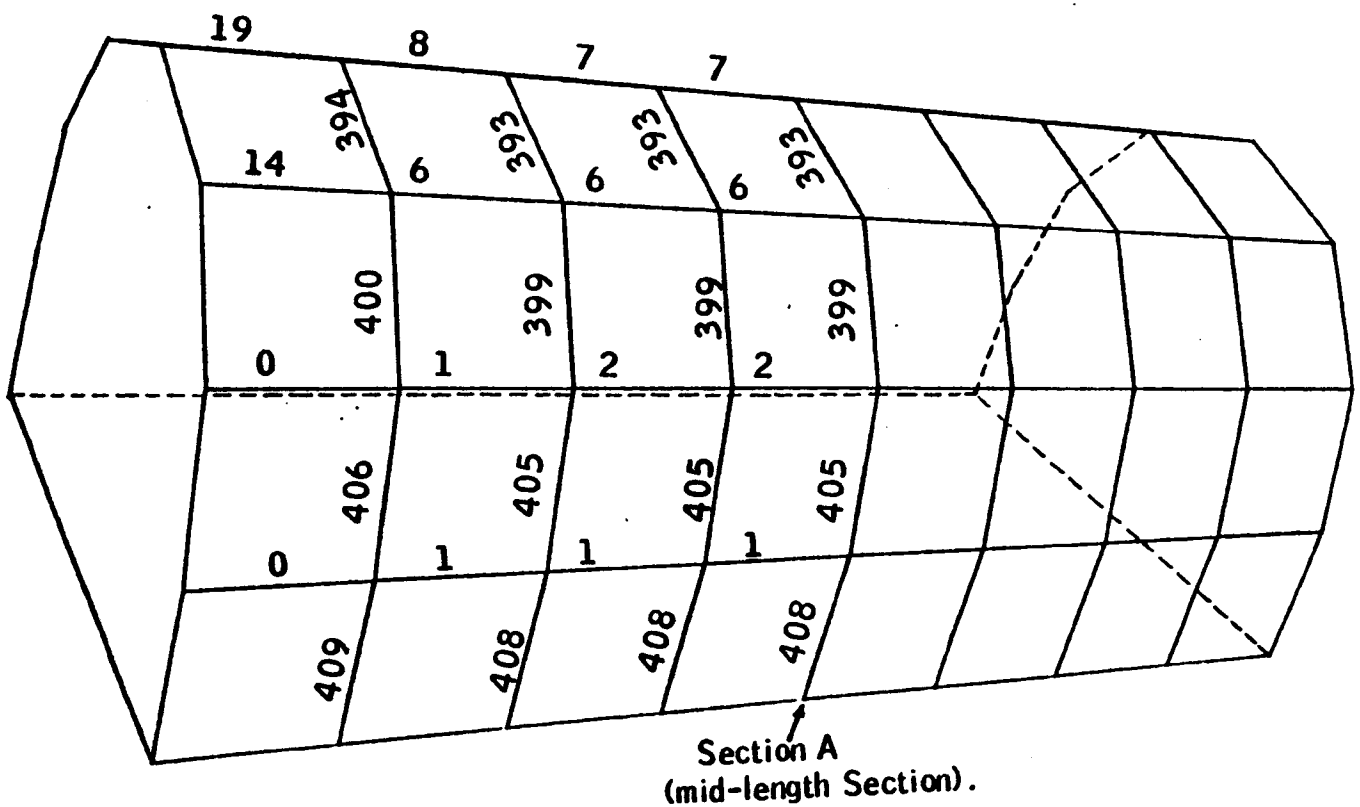

Figure 2.15 a2 - Tension forces in the cables (in kN)

Structure : Type 1 (16 m long)
Cable spacing : 2 m
Height of water in the structure : 4.0 m.

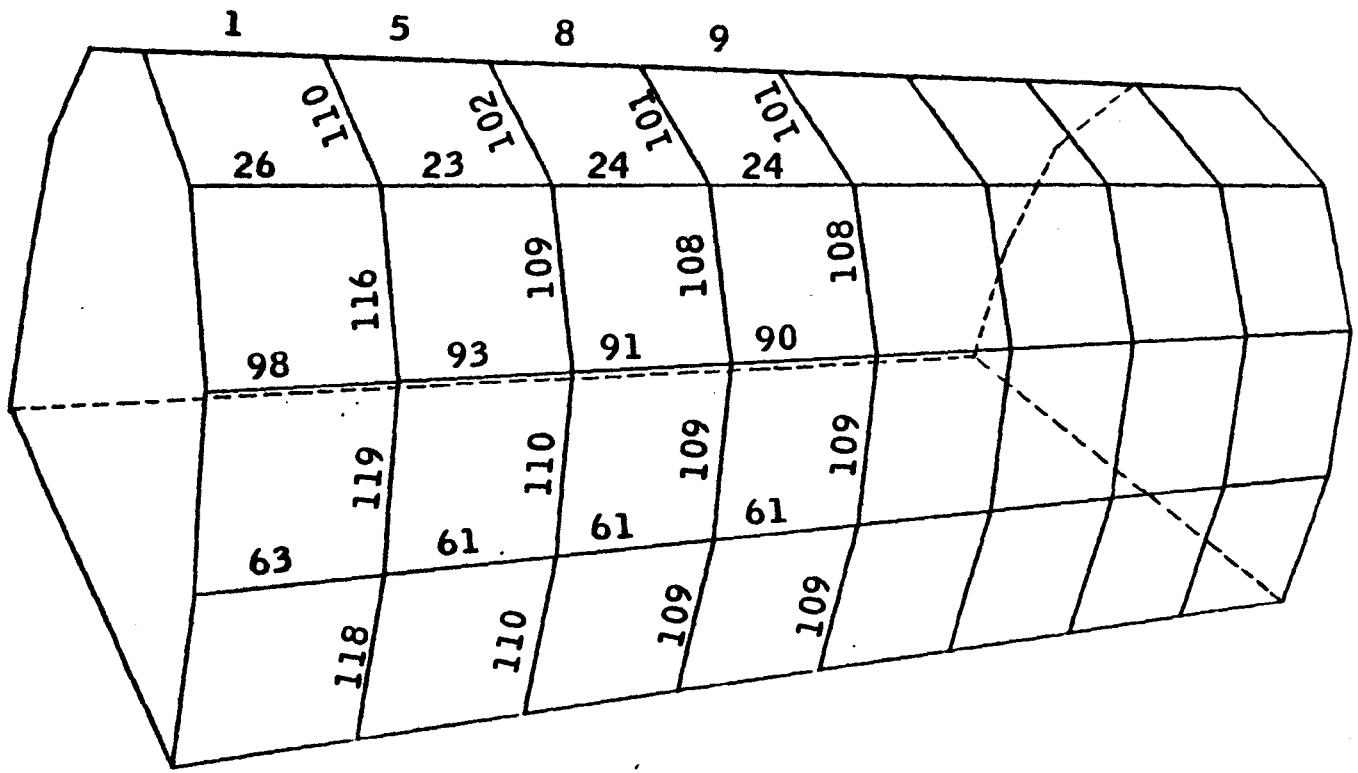

Figure 2.16a1 - Tension forces in the cables (in kN)

Structure : Type 1 (8 m long)

Cable spacing : 2 m.

Height of water in the structure : 0.0 m.

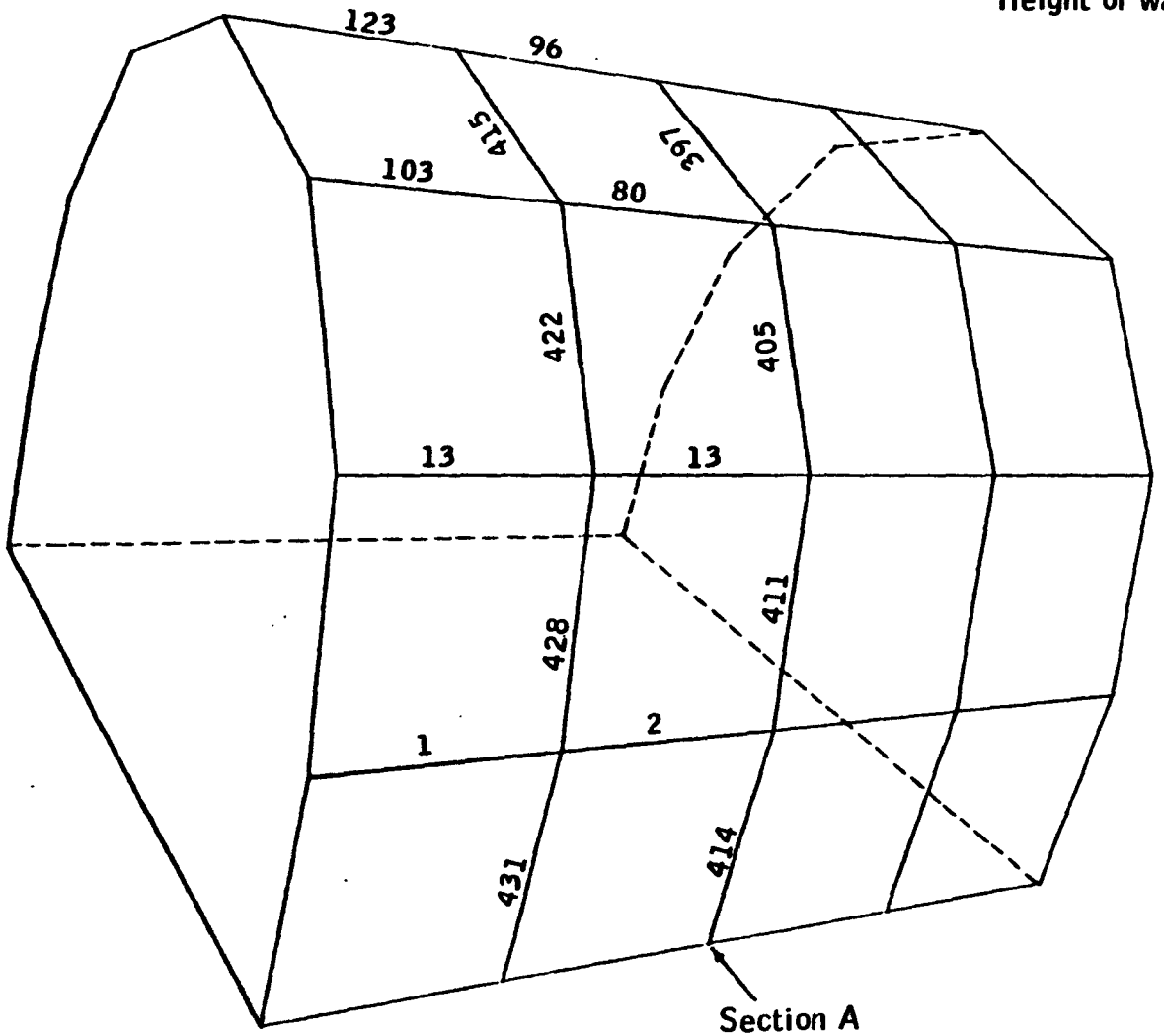

Figure 2.16a2 - Tension forces in the cables (in kN)

Structure : Type 1 (8 m long)

Cable spacing : 2 m.

Height of water in the structure : 2 m.

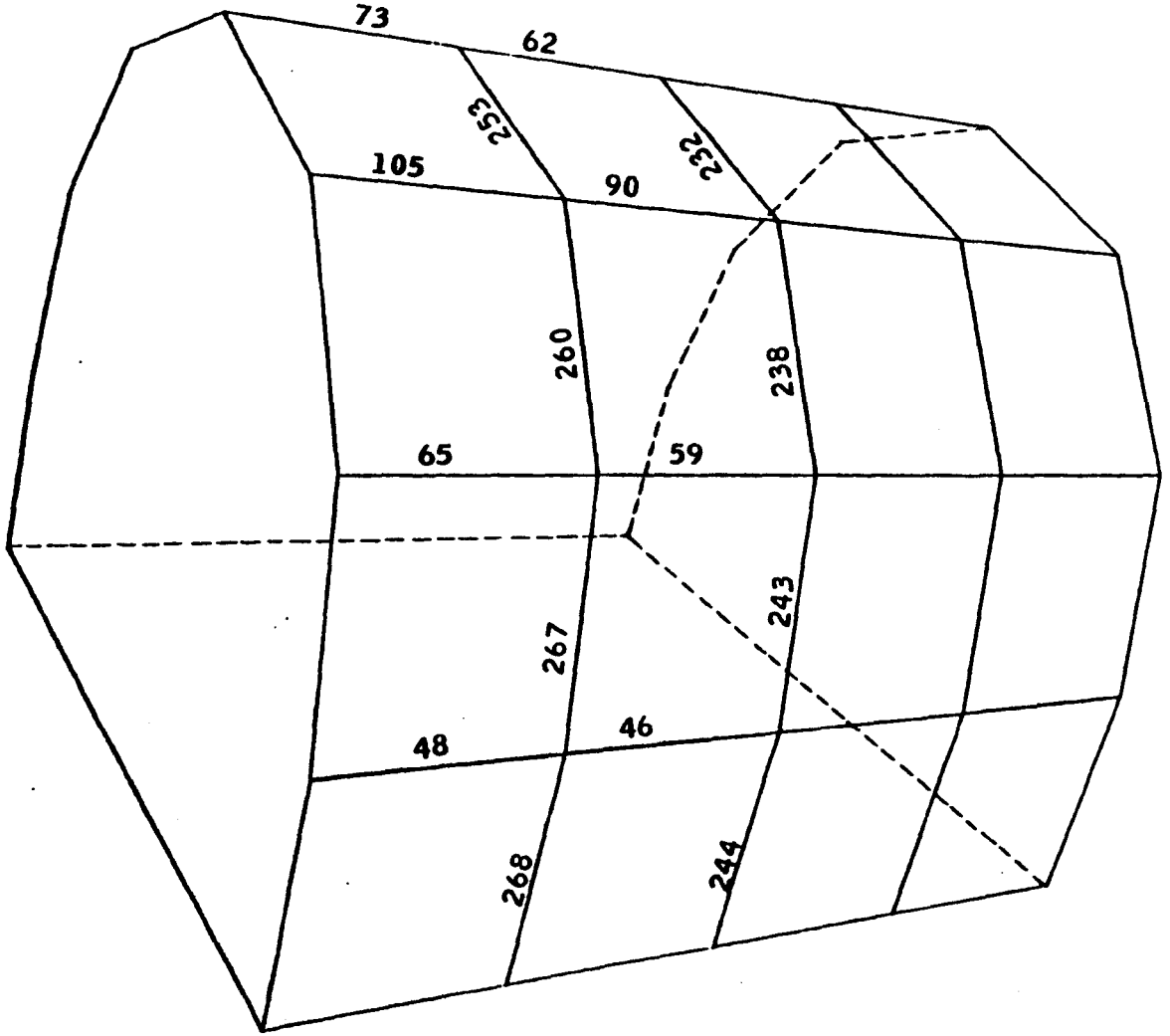

Figure 2.16a3 - Tension forces in the cables (in kN)

Structure : Type 1 (8 m long)

Cable Spacing : 2 m.

Height of water in the structure : 4 m.

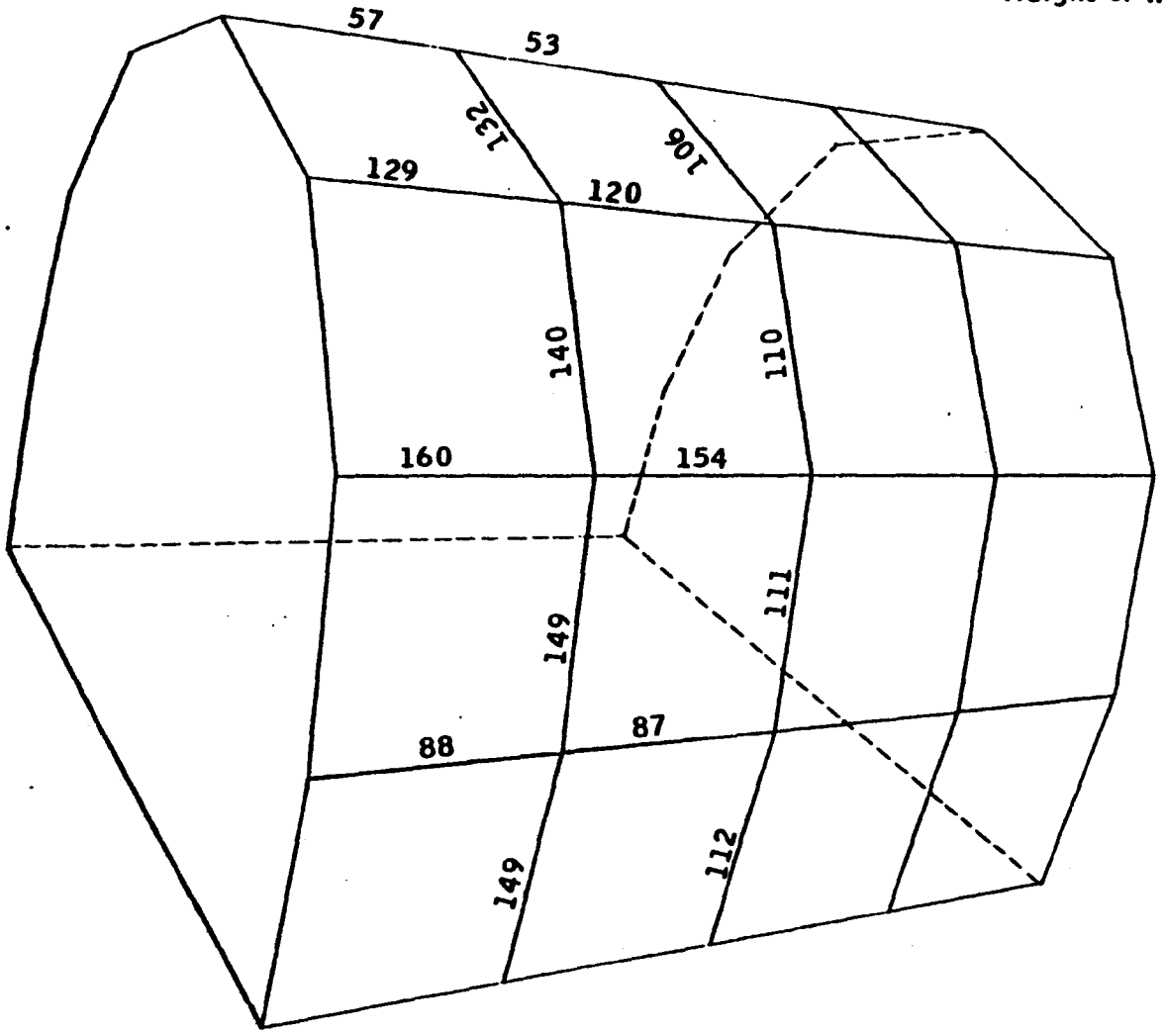

Figure 2.17a1 - Tension forces in the cables (in kN)

Structure: Type 1 (8 m long)

Cable spacing: 1 m.

Height of water in the structure: 0.0 m.

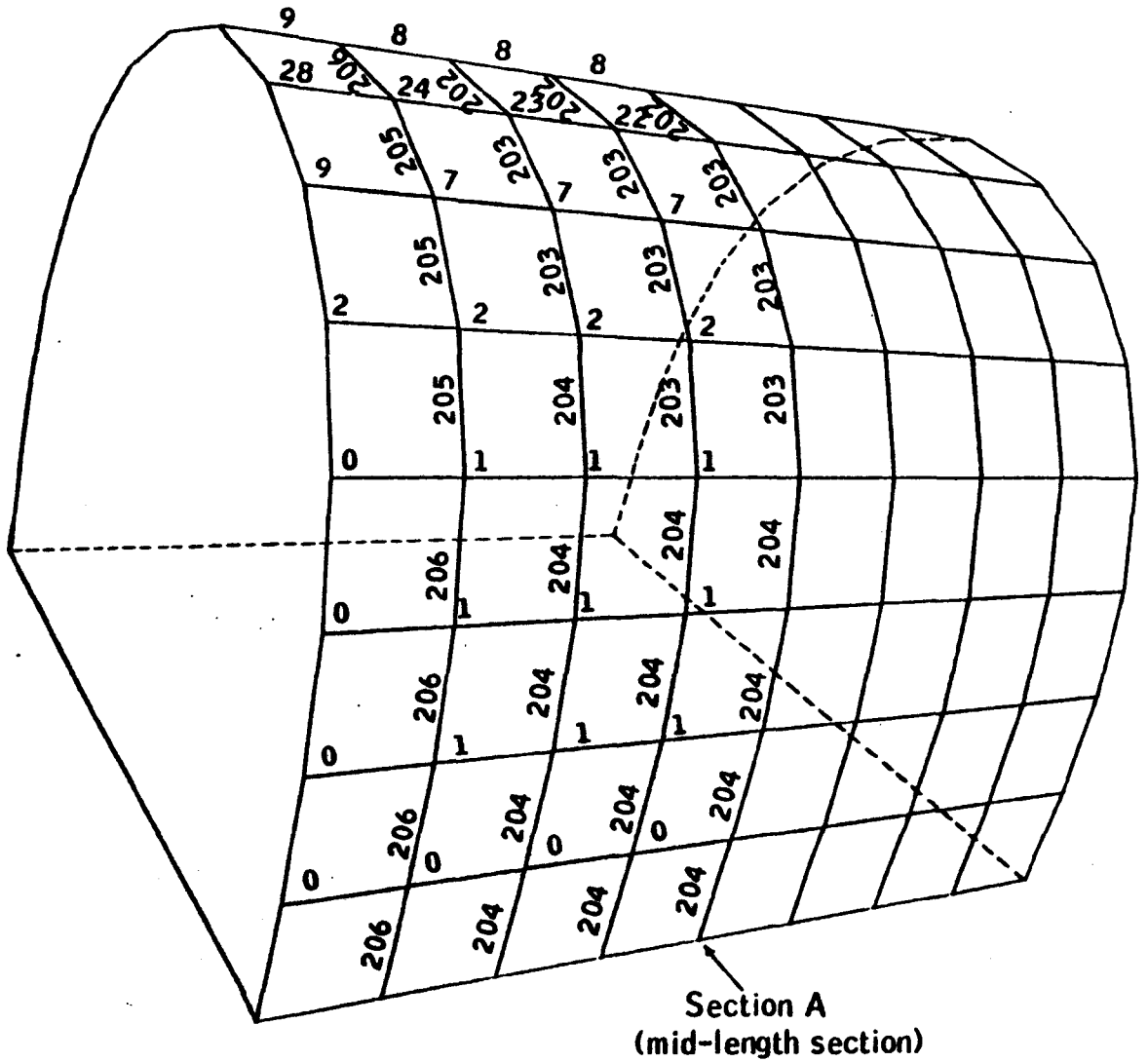

Figure 2.17 a2 - Tension forces in the cables (in kN)

Structure : Type 1 (8 m long)

Cable spacing : 1 m.

Height of water in the structure : 2.0 m.

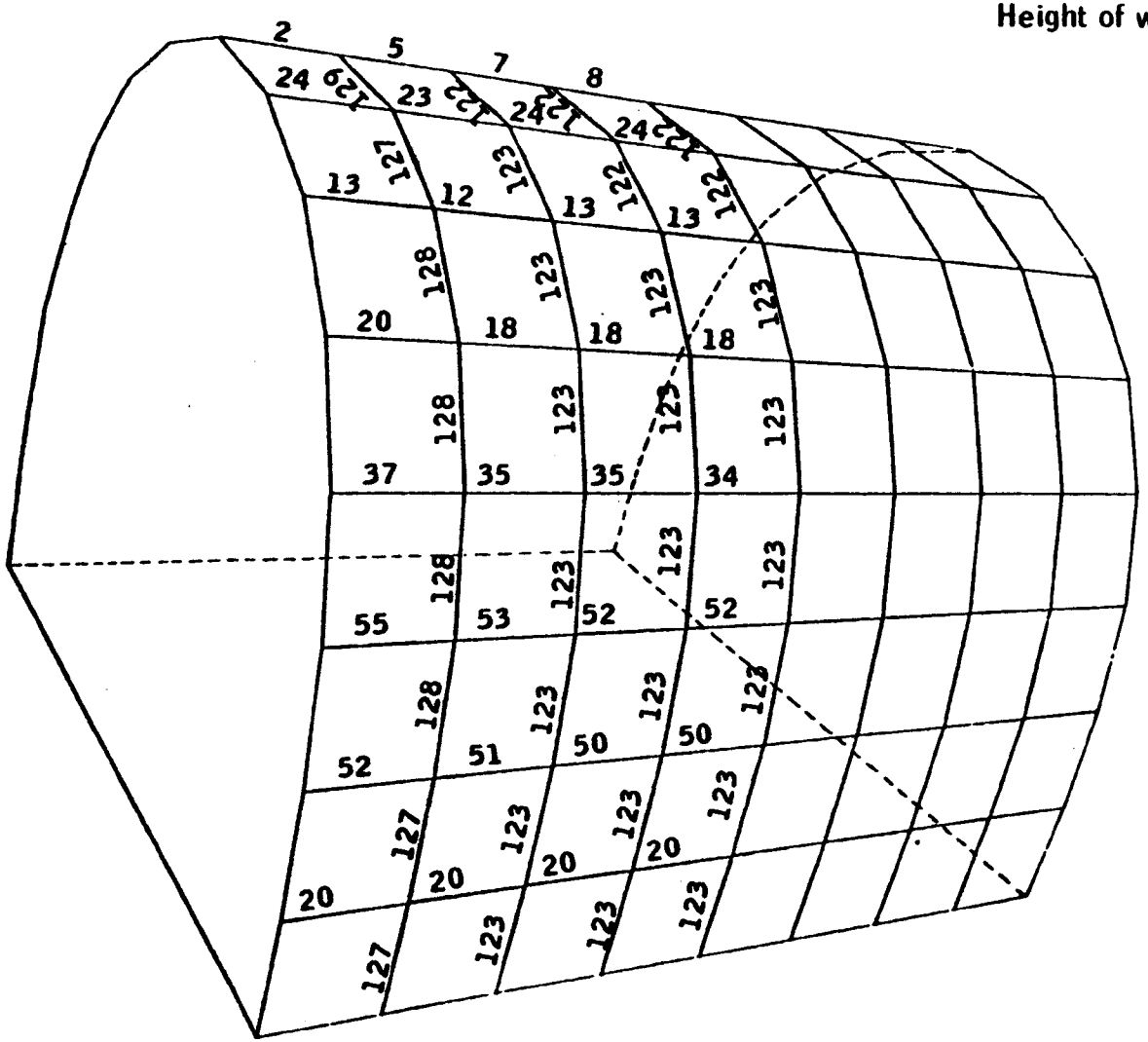

Figure 2.17 a3 - Tension forces in the cables (in kN)

Structure : Type 1 (8 m long)

Cable spacing : 1 m.

Height of water in the structure: 3.0 m.

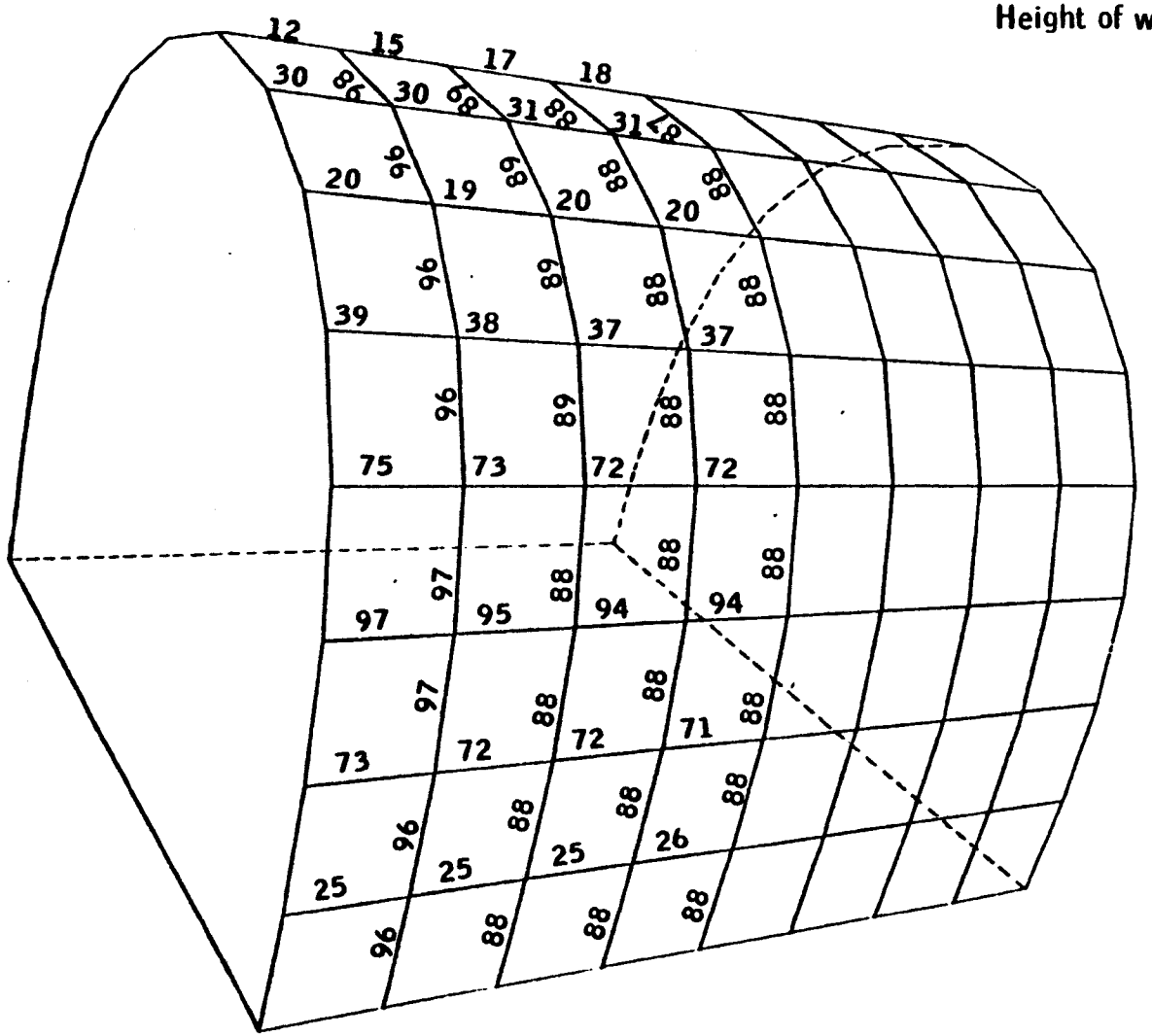

Figure 2.17 a4 - Tension forces in the cables (in kN)

Structure: Type 1 (8 m long)

Cable spacing : 1 m.

Height of water in the structure : 4.0 m.

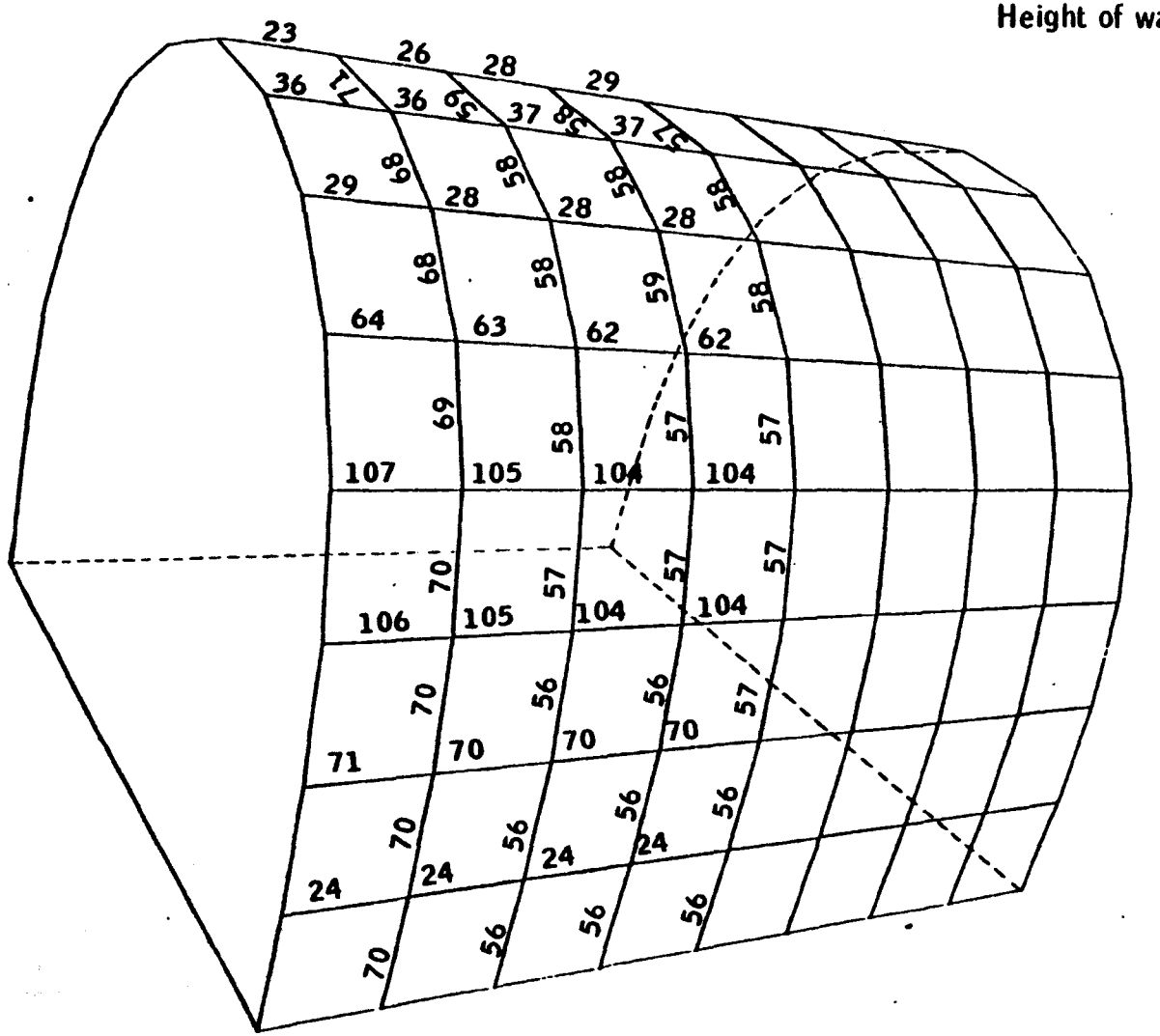

Fig. 2.17 b - Cross Section A in the X-Y plane.

Structure : Type 1.

Cable spacing : 1 m.

—×—×—×— Structure full of gas.

—▲—▲—▲— Height of water in the structure 2.0 m.

—◆—◆—◆— Height of water in the structure 4.0 m.

Scale 1:50.

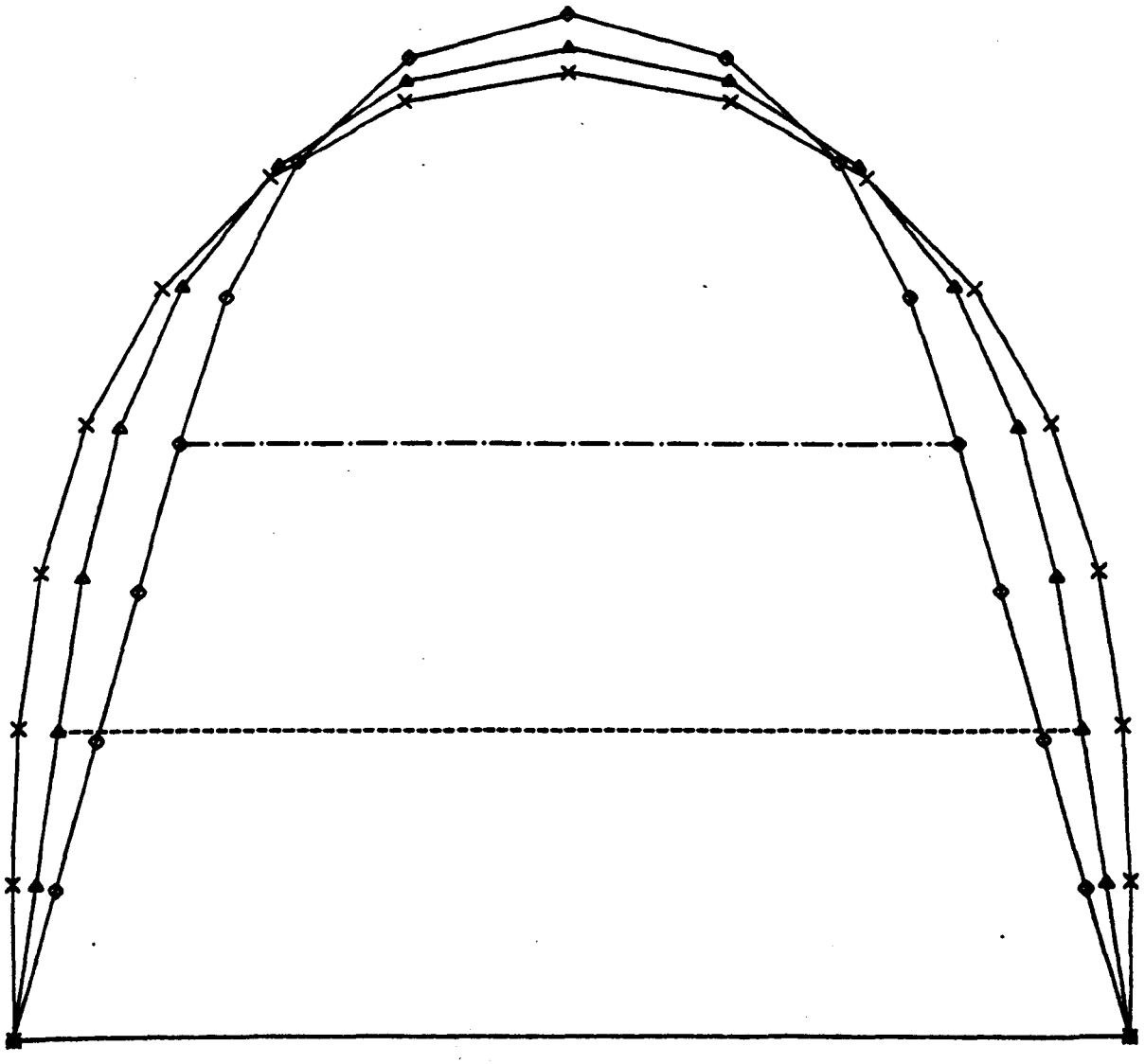

Figure 2.18 a1 - Tension forces in the cables (in kN).

Structure : Type 2 (39.5 m long)

Cable spacing : 2.0 m.

Height of water in the structure : 0.0 m.

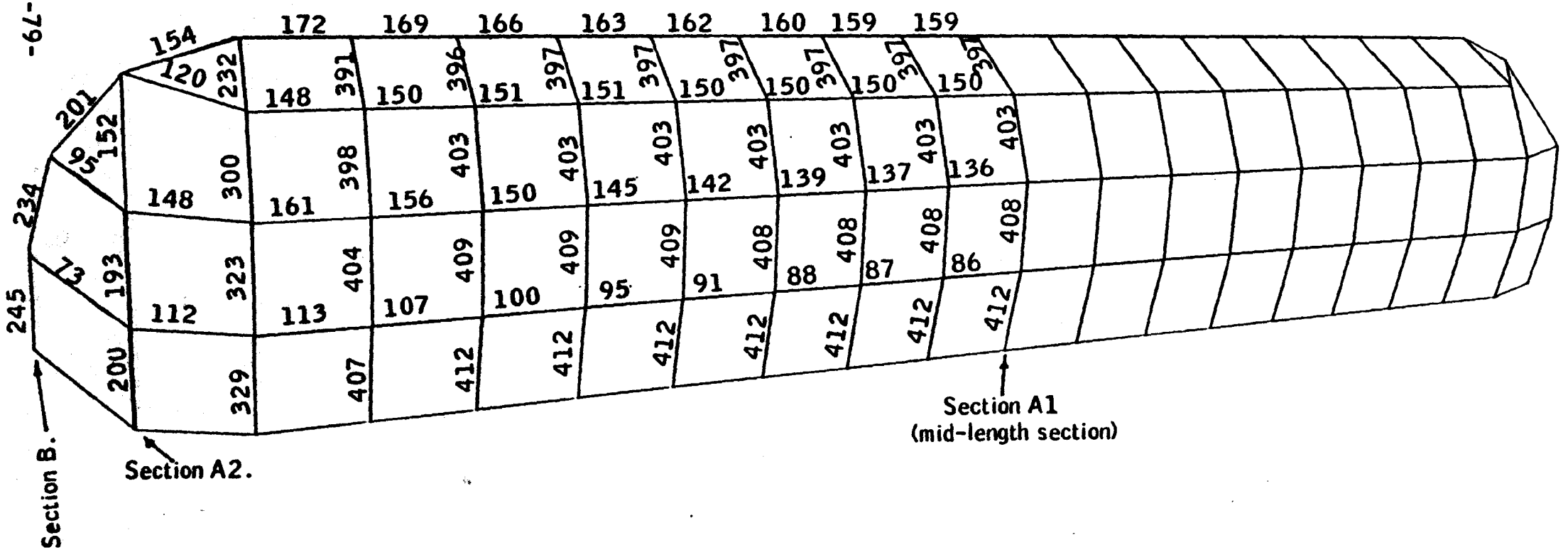

Fig. 2.18 a2 - Tension forces in the cables (in kN).

Structure : Type 2 (39.5 m long)

Cable spacing : 2.0 m.

Height of water in the structure : 2.0 m.

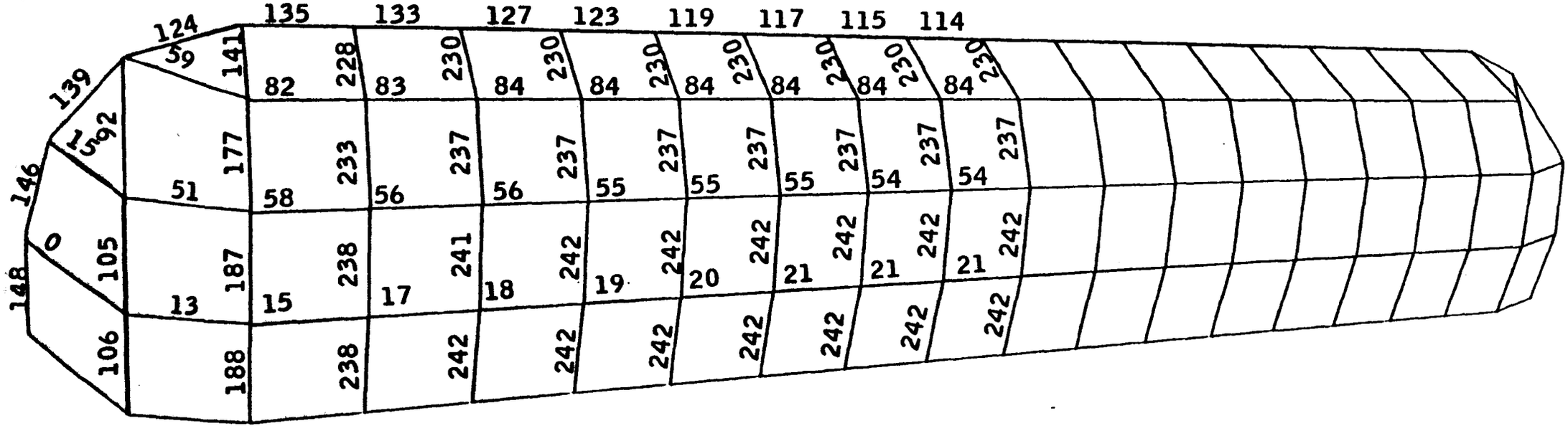

Fig. 2.18 a3 - Tension forces in the cables (in kN)

Structure : Type 2 (39.5 m long).

Cable spacing 2 m.

Height of water in the structure : 4.0 m.

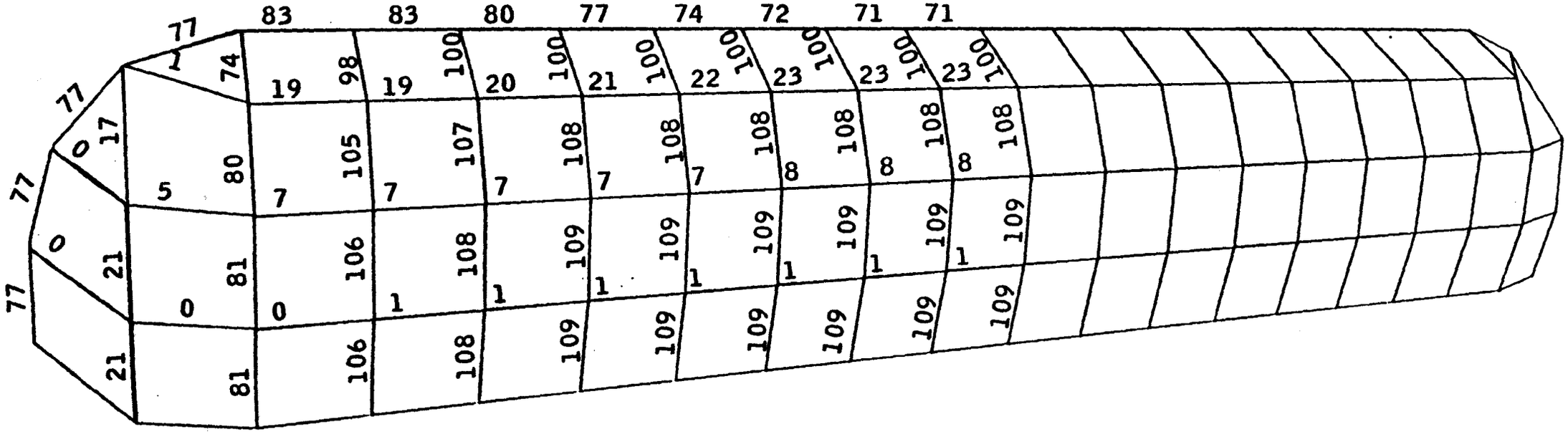

Figure 2.18 b - Cross sections A1 and A2 in the X-Y plane.

Structure : Type 2.

Cable spacing : 2.0 m.

—×—×—×— Structure full of gas.

—▲—▲—▲— Height of water in the structure : 2.0 m.

—◆—◆—◆— Height of water in the structure : 4.0 m.

Scale : 1:50.

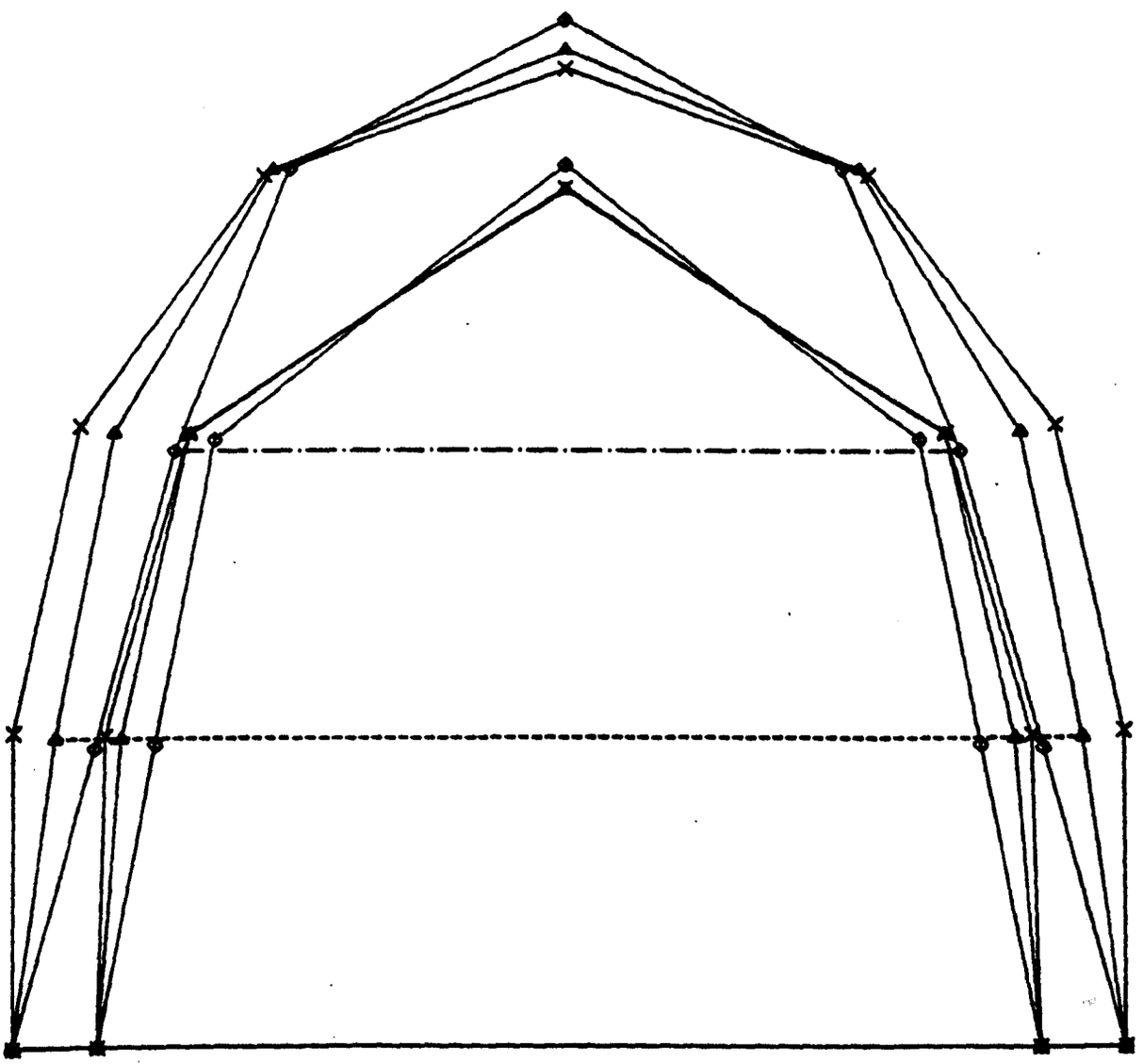

Figure 2.18 c - Cross-section B in the Y-Z plane.

Structure : Type 2

Cable spacing : 2.0 m.

—×—×—×— Structure full of gas.

—▲—▲—▲— Height of water in the structure : 2.0 m.

—◆—◆—◆— Height of water in the structure : 4.0 m.

Scale : 1:50.

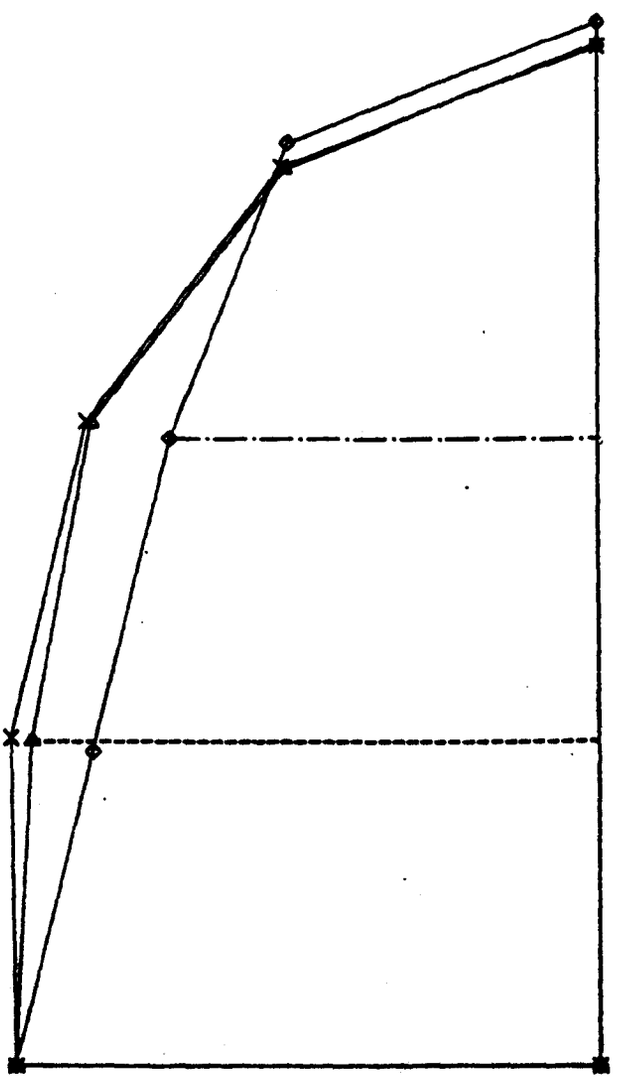

Figure 2.19 a1 - Tension Forces in the cables (in kN)

Structure : Type 2 (23.5 m long)

Cable spacing : 2.0 m.

Height of water in the structure : 0.0 m.

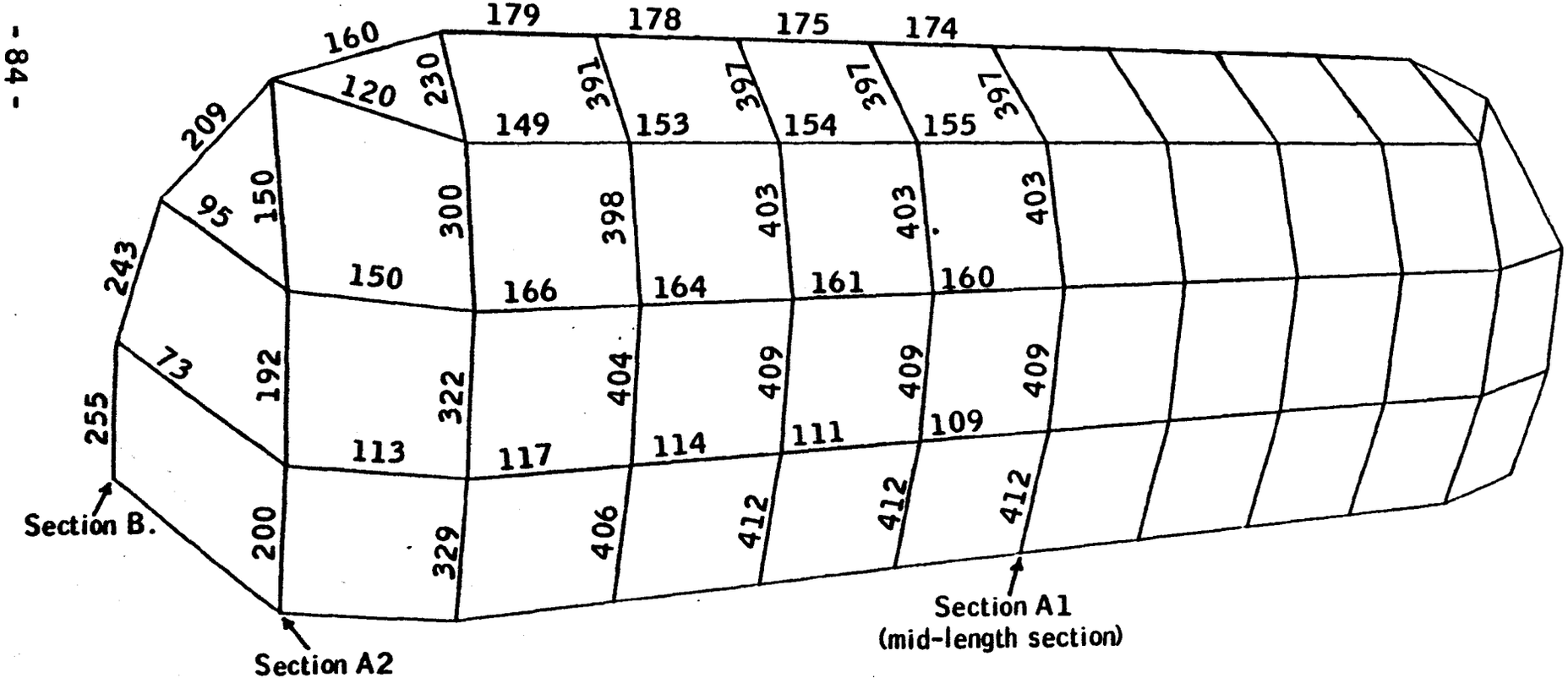

Figure 2.19 a2 - Tension forces in the cables (in kN).

Structure : Type 2 (23.5 m long)

Cable spacing 2.0 m.

Height of water in the structure 2.0 m.

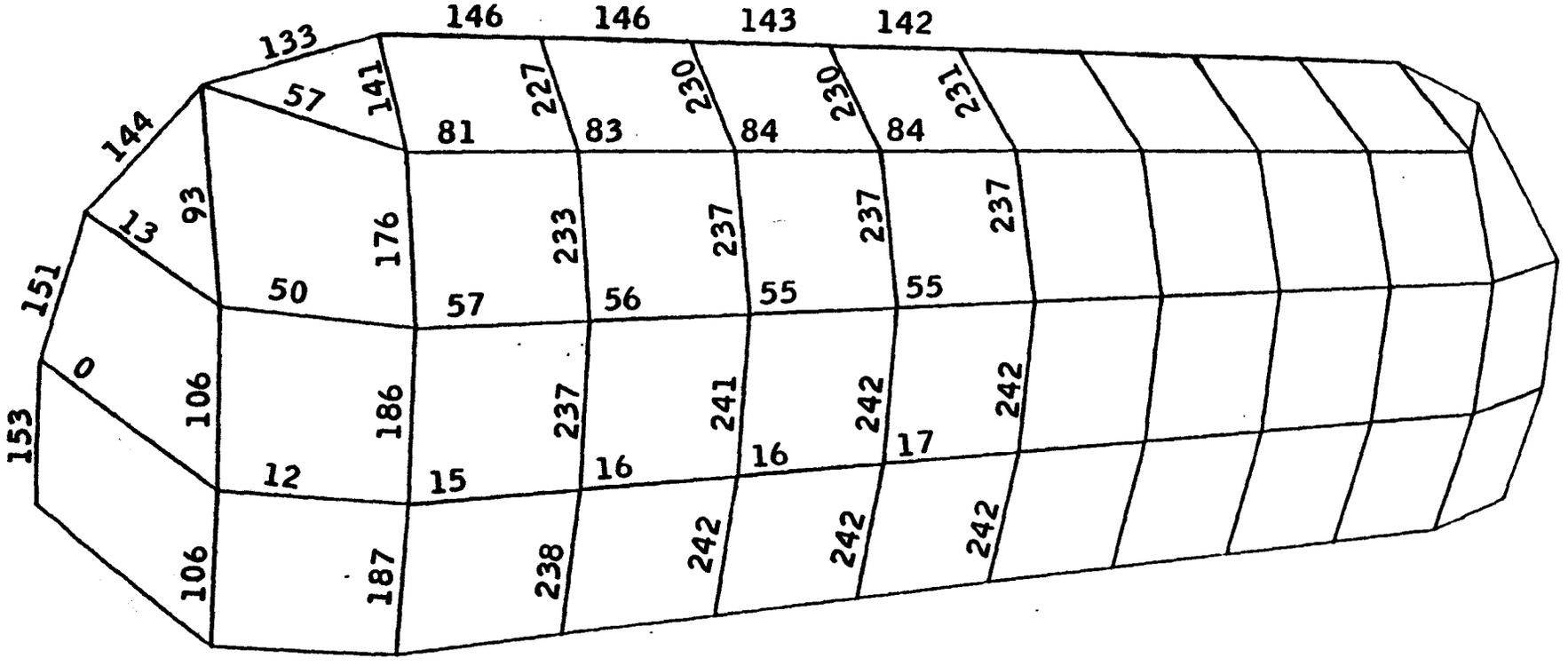

Figure 2.19 a3 - Tension forces in the cables (in kN).

Structure : Type 2 (23.5 m long)

Cable spacing: 2.0 m.

Height of water in the structure: 4.0 m.

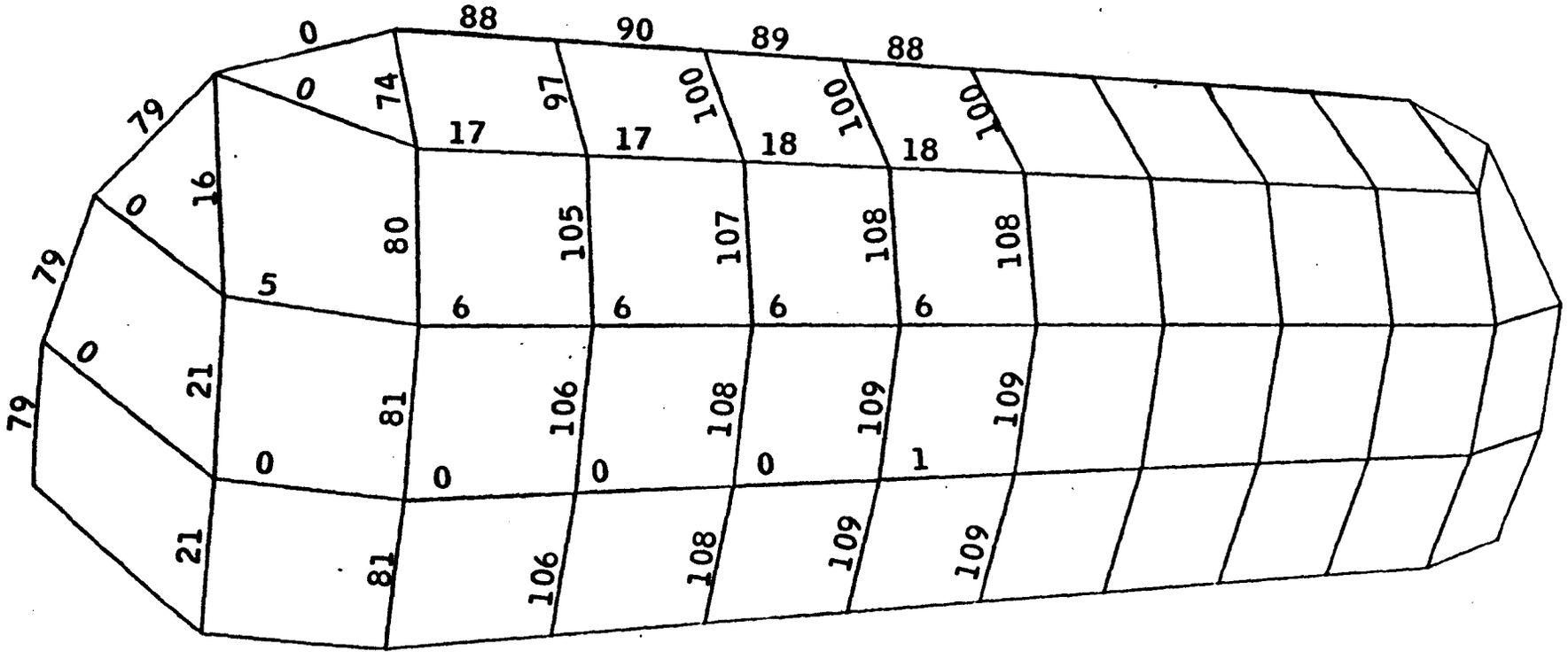

Figure 2.20 a1 - Tension forces in the cables (in kN)

Structure : Type 2 (15.5 m long)

Cable Spacing : 2.0 m.

Height of water in the structure : 0.0 m.

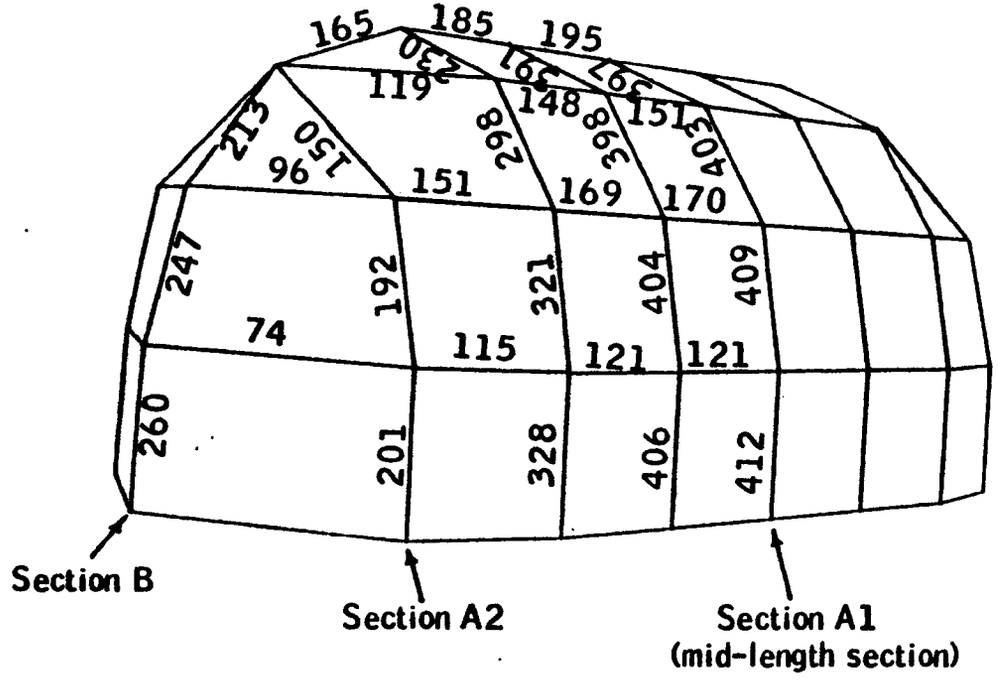

Figure 2.20 a2 - Tension forces in the cables (in kN)

Structure : Type 2 (15.5 m long)
Cable spacing : 2.0 m
Height of water in the structure : 2.0 m.

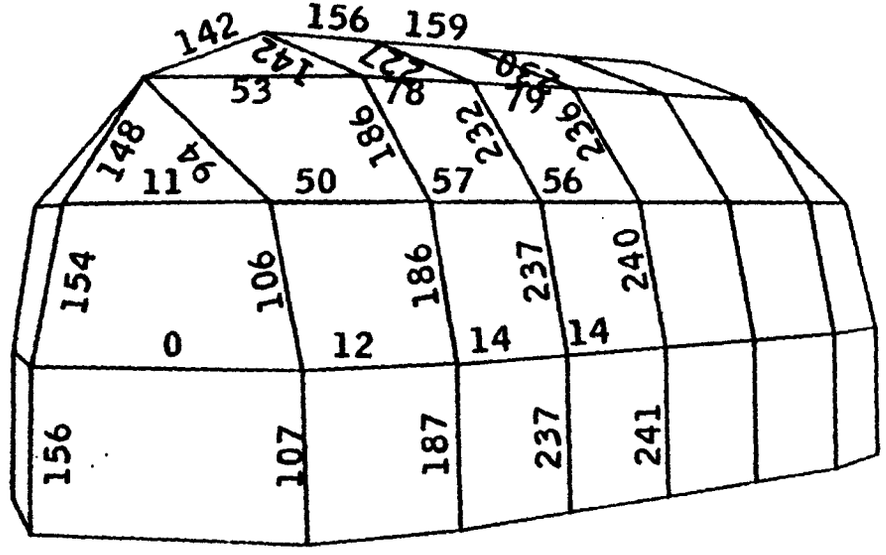

Figure 2.20 a3 - Tension forces in the cables (in kN).

Structure : Type 2 (15.5 m long)
Cable spacing : 2.0 m
Height of water in the structure : 4.0 m.

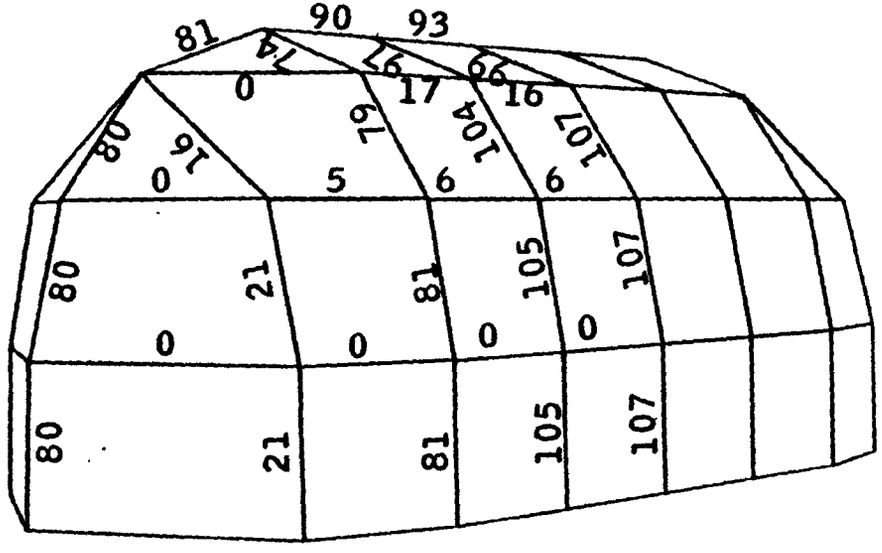

Figure 2.21 a1 - Tension forces in the cables(in kN)

Structure : Type 2 (15.5 m long)

Cable spacing : 1 m.

Height of water in the structure : 0.0 m.

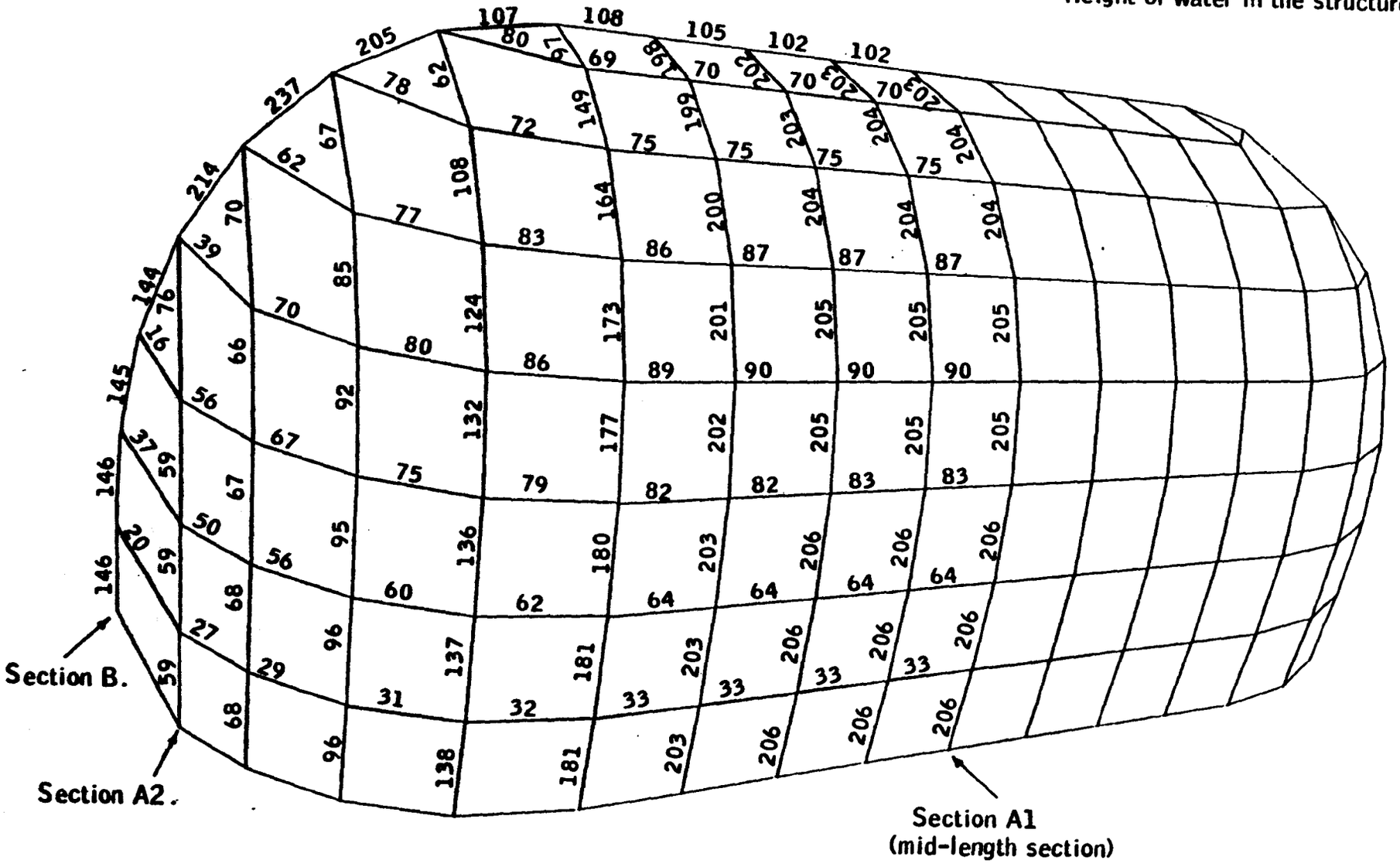

Figure 2.21 a2 - Tension forces in the cables (in kN)

Structure : Type 2 (15.5 m long)

Cable spacing : 1 m.

Height of water in the structure: 2.0 m.

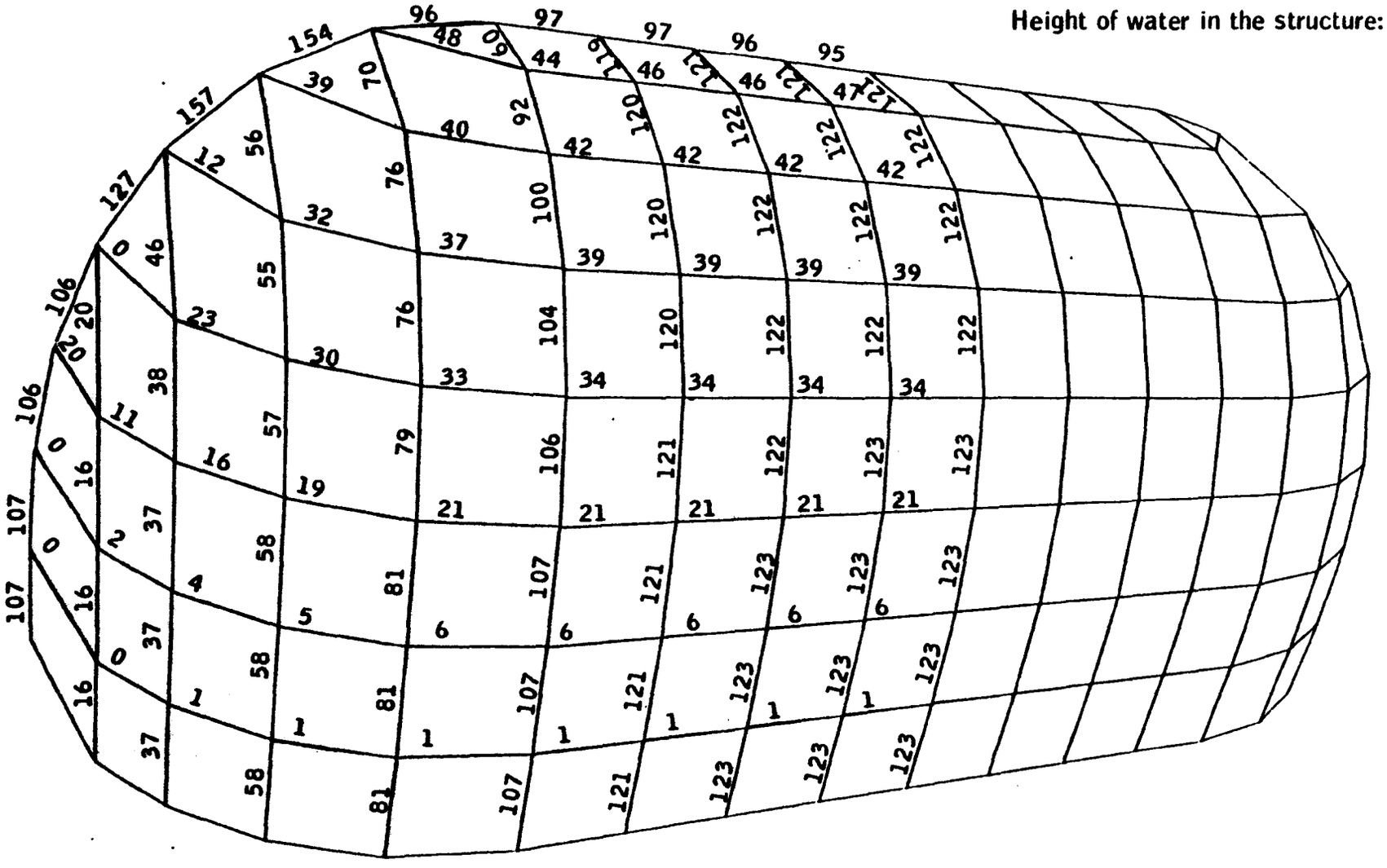

Figure 2.21 a3 - Tension forces in the cables (in kN)

Structure : Type 2 (15.5 m long)

Cable spacing : 1 m.

Height of water in the structure: 4.0 m.

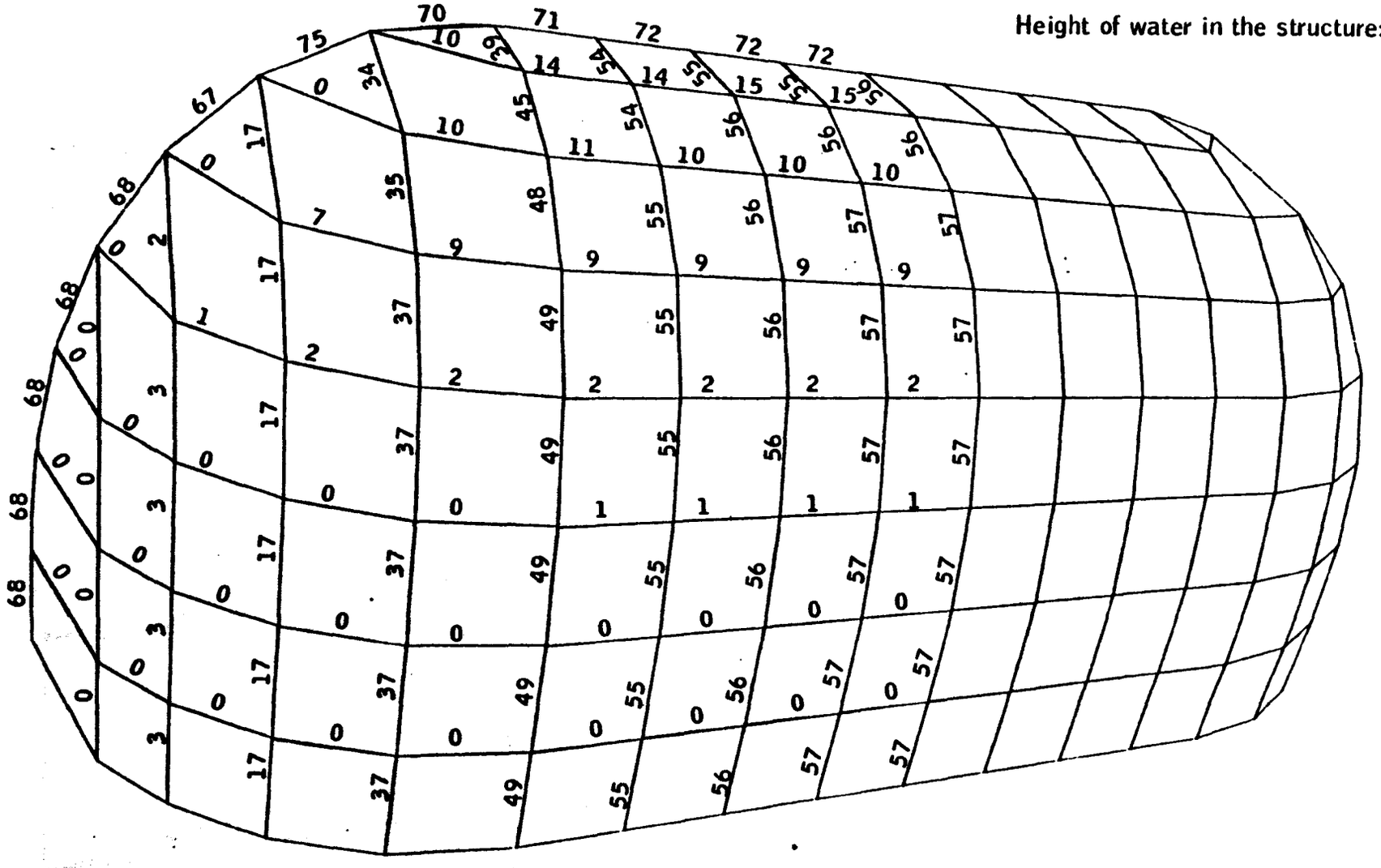

Figure 2.21b - Cross-sections A1 and A2 in the X-Y plane.

Structure : Type 2.

Cable spacing : 1 m.

—×—×—×— Structure full of gas.

—◆—◆—◆— Height of water in the structure: 2.0 m.

—◆—◆—◆— Height of water in the structure: 4.0 m.

Scale: 1:50.

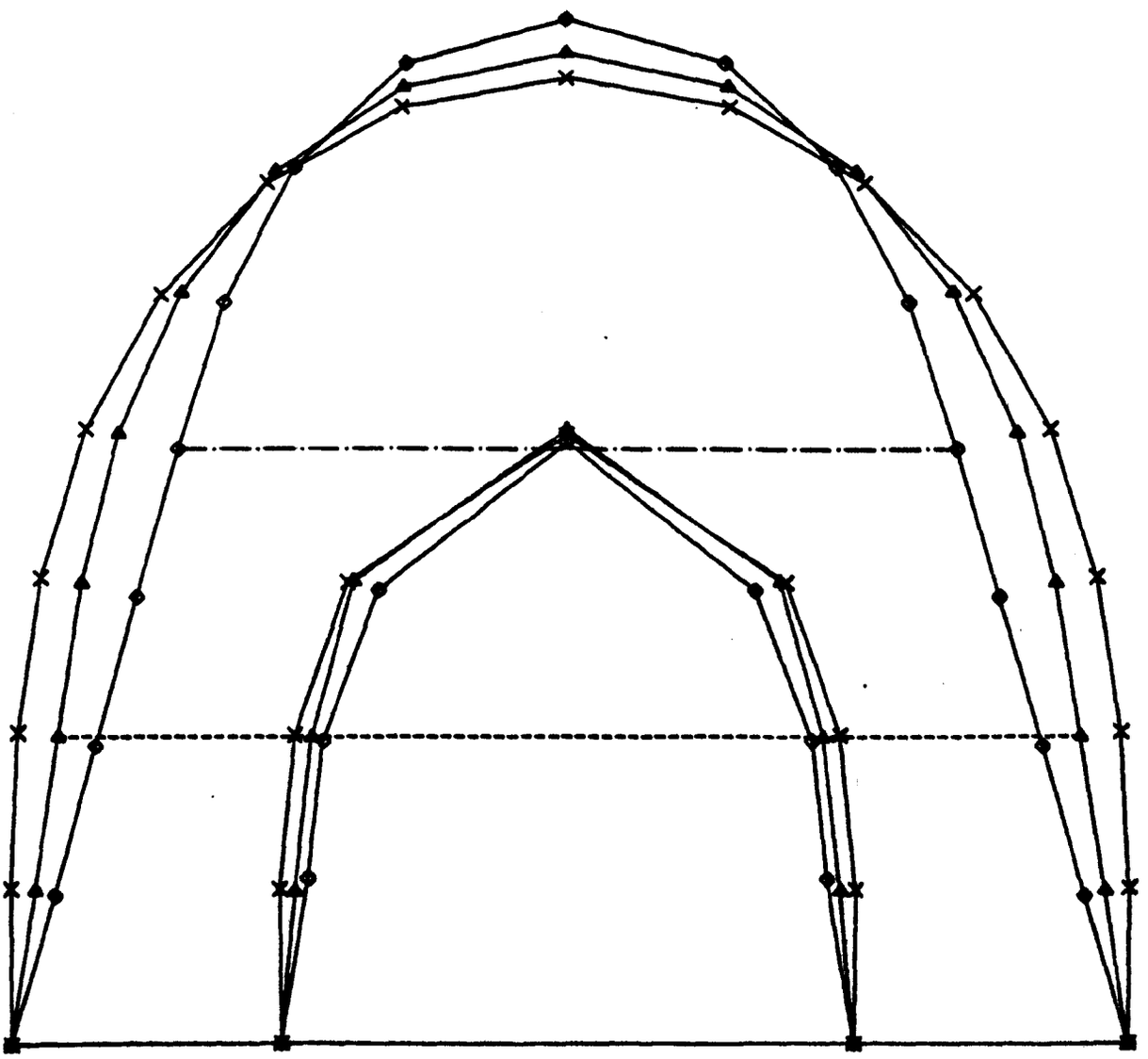

Figure 2.21c - Cross Section B in the Y-Z plane.

Structure : Type 2.

Cable Spacing : 1 m.

—×—×—×— Structure full of gas.

—▲—▲—▲— Height of water in the structure: 2.0 m.

—◆—◆—◆— Height of water in the structure: 4.0 m.

Scale: 1:50.

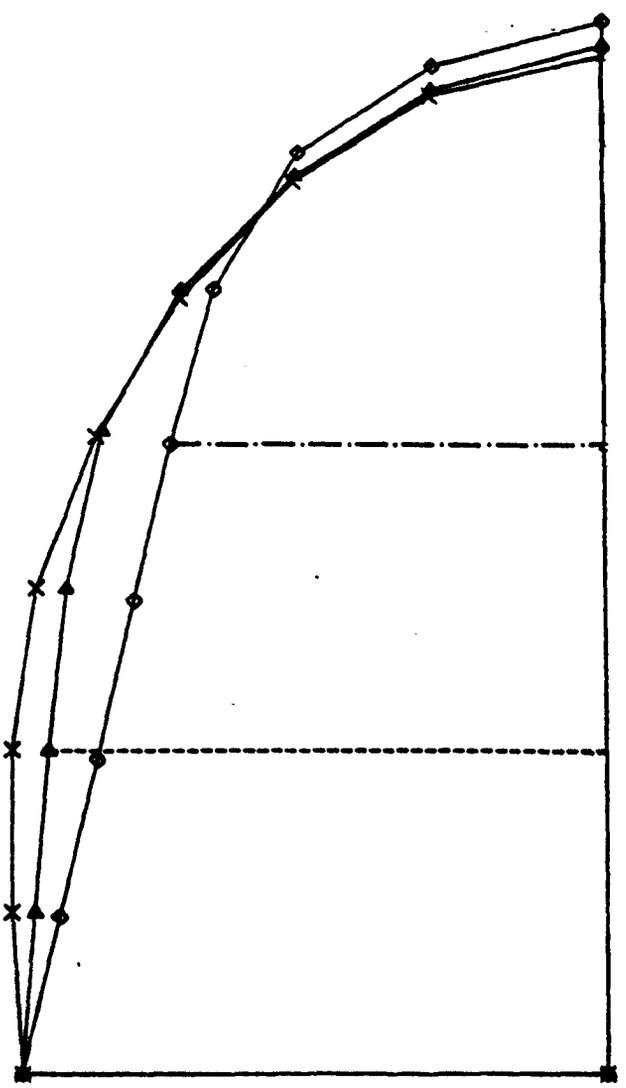

Figure 2.22a1 : Tension forces in the cables (in kN).

Structure : Type 3.

Cable spacing : 2 m.

Height of water in the structure : 0.0 m.

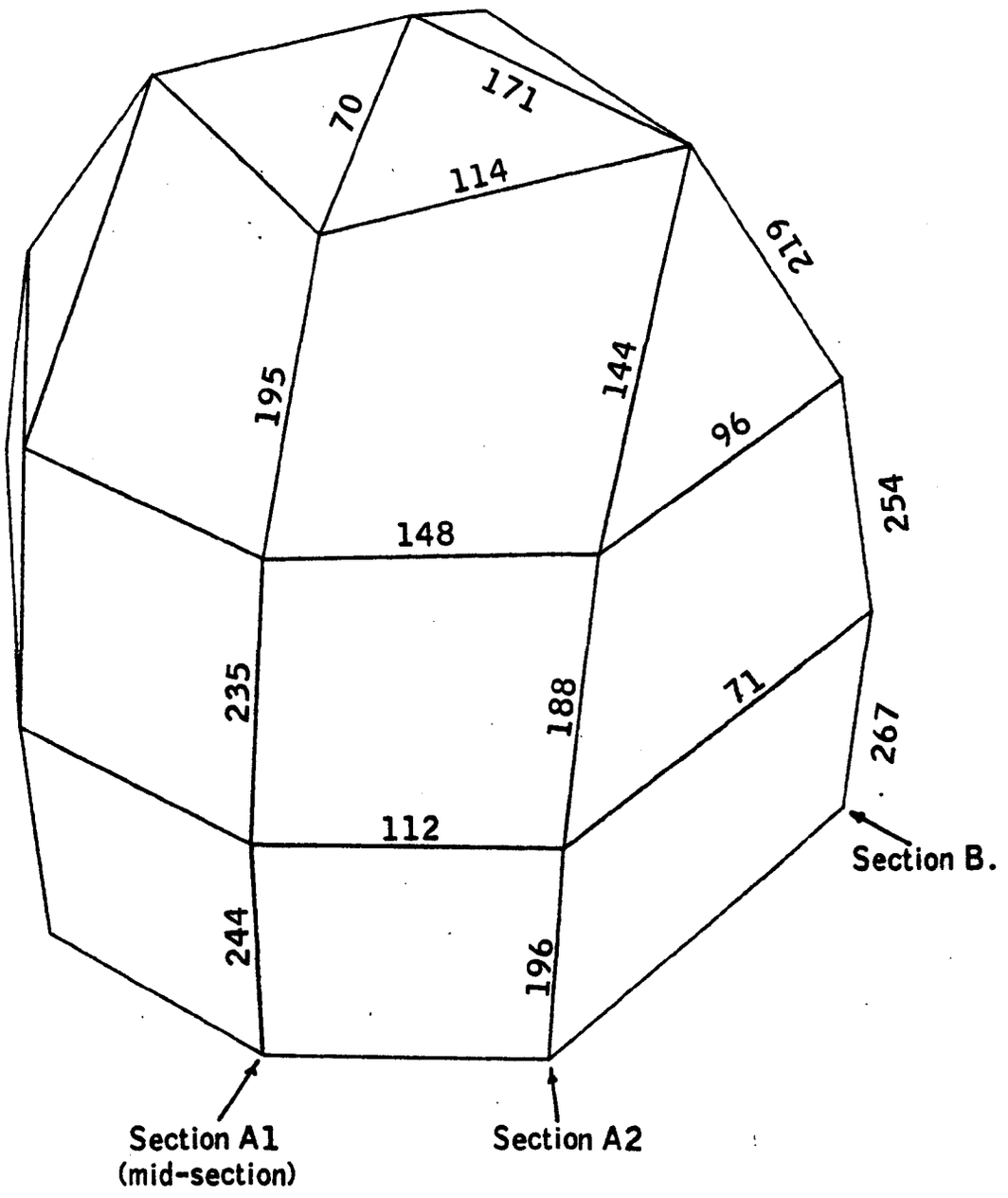

Figure 2.22a2 : Tension forces in the cables (in kN).

Structure: Type 3

Cable spacing : 2.0 m.

Height of water in the structure : 2.0 m.

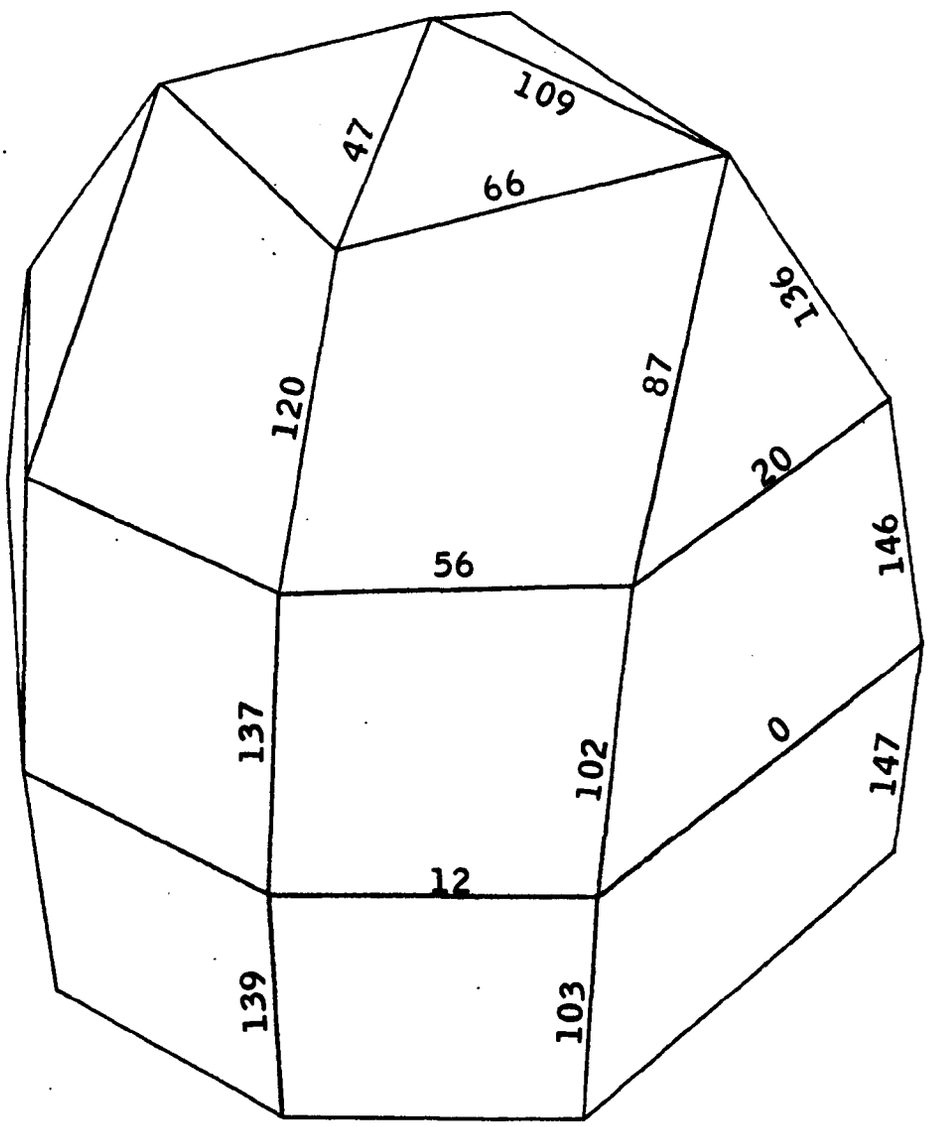

Figure 2.22 a3 : Tension forces in the cables (in kN)

Structure : Type 3.

Cable spacing : 2 m.

Height of water in the structure : 4.0 m.

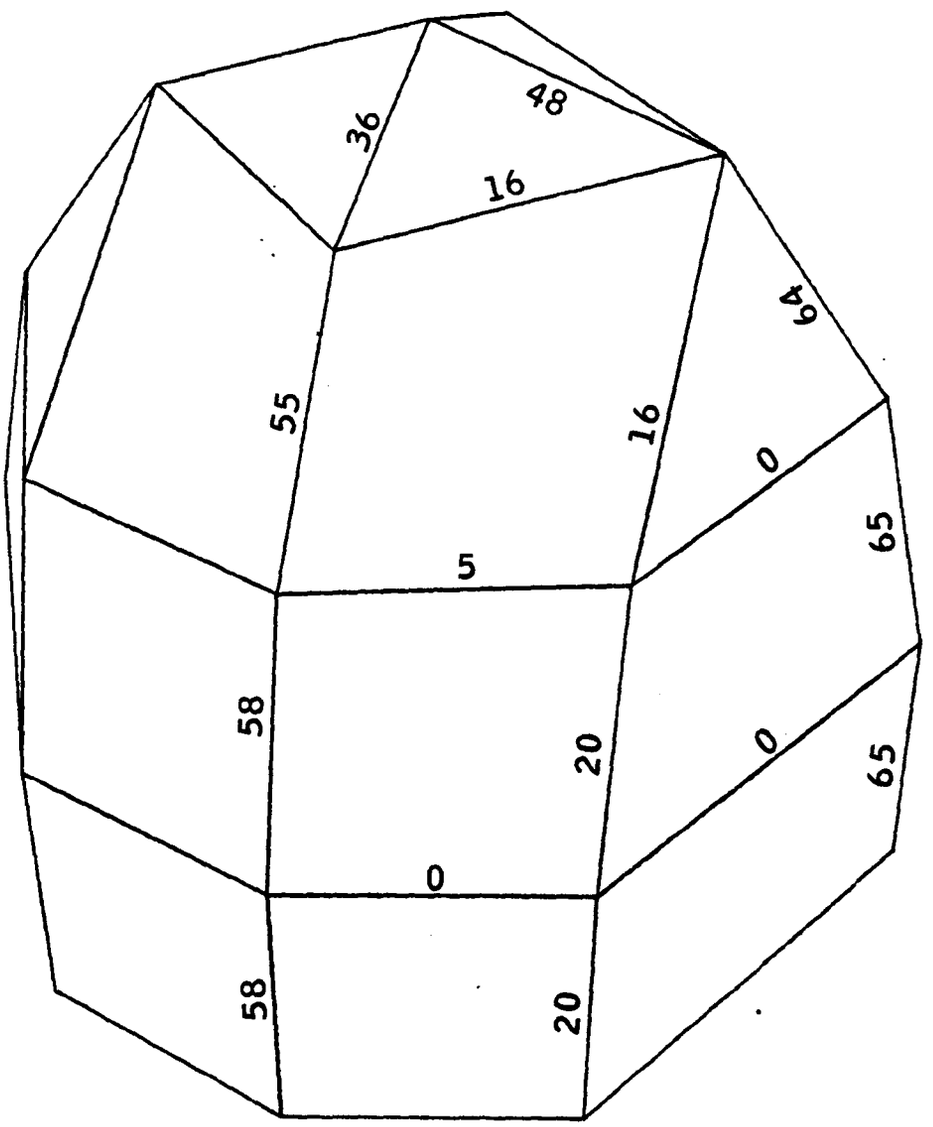

Figure 2.22 b : Cross-sections A1 and A2 in the X-Y plane.

Structure : Type 3.

Cable spacing : 2 m.

—×—×—×— Structure full of gas.

—♦—▲—♦— Height of water in the structure : 2.0 m.

—♦—◇—♦— Height of water in the structure : 4.0 m.

Scale : 1:50.

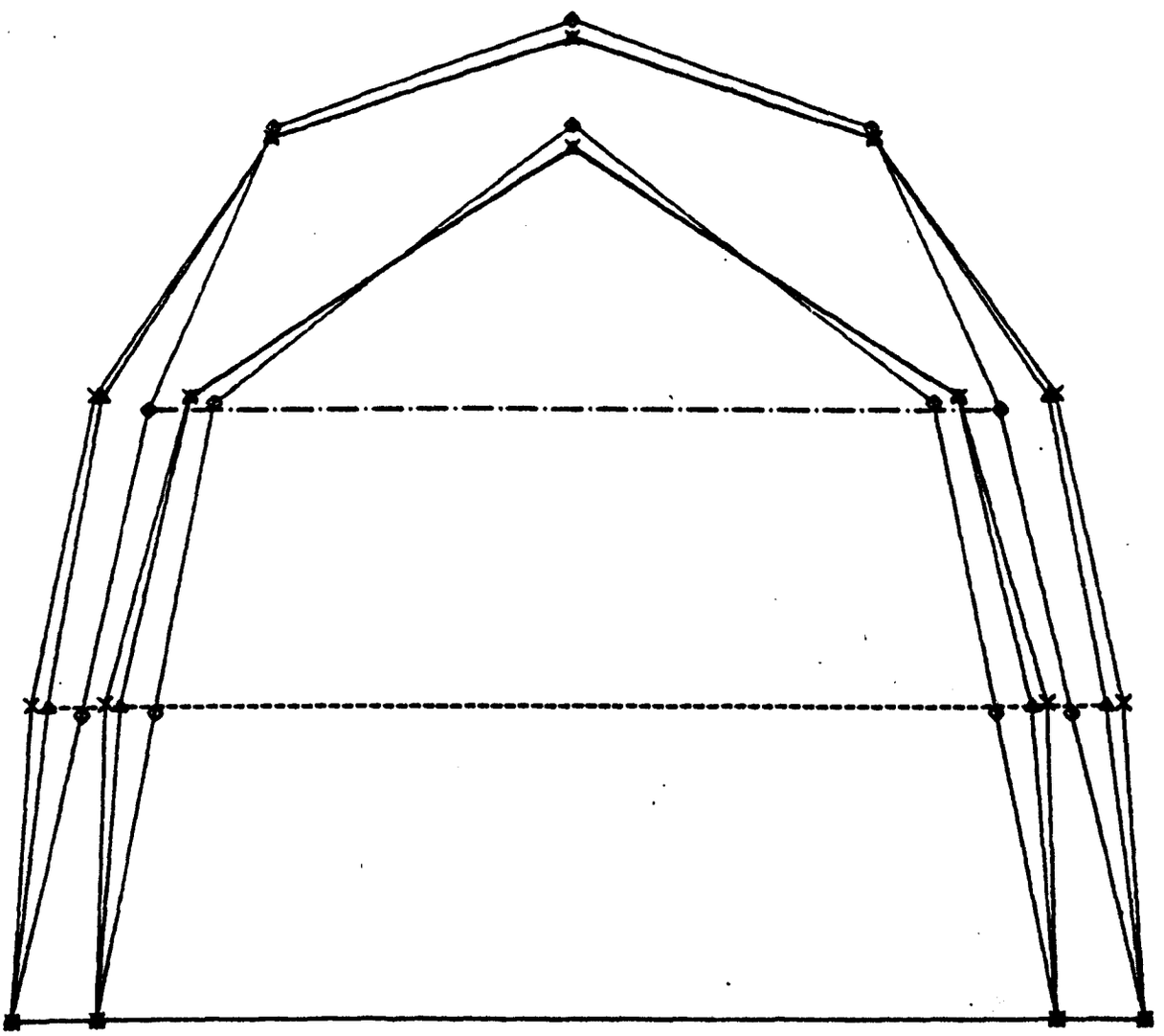

Figure 2.22 c : Cross-section B in the Y-Z plane.

Structure : Type 3.

Cable spacing : 2 m.

—x—x—x— Structure full of gas.

—•—•—•— Height of water in the structure : 2.0 m.

—◊—◊—◊— Height of water in the structure : 4.0 m.

Scale : 1:50.

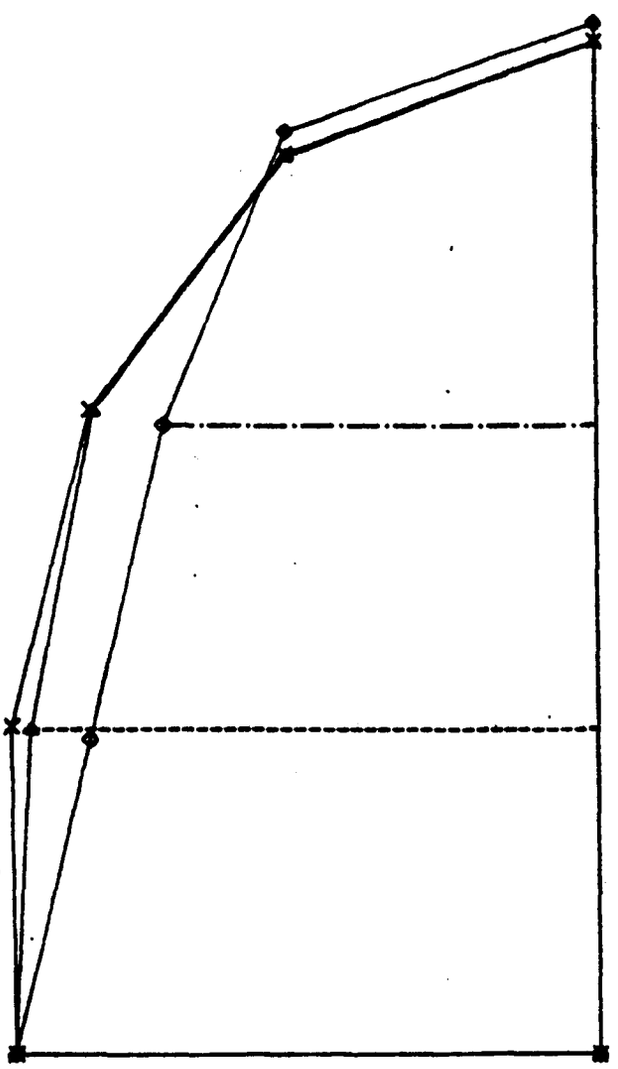

Figure : 2.23 a1 : Tension Forces in the Cables (in kN).

Structure : Type 3.

Cable spacing : 1.0 m.

Height of water in the structure : 0.0 m.

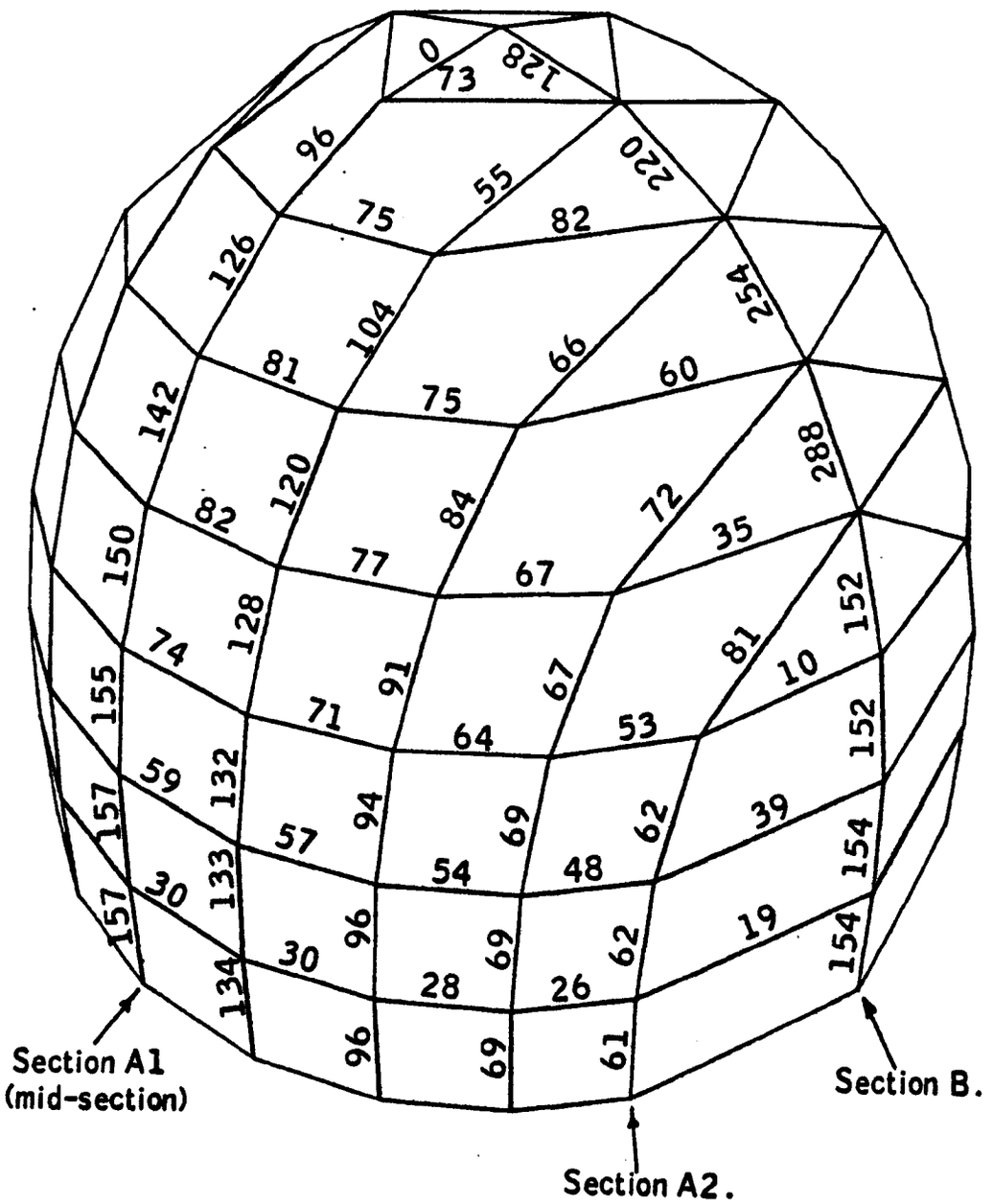

Figure 2.23 a2 : Tension forces in the cables (in kN).

Structure : Type 3.

Cable spacing : 1.0 m.

Height of water in the structure : 2.0 m.

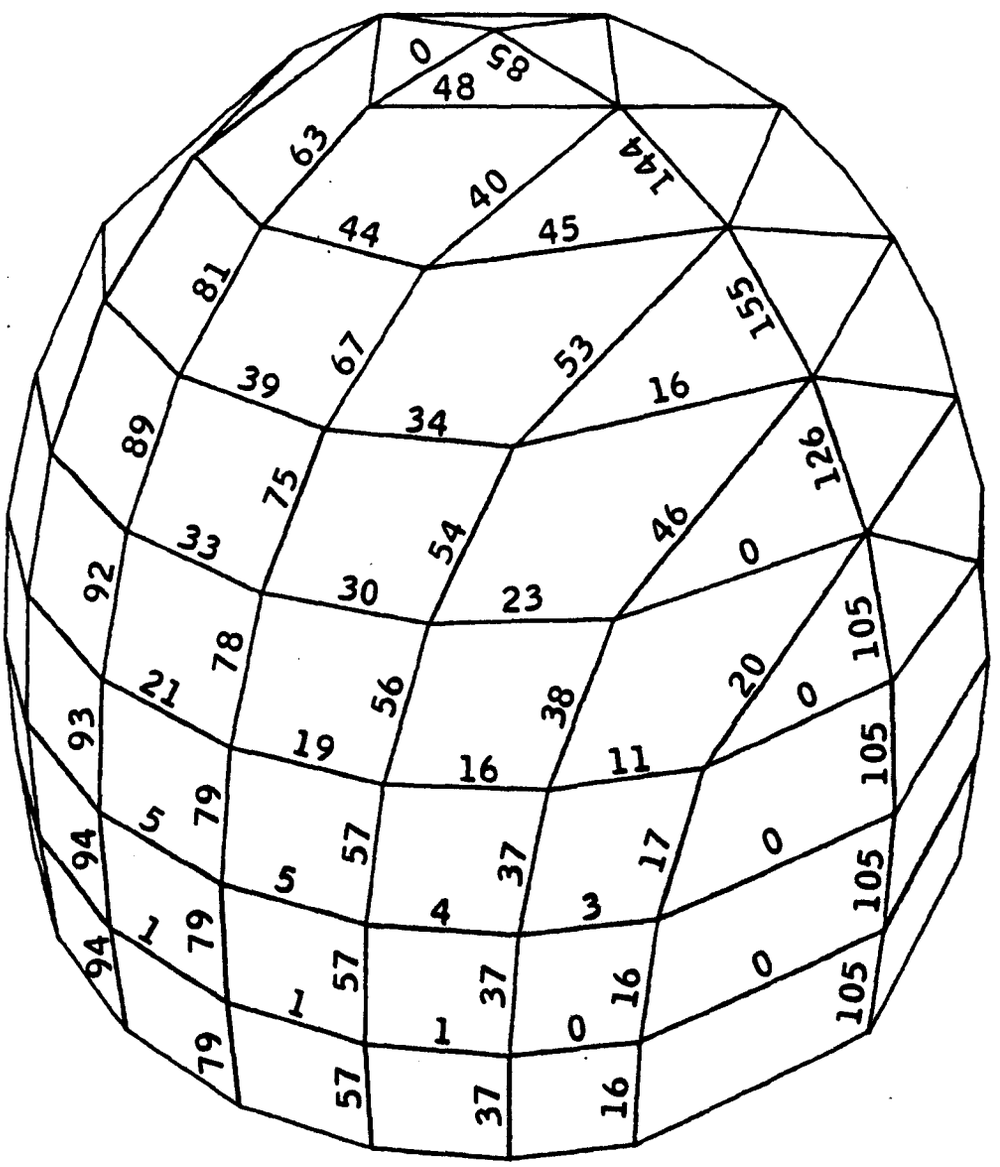

Figure 2.23 a3 - Tension forces in the cables (in kN).

Structure : Type 3.

Cable spacing : 1.0 m.

Height of water in the structure : 4.0 m.

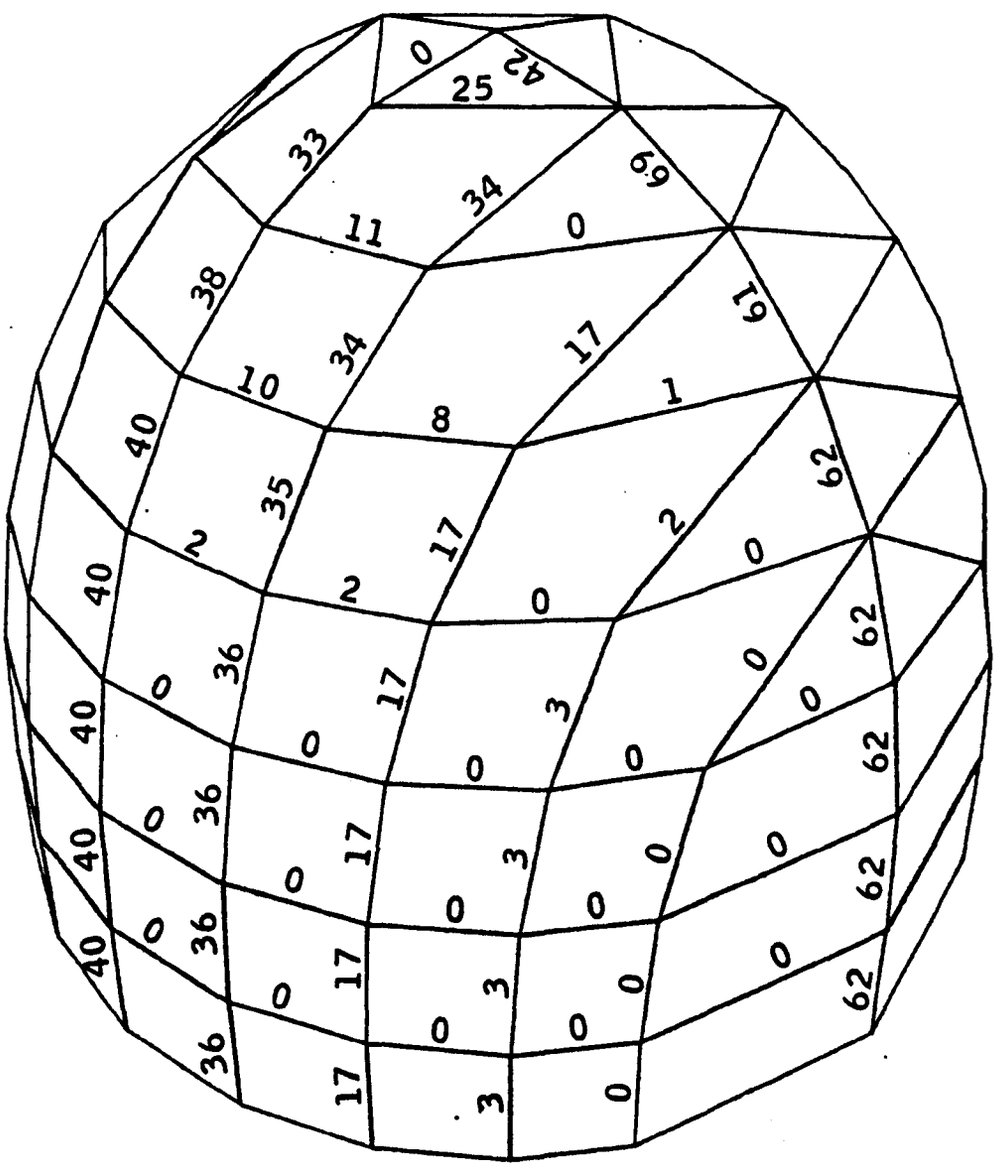

Figure 2.23b - Cross-sections A1 and A2 in the X-Y plane.

Structure : Type 3.

Cable spacing : 1 m.

—×—×—×— Structure full of gas.

—▲—▲—▲— Height of water in the structure : 2.0 m.

—◆—◆—◆— Height of water in the structure : 4.0 m.

Scale : 1:50.

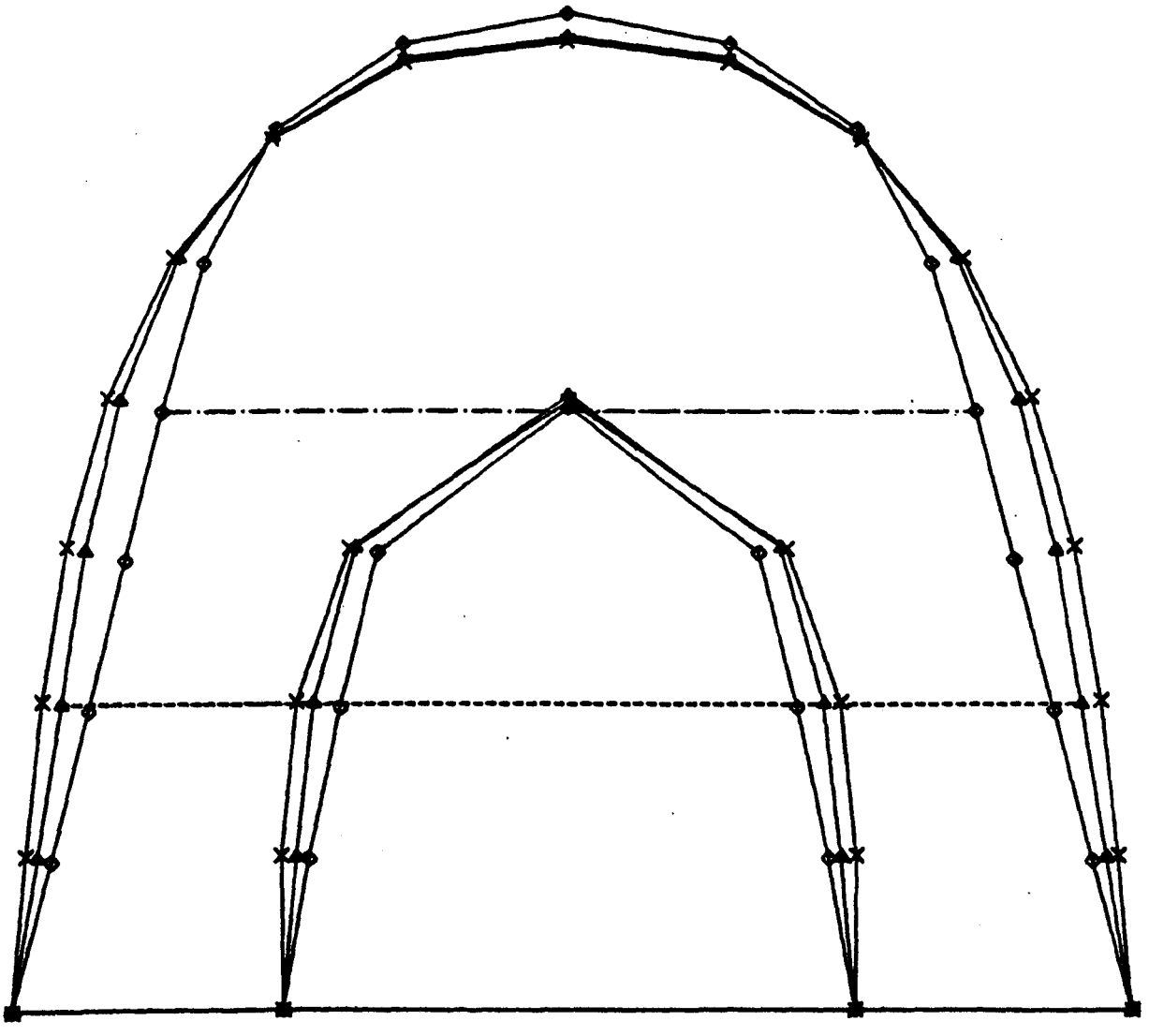

Figure 2.23c - Cross-section B in the Y-Z plane.

Structure : Type 3.

Cable spacing : 1 m.

—×—×—×— Structure full of gas.

—▲—▲—▲— Height of water in the structure : 2.0 m.

—◇—◇—◇— Height of water in the structure : 4.0 m.

Scale : 1:50.

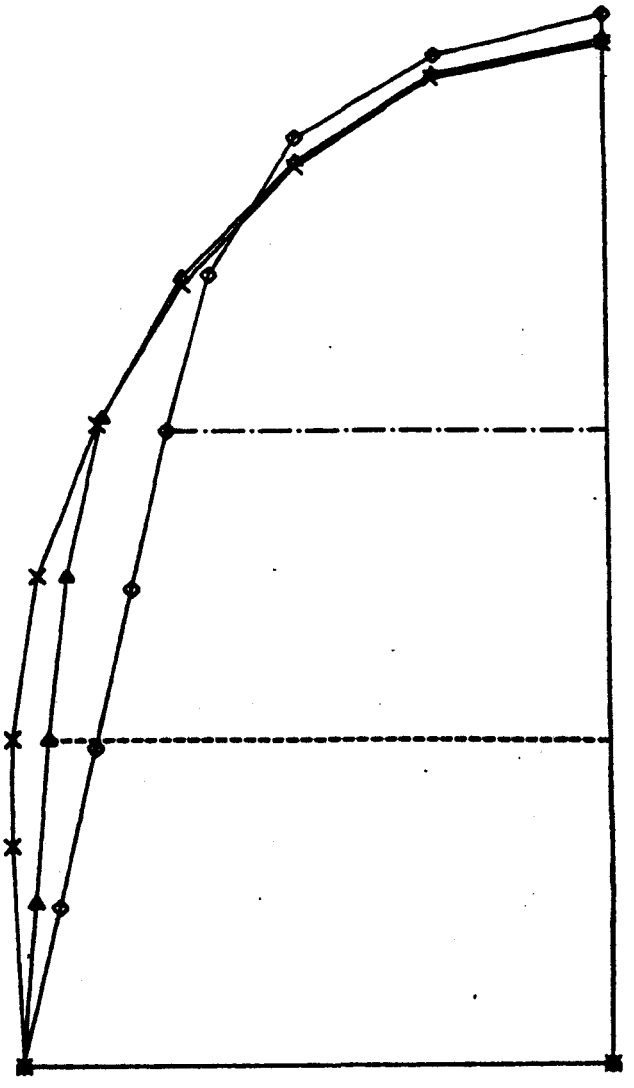

Figure 2.24 a1 - Tension forces in the cables (in kN).

Structure : Type 3.

Cable spacing : 0.6 m.

Height of water in the structure : 0.0 m.

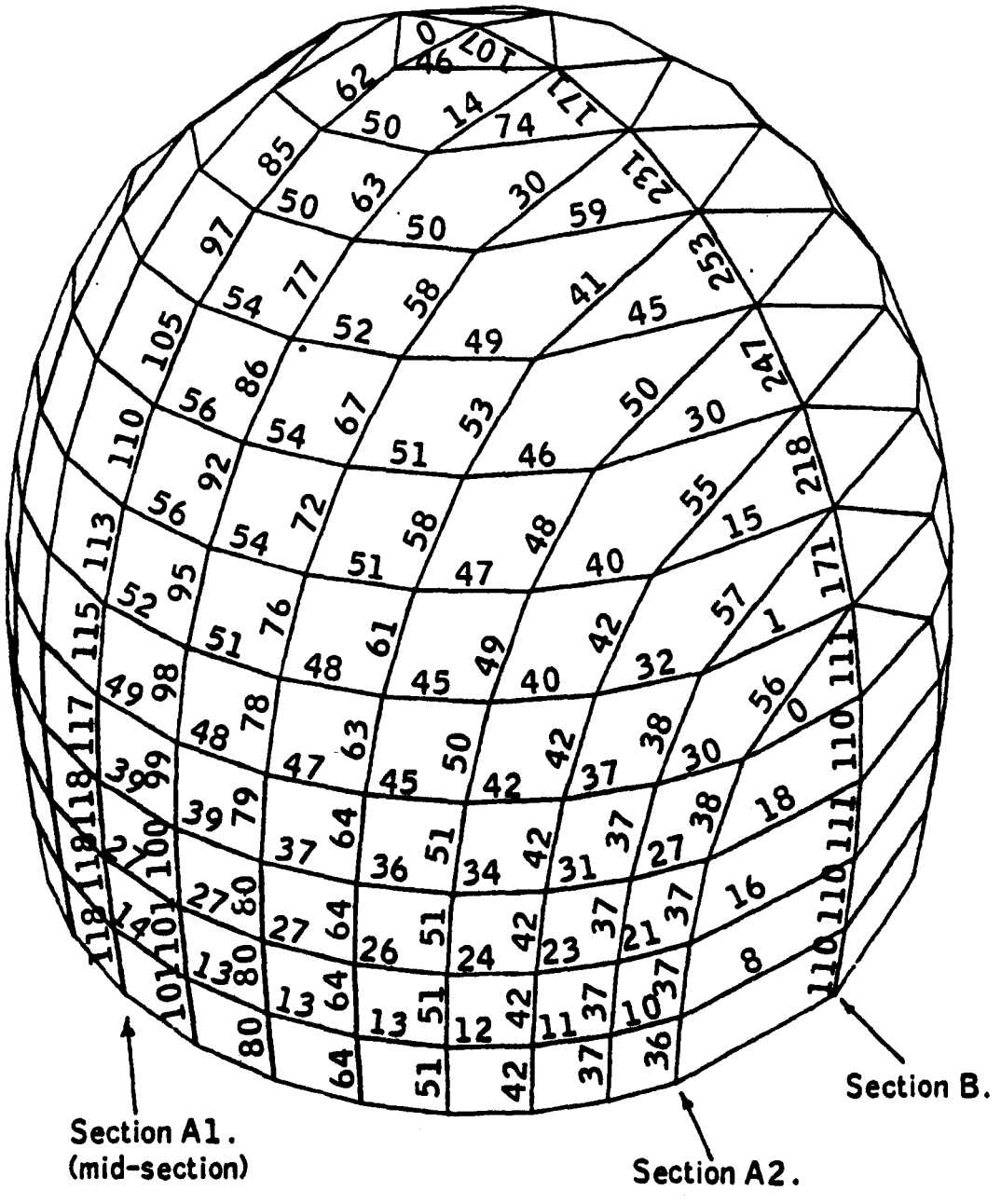

Figure 2.24 a2 - Tension forces in the cables (in kN)

Structure : Type 3.

Cable spacing : 0.6 m.

Height of water in the structure : 2.0 m.

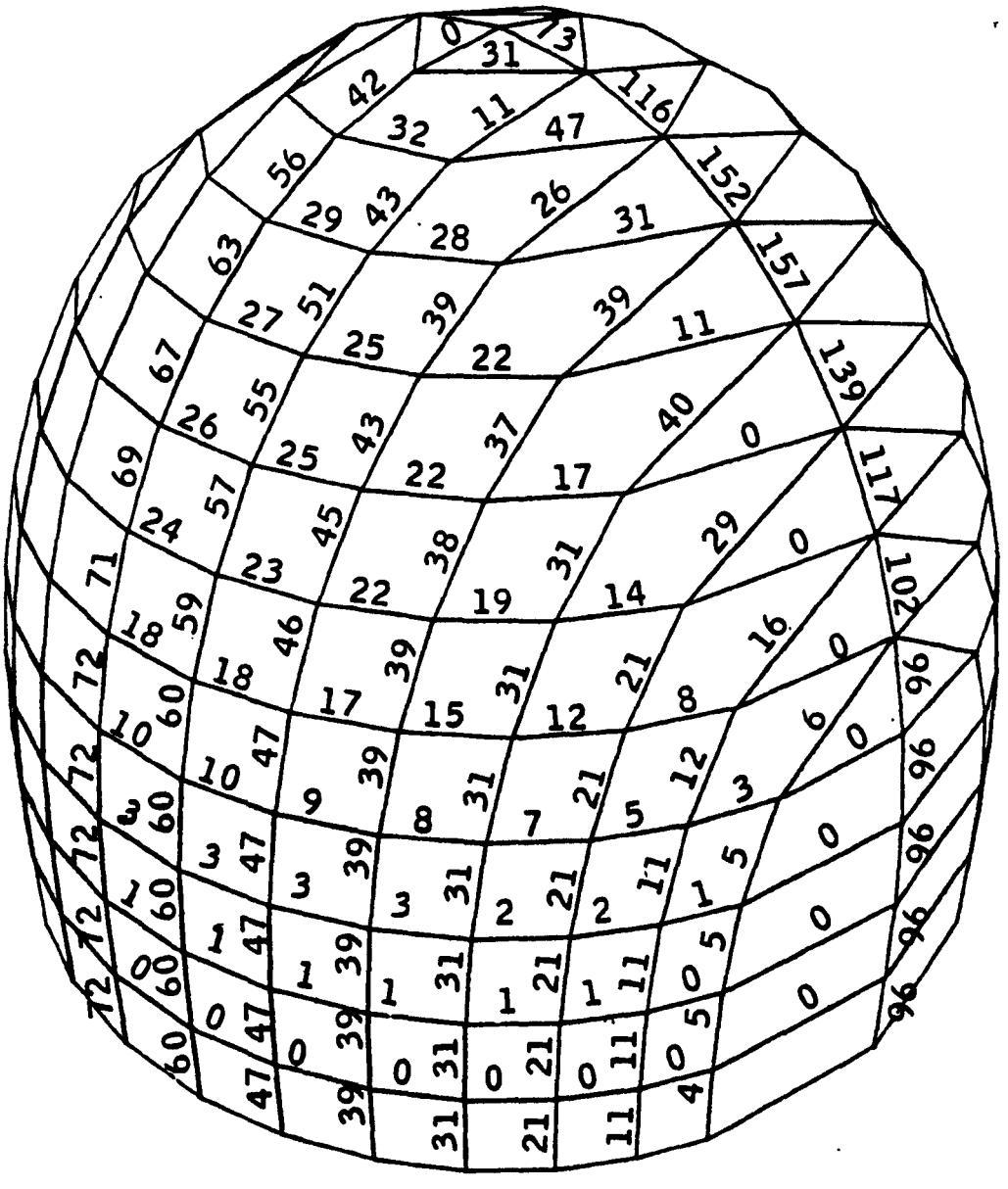

Figure 2.24 b - Cross-sections A1 and A2 in the X-Y plane.

Structure : Type 3.

Cable spacing : 0.6 m.

—×—×—×— Structure full of gas.

—▲—▲—▲— Height of water in the structure : 2 m.

Scale : 1:50.

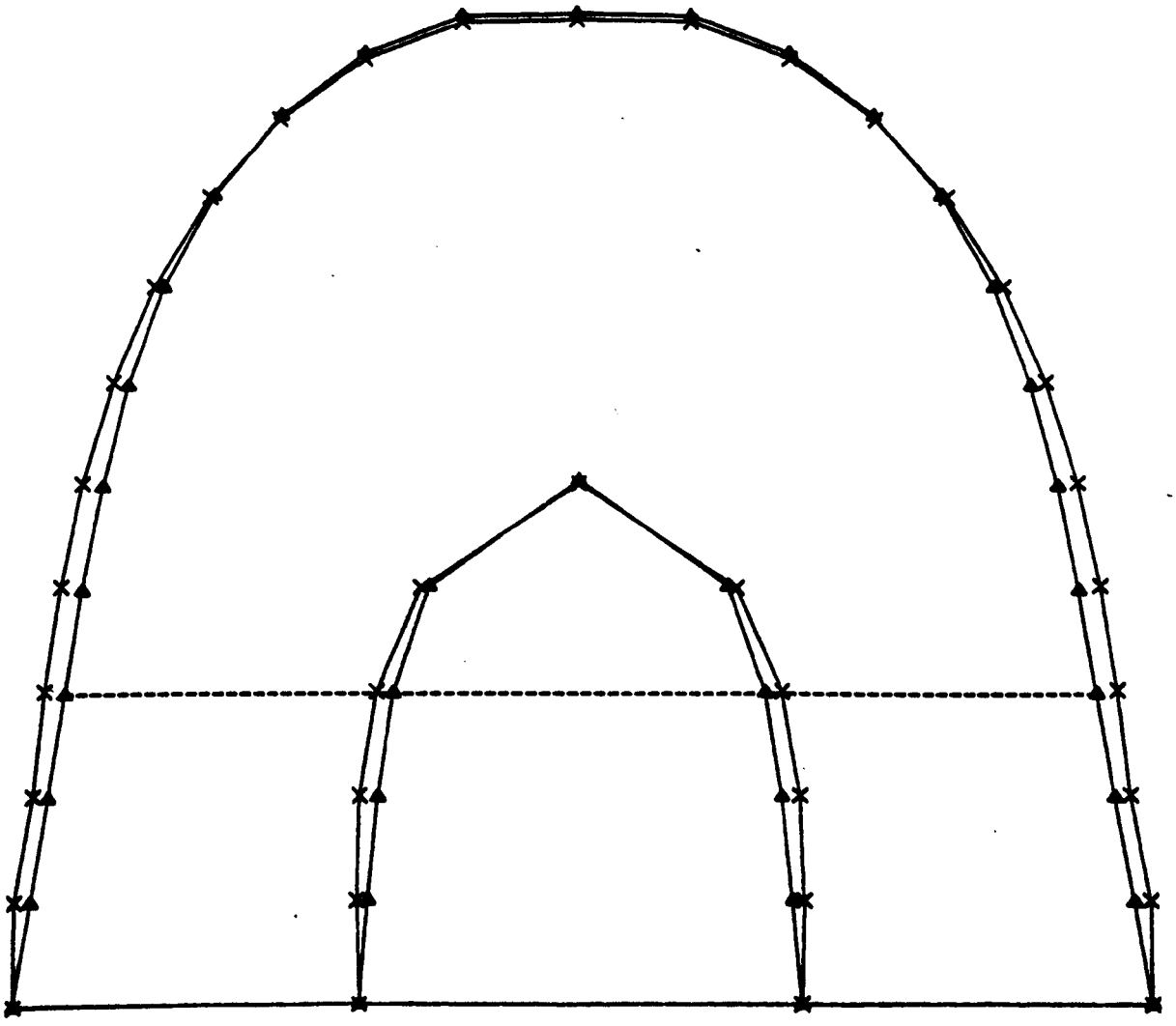

Figure 2.24 c - Cross-section B in the Y-Z plane.

Structure : Type 3.

Cable spacing : 0.6 m.

—x—x—x— Structure full of gas.

—▲—▲—▲— Height of water in the structure : 2 m.

Scale : 1:50.

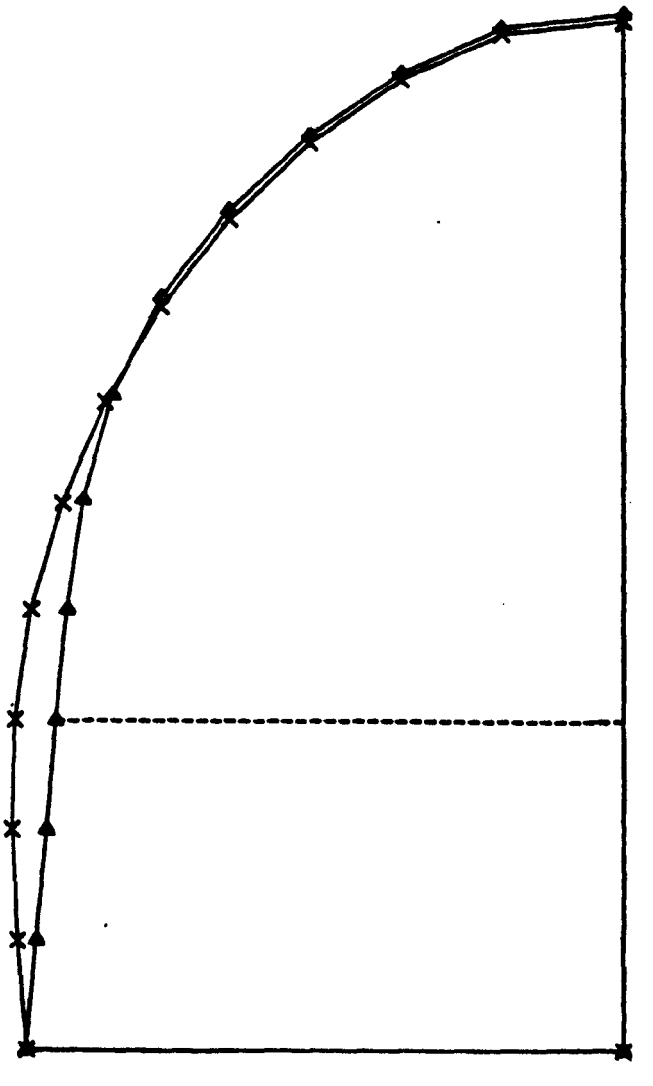

Figure 2.26 - Profiles for Partially Drawing Off of Gas at Different Stages (non-reinforced membrane).

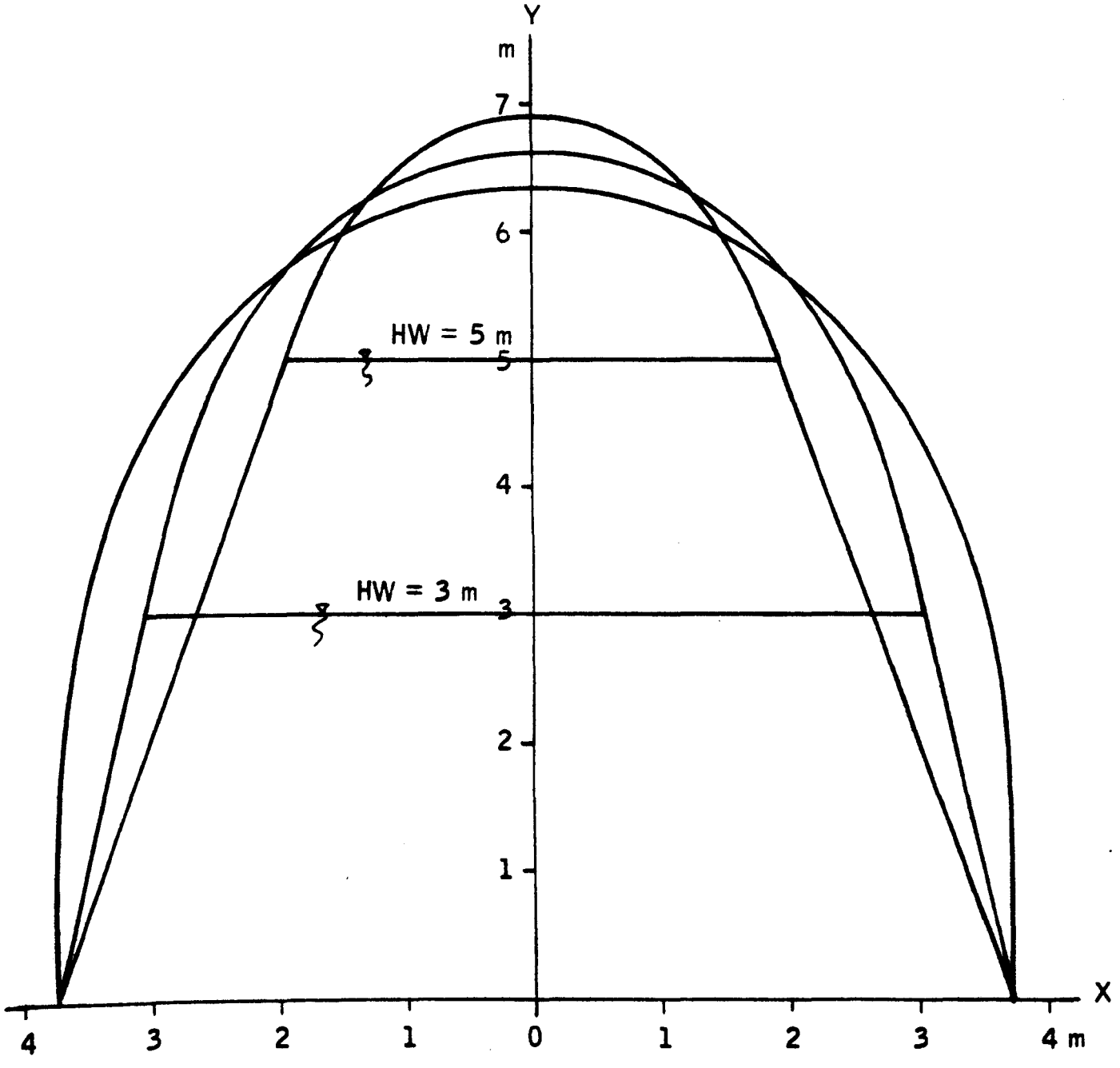

Figure 2.27 - Comparison of the profiles of reinforced and non-reinforced membrane structures for the case when the height of water in the structure is 0.0 m and 3.0 m.

Reinforced membrane, height of water : 0.0 m.

Non-reinforced membrane, height of water : 0.0 m.

Reinforced membrane, height of water : 3.0 m.

Non-reinforced membrane, height of water : 3.0 m.

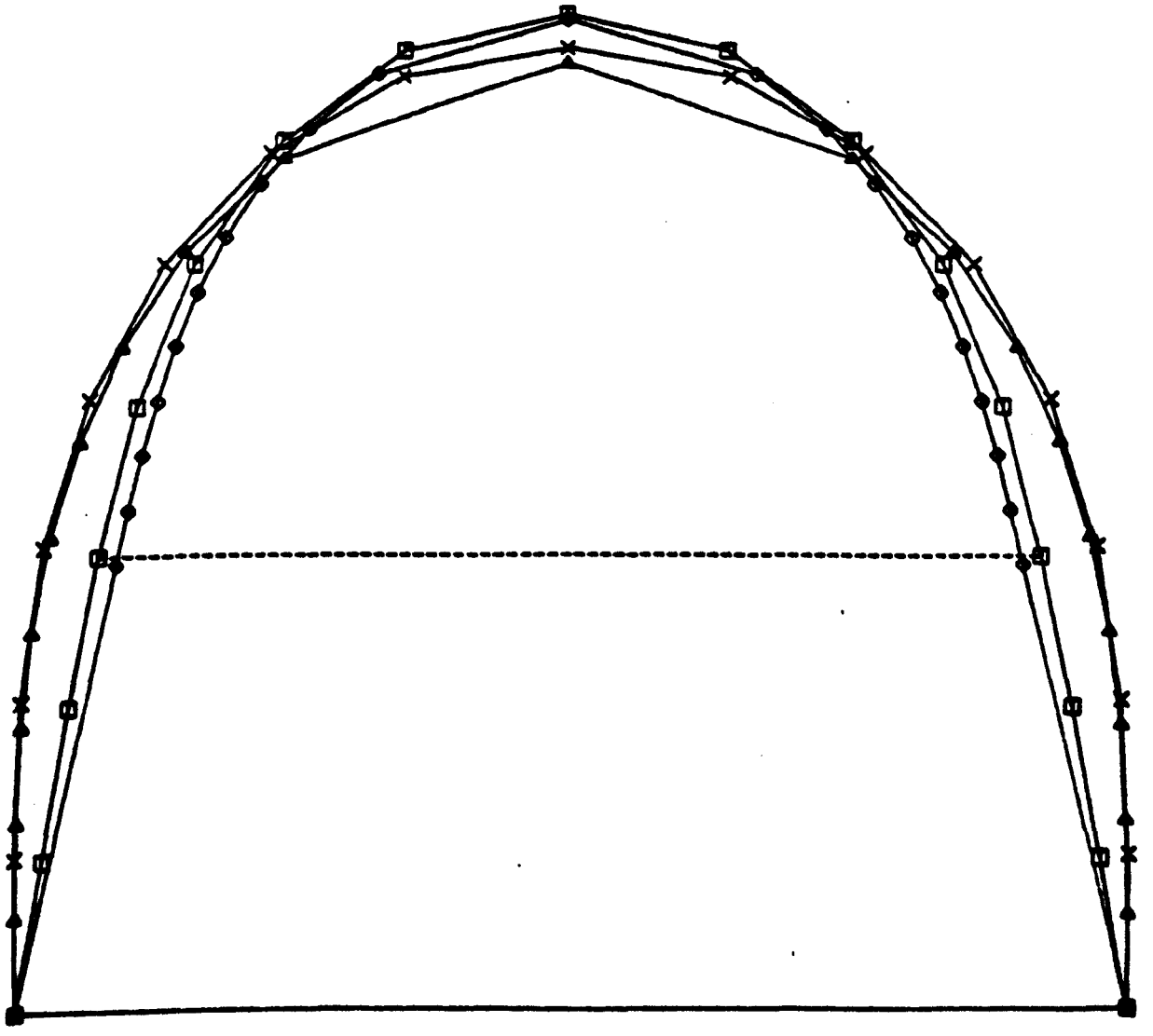

Graphs in Chapter Two

Graph 2.1 - Graph of Area (A) Against Base Angle (ϕ_o) for different Base Widths (B)

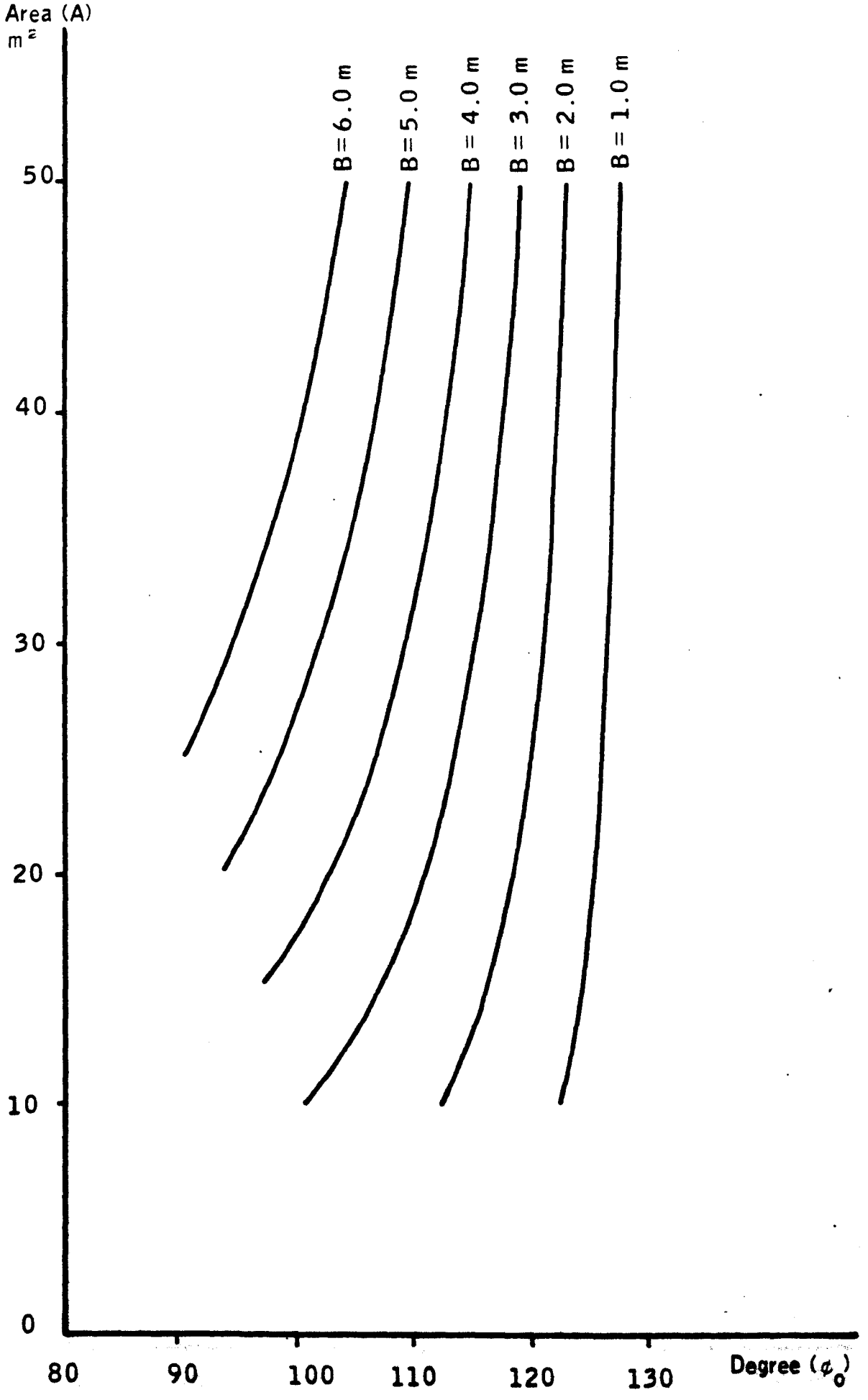

Graph 2.2 - Graph of Perimeter (S) against Base Angle (ϕ_o) for Different Base Widths (B)

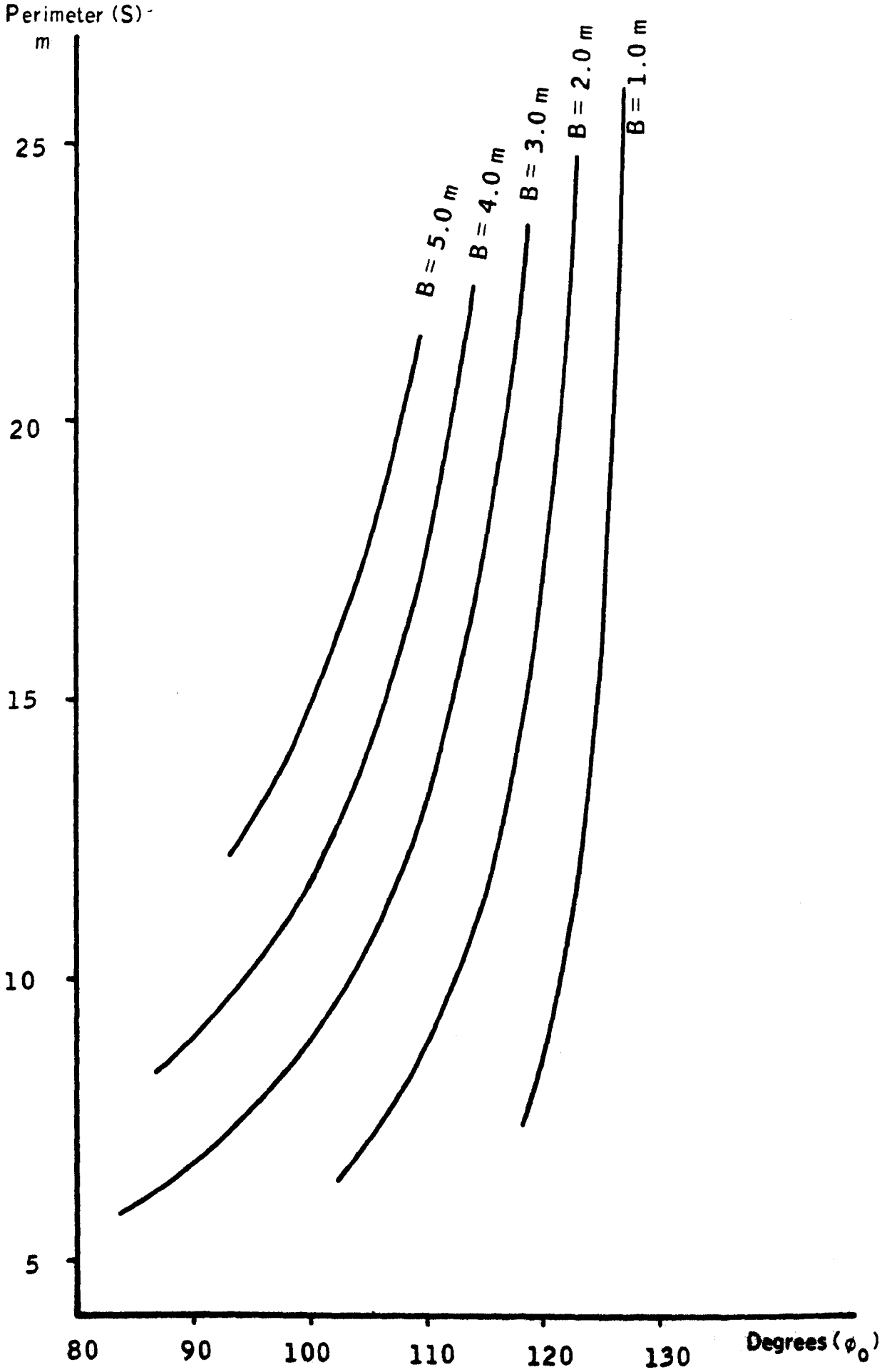

Graph 2.3 - Graph of Tension (T) Against Base Angle (ϕ_o) for Different Base Widths (B).

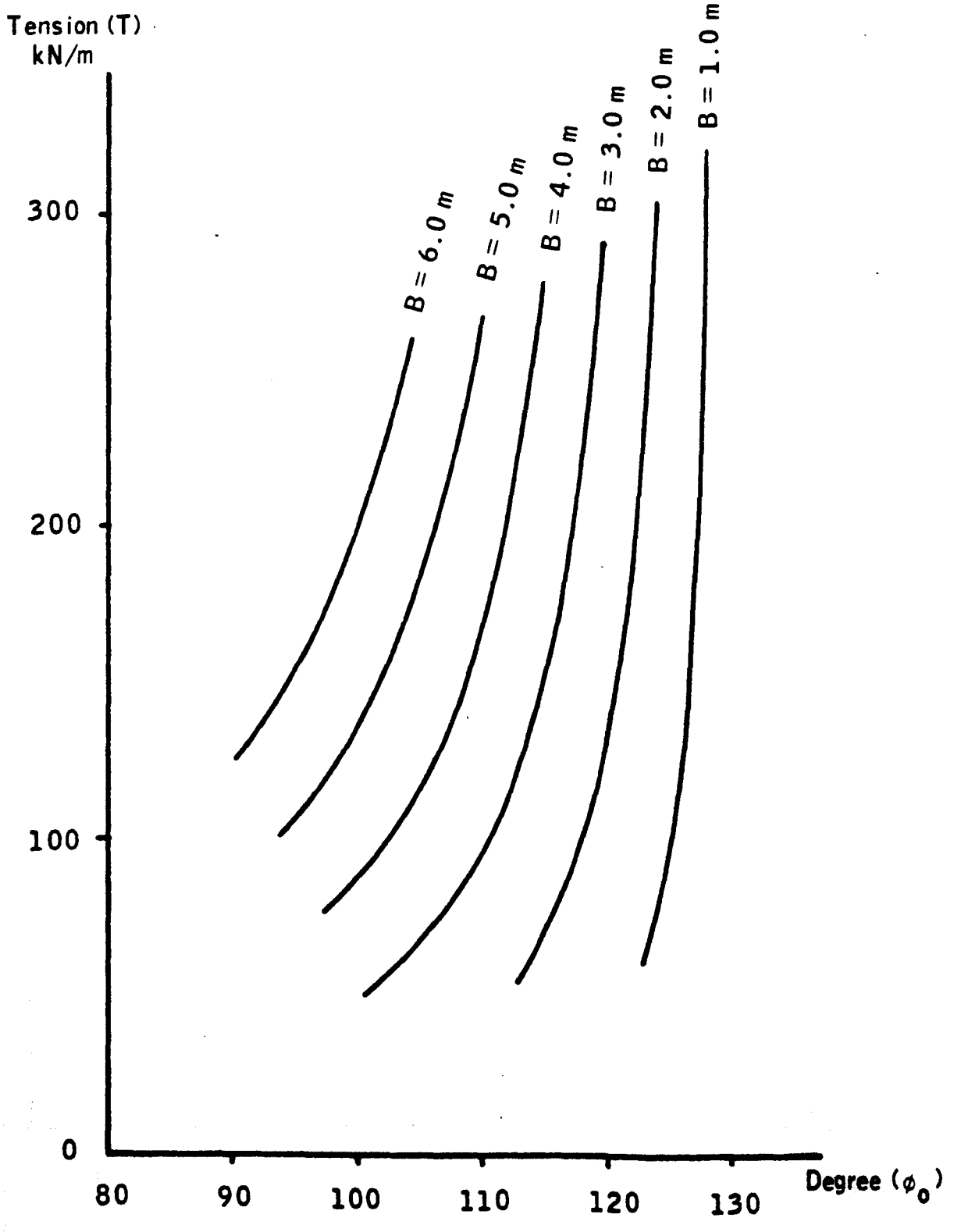

Graph 2.4 - Graph of Perimeter (S) Against Base Width (B) for Different Areas (A)

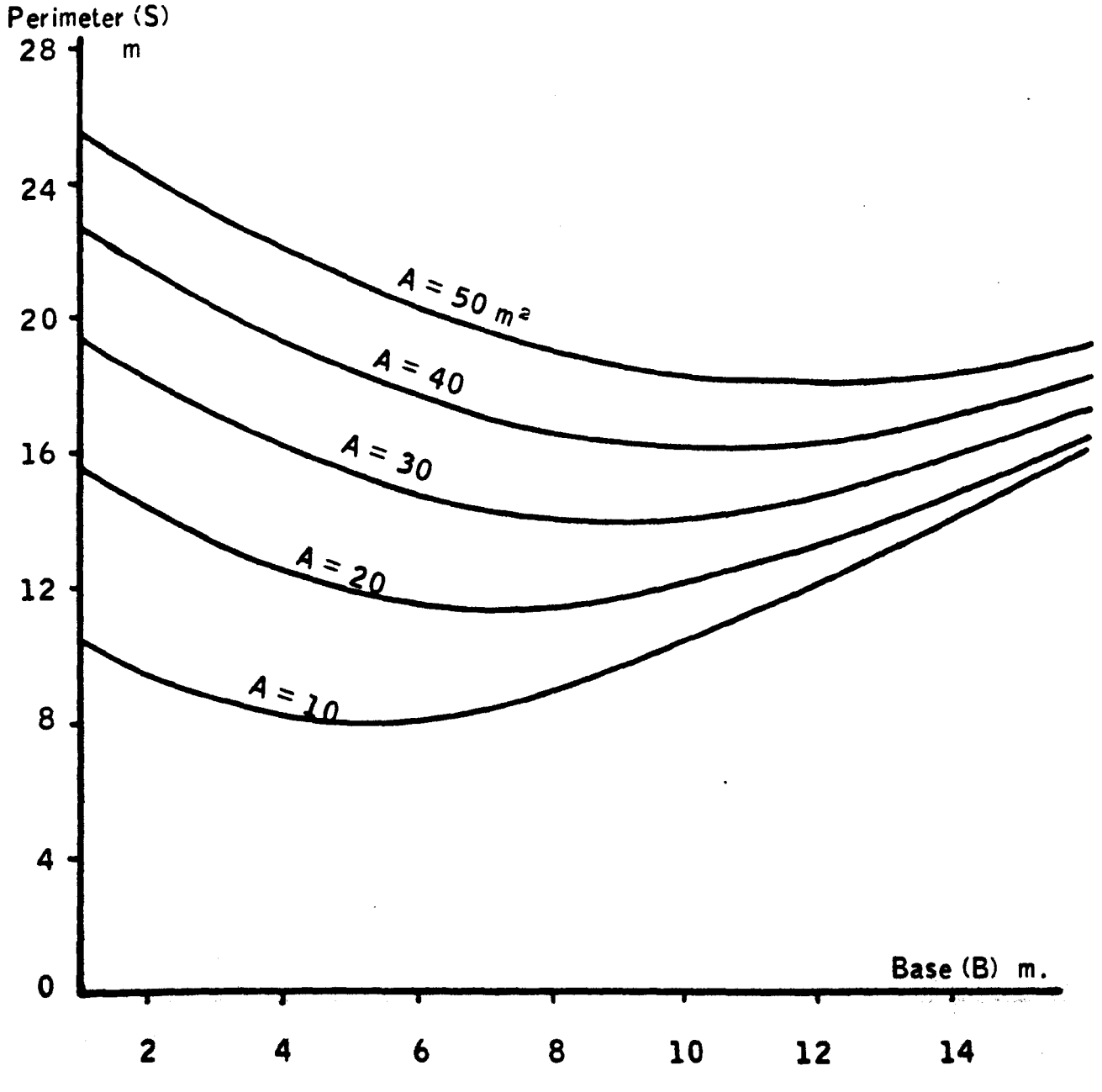

Graph 2.5 - Graph of Tension (T) Against Base Width (B) for Different Areas (A)

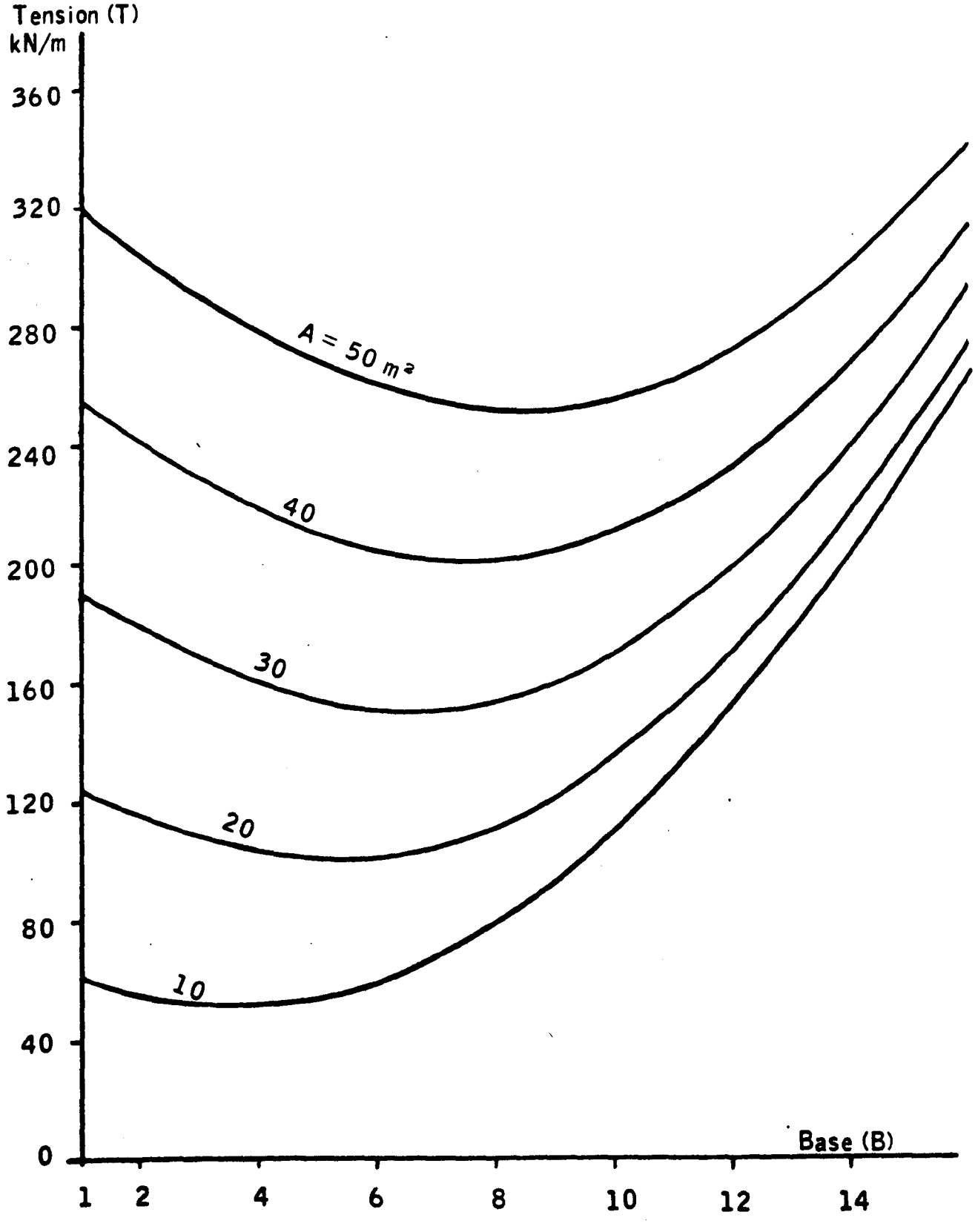

Graph 2.6 - Graph of Tension (T) and Perimeter (S) against Base Width (B).

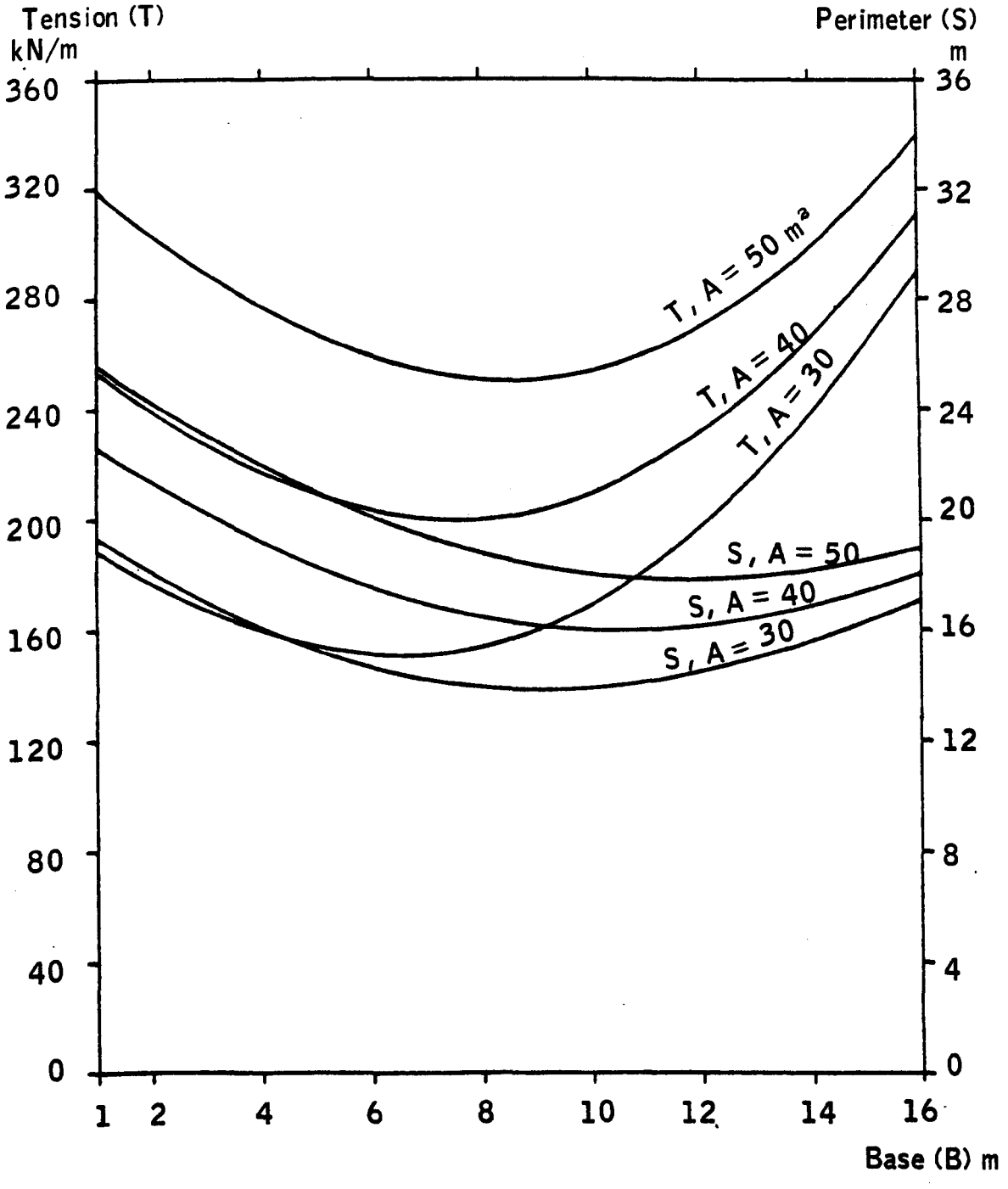

Graph 2.7 - Graph of Tension (T) Against Strain (ϵ)

Av. Yield Load = 43 kN/m

$$Et = \frac{T}{\epsilon} = \frac{18}{0.1} = 180 \text{ kN/m}$$

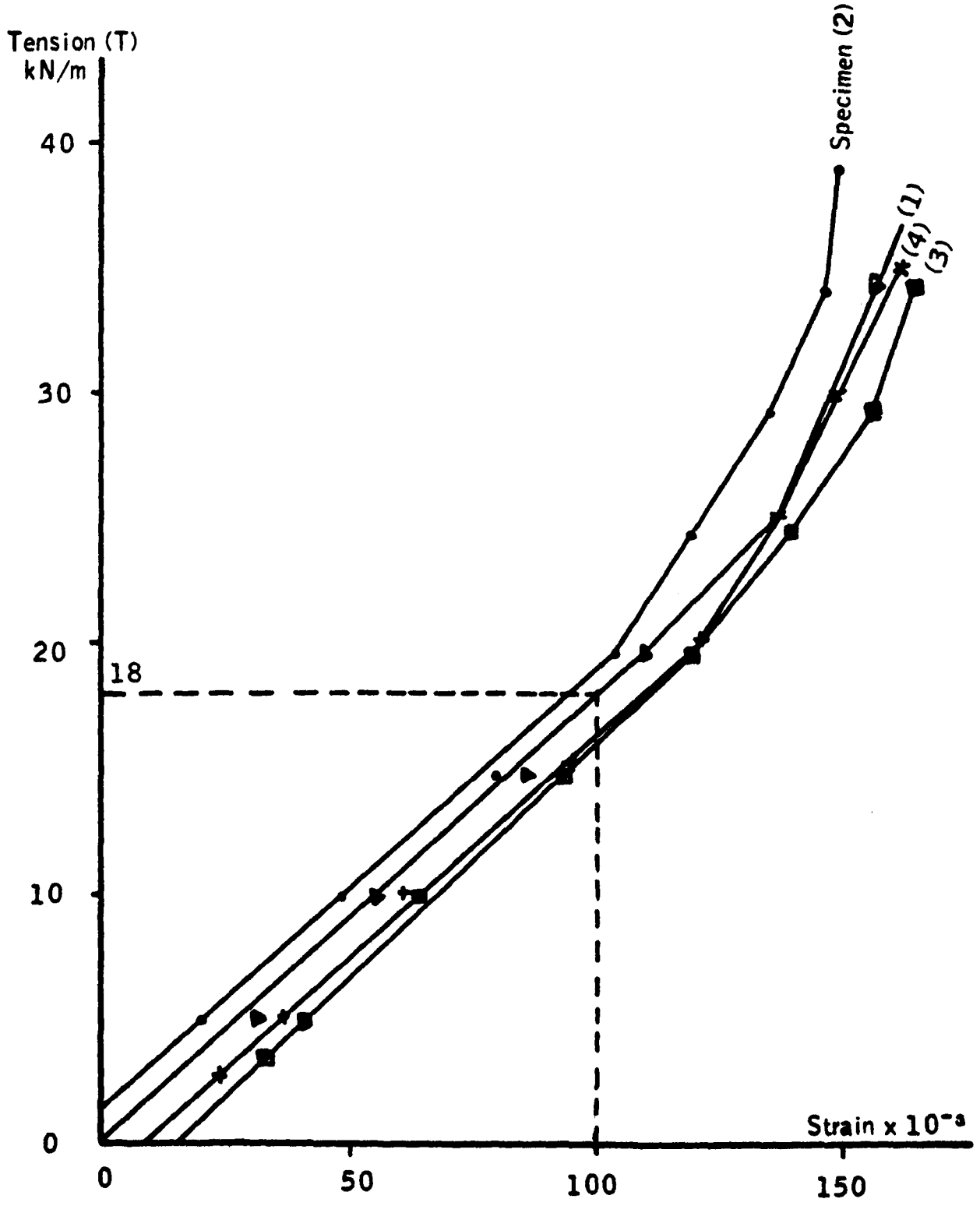

CHAPTER THREE

HYDRODYNAMIC ANALYSIS

List of Notations in Chapter Three.

a	axis which lies in the direction of flow
A	projected frontal area
b	axis which is perpendicular to the direction of flow
C_a	coefficient of inertia
C_d	coefficient of drag
C_m	added mass coefficient
C_p	pressure coefficient
D	linear dimension of the object
$E(\gamma, \varphi)$	incomplete elliptic integral of the second kind
F	wave force
K_c	Keulegan-Carpenter number
p	pressure on the object
P	pressure at infinity
s	length along the perimeter
t	2 x the axis which lies in the direction of flow
T	wave period
U	horizontal component of wave particle orbital velocity
U_o	undisturbed velocity at infinity
U_m	maximum particle velocity of the undisturbed wave at the position of the center of the object.
V	volumetric displacement
x	co-ordinate
y	co-ordinate

θ	momentum thickness
λ	shape factor
ν	kinematic viscosity
ρ	fluid density
τ_o	shear stress
ω	complex potential

3.1 Introduction.

In the previous chapter, an inflated membrane structure for underwater use has been statically analysed. Since the structure has been designed mainly for use in the ocean environment, the elements of the ocean environment which might affect the safety of the proposed structure have to be investigated. The main environmental factors which affect an offshore structure are wind, waves, currents, water pressure, earthquakes and the reactive forces of the foundation medium. In this chapter the effect of some of these offshore parameters which are likely to have a more pronounced influence on the behaviour of the proposed structure, are examined.

The proposed structure has its main application in the storage of gas. In view of the results of the structural analysis, it is deduced that by locating the structure in deeper water, a greater quantity of gas can be stored in the structure due to its higher internal pressure. It is therefore decided to design the structure for deep water conditions and assume that the dimensions of the submerged structure are small compared to the depth of the water and the wavelength of the incident waves. Under the above conditions the hydraulic actions due to deep ocean currents and buoyancy forces and the reactive forces of the foundation medium are of principal importance in the design of the proposed structure but the effect of wind and wave disturbances are insignificant.

The buoyancy force on a submerged object is a surface directed force and its value is equal to the weight of water displaced by the structure. This uplift force is usually resisted by the suitable choice of the anchorage system of the structure.

The main forces arising from ocean currents are primarily those of drag. One method of estimating the drag force on a submerged object is by studying the pressure distribution due to currents around the surface of the object. A theoretical analysis has been carried out in section 3.3.1., based on the potential flow theory for the prediction of the pressure distribution around the object placed in a steady current. This is followed in section 3.3.2., by some

experimental examination into the effect of steady currents on submerged objects. The changes produced by the steady currents on the pressure distribution around the proposed structure are estimated from the results of the theoretical and the experimental investigations. The effect that these pressure changes have on the shape of the structure and on the forces of the reinforcing cables are then calculated in section 3.3.4.

One of the problems associated with a bottom-fixed structure is the abrupt change in the sea-bed elevation around the interface of the structure with the sea-bed. These changes are known as local scour and are due to the erosion of the bed material which are mainly caused by the large-scale system of vortices that develops about the bottom fixed object by the local flow. In order to ensure the stability and the integrity of the structure foundation in the face of gross instability of the sea-bottom, it is essential to obtain a general geological knowledge of the given area and to estimate the ultimate depth of scour so that a suitable site can be selected for laying the proposed structure. The geological data are available from Oceanography stations. Experiments have been conducted in section 3.5 in order to study the pattern of scour around a model of the proposed structure. The ultimate depth of scour can then be estimated by a semi-empirical method based on experimental observations made during the early stage of the scouring process.

Although for structures located in deep water, the magnitude of forces induced by waves is insignificant, nevertheless the determination of these forces is essential to their design. Therefore a brief investigation has been carried out, in section 3.4, into the effect of waves on the proposed structure. This investigation is based on the assumption that the size of the structure is small compared to the wavelength and hence the presence of the structure does not materially affect the wave field except in the region adjacent to the body where flow separation and attendant vortex shedding are predominant. When this condition prevails, the well-known Morison's equation which assumes that the force is simply the sum of a component due to drag and one due to inertia can be applied. The successful application of Morison's equation, however, depends on the proper choice of the two coefficients pertaining to the drag and the inertia. The choice may not be all that straightforward in realistic situations as shown by

Hogben et al.[29], but these coefficients can be estimated by experiments. The effect that these estimated wave forces have on the profile of the structure and the tension in the cable reinforcements is thought to be insignificant when the structure is located in deep water.

In section 3.2 some of the less important environmental factors which might affect the design of the proposed structure are briefly outlined. These include the installation and operational forces. Among operational characteristics to be considered is the effect of marine fouling over the lifetime of the structure. In addition to corrosive action, marine fouling will also increase the size and the roughness of the structure with regard to hydrodynamic drag and inertia forces. Another factor which has to be considered in the design of any ocean structure is the effect of impact from floating objects. The dynamic behaviour of the proposed structure has not been looked at in detail in this study because in small structures, the fundamental periods of vibration are much shorter than those of waves with significant energy content and therefore the possibility of violent oscillatory behaviour in such structures is small.

3.2 Hydraulic Forces on Underwater Structures.

In order to design any structure, it is necessary to know the requirements of the proposed use of the structure and the characteristics of the environment in which the structure is to be located. These requirements are well defined for most structures which are built on dry land but have not been fully developed in the case of offshore structures. This is mainly due to the very complicated nature of structure-fluid interaction and the complex behaviour of the water waves and currents in the real situations. It is therefore of prime importance to predict as accurately as possible the design requirements of the fluid environment in which the proposed structure is to be located. Since there are no accurate theoretical methods for the calculation of fluid forces on offshore structures, most of the design requirements for these structures have to be determined by experimental methods. In spite of the uncertainties and limitations involved in small-scale model experiments, these experiments are the most common method of predicting the behaviour of offshore structures in the fluid environment.

The elements of the environment which might affect the design of the proposed structure are waves, currents, water pressure, earthquakes, corrosion, impact from floating objects and the reactive forces of the foundation medium. Several of these elements have a dynamic nature. Of fundamental importance among these are the wave loads and the hydrodynamic pressure due to earthquakes. Due to the fact that the fundamental periods of small sized structures are much shorter than those of waves in the ocean environment, a quasi-static analysis of the fluid loading on these structures may suffice. However, a dynamic analysis would assist in determining the structural behaviour with better accuracy. The dynamic characteristics of a structure which affect its response in the state of submergence are the natural period of vibration and damping. A system has a longer period of vibration and a higher damping when vibrating in water compared to that in air. It has been concluded by Chandrasekaran[13] that the increase in the natural period of vibration of a system is only attributed to an increase in the apparent mass of the system due to the participation of the surrounding water in the motion. The hydrodynamic pressure effects can therefore be represented on the basis of the virtual mass concept as described by Altinisik[1].

In the hydrostatic analysis of a submerged offshore structure, the first and foremost force which has to be considered is the force exerted on the structure due to its state of submergence in the fluid environment. By Archimedes' principle a submerged object is buoyed up by a surface-directed force equal to the weight of the displaced liquid. Hydrostatic forces due to submergence are the most critical forces acting on a structure in the ocean environment. The buoyancy force on the proposed flexible membrane structure is the largest force acting on the structure and has to be considered in the design of its anchorage system. It has been shown by C.M. Hix[28] that solid mass anchors that have a submerged weight equal to the buoyancy force of an offshore structure have a factor of safety against uplift and are therefore a suitable method of anchoring the proposed structure. The second largest force on an offshore structure is the static pressure force of the fluid environment. It is the main factor that has to be considered in the design of the structure properties and shape. In spite of the fact that the static pressure in a fluid increases with the depth of the fluid, this does not imply that the

pressure force on the membrane increases with depth in this particular case. It does, however, imply that the internal pressure of the structure should increase in order that the designed equilibrium configuration is obtained.

The second important set of factors which has to be dealt with in the design of offshore structures are those associated with waves and currents. In general current effects are important mainly as a velocity vector addition to the wave celerity vector. Current velocities are the principal source of loads for deep sea-based structures; as a transport mechanism, they cause the gradual erosion of the sea-bed and as a hydraulic impediment they cause changes in the pressure distribution on the structure which give rise to a drag force. Wave forces are due to the pressures and orbital velocities of water particles. The magnitude of the wave force on a structure depends upon the size and shape of the structure and upon the total energy being transmitted by the wave. Wave forces diminish exponentially with depth from the free surface and their effects become negligible at depths greater than one-half the length of the wave as is shown by Wiegel[66]. In cases where the size of the structure is small compared to the wavelength of the incident wave, the wave force can be determined by applying the well-known Morison's equation which simplifies the general problem of wave-structure interaction in that it allows the assumption that the presence of the structure has no effect on the incident wave. Accordingly it may be assumed that the flow field existing at the centre of the structure extends to infinity and the force due to wave can be represented as the sum of two independent components, namely drag and inertia which are in phase with velocity and acceleration respectively. By using Morison's equation,the magnitude of these force components can be estimated by invoking two parameters known as the drag coefficient and the inertia coefficient respectively. These two parameters must be chosen mainly on the basis of empirical data. Due to viscosity of fluids, the evaluation of these two parameters has always presented problems of similarity and scale. It is often the case that the prototype has large values of Reynolds number which is difficult to reproduce in the laboratory.

Nevertheless, until a theoretical method for calculation of such forces is developed, designers have to rely on experimental methods for determination of these coefficients. Since the main effect of current velocities is to add vectorially to the wave velocity vector, the evaluation of forces due to currents impose similar problems to those associated with the evaluation of forces due to waves.

The hydraulic forces explained above are all of deterministic type and are transmitted by fluid pressure fluctuations normal to immersed surfaces which are caused by the relative motion between the fluid medium and the structure. Three types of loads which are not transmitted by fluid pressure fluctuations are (Leonard[42]): the geotechnical forces, the surface forces and the installational and operational forces. In the case of bottom-fixed structures in deep waters, which do not have any structural components on or above the ocean surface, the surface forces such as ice or wind loads are negligible and need not be considered. However, the effects of geotechnical forces which are transmitted to such structures by motion of the sea floor have to be investigated. The primary geotechnical force which has to be considered with regard to a bottom fixed structure is that caused by a seismic event. A structure which is rigidly connected to the ocean floor will be more susceptible to damage but a structure attached in a flexible manner will not be subjected to such severe forces. In the seismic analysis of offshore structures, the effects of both added mass and hydrodynamic damping on structural motions must be included since these two parameters significantly affect the structural mass and damping matrices such that lower natural frequencies are obtained. Other geotechnical forces such as those produced by seabed destabilization due to extensive erosion or scour should also be looked at. A study of the physical properties of sediments on the sea-bed where the structure is to be located and a general geological knowledge of the location should be carried out so that hazardous environmental factors can be avoided. Subsurface conditions are generally such that the allowable bearing capacity of the sediment is not great enough to support the weight of the structure without an extensive foundation structure.

Loads applied to an offshore structure during implantation of the system need to be carefully considered because the primary design may have been based on a certain configuration of the structure or on loads which may not be present

during installation. One of the operational characteristics to be considered is the effect of marine fouling over the lifetime of immersed structural components. Some marine foulings have corrosive actions which might lead to the destruction of the structural components. The effect of marine fouling therefore plays an important role in the choice of the material of the structure and its maintenance. In addition to corrosive action, marine fouling can also increase the size and roughness of structural members with regard to hydrodynamic drag and inertia forces. Another factor which has to be considered in the design of an ocean structure is the possibility of the structure being struck by a floating or falling object. Fixed structures which have components projected up to and above an elevation of 20 m below the water surface, are in danger of collision by passing ships. The impact by falling objects cannot be predicted. If the structure is flexible or if the anchorage system is flexible, there will be a smaller instantaneous force acting in a collision compared to the case where the structure and the anchorage are rigid. In some cases it might be possible to design a protective cover for the structure or to provide hazard markings so that the possibility of damage due to falling or floating objects is reduced.

In the design of most offshore structures certain phenomena such as chemical, electrolytic and thermal reactions must be considered. The most important chemical and electrolytic reaction in offshore structures is that of corrosion. The rate at which a structure or a section of it is corroded is strongly dependent on its material and the environment in which it is placed. Galvanic corrosion in sea water occurs because the water is a good electrolyte and the system of the structure acts as a battery. Many types of protective coatings have been designed for different common materials against corrosion. Consideration must also be given to forces caused by expansion and contraction of structure members due to temperature changes inside and outside the structure (Hix[28]). A maximum average annual variation in temperature of about 8° C has been reported by Hill[27] for the ocean as a whole. Depending on the material of the structure members, they will experience some changes in their dimensions when they are subjected to this change in temperature. If the structure is used for storage purposes, the internal temperature changes of the structure due to loading and unloading of the stored substance must be considered and the balance of internal and external temperature has to be studied. The effect of external

temperature changes on the expansion and contraction of the stored substance should also be allowed for. Fixed storage structures should not be constructed in areas where icebergs may be encountered because firstly in iceberg regions, the minimum water temperature is very low and therefore there will usually be high temperature differences between the surrounding ocean environment temperature and the temperature of the stored substance and secondly icebergs are a threat to structures due to the great momentum of the floating icebergs.

In the following sections the effect of some of the more important hydraulic forces on the proposed structure will be examined.

3.3 Ocean Currents.

There are several main types of currents in the oceans. Wind-drift currents are those developed from friction exerted on the surface of the water by steadily blowing wind. Tidal currents are caused by tidal actions and are of three types; the rotary type, the reversing type and the hydraulic type. In the open ocean tidal currents are usually rotating due to the effect of the Coriolis force. Density currents are caused by difference in the density of water. Wave-induced currents are generated by the wind blowing over the water surface. Part of the energy transmitted by the wind to the water is in the form of surface currents. Major ocean currents are generally considered to be a part of the oceanic circulation due to the distribution of mass in the ocean which is developed by heating at the tropics and cooling at the poles. Far more is known of the surface currents of the ocean than of the deeper currents mainly because of the difficulties encountered in studying deep ocean currents. Nevertheless, design data are available for both shallow and deep ocean currents. In general currents cause the following effects:

(a) As a hydrodynamic impediment they cause a drag force proportional to the square of the velocity.

(b) As a transport mechanism they cause a drift effect on floating equipment or debris. The transport of debris which is proportional to the first power of velocity gives rise to scouring on the sea-bed.

(c) As a source of vertical and horizontal shear, they can seriously interfere with cables or subsurface operations.

In relation to the proposed structure, the most pronounced effect of currents is the drag force caused by deep ocean currents. In this section, this effect is studied both theoretically and experimentally. The scouring effect of the currents is studied in a later section.

3.3.1. Theoretical analysis of the effect of ocean currents.

An accurate theoretical analysis of the effect of currents on offshore structures is hardly possible because of the complications due to many factors including the turbulent flow process about the structures, non-uniformity of currents in the real situations, the effect of the boundary layer and the natural variability of the forces related to vortex shedding. The analysis can however, be greatly simplified if it is assumed that the flow is incompressible, irrotational, frictionless and uniform and the effect of the boundary layer is neglected in which case the incompressible potential flow theory can be applied. In most cases including the case of the proposed structure, the potential flow theory leads to a conservative analysis and is therefore safe to use. The analysis is further simplified by assuming that the structure is two dimensional, rigid and the undisturbed flow velocity at infinity is parallel to the minor axis of the structure although currents in the ocean are in different directions. It is observed that the cross-section of the proposed prototype can very nearly be approximated by the shape of a semi-ellipse whose major and minor axes are 6.84 and 3.93 m respectively. Figure 3.1 shows the comparison of the actual cross-section of the proposed structure and the above mentioned semi-ellipse. Because of the close similarity of the cross-section of the proposed structure to this semi-ellipse and due to the fact that the application of the potential flow theory to the streaming past an elliptic cylinder is an easier task and solutions have been obtained by Lamb[35] and Milne-Thomson[45], it is decided to carry out the theoretical analysis of the effect of ocean currents on the elliptic cylinder whose cross-section is shown in figure 3.1. Although the available

solutions in the above mentioned references are all related to the case of the elliptic cylinders whose major axes are in the direction of the flow, they can be easily changed to be used for the case of the proposed structure which is assumed to have its minor axis in the direction of the flow. Furthermore, because the effect of the boundary layer is ignored, by taking advantage of the symmetry, the solution to a full-elliptic cylinder can be applied to a semi-elliptic cylinder.

The detailed solution of the problem is given by Milne-Thomson[45] It is found that the complex potential ω is given by

$$\omega = \tfrac{1}{2} U (a + b) \left\{ \frac{[z - \sqrt{z^2 - (b^2 - a^2)}]}{b - a} - \frac{[z + \sqrt{z^2 - (b^2 - a^2)}]}{a + b} \right\} \quad (3.1)$$

where U is the undisturbed velocity at infinity, a is the axis which lies in the direction of the flow or the minor axis in this case and b is the other axis. These parameters are shown in figure 3.2 below. It can

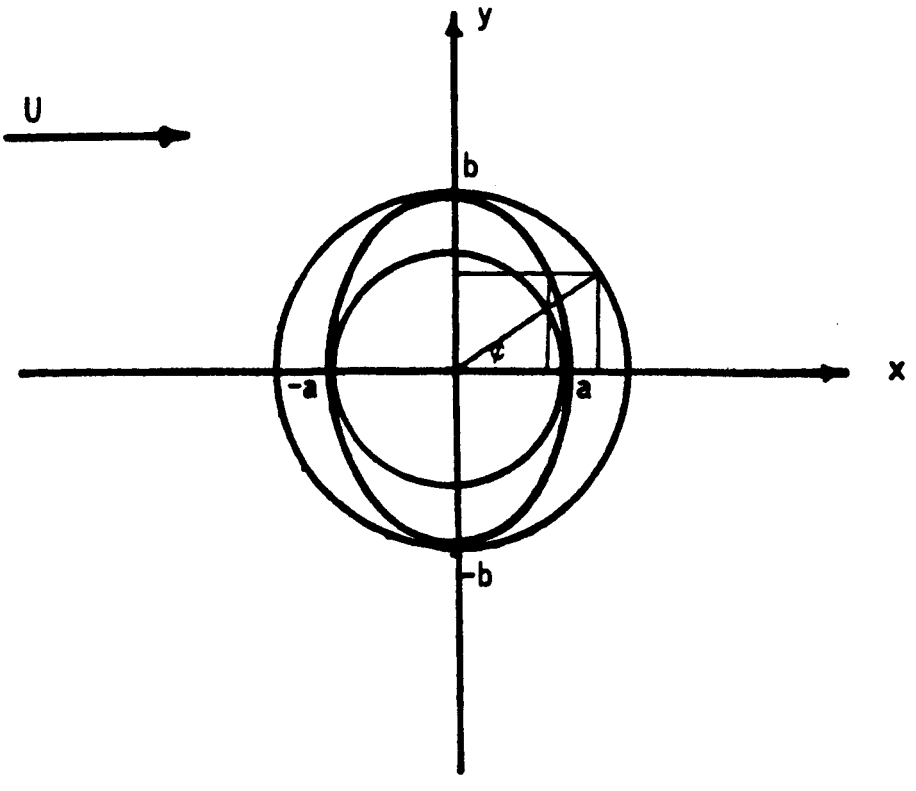

Figure 3.2 - Geometry of an ellipse.

be seen from figure 3.2 that the co-ordinates of any point on the ellipse are given by

$$x = a \operatorname{Cos} \varphi \; ; \quad y = b \operatorname{Sin} \varphi \tag{3.2}$$

The potential velocity of the fluid at any point on the surface of the elliptic cylinder is found to be:

$$u(\varphi) = U \frac{(1+k)}{\sqrt{1+k^2 \operatorname{Cot}^2 \varphi}} \tag{3.3}$$

where $k = \frac{b}{a}$.

The computer program developed in chapter two analyses the proposed structure on the basis of the pressure distribution around its surface. It is therefore wiser to find the change in the pressure distribution around the structure due to the steady current of velocity U, rather than calculating the drag force due to that current. Using Bernoulli's theorem, the pressure p at any point on the surface of the elliptic cylinder is given by:

$$\frac{p}{\rho} + \tfrac{1}{2} U^2 \frac{(1+k)^2}{1+k^2 \operatorname{Cot}^2 \varphi} = \frac{P}{\rho} + \tfrac{1}{2} U^2 \tag{3.4}$$

in which P is the pressure at infinity and ρ is the fluid density. To find where the pressure is greatest and least, the derivative $\frac{dp}{d\varphi}$ should be equated to zero, which leads to a value of $\varphi = \frac{\pi}{2}$ for the point of minimum pressure and a value of $\varphi = 0$ and π for the point of maximum pressure. The point given by $\varphi = 0$ is the stagnation point. Normally the pressure distribution around a structure is expressed in terms of the pressure coefficient C_p which is defined as:

$$C_p = \frac{p - P}{\frac{1}{2} \rho U^2} \tag{3.5}$$

In the case of the elliptic cylinder, the pressure coefficient is found to be

$$C_p = \frac{k^2 + \operatorname{Sin}^2 \varphi (-2k^2 - 2k)}{k^2 + \operatorname{Sin}^2 \varphi (1 - k^2)} \tag{3.6}$$

which has a value of 1 at stagnation point and has a minimum value of $(-k^2 - 2k)$ at $\varphi = 90^0$ and is symmetrical about the $\varphi = 90^0$ point.

In order to plot the distribution of C_p along the perimeter of the elliptic cylinder, the relation between s, the length along the perimeter and the angle φ should be known. For the case of $k > 1$, this relation is given by:

$$s = a\,k\,E(\gamma, \varphi) \tag{3.7}$$

where

$$\gamma = \arcsin\sqrt{1 - \frac{1}{k^2}} \tag{3.8}$$

and E is the incomplete elliptical integral of the second kind. The distribution of the pressure coefficient C_p against s, distance along the perimeter is calculated on the basis of the potential flow theory and is plotted in graph 3.5a. It is well understood that the pressure coefficient in a real situation cannot be exactly predicted using potential flow theory and that the distribution of C_p in real fluid situations, deviates greatly from the distribution of C_p in the ideal fluid situation, except for a short distance close to the stagnation point. Nevertheless, at relatively high Reynolds numbers, the pressure distribution at the upstream region of the structure does not differ greatly from the theoretical results. The case of the real fluid is better understood by experiments which are explained, together with the results, in the next section.

The main cause of the descrepancies between the theoretical results and the actual behaviour of the real fluid is that the potential flow theory is based on the assumption that the fluid is frictionless. Although in regions far from the structure, the friction of the fluid is unimportant and the flow is essentially ideal, near the structure, the fluid develops a shear layer where the viscosity is important. The boundary layer is developed as a result of the viscous action in the fluid and is the cause of the formation of wake behind the structure. The wake which is generally a region of high turbulence and low pressure, is due to the separation of the boundary layer from the surface of the body and gives rise to a friction drag on the structure. The concept of boundary layer is explained in detail by Schlichting[58]. In order to find the point of separation of the flow from the structure, the boundary layer equations must be solved. These

equations are not valid after the separation point because the assumptions on which they are based, no longer apply. An approximate method has been suggested by K. Pohlhausen[54] for the calculation of laminar boundary layer and the method has been applied to the case of elliptic cylinders whose major axes are parallel to the direction of the flow. In this study the same method is applied to the case of the elliptic cylinder shown in figure 3.2, which has its minor axis parallel to the direction of the flow and the results are plotted in graphs 3.1 to 3.4. The results would still not give the accurate solution to the effect of current on the proposed structure because firstly in the real situation the boundary layer is not laminar but is turbulent and secondly the cross-section of the proposed structure is similar to a semi-ellipse and not a complete one and therefore the stagnation point might not coincide with the point of $\varphi = 0$. Nevertheless, the results obtained from the boundary layer calculations are bound to improve the results of the potential flow calculations and may be used as a better guide for design purposes.

In order to calculate the laminar boundary layer, the first derivative of the velocity with respect to the distance along the perimeter is required. This derivative is found to be:

$$\frac{d\frac{u_o}{u_\infty}}{d\frac{s}{t}} = \frac{2(1+k)k^2 \cos\varphi}{(\sin^2\varphi + k^2\cos^2\varphi)^2} \qquad (3.9)$$

The variation of this derivative has been plotted in graph 3.1 against the length along the perimeter. It is observed that the curve initially rises gradually to a maximum but then it falls sharply to zero at the mid-point along the half-perimeter of the ellipse. Equation 3.9 is used in the approximate method of solution of the boundary layer equation. It is found that the separation point of the laminar boundary layer occurs at $s = 0.535S$ where S is the length of the half-perimeter of a full ellipse and s is measured from the stagnation point ($\varphi = 0$). The variation of the momentum thickness of the boundary layer, the shape factor and the shear stress have been plotted against the perimeter length of the ellipse in graphs 3.2, 3.3 and 3.4 respectively. From graph 3.3 it is observed that the shape factor starts at $\lambda = 7.05$ and increases

to a maximum value of about 8.6 at $s = 0.35\ S$, after which it falls rapidly. The increase of the shape factor shortly after stagnation point is due to the increase in the velocity gradient at that region. The curve of the momentum thickness in graph 3.2 shows that the momentum thickness starts from a value of about 0.2 and decreases to a minimum value of 0.16 after which it tends to rise. The minimum value of the momentum thickness occurs between the point of minimum pressure and the point of inflection of the pressure. The curve in graph 3.4 shows that the shear stress increases sharply to a maximum value of about 10 at the point $s = 0.45\ S$ and then falls rapidly to zero at the point $s = 0.53\ S$.

As mentioned earlier, in the real flow situation the boundary layer would not be laminar and would exhibit a turbulent characteristic feature. At the present time, the complicated turbulence phenomena are far from being understood completely but there are in existence several semi-empirical methods of calculation which lead to comparatively satisfactory approximate results. The empirical relations which have been used for the study of flows past different shaped objects do not suffice for the development of such semi-empirical methods and additional hypotheses become necessary (Schlichting[58]). Because of the complications and the inaccuracies involved in the available semi-empirical methods of calculation of the turbulent boundary layers, it is decided not to carry out any such calculations in this study.

3.3.2. Experimental Study on the Effect of Current.

The importance of an adequate estimation of the effect of ocean currents on the proposed structure has been discussed in a previous section. In section 3.3.1 it has been concluded that the real behaviour of the pressure distribution around a structure due to current, cannot be obtained by any theoretical analysis developed up to the present time. It is fairly obvious that until a better theoretical method for the prediction of the effect of current is developed, designers are forced to rely upon experimental methods for the design criteria. These experimental methods may

be either model studies or full-scale studies. Since full-scale studies are not feasible in the case of the proposed structure due to various problems including the expenses involved, model studies have been adopted for the study of the effect of current on the proposed structure. Model studies are comparatively cheap and easy to construct and are convenient to test. However, it is well understood that the results of the experimental tests on models can only provide an indication of the behaviour of the structure in the real situation and the exact behaviour of the structure cannot be modelled because of the limitations imposed by scale effects. These limitations are enhanced in the case of experimental studies in the effect of oceanic waves and currents on offshore structures mainly due to the restricted sizes of the laboratory flumes and the impossibility of generating waves and currents of characteristics similar to those of the real situation.

In the experimental work conducted in this study, an important simplification has been adopted. This simplification is that all the experiments have been carried out on rigid models instead of flexible ones. The reason for not using flexible models is that it would be difficult to measure the pressure on the surface of a flexible model. The Reynolds number $(\frac{DU_o}{\nu})$ in the real situation is high and in the order of $10^7 - 10^8$. It would have been ideal if such high Reynolds numbers could be reached in the current flume but the size of the existing flume restricts the size of the model and the small rate of discharge of the flume prevents the desired high velocities to be reached. As a result, it is not possible to obtain Reynolds numbers greater than 2×10^4 in the existing flume. It is therefore decided to use the wind tunnel instead. The maximum Reynolds number which can be obtained in the available wind tunnel is about 1.1×10^6 which although is not high enough, is an improvement to that obtainable in the current flume.

On the whole, four sets of experiments have been conducted on the effect of current on the structure. In all the experiments, the pressure distribution at a number of points on the surface of the model has been measured and the values of the pressure coefficients C_p have been

calculated for those points. The distribution of these pressure coefficients is then represented in the form of a curve for each experiment. Later, these curves are used for estimation of the pressure distribution due to current on the proposed structure. The estimated values of the pressures are then fed into the computer and the changes in the profile and also the changes in the tensions of the cables of the proposed structure due to current are computed by the computer.

The cross-section of the main model for the purpose of this experiment is very similar to that of the proposed structure and of scale 1:100. Since it is a difficult task to make a rigid model with that cross-section, it is decided to make only one model in that shape. Also, because the material chosen for the construction of this model is not suitable for tests in water, the model is made such that it can be fitted and tested in the wind tunnel. Although it would be preferable to test the model in the current flume as well as in the wind tunnel, as mentioned earlier with regards to the Reynolds number, the tests in the current flume would not have resembled the case of the high Reynolds numbers in the real situation. In the theoretical analysis of the effect of current on the structure (section 3.3.1.) it has been assumed that the cross-section of the structure is a semi-ellipse. In order to establish the similarity between the actual cross-section of the structure and the semi-ellipse of the theoretical analysis, from the point of view of the effect of current, a scaled model of that semi-elliptical cylinder has been constructed in the same way as the model of the proposed structure and it is tested under exactly the same conditions as that of the main model. The results of the two sets of experiments can then be compared.

Since there are no such experimental results for the main model, in the literature and only one set of experimental results has been found in the literature, for elliptical cylinders whose minor axes are in the direction of flow (Modi[47]), the correctness of the experimental procedures and the accuracy of the results of the tests in this study cannot be checked. It is therefore decided to perform the same experimental procedure on a full circular cylinder and a semi-circular cylinder, for which results of such experiments are readily available in the literature for the purpose of

comparison so that the accuracy of the experimental method adopted can be checked. In the case of the semi-circular cylinder, a series of tests have been conducted in the current flume and the results have been compared with those of the wind tunnel at approximately the same Reynolds numbers .

In this section,first each of the four models made for these experiments are described in detail. Then the wind tunnel and the current flume used are briefly discussed. Next, the measuring apparatuses used during these tests are described followed by full explanations of the experimental procedures carried out both in the wind-tunnel and the current flume tests. Finally the results obtained in these experiments are discussed.

3.3.2.1. The Models for the Experiments on the Effect of Current.

In the experiments on the effect of current, a total of four models have been used. All the models are cylindrically shaped. The sizes of the cross-sections of the models have been chosen such that they are as small as possible from the construction and measurement points of view. This is because it is desirable to minimize the blockage ratio in the wind-tunnel so that the effect of wall interference is as little as possible. The length of the models are such that they run across the total internal depth of the wind tunnel or the total width of the current flume and the ends of the models are close enough to the side walls of the tunnel (or flume) so that the flow is restricted past the ends. The detailed description of the models are as follows:

Model 1 - Scaled Model of the Proposed Structure (Photo 1). The cross-section of this model is shown in Photo 1. The scale of the model relative to the proposed prototype is in the ratio of 1:100. The model has been made up of sixteen strips of Balsa wood, each being 11 mm wide and 300 mm long. The width of each strip is 1/16th of the perimeter of the model.

At the center of each strip, a long polythene tube is inserted for measuring the pressure at that point. The external and the internal diameter of the tubes are 4 mm and 2 mm respectively. Four pieces of Balsa wood are then cut in the shape and size of the cross-section of the intended model. These pieces provide the supporting stiffeners inside the model and they prevent distortion of the model. They are equally spaced apart and the strips are glued onto them and to each other side by side to form a cylindrical shape. The glue used for this purpose is Balsa cement which is also used in model aircraft making. The outer surface of the model is then smoothed and varnished. The tubes which run to the inside of the model are cut from the outside flush with the model surface so that there are no discontinuities at the outer surface of the model. The tubes are then numbered according to the positions of the strips through which they run. Ideally the total number of the strips used for making up such models should be as high as possible and the width of the strips should be minimum. In the case of this model, a width of 11 mm for each strip is considered to be acceptable mainly because of the plastic tubes which have to be inserted in the strips. The model is then mounted on a rectangular piece of board which is 335 x 225mm. The board has a 25 x 50 mm hole at its centre through which all the sixteen tubes come out. This board replaces a section of a side wall of the wind tunnel such that there are no discontinuities inside the wind tunnel at that side wall except for the model itself. In this way, the base of the model is at exactly the same level as the inner surface of the side wall on which it has been mounted. The sixteen plastic tubes run outside the wind tunnel to be connected to the measuring apparatus.

Model 2 - A Semi-Elliptical Cylinder (Photo 1).

The cross-section of this model is in the form of a semi-ellipse. The dimensions of the cross-section is 1/100th of the

dimensions of the ellipse analysed in section 3.3.1. and it looks as if that ellipse has been cut along its minor axis. The model is constructed in exactly the same way as the previous model and therefore it will not be described any further. Photo 1 illustrates the two models side by side for comparison of the cross-sections. The position of the model in the wind tunnel can be seen in photo 2.

Model 3 - A Full-Circular Cylinder

This model is simply a hollow perspex tube of external diameter 63.5 mm and it is 300 mm long. Mid-way along its length it has a 1 mm diameter hole. One end of the cylinder is completely blocked and the other end is fitted with a circular plate through which a narrow plastic tube runs. All the pressure of the inside of the model which is due to the pressure at the tapping point, is transmitted to the measuring apparatus by the plastic tube. The model is mounted on a section of the wind tunnel side wall so that the length of the model runs across the inside width of the wind tunnel. The model is then connected to a rotating disc from the outside of the tunnel in such a way that the model can be rotated manually and the position of the tapping point on the model can be adjusted at different angles relative to the direction of the flow. The rotating disc is shown in Photo 3.

Model 4 - A Semi-Circular Cylinder (Photo 4).

This model has originally been designed for tests in the current flume and then it is reduced in length so that it can be fitted into the wind tunnel. The idea of having a rotating model with only one tapping point is used as in Model 3. The semi-circular model consists of a 110 mm diameter p.v.c. circular cylinder. The cylinder is divided into three parts. The two end parts are fixed but the middle part can rotate about its central axis. A brass plug which has a 1 mm hole, is inserted in the middle part of the model. One

end of a long narrow plastic tube is connected to this hole to transmit the pressure to the measuring apparatus. The cylinder is marked around its perimeter at ten degree intervals. When the model is used in the current flume, it rests on the bottom of the flume horizontally. A piece of horizontal perspex plate as wide as the flume is then connected to each side of the model such that only one half of the cross-section of the model stands above the perspex plates. In this way the perspex plates form a secondary base to the flume and the model appears as a semi-circular cylinder resting on the perspex base. The length of this secondary base is increased along the length of the flume by using two horizontal wooden boards. The boards are wide enough to cover the whole width of the flume and their heights above the actual base of the flume are adjusted so that there are no discontinuities along the secondary base. The positioning of this model in the current flume is shown in photo 4. In order to use this model in the wind tunnel, it is cut such that the tapping point stays midway along the total length of the model. The model is then fitted to a section of a side wall of the wind tunnel vertically such that exactly one half of its cross-section stays inside the wind tunnel and the rest of its cross-section is left outside. The model thus behaves as a semi-circular cylinder inside the wind tunnel.

The tests on the four models in the wind tunnel and the test on model number 4 in the current flume are discussed in a later section.

3.3.2.2. The Wind Tunnel.

The wind tunnel in which the experiments are conducted is shown in Photo 5. It is basically a closed jet, open-circuit low speed type wind tunnel with two contra-rotating fans which run independently. The air speed inside the tunnel can be

varied in the range of about 5 to 35 m/s. The intake area is about 6 times that of the working section. The square cross-section of the working area has a rather small internal dimension of 300 x 300 mm. The effect of wall interference is therefore considerable and has to be accounted for in the results of the experiments. Prior to conducting the experiments the spatial distribution of velocity in the working section is determined by measuring the variation of pressure at different points in that section using a pitot-static tube. The velocity distribution obtained in this way has shown that in a 250 x 250 mm area in the center of the tunnel cross-section, the velocity is almost uniform. Each of the side walls of the working section of the tunnel has of a number of easily replacable sections. The model which is to be tested, is mounted on a suitable piece of board and the board replaces one of these sections. Apart from the usual uniform velocity profile, a velocity profile simulating a boundary layer can also be generated in the wind tunnel. This is done by placing a series of rods at the most upstream part of the tunnel. The spacing between the rods can be adjusted to produce any desired velocity profile in the tunnel.

3.3.2.3. The Current Flume.

The current flume used for the test is basically a rectangular tank which has a height of 300 mm and a width of 610 mm. The overall length of the tank is approximately 6.5 m. The water is circulated by means of a pump and variation in the flow rate can be achieved by suitable adjustment of a flow control valve situated adjacent to the pump. The flow rate is measured by a turbine flow meter. The water discharges freely at the downstream end of the flume. The depth of water in the tank can be varied by means of placing appropriate numbers of weir elements at the outlet end of the flume. In testing the proposed

model, the maximum velocity which can be obtained in the flume without occurence of a hydraulic jump is 0.35 m/s. In order to verify that uniform flow conditions are present, the horizontal and vertical profiles of the flow are determined at the position just upstream of the model. This is carried out in the absence of the model. The pressure at a number of different heights above the tank bottom along a vertical and a horizontal line is measured by a pitot tube and the distribution of velocity in the horizontal and the vertical directions is determined. The result of the vertical velocity distribution has shown that the boundary layer at the position of the model is quite thin.

3.3.2.4. The Measuring Apparatus.

The pressure measurements in these experiments have all been carried out by use of different types of manometers. In the experiment in the current flume, a U-tube manometer is used. The maximum accuracy which can be acquired with it is about 1 mm of water. In the wind tunnel experiments on the circular and the semi-circular cylinders where only one tapping point is involved, a single tube variable inclination manometer is used. The maximum accuracy obtainable with this manometer is 0.05 mm of water. In the experiments on Model 1 and Model 2 for each of which pressure at sixteen tapping points has to be measured, a multi-tube variable inclination manometer is used. The advantage of using a multi-tube manometer is that it not only reduces experimental time, but also because the pressure at all the tapping points is measured simultaneously, the inaccuracies involved in trying to produce exactly the same flow velocities for each of the sixteen tapping points is considerably reduced. The reference pressure can also be connected to one of the tubes of the multi-tube manometer. The accuracy of the measurements can be increased by tilting the plate on which the tubes are mounted.

3.3.3. Experimental Procedure.

(a) Wind Tunnel Experiments. The model is placed in the wind tunnel and it is ensured that there are no leaks in the working section of the wind tunnel. A pitot-static tube is placed in the wind tunnel upstream of the model and 60 cm away from it. In order to measure the velocity in the tunnel and to ensure that it does not change during the experiment, the pitot-static tube is constantly connected differentially to the inclined manometer or to two separate tubes of the multi-tube manometer and the pressure differential across the two ends of the pitot-static tube is recorded. The wind velocity in the tunnel can then be calculated from the measured value of the pressure differential. A pitot-static tube is traversed horizontally across the working section of the tunnel and the distribution of the local static pressure across the model is measured in the presence of the model. The local static pressure distribution hence obtained differs from the static pressure measured upstream of the model since it bears the effect of presence of the model.

In the experiments on the models which have sixteen tapping points, each tapping point is connected to a seperate tube of the compound manometer and the total pressure at each tapping point is recorded from the manometer. The dynamic pressure at each point is then obtained by subtracting the value of the corresponding local static pressure from the measured value of the total pressure at that point. In the experiments on the models with one tapping point, a static probe is placed in the wind tunnel upstream of the model and it is connected to one end of the inclined manometer while the tapping point of the model is connected to the other end. The pressure differential is measured from the manometer at every ten degree intervals of the position of the tapping point relative to the direction of flow. The measured pressure is later corrected for the difference between the local static pressure and the upstream static pressure.

(b) Current Flume Experiment. As mentioned earlier, the semi-circular model is tested in the current flume as well as the wind tunnel. The pressure on the model is measured by an inclined U-tube manometer. One end of the manometer is left open and the other end is connected to the model tapping point via a 'T' piece. The free branch of the T piece is connected to a static probe placed in the flume. The tubing of any branch of the 'T' piece which is not being measured is closed firmly by a hose clamp. Before taking any measurements, the manometer and all the tubings are kept in water for a while so that all the air in the system is released. Throughout the experiment great care is taken in ensuring that the manometer and the leading tubes are completely airtight. The static pressure at the upstream is measured a few times during the experiment. The model is rotated gradually so that the position of the tapping point relative to the direction of the flow changes from 0^0 to 180^0 at 10^0 intervals. At each interval the pressure at the tapping point is measured by the manometer. The draw down of the water surface due to the presence of the model is measured by a vertical vernier probe at 2 cm horizontal intervals in the vicinity of the model. The dynamic pressure at each point on the model is obtained by subtracting the upstream static pressure from the measured total pressure at that point and then correcting it by allowing for the effect of the draw down. Also, the static probe is traversed horizontally across the model and the value of the local static pressure is recorded directly at 2 cm intervals. The dynamic pressure at each point on the model can also be obtained by subtracting the corresponding measured local static pressure from the measured total pressure at that point. The two methods of measuring the dynamic pressure lead to exactly the same result.

3.3.4. Experimental Results.

The experiments on the model of the proposed structure and on the semi-elliptical model are carried out in the wind tunnel at two different Reynolds numbers of around 1.1×10^6, and 1.5×10^5. The pressure coefficients C_p are plotted against distance along the perimeter

in graphs 3.5a and 3.5b. The distribution of pressure around the cross-section of the model of the proposed structure at a Reynolds number of 1.5×10^5 is shown in figure 3.3.

The full circular cylinder is tested in the wind tunnel at Reynolds numbers of 1.6×10^5 and 1.2×10^5. The results are shown simultaneously in graph 3.6.

The experiment on the semi-circular cylinder in the wind tunnel is conducted at Reynolds numbers of 1.3×10^5, 0.9×10^5 and 1.6×10^4. The results are plotted in graph 3.7. Later the wind tunnel is fitted with the rods which produce a particular velocity profile across the tunnel and the pressure distribution around the semi-circular model is measured under the same flow that leads to a Reynolds number of 0.9×10^5 in the absence of rods. The result is shown in figure 3.4 together with the result of the similar experiment which is conducted in the wind tunnel before fitting the rods. The experiment on the semi-circular cylinder in the current flume is carried out at Reynolds numbers of approximately 1.6×10^4 and 1.2×10^4. The results are plotted in graph 3.7. The results of the experiment on the semi-circular cylinder in the wind tunnel and in the current flume at the same Reynolds number of 1.6×10^4 can thus be seen together in graph 3.7 for comparison.

3.3.5. Discussion of Experimental Results of the Effect of Current.

The experiment on the full circular cylinder has been conducted in order to provide a means of checking the validity of the experimental results as compared to the results already available in the literature. The result of Goldstein[23] which corresponds to wind tunnel tests on a 7.4 cm diameter cylinder at a Reynolds number of 1.06×10^5 is shown in graph 3.6 together with the results of this study on the 6.4 cm diameter cylinder at Reynolds numbers of 1.2×10^5 and 1.6×10^5. The general shape of the curves is similar and the results are in good agreement. The minimum pressure coefficients in the result of

Goldstein[23] and in the result of the present study at Reynolds number of 1.2×10^5, are both around -1.2 and they both occur between $\theta = 70^0$ and $\theta = 80^0$ where θ is the angular distance from the stagnation point. The points of separation of the boundary layer in those two results are also the same in both cases and are in the regions of $\theta = 82^0$ The region of fairly constant pressure at the back of the models are almost along the same positions in both curves. The biggest difference between the two curves is the angular distance at which zero pressure coefficient occurs; this angle is about 34^0 according to the published result whereas it is about 42^0 in the result of this study. Considering the difference in the size of the tunnels in which the two experiments are conducted and the experimental errors involved, this difference is considered as acceptable. The present results are also compatible with those of Roshko[57], Batham[6] and Vance[62] for circular cylinders.

The curves corresponding to the experiments on the semi-circular cylinder in the wind tunnel and the current flume are shown together in graph 3.7. Comparing the results of the two experiments at similar Reynolds numbers, it is observed that there is a 10 percent difference at the starting point of the two curves at $\theta = 0^0$. This difference may be due to the fact that the boundary layer thickness which develops along the wind tunnel and the current flume is different at the position where the model is placed in the two experiments. The general shape of the two sets of curves is similar but the pressure at the back of the model after the separation point is 30 percent higher in the case of the test in the current flume. In figure 3.4 the pressure distribution around the model due to a varying wind velocity is compared to the pressure distribution due to a uniform wind velocity. It can be seen that the general shape of the two pressure distributions is the same in both cases but the value of the pressure at every point on the model is always lower in the case of the varying wind velocity. The difference in the value of the pressure in the two cases is on average higher at the upstream side of the model. Graph 3.7 shows the distribution of the pressure coefficient on the semi-circular cylinder at Reynolds numbers of 1.3×10^5, 0.9×10^5 and 1.6×10^4. It is observed that the point at which the minimum pressure coefficient occurs and also the point of separation of

the boundary layer moves farther around the cylinder as the Reynolds number increases. This result is consistent with that of Goldstein[23] on full circular cylinders.

The results of the experiments on the semi-elliptical cylinder and the model of the proposed structure are shown ingraphs3.5a and 3.5b respectively. The curves for the model of the proposed structure correspond to two different Reynolds numbers of around 1.5×10^5 and 1.1×10^6. It can be seen that the pressure coefficient falls from its maximum value of about 1 at just after the leading edge, to a minimum value and then rises slightly and from around 0.55 of the perimeter to the back edge of the model it remains fairly constant. The comparison of the curves for the two models shows that from the pressure coefficient point of view,the model of the proposed structure behaves very similarly to the semi-elliptical cylinder model. In both cases the point of zero pressure coefficient occurs at about the same distance from the leading edge of the two models, the same is true for the point of minimum pressure coefficient and the point of separation of the boundary layer on the two models. The points of zero pressure coefficient and the minimum pressure coefficient occur at about 0.3 and 0.46 of the perimeter respectively while separation occurs around 0.54 of the perimeter from the leading edge. The experimental value of the separation point is in good agreement with the theoretical result for the full elliptical cylinder in a laminar boundary layer. At Reynolds number of 1.1×10^6, the minimum pressure coefficient on the semi-elliptical model is about -1.7 and on the model of the proposed structure is about -2.4. The pressure coefficients at the back of the two models are -0.65 and -0.45 respectively. Figure 3.3 shows the distribution of pressure around the model of the proposed structure at a Reynolds number of 1.5×10^5. In graph 3.5a the distribution of the pressure coefficient on the semi-elliptical cylinder obtained experimentally is compared with the theoretical results of section 3.3.1. It is observed that the two results differ considerably especially at the value of the minimum pressure coefficient and the behaviour of the curve at the back of the model. This discrepancy is not unexpected since the theoretical results have been based on the potential flow theory which does

not take into consideration the effect of the viscosity of the fluid and therefore it ignores the formation of the boundary layer along solid boundaries.

In the next section, the effect of pressure changes due to current on the proposed flexible structure is examined.

3.3.6. Effect of Current on the Profile of the Structure.

In sections 3.3.1 and 3.3.2 the effect of a uniform current on the pressure distribution around the structure has been studied theoretically and experimentally. In this section it is intended to use these results and to estimate the changes in the configuration of a fixed-ended cylindrical membrane structure, due to a uniform current in the direction perpendicular to the longitudinal axis of the strucutre. In order to be able to use the results of sections 3.3.1. and 3.3.2, it has to be assumed that the pressure distribution around a flexible structure due to a uniform current is almost the same as the pressure distribution due to the same uniform current on a rigid structure whose shape and size are exactly similar to the flexible one. It is also assumed that the theoretical pressure distribution around the proposed structure is the same as that around a semi-elliptical cylinder. Under these assumptions, the graphs of pressure coefficients C_p obtained in the last two sections can be used directly and the changes in the profile of the proposed flexible structure can be computed.

The velocity of deep ocean currents is usually taken as 1 m/s in the design of some offshore structures (Myers et al.[49]). It is therefore decided to study the effect of a uniform current of that velocity on the proposed structure. The Reynolds number produced under this condition is in the order of 10^7. Since there are not any experimental or theoretical curves available on the distribution of pressure coefficient on the proposed structure under such high values of Reynolds number, the curve corresponding to the highest Reynolds number available, which is 1.1×10^6,

is used. At Reynolds numbers of about 10^7, the flow is turbulent. In modelling techniques, it is usually accepted that for turbulent flow, the drag force changes very little with increasing the Reynolds number. However, there will be some changes in the shape of the pressure coefficient curve when the Reynolds number is increased. The most significant change produced by a higher Reynolds number is the reduction of the value of the minimum pressure coefficient. In fact it has been found by Roshko[57] that by increasing the Reynolds number, the pressure coefficient curve tends to get nearer to its theoretical curve obtained by the potential flow theory. It is therefore decided to calculate the changes in the structure profile on the basis of the pressure coefficients obtained theoretically as well as the pressure coefficients obtained experimentally at the Reynolds number of 1.1×10^6. In the experimental results of section 3.3.2. it has been shown that the distribution of the pressure coefficient around the model of the proposed structure is similar to that around a semi-elliptical cylinder. Thus, the result of the potential flow theory on the elliptical cylinder (section 3.3.1.) is used for the calculation of the changes in the profile of the proposed structure.

The method of incorporating the effect of the pressure due to current into the equilibrium equations is as follows: At the positions of the points of intersections of the cables on the circumference of the structure, the pressure values due to current are read off from the corresponding curves in graphs 3.5a and 3.5b. These pressure values are then combined with the values of the static pressure at the nodes. The resultant pressure at each node is equal to the algebraic difference between the two pressure values at that node. The deformation of the structure due to the effect of current is then computed based on the experimental and the theoretical values of the pressure coefficients. The results show that there are hardly any changes in the profile of the structure in connection with the changes in the pressure distribution around the structure under the effect of current. In fact in the case where the results of the potential flow theory are used in computing the change of profile of the structure due to the effect of current, it is observed that the maximum

displacement of the nodes is less than 6.0 percent of the displacement under static pressure condition. In the case where the experimental results of the effect of current are used, the corresponding maximum displacement of the nodes does not exceed 2 percent of the displacement under static conditions. As mentioned before, the Reynolds number for the proposed structure in a stream velocity of 1 m/s is in the order of 10^7. At this Reynolds number the curve of the distribution of the pressure coefficient is likely to lie somewhere between the curve obtained by the potential flow theory and that obtained experimentally for a Reynolds number of 1.1×10^6. It is therefore reasonable to expect that the deformed profile of the structure corresponding to a Reynolds number of 10^7 would lie somewhere between the two deformed profiles and the deformations would not exceed that of the potential flow curve. So the profile change due to the results of the potential flow theory, is the maximum change of profile that would occur in the structure. As stated above, the maximum displacement under this condition is less than 6.0 percent of the displacement under hydrostatic pressure and therefore it can be concluded that the effect of pressure due to deep ocean currents on the proposed structure is insignificant as compared to the hydrostatic pressure on the structure.

Apart from the changes in the profile of the structure due to the effect of current, it is evident that there will be some changes induced in the tension of the membrane and the tension in the reinforcing cables. The forces in the reinforcing cables of the structure have been computed for the two cases of the experimental and the theoretical estimation of pressure distribution due to the effect of current. The results obtained are shown on the corresponding cable segments in figures 3.5a and 3.5b. It is observed that the tension forces in all the circumferential cables are reduced under the effect of pressure changes due to current. In the case where the theoretical results of current is used, there is a reduction of around 3 percent in the tension of the circumferential cables whereas in the case of the experimental results of the effect of current, the corresponding reduction in the tension of the cables is about 1.0 percent. In the latter case, the forces in the cables on the upstream and

on the downstream of the structure are different due to the asymmetry of the pressure distribution on the two sides. The reason for the reduction of cable forces under the effect of current is that on some points on the structure, the current increases the external pressure on the membrane. This increase in the external pressure further balances the internal pressure of the structure and therefore leads to a reduction in the value of the resultant pressure acting on the membrane and the cables.

In view of the results of the investigations into the effect of current on the proposed structure, it has been concluded that the changes in the profile of the structure and the changes in the forces of the cables are not significant compared to the effect of the hydrostatic pressure and therefore the analysis of the structure on the basis of the hydrostatic pressure may suffice. However, the hydrodynamic effect of non-uniform currents which may induce dangerous vibrations in the structure, has not been investigated in this study. The scouring effect of currents are examined in section 3.5.

3.4 Ocean Waves and their Effects on the Proposed Structure.

Since all structures placed in the ocean are subjected to wave forces, it is important to predict the response of these structures to ocean waves. The problem of wave forces on submerged cylindrical objects is not completely understood because of the very complicated nature of the flow. These forces are influenced by several factors such as the Reynolds number, the roughness of the structure, the angle of skew and the proximity of the free stream and the ocean bottom, as explained by Wright and Yamamoto[68]. Most of the analytical methods available for the calculation of such forces do not incorporate all these factors at the same time. However, these methods have been proved to produce valid approximate solutions for the special cases to which they correspond. This is because the effects of some factors are less significant in those cases and these factors can be neglected without violating the validity of the solutions.

In determining the wave forces on submerged objects normally two cases are considered. The first case is when the size of the object is comparable with the wavelength. In this case the incident wave is scattered upon encountering the surface of the object. The amount of scattering depends on the geometry of the object, the depth of water and the wave characteristics. The analysis used for the solution of this case is generally referred to as the diffraction theory. In this analysis, viscous effects are neglected and the problem is solved in terms of the velocity potential that must satisfy appropriate boundary conditions for the problem. Once the potential function is obtained, the pressure distribution on the immersed surface as well as the resulting forces and moments are easily determined. Application of diffraction theory in the evaluation of wave forces on submerged objects has been used by Chakrabarti[11], Garrison and Seetharama[21], Garrison and Chow[22], Efthymiou and Narayanan[18] and many others. If the waves are of small amplitude and the object is relatively large so that the ratio of wave height to object size is small, the flow separation from the body would not be a dominant parameter and linear wave theory can be successfully applied, otherwise nonlinear wave theory must be used. The applicabilities of various wave theories are examined by Dean[15].

The effect of the free surface on the reflected wave can be incorporated in the analysis but this effect is negligible if the ratio of the water depth to the size of the object is sufficiently large.

The second case arises when the linear dimensions of the object are small compared to the wavelength. This condition simplifies the general problem of wave-structure interaction in that it allows the assumption that the presence of the body does not materially disturb the incident wavefield except in the region adjacent to the body where flow separation and attendant vortex shedding are predominant. Accordingly it may be assumed that the flow field existing at the centre of the object extends to infinity and the wave force can be represented as the sum of two components, drag and inertia. The expression for wave force which involves these two terms was originated by Morison[48] and is known as Morison's equation:

$$F = \tfrac{1}{2} \rho C_d A U |U| + \rho V C_a \frac{dU}{dt} \qquad (3.10)$$

In this equation ρ is the water density, U is the horizontal component of wave particle orbital velocity and V and A are the volumetric displacement and the projected frontal area of the structure respectively. The successful application of Morison's equation depends on the proper choice of the two coefficients pertaining to the drag and the inertia. These coefficients are for the most part obtained experimentally using either a laboratory model or a field prototype. Measured forces are correlated with either experimentally measured or theoretically calculated fluid velocities and accelerations. If the theoretical method is to be used for the calculation of the fluid velocity and acceleration, an appropriate wave theory has to be applied.

Since the proposed structure is used more efficiently in deeper waters (section 3.2), it would be ideal to estimate the wave forces on this structure in water-depths of about 100 metres. A typical set of design data for that water depth has been taken from 'Offshore installations: Guidance on design and construction'[16], which gives the fifty year storm wave data for the North Sea. This data is shown in Table 3.1.

Site	Approximate water depth (m)	Wave period (s)	Wave length (m)	Wave height (m)
North Sea	100.0	12	223	13

Table 3.1 - Fifty-year storm wave data.

Under this condition, it is observed that the size of the proposed prototype which is less than 7.0 m high, is small compared to the wavelength of the incident wave and the depth of the water. As mentioned above, when this condition prevails, Morison's equation can be safely used for the calculation of the wave forces on the structure. A prerequisite to the employment of Morison's equation is the correct evaluation of the coefficients of drag and inertia by model studies. It has been shown by Efthymiou and Narayanan[19] that when the Keulegan-Carpenter number ($K_c = \frac{U_m T}{D}$) is less than 4, drag effects may be neglected. Considering the design wave conditions in Table 3.1, it is found that drag effects can be neglected. An experiment has therefore been conducted on the model of the proposed structure in a wave tank in order to find the coefficient of inertia. The details of the experimental procedures and results are given in Appendix III. The application of Morison's equation to the proposed structure is explained in the next section.

3.4.1. Application of Morison's Equation.

It has been explained in the previous section that the relation between the size of the proposed structure and the characteristics of the typical wave conditions for which the structure is designed, allows the application of Morison's equation for the evaluation of the forces due to waves acting on the structure. As mentioned before, when this condition prevails the effect of wave scattering is negligible and the wave force can be approximated by the sum of two components, namely drag and inertia. The component due to drag is proportional to the product of a drag coefficient, C_d, and the square of the velocity. The component due to inertia on the other hand is proportional to the sum of two components: the Froude-Krylov force and the added mass effect, both of which are proportional to the local fluid acceleration. The inertia coefficient C_a is the

sum $(1 + C_m)$ in which C_m is the added mass coefficient. The relative importance of the drag force over the inertia force is specified by the magnitude of the Keulegan-Carpenter number $K_c = U_m T/D$ where U_m is the maximum particle velocity of the undisturbed wave at the position of the center of the cylinder, T is the wave period and D is the characteristic linear dimension of the object. As the value of K_c increases, the flow is progressively modified by viscosity in the vicinity of the object but as K_c tends to zero, the wave force is inertia dominated. It is shown by Efthymiou and Narayanan[19] that for horizontal cylinders, if K_c is less than 4, drag effects may be neglected, if K_c is between 4 and 20, inertia force is greater than drag force and if K_c is greater than 20, drag force dominates.

To use Morison's equation, force coefficients have to be obtained experimentally using either a laboratory model or a field prototype. Measured forces are correlated with either measured or calculated fluid velocities and accelerations. If a theoretical method is to be used for the calculation of fluid velocities and accelerations, an accurate wave theory has to be used in order to predict the kinematics. In the experimental investigation carried out in Appendix III, Linear or Airy wave theory has been used because of its relative simplicity. With the wave design data considered for the proposed structure, it can be seen that the ratio of the water depth to wave length is in the order of 0.45 which according to wave classification by Ippen[32] corresponds to "intermediate depth" type of wave. Using the wave data of Table 3.1, the maximum particle velocity of the undisturbed wave at the position of the center of the structure is found to be about 0.4 m/s and the magnitude of the Keulegan-Carpenter number K_c for the case under study is found to be 0.76. Since for K_c values of less than 4., the drag effects are negligible, in the experimental investigation of Appendix III, it is aimed to find only the coefficient of inertia.

Due to the limitations of laboratory facilities and different scale effects detailed in Appendix III, the results of the wave effects on the model of the proposed structure obtained experimentally, can only be used within the experimental range. Using sinusoidal waves, it is found that the

average value of the inertia coefficient is about 3.6 for the horizontal force and about 2.8 for the vertical force. These values correspond to the case where the water depth is 4 times the height of the structure. If the same Keulegan-Carpenter number and the same ratio of particle velocity ratio is used for both the model and the prototype, it is found that the horizontal and vertical wave forces on a unit length of the prototype will be about 55 kN and 9.0 kN respectively, when the prototype is located in 28 m deep water and is subjected to sinusoidal waves of 88 m wavelength and 4.0 m wave height. However, the prototype is designed for water depths of 100 m or more and it is shown by Hix[28] that wave disturbance diminish exponentially with depth, therefore, the horizontal wave force on the structure will be less than 55 kN per unit length. In fact, if the same inertia coefficient applies to all water depths and all wave conditions, it is found that the horizontal wave force on the proposed structure under the design wave condition is about 31 kN per unit length of the structure. These results, together with the measured pressure distribution around the structure due to the action of waves, as shown in figure AIII.1, suggest that the forces due to the action of waves are not likely to cause any significant disturbances on the proposed structure. Although it is possible to incorporate the pressure measurements due to wave action into the structural analysis as in the study of current, since the procedure is similar and the pressure values are small, it is decided to leave this for future investigation.

3.5 Study of Scour Around the Proposed Structure.

Local scour is defined as the abrupt change in the bed elevation near a sea-based structure, due to erosion of bed material by the local flow pattern induced by the structure. The general characteristics which should be basic to any detailed analysis of local scour are given by Laursen[37] as:

1. The rate of scour will equal the difference between the capacity for transport out of the scoured area and the rate of supply of material to that area.
2. The rate of scour will decrease as the flow section is enlarged.
3. There will be a limiting extent of scour which will be approached asymptotically.

When a structure is placed on the sea-bed, it disrupts the flow pattern. The

dominant feature of the disrupted flow pattern near a structure is the large scale eddy vortices which develop about the structure. These vortex systems are the basic mechanisms of local scour because they introduce some changes in the bed configuration in order to conform to the new flow pattern. This implies a limit to the extent of the scour when the bed configuration and the flow pattern match each other. It is this limiting or equilibrium extent of scour which is important. Research in this area showed that the significant factors in scour patterns are the geometry of the structure, the flow pattern and the sediment characteristics, but the magnitude of the equilibrium scour pattern is primarily a function of flow pattern as determined by the boundary geometry of the structure, the bed configuration, characteristic velocities and fluid properties (Ven Te Chow[63]). In the design of any offshore structure which rests on the sea-bed, due consideration must be given to the local stability of the structure at the structure-soil interface so that hazardous environmental factors are avoided, as much as possible.

Analytical methods of estimating the ultimate depth of scour have been suggested by Shen et al[60] and Blaisdell et al[8]. Since there are no theoretical methods available, scouring process can only be examined empirically. In this section, some experiments which have been carried out to investigate the scouring process in relation to the proposed structure are described. In these experiments, the scour patterns around two different models in a number of flow directions have been examined.

3.5.1. Experimental Approach for the Study of Scour.

The study of the scouring process around a sea-based structure is important in the design of any offshore structure. In this section, a number of experimental observations have been carried out on the phenomenon of scour in relation to the proposed structure. In these experiments, the scour patterns around two models of the same shape but different sizes have been studied for different directions of flow and using two different types of sand. The scour patterns obtained are photographed and also a series of transverse profiles have been drawn for the affected area.

One of the methods of anchoring the proposed structure is by dead weight. A schematic diagram of using a dead-weight anchorage system is shown in figure 1.1. This diagram suggests that a suitable model for the study

of the scour phenomenon would have a rectangular base. Since the model of the proposed structure is difficult to make, it is decided to use semi-circular cylinder models instead. Each model consists of a semi-circular cylinder glued to a rectangular base. The models are both hollow and have been filled with lead pieces in order to provide the required anchorage and to prevent buoyancy.

The experiments are conducted in a flow tank, 2.75 m long, 0.61 m wide and 0.2 m deep (Photo 6). The working section of the flume is covered with a layer of sand which is deep enough to embed the base of the model. A pump circulates the water in and out of the tank. The water enters an inlet tank at one end of the flume, through a perforated plate baffle. It is then discharged over an inlet weir onto the sand bed. It then flows over the level control weir and into the discharge tank where it is recirculated by the pump once more into the inlet tank. The control console is situated at the downstream end of the flume. It houses the 'start' and 'stop' switches, the regulating valve,'increase' and 'decrease' switches and the flow meter controls and the readout meter which shows the rate of flow of water. The flow rate can be varied between 0 and 4.2 l/s. The water level in the tank can be increased to about 0.16 m above the bottom of the tank, by raising the level control weir which is hand controlled. The water in the tank can be drained off through a drain on the floor of the working section of the tank. The contours of the sand bed produced during each experiment are mapped using the depth gauge supplied. The depth gauge is provided with a stainless steel pointed rod and incorporates a vernier scale which enables vertical levels to be determined accurately. The gauge is mounted on the instrument carrier assembly which can be positioned over any point of the working area. The main carrier can traverse longitudinally and is provided with a locking device and a cursor to operate in conjunction with the instrument rail scale fitted to the rail. The sub-carriage is used for transverse traverse and operates on rails provided by the main carriage. There is again a transverse scale and locking device. The gauge has therefore the freedom of movement in all three directions which enables

the location of any point in the working section of the tank to be measured by a system of co-ordinates. Hence the patterns of scour contours and also the depth of water in the tank can be determined.

The sand which is spread over the base of the working section of the tank, is analysed for particle size distribution prior to the experiment. Two types of sand are used in this experiment. The results of the sieve analyses of the sands are shown in figure 3.6. The depth of the layer of sand in each experiment is almost equal to the height of the base of the model used. The sand should be well washed to remove any clay which would otherwise tend to cloud the water.

Before starting the flow, it is ensured that the level of sand is uniform everywhere in the tank. It is also important not to disturb the sand bed by an initial surge of water on starting the flow, so initially the flow rate is kept very low and is then gradually increased until it reaches its required value. Sufficient time of around 2 hours has to be allowed for an equilibrium state to be reached. The water is then drained off completely and a few hours is allowed for the sand to dry out. An example of the scour patterns obtained is shown in Photo. 7. For each test a series of transverse profiles are drawn in the scoured region around the model, using the depth gauge and the scale provided. The results are shown in the next section.

3.5.2. Discussion of the Results of Scour Experiment.

The experiment on the scouring effect is carried out in the flow tank, on two similar models using two different types of sand. The average flow rates obtained in the tank in different tests vary between 3.3 and 4.0 litres per second. One of the problems encountered in this experiment is that the flow velocity in the tank is not high enough to produce Reynolds numbers of the same order of magnitude as those of the prototype. Although the velocity can be increased by reducing the water depth in the

tank, the water depth has to be kept at its maximum value of about 0.16 m throughout the experiment. This is because ideally, deep water conditions have to be represented by this model study and if the depth of water is reduced any further from its maximum level, only very shallow conditions are generated. The flow velocity in these experiments varies between 0.03 and 0.04 meters per second depending on the flow rate obtained in each test. The maximum Reynolds number obtained in the test on the smaller model is about 0.15×10^4 and the maximum obtained on the larger model is about 0.22×10^4.

Since the direction of the flow relative to the longitudinal axis of the proposed structure in the prototype situation is not exactly known and is thought to be variable, it is decided to conduct the experiment for different flow directions. The experiment on the smaller model is conducted for three different angles of 0^0, 45^0 and 90^0 between the direction of flow and the longitudinal axis of the model while in the experiment on the larger model, 60^0 and 90^0 angles have been tested. The values quoted for the angles, correspond to the position of the model in the tank before starting the flow. It is found that these angles do not remain the same once the flow is started. This is because the leading edge of the model shifts slightly in the flow direction due to the strength of the flow. The models are usually placed in the center of the tank so that any wall effects are minimized. In the tests where the flow direction makes angles of 60^0 and 90^0 with the longitudinal axis of the model, in addition to testing the model in the center of the tank, the model is placed in contact with a side wall of the tank and tested in those positions as well. These latter positions are supposed to represent infinite length condition of the prototype. The details of the experimental work on the effect of scour are summarized in Table 3.2.

Table 3.2 - Summary of the experiments on the effect of scour.

Experiment number	Size of the model			Position in the flow tank		Average flow velocity (cm/s)
	Width (cm)	Length (cm)	Overall height (cm)	distance from the side wall of the tank (cm)	angle of the model with the direction of flow	
1	8.0	25.0	8.0	26.0	0^{o}	4.7
2	8.0	25.0	8.0	18.0	45^{o}	4.4
3	8.0	25.0	8.0	18.0	90^{o}	4.9
4	8.0	25.0	8.0	0.0	90^{o}	4.7
5	11.0	28.5	9.5	16.3	60^{o}	4.7
6	11.0	28.5	9.5	0.0	60^{o}	4.7
7	11.0	28.5	9.5	16.3	90^{o}	4.7
8	11.0	28.5	9.5	0.0	90^{o}	4.7

The scour contours obtained by the depth gauge are illustrated in figures 3.7 to 3.14. It can be seen from these results that the general pattern of scour is almost the same in every experiment regardless of the size of the model and the direction of flow. The area around the upstream corner of the model is usually the most eroded region and is marked by scour patterns in the form of parts of circles. The center of these circular scours is the front corner of the model; this point experiences the deepest scour in most experiments. The depths of the scours decrease as their distances from the front corner point increase. Some of these circular scour contours tend to become longitudinal and run along the length of the model. The eroded material of the upstream region is transported downstream where it is deposited. The region around the model on the downstream side is therefore marked by deposition contours. These contours are also almost circular around the downstream corner of the model. In the experiments where the model is positioned symmetrically with respect to the tank, it is observed that the scour patterns are more or less symmetrical. The comparison of the results on the different positions of the models suggests that the depths of scour contours reduce as the angle between the longitudinal axis of the model and the direction of the flow is decreased. For the same angle of incidence, it is observed that the depth of scour increases by increasing the Reynolds number. This result is in agreement with the results obtained by Schen et al[60]. However it is not possible to establish any relationship between the scour depth and the flow Reynolds number from the results of this study since the data obtained is not sufficient for this purpose. The variation of the scour depth with time is not investigated in these experiments but from the observations made in the tests it appears that most of the scouring patterns develop in the first twenty minutes or so of the test run and the changes in the scour patterns after this period of time is comparatively insignificant.

It must be emphasized that these tests provide only qualitative results of the pattern of erosion and deposition in the prototype case and they are by no means sufficient for making any decisions on the location of the proposed structure or its foundation requirements and the type of anchorage system

required. A careful study of the general geological characteristics of the region considered for locating the structure is a necessary prerequisite to the final decision on the exact location of the structure. It is important that the structure is laid in a region where significant scouring of the sea bottom is not likely to occur or that no portion of the structure is laid on harder or non-scouring materials because then a span will be left suspended over other portions of the bottom which do scour.

3.6 Conclusion.

An inflatable membrane structure has been proposed for the storage of gas underwater. An important area of investigation in the design of the proposed structure is the hydrodynamic aspect. In this chapter, a brief hydrodynamic analysis of the proposed structure is carried out.

Since the quantity of gas that can be stored in this structure increases with the depth of water at which it is located, the structure is designed for deep water conditions. In these conditions, the elements of the fluid environment which might affect the design of the proposed structure are: water pressure, current, wave, earthquakes, corrosion, temperature, reactive forces of the foundation medium and the impact from floating objects. Although several of these elements have a dynamic nature, the present study is principally concerned with the hydrostatic analysis of the structure. The effects of waves and currents have been investigated in some detail but the other environmental factors have only been briefly discussed.

The largest hydrostatic forces on the structure are the buoyancy force and the water pressure force. They are both dependent on the state of submergence of the structure in the fluid environment. The static pressure of water is the main determinant factor in the development of an optimum design for the proposed structure. The consideration of the buoyant force is especially important in the design of the anchorage system. Since the proposed structure is bottom-fixed, the effects of geotechnical forces such as earthquakes and destabilization due

to extensive erosion have to be investigated. The phenomena such as chemical and electrolytic reactions which are responsible for the corrosion of the structure in water should be carefully examined. External and internal temperature changes of the structure are caused by the variation in ocean temperature and the variation in the temperature of the stored gas. The forces caused by expansion and contraction due to these temperature changes have to be accounted for in the design of the proposed structure. Impact from floating objects and the growth of marine fouling are two of the dangers which the structure has to face and should therefore be considered in the design of the structure. Since the proposed structure is designed for deep water conditions, the direct effects of winds, icebergs and sheet ice are insignificant.

The effect of current on the proposed structure is investigated theoretically and experimentally. In this investigation, it is assumed that the pressure distribution on the structure due to the action of current, is the same irrespective of whether the structure is flexible or rigid. The analysis is therefore carried out on a rigid structure for simplicity. Since the cross-section of the proposed structure is similar to a semi-ellipse, the pressure distribution due to a uniform current on a semi-elliptical cylinder is theoretically obtained. The theoretical analysis is based on the potential flow theory in which the effect of the viscosity of water is not considered. Although the results are slightly improved by incorporating the effect of a laminar boundary layer, they still do not correctly predict the pressure distribution around the proposed structure due to current. A better estimation can be obtained by experimental studies. Experiments are carried out on four models in a wind-tunnel where Reynolds numbers as high as 1.1×10^6 are achieved. The models are a circular, a semi-circular and a semi-elliptical cylinder and a model of the proposed structure. The semi-circular cylinder is tested in a current flume as well. In all these experiments, the pressure distribution around each model due to uniform currents of different velocities is measured. Using these results, the pressure-coefficient curves are plotted for all the models. The results of the experiment on the circular cylinder model are in good agreement with those in the literature for similar experiments. The results of the two experiments on the semi-circular cylinder model in the wind tunnel and in the current flume are quite consistent. The

theoretical pressure coefficient distribution for a semi-elliptical cylinder deviates considerably from the experimental results. However, the result of the theoretical calculation of the boundary layer has predicted the position of the separation point well. The comparison of the experimental results for the semi-elliptical model and the model of the proposed structure shows a close similarity in the pressure distribution around the two objects.

The experimental and the theoretical results of the pressure distribution around a semi-elliptical cylinder and the model of the proposed structure, due to a uniform current are used to estimate the deformation of the proposed cable-reinforced membrane structure and to find the changes in the cable forces for the case when the structure is subjected to a uniform current of 1 m/s velocity. It is found that the changes in the structure profile are very small, and the cable forces do not increase. In fact, the tensions in some cables reduce by as much as 3 percent. It is therefore concluded that statically, the effect of current on the proposed structure is insignificant.

The scouring effect of current is examined experimentally on two rectangular based models placed in a flow tank. The scour contours show that the region adjacent to the upstream side of the model is eroded in the form of circular arcs and the region on the downstream side of the model is marked by deposition contours. The depth of scour patterns reduces as the angle between the direction of flow and the longitudinal axis of the model is decreased.

The effect of sinusoidal waves on the proposed structure is briefly investigated. This investigation is based on the assumption that the size of the structure is small compared to the wavelength and so the presence of the structure does not disturb the incident wavefield. Under this assumption Morison has suggested that the wave force can be represented as the sum of the two components, namely drag and inertia. The evaluation of the coefficients of drag and inertia is essential for the calculation of the wave force. Since there are no theoretical methods for the calculation of these coefficients, they have to be found experimentally. The force coefficients obtained experimentally in Appendix III are used to estimate the effect of a design wave on the proposed structure. The

result shows that the value of the wave force on the structure is not significant.

The hydraulic analysis of the proposed structure is very briefly developed in this chapter. The analysis has mostly been concentrated on the static effect of waves and currents on the proposed structure when located in deep water conditions. The results have shown that the above effects are small compared to the water pressure effects. However, hydrodynamic effects of waves and currents which may induce dangerous vibration of the structure, have to be investigated. A more detailed hydrodynamic analysis is therefore required before the structure can be fully developed.

Figures of Chapter Three

Figure 3.1 - Comparison of the cross-section of the proposed structure with a semi-ellipse whose axes are 6.84 and 3.93 m.

—×—×—×— Proposed structure.

—▫—▫—▫— semi-ellipse.

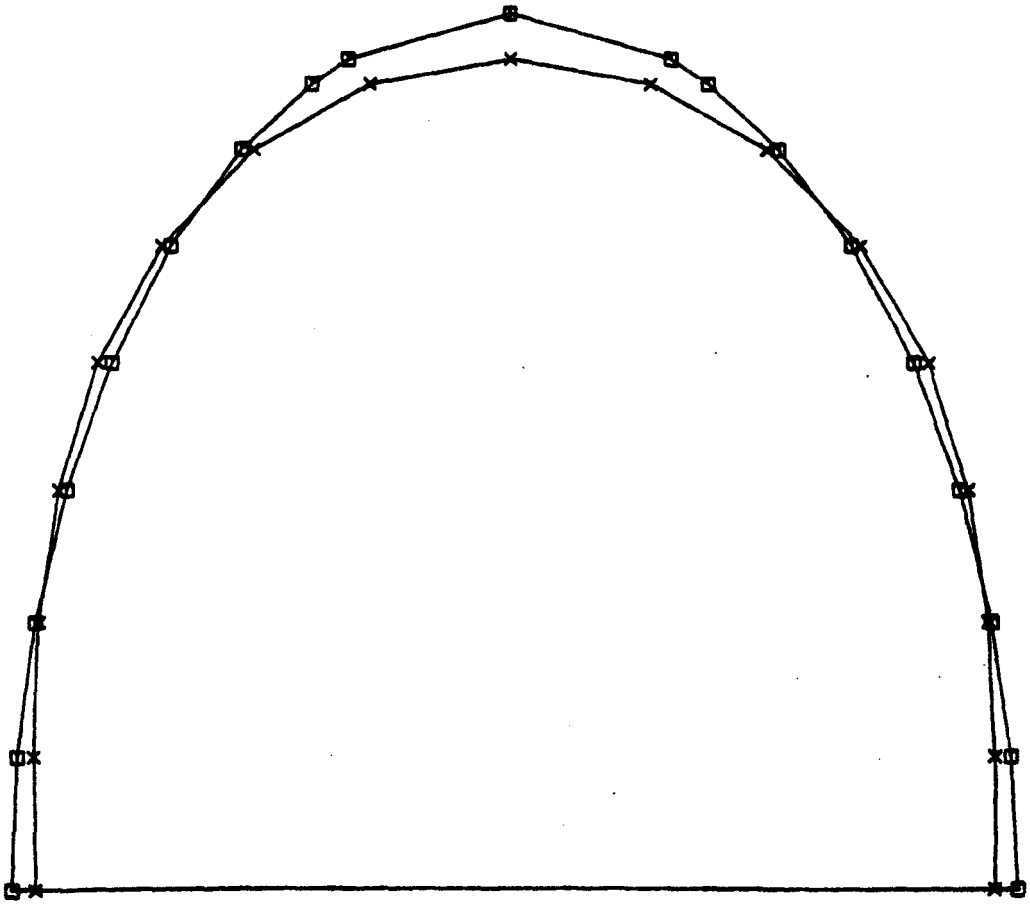

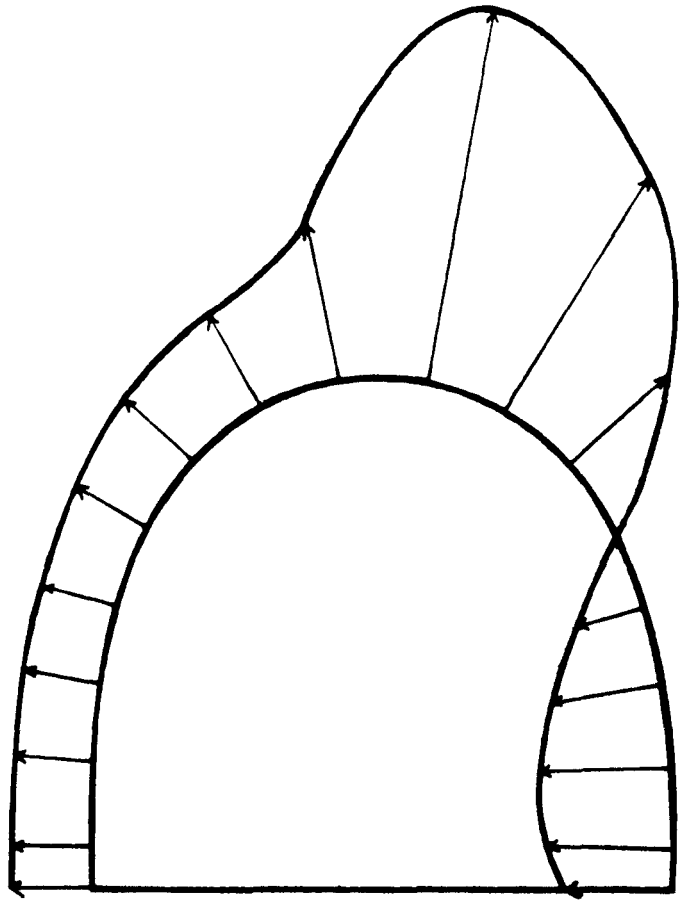

Figure 3.3. - Pressure distribution due to a uniform current, around the model of the proposed structure (Re = 1.1×10^6).

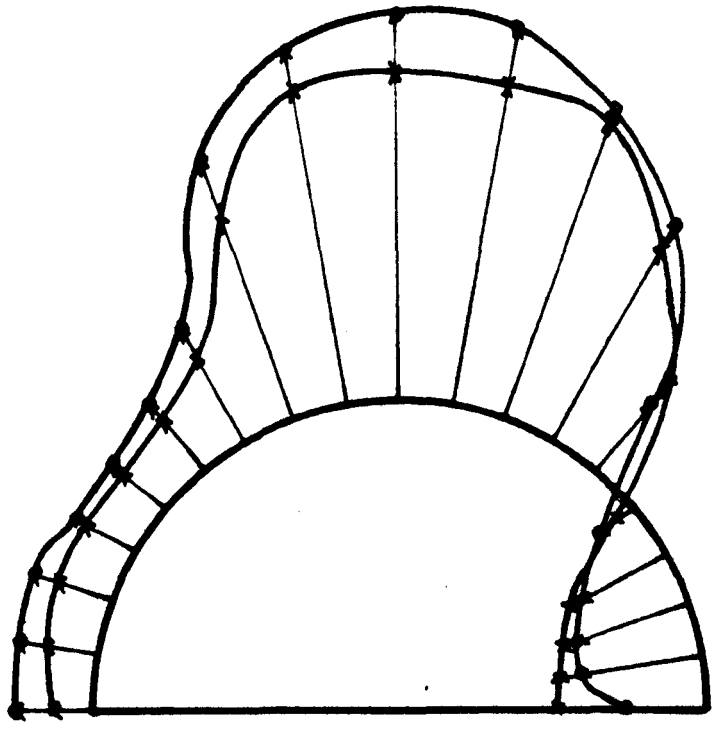

Figure 3.4. - Pressure distribution around the semi-circular model.

—●—●— pressure distribution due to a uniform wind velocity.

—×—×— pressure distribution due to a varying wind velocity.

Figure 3.5a - Tension forces in the cables (in kN) using the theoretical results of the pressure distribution due to current.

Current velocity : 1 m/s
length of structure : 8 m.
cable spacing : 1 m.

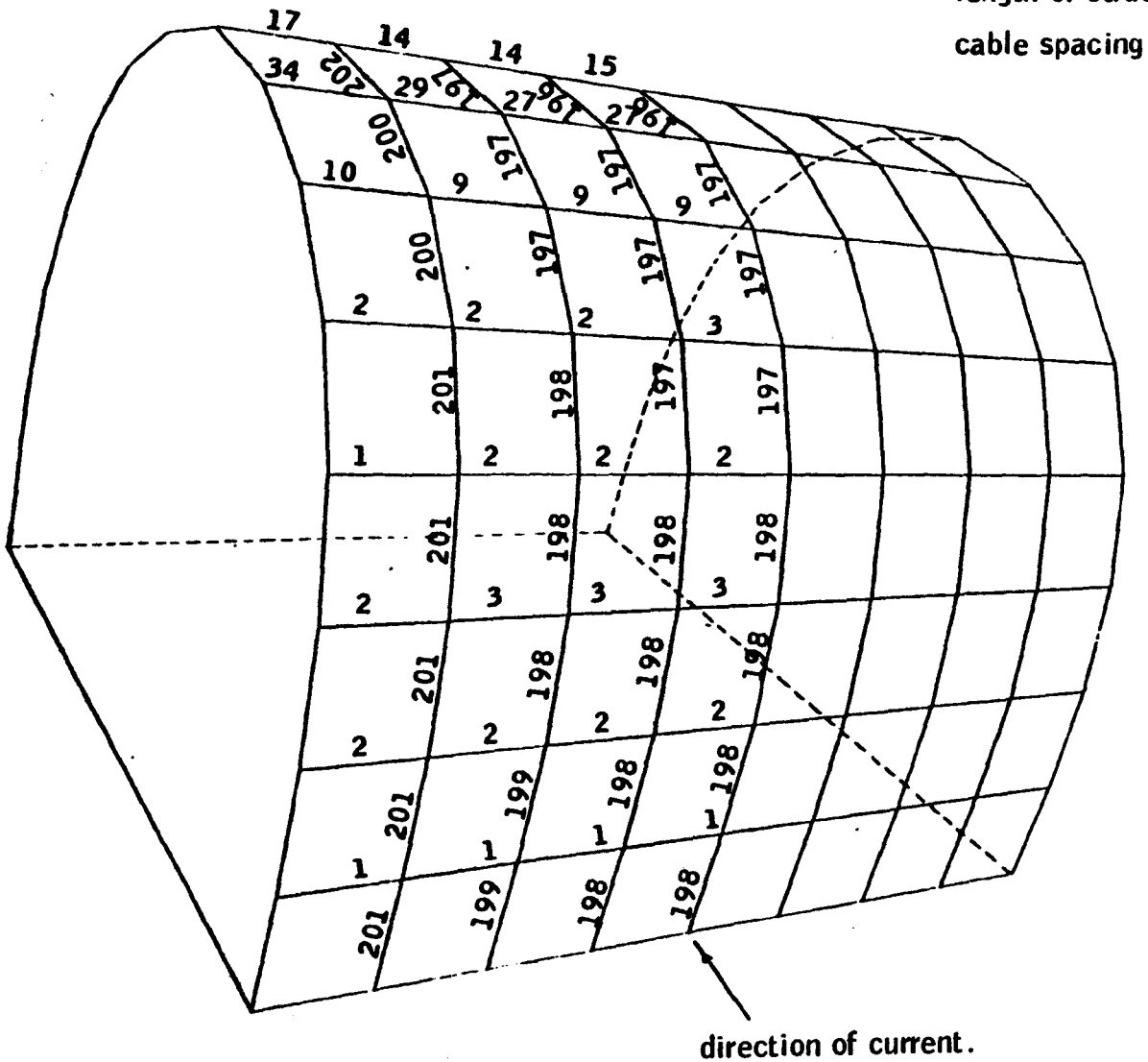

Figure 3.5b - Tension forces in the cables (in kN) using the experimental results of the pressure distribution due to current.

current velocity : 1 m/s
length of structure : 8 m
cable spacing : 1 m.

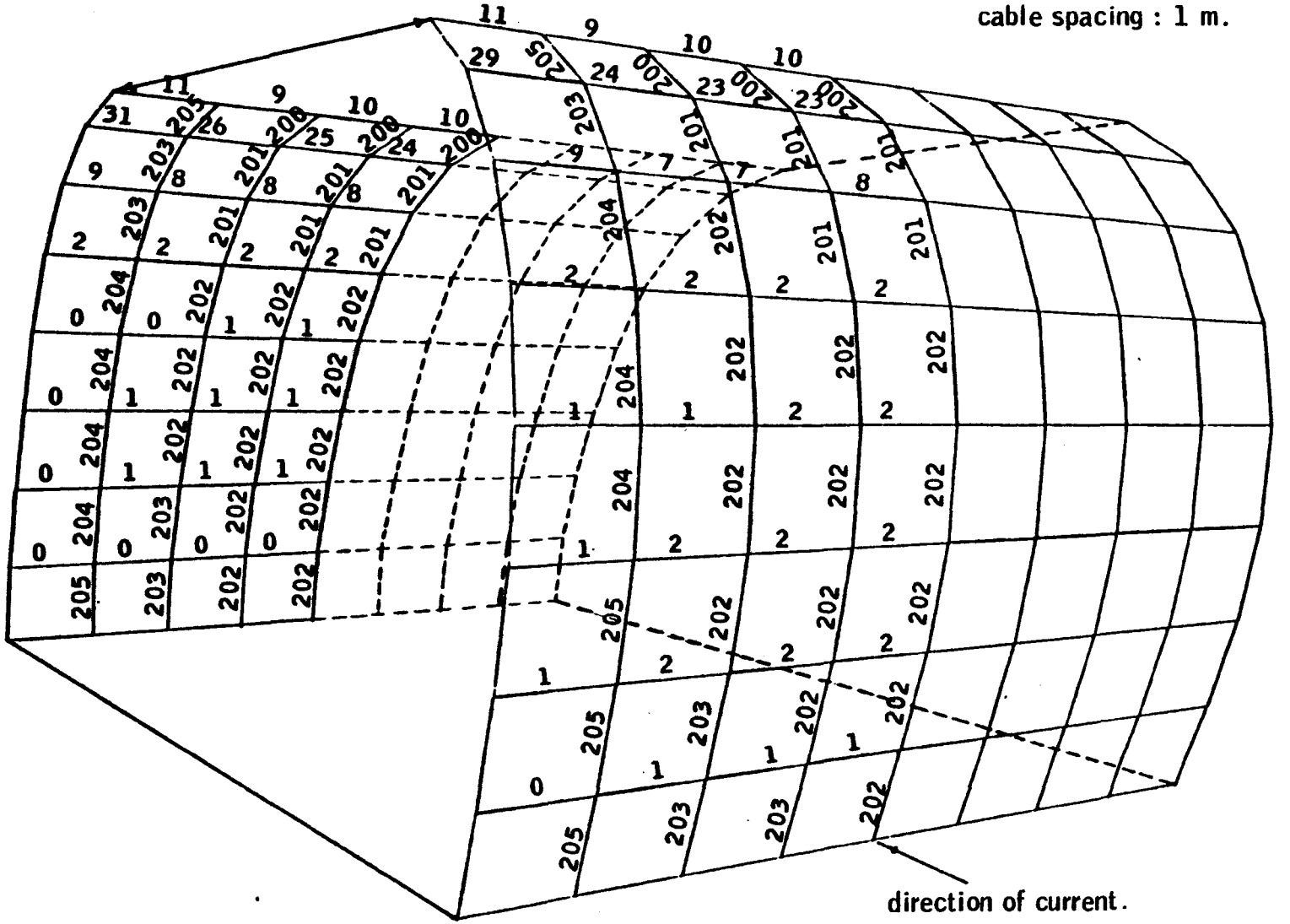

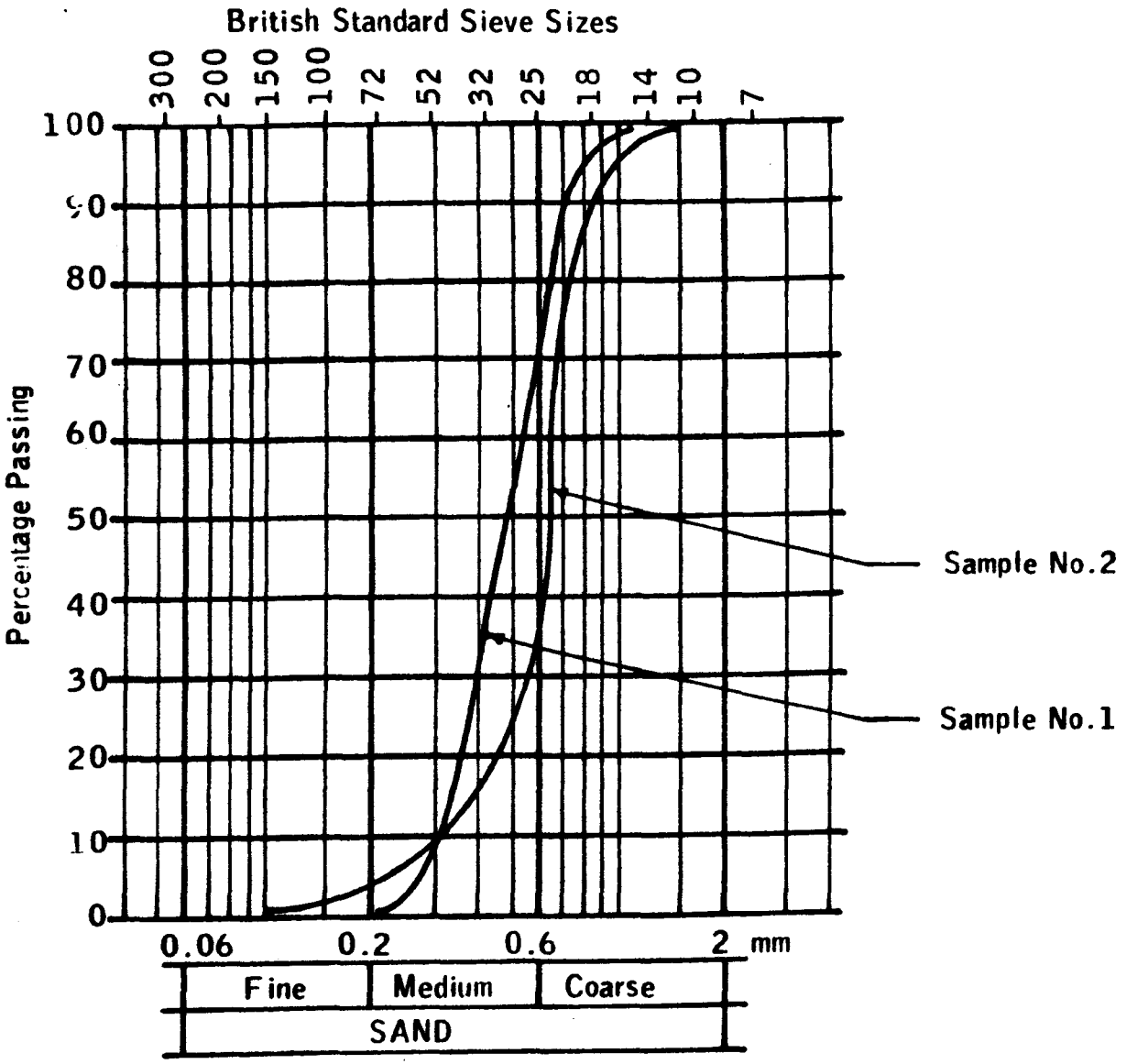

Figure 3.6 - Particle size distribution of the two types of sand used for the scour experiment.

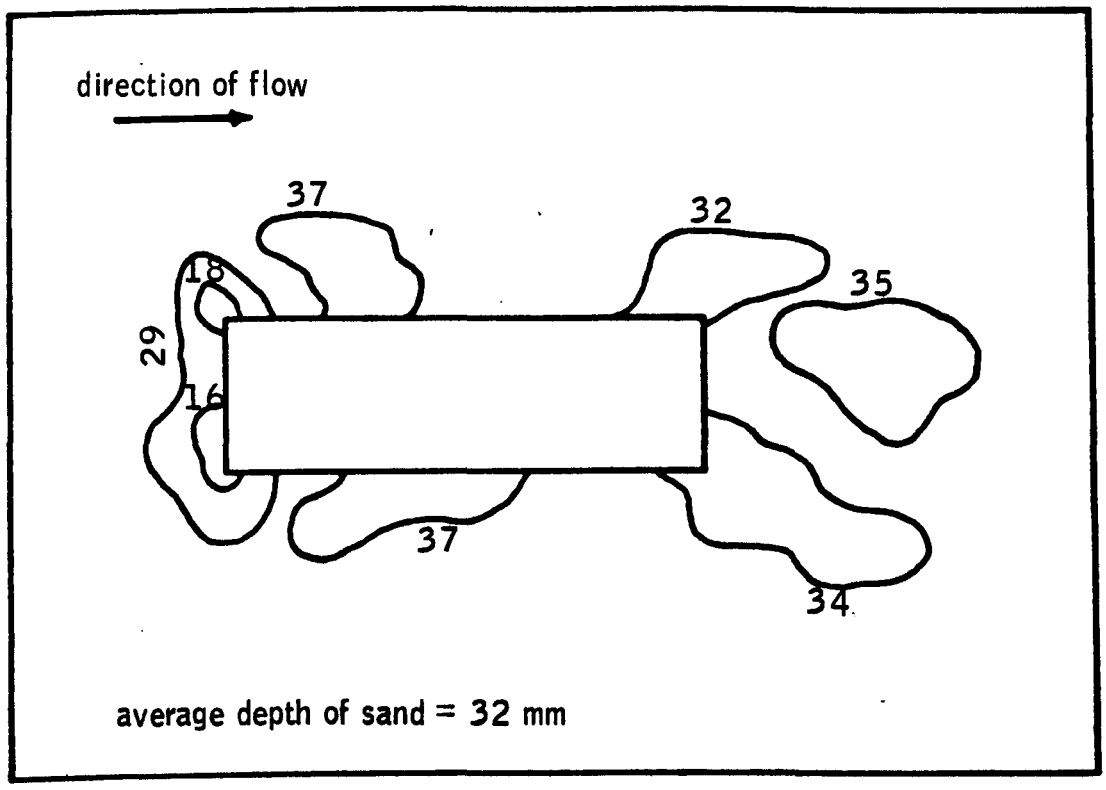

Figure 3.7 - Scour patterns in experiment 1 (contours in mm)

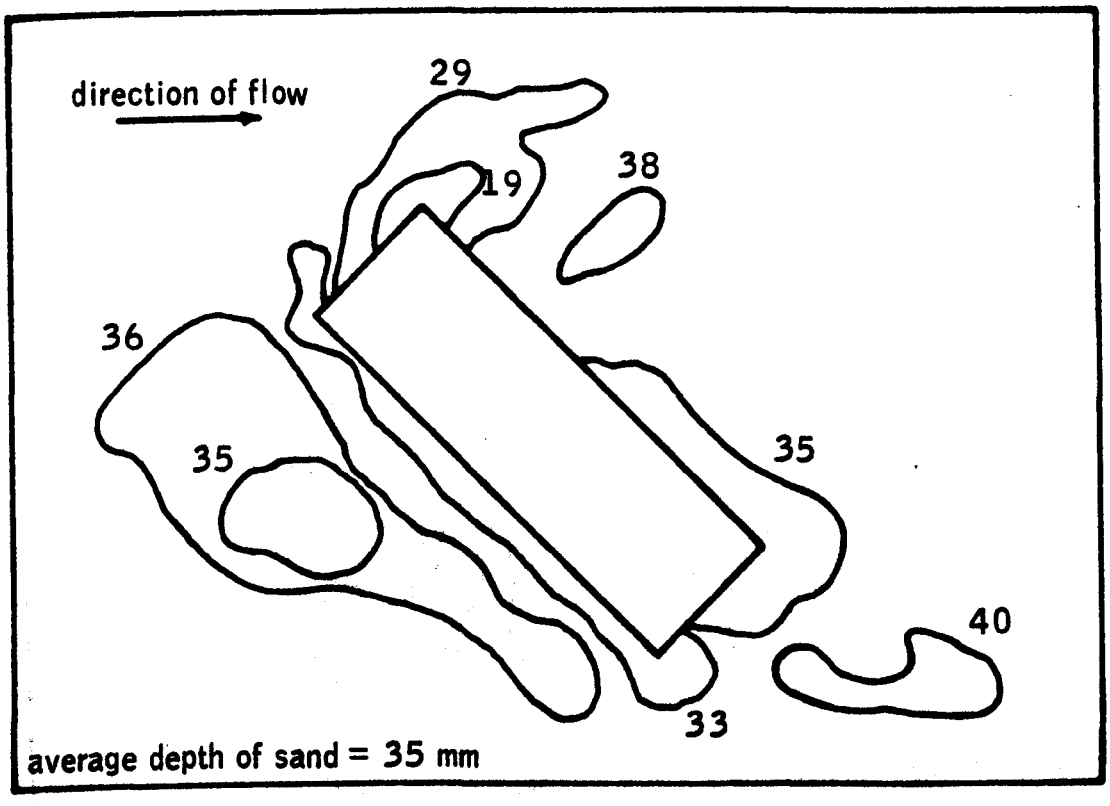

Figure 3.8 - Scour patterns in experiment 2 (contours in mm)

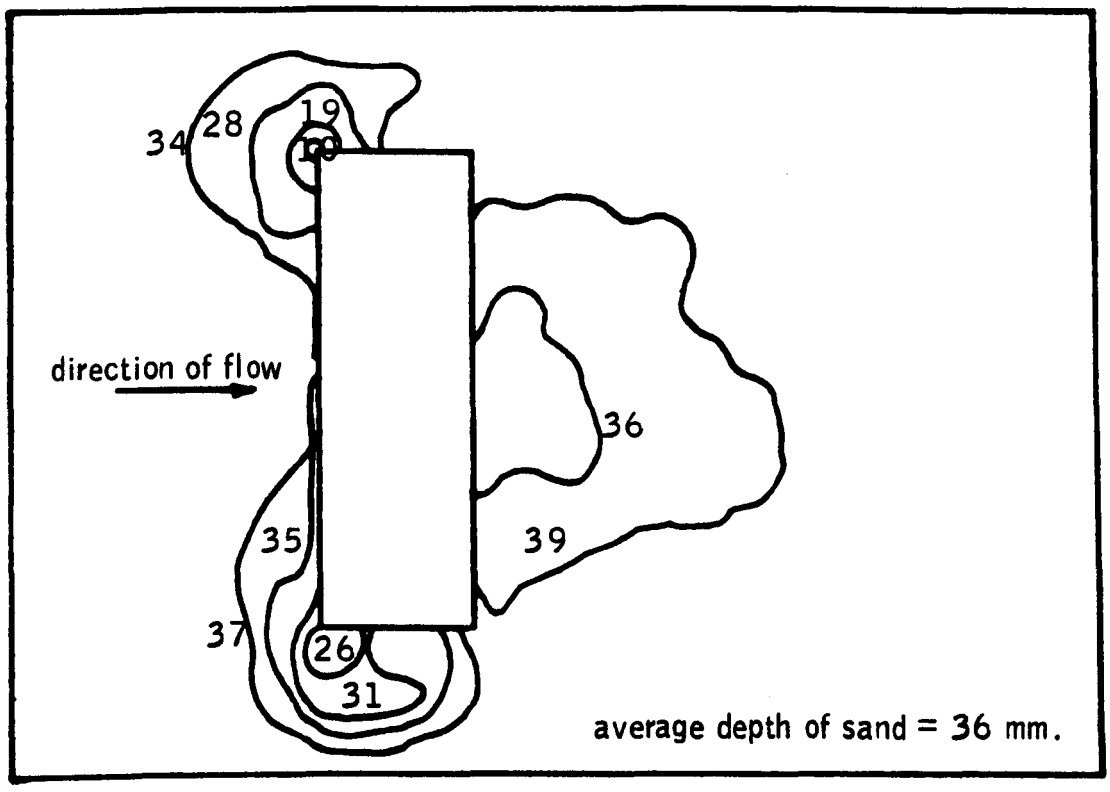

Figure 3.9 - Scour patterns in experiment 3 (contours in mm)

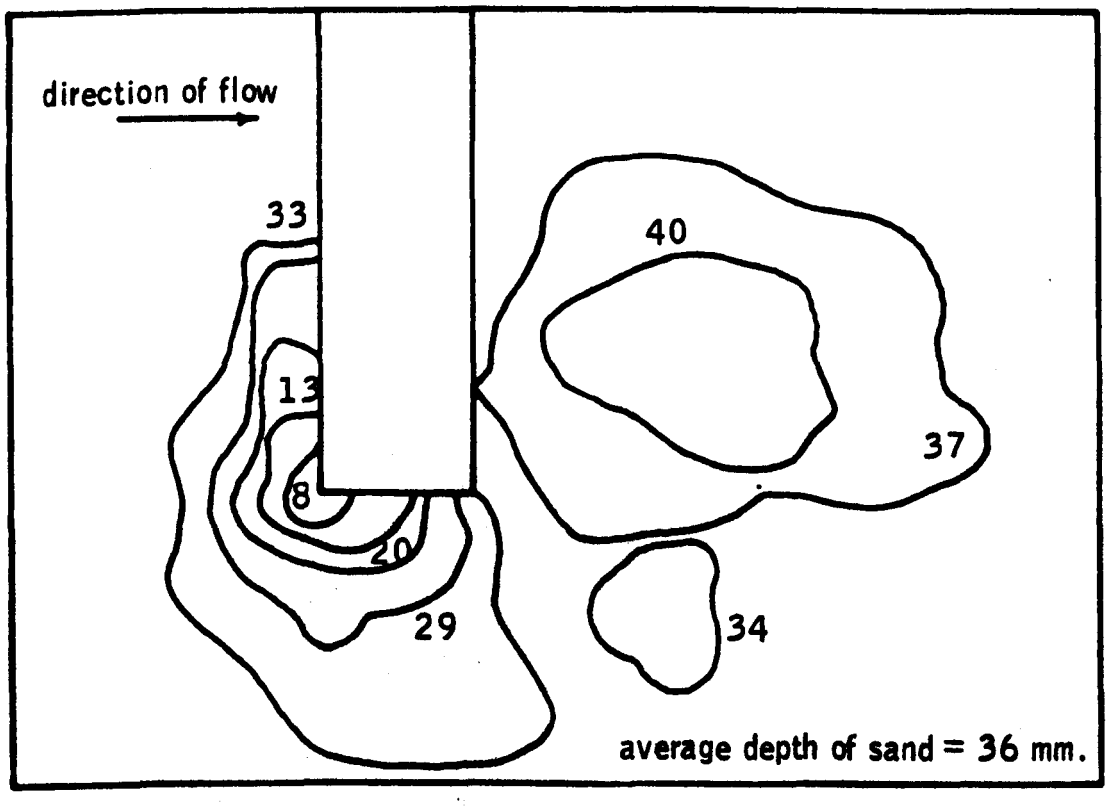

Figure 3.10 - Scour patterns in experiment 4 (contours in mm)

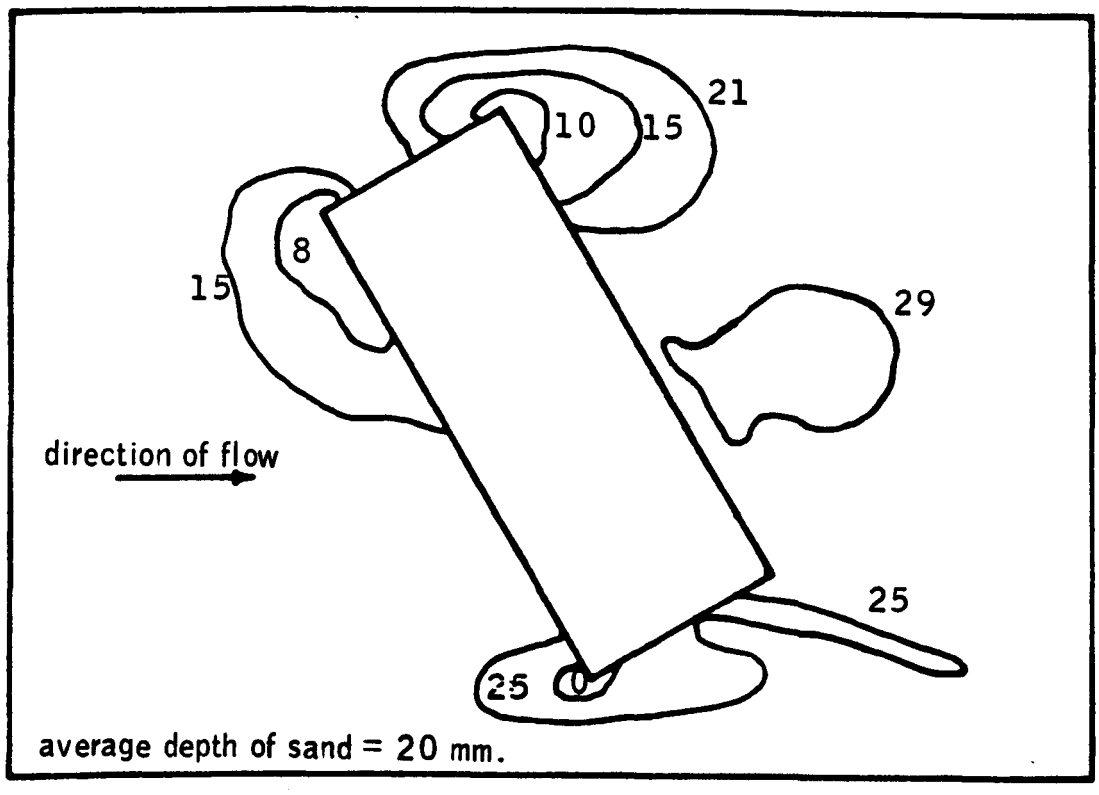

Figure 3.11 - Scour patterns in experiment 5 (contours in mm)

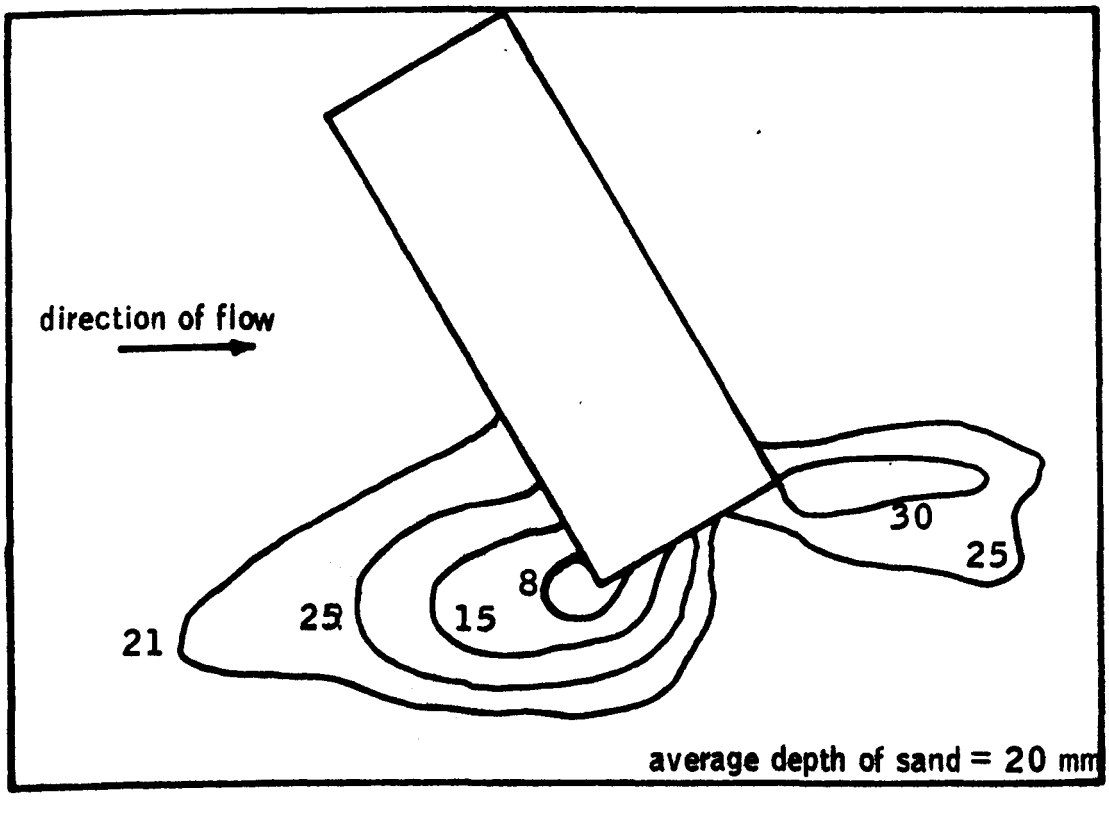

Figure 3.12 - Scour patterns in experiment 6 (contours in mm).

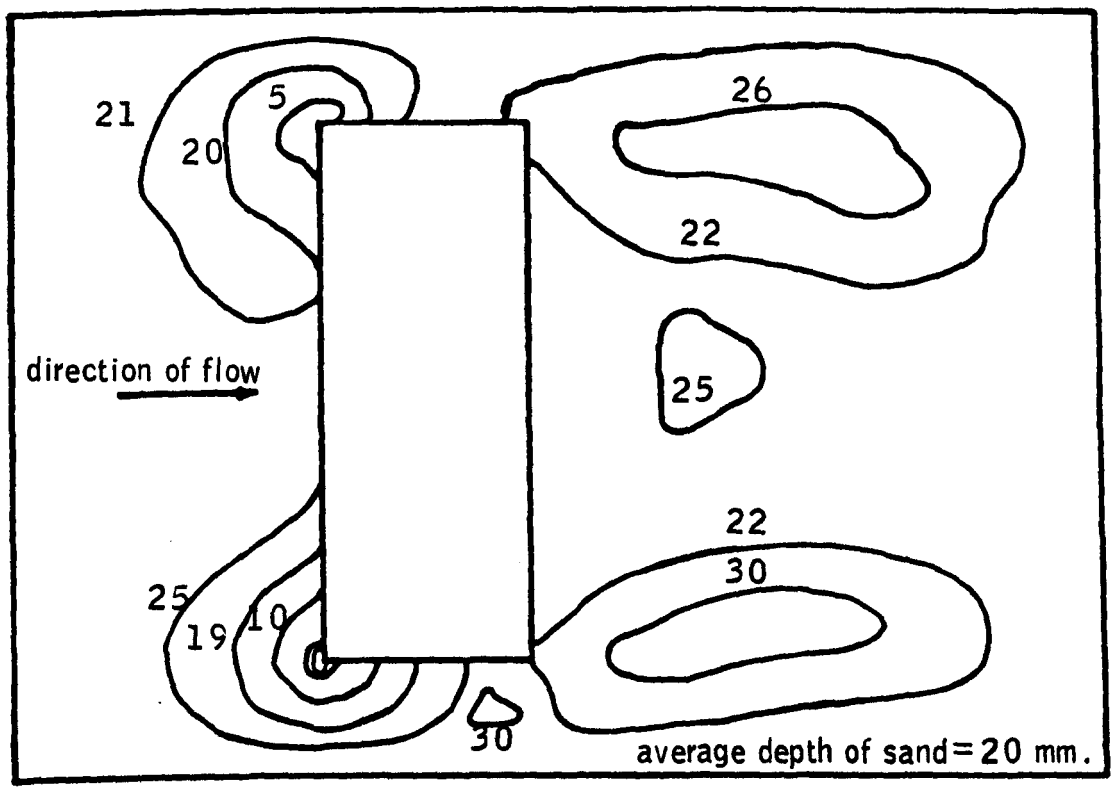

Figure 3.13 - Scour patterns in experiment 7 (contours in mm).

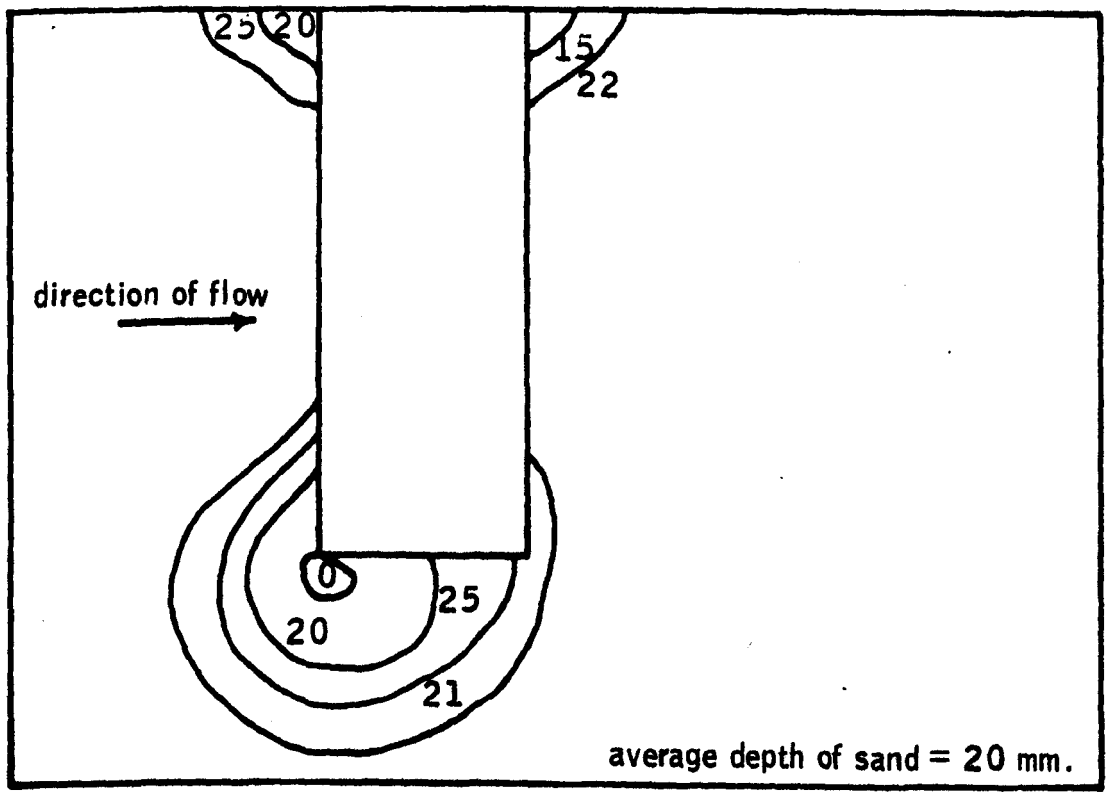

Figure 3.14 - Scour patterns in experiment 8 (contours in mm).

Graphs of Chapter Three

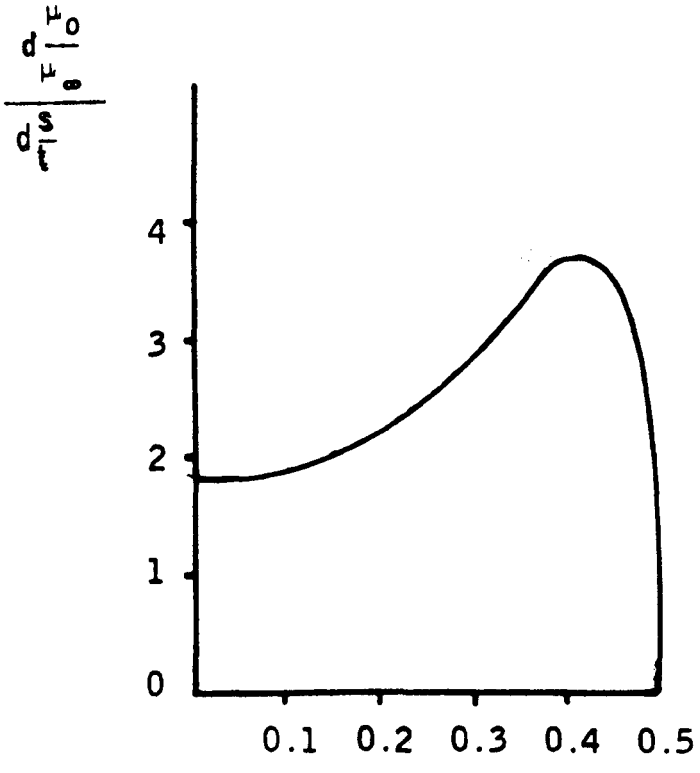

Graph 3.1 - Variation of the first derivative of velocity with distance along half-perimeter of the ellipse

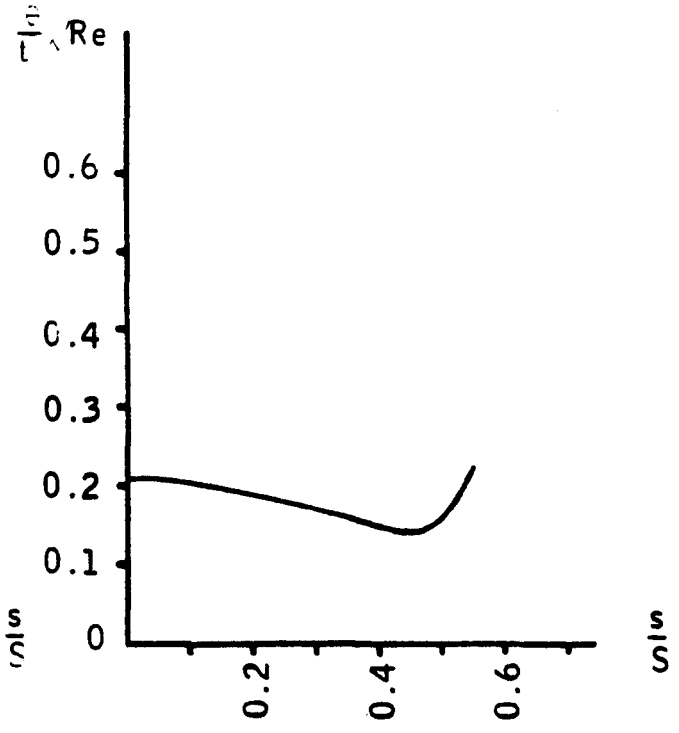

Graph 3.2 - Variation of the momentum thickness with distance along half-perimeter of the ellipse.

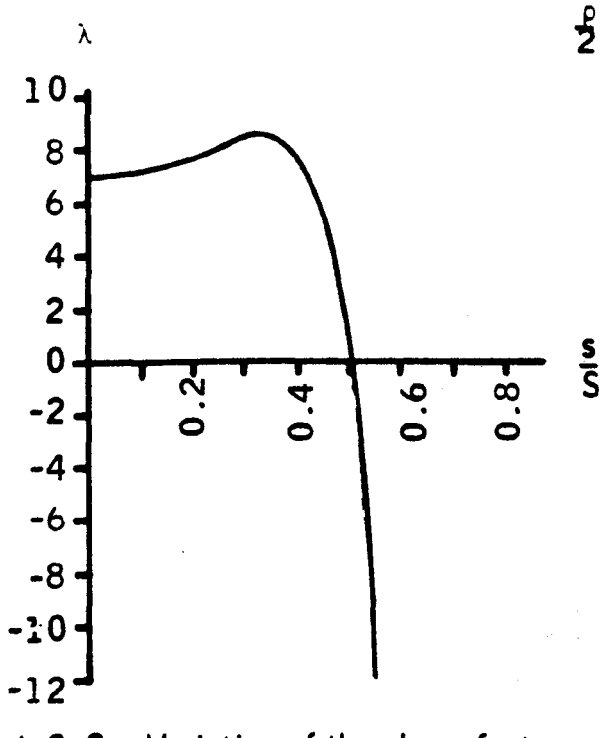

Graph 3.3 - Variation of the shape factor with distance along half-perimeter of the ellipse.

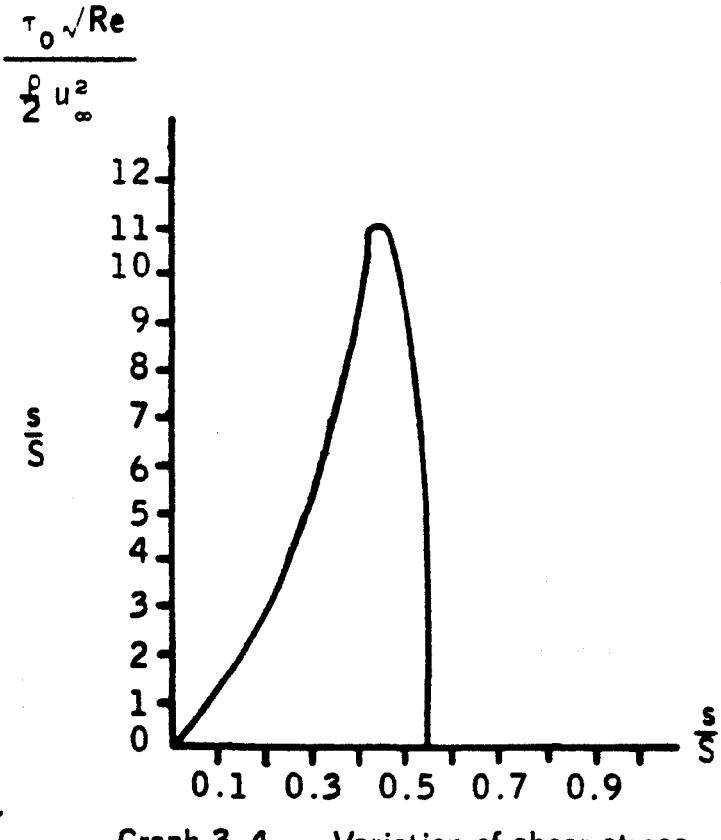

Graph 3.4 - Variation of shear stress with distance along half-perimeter of the ellipse.

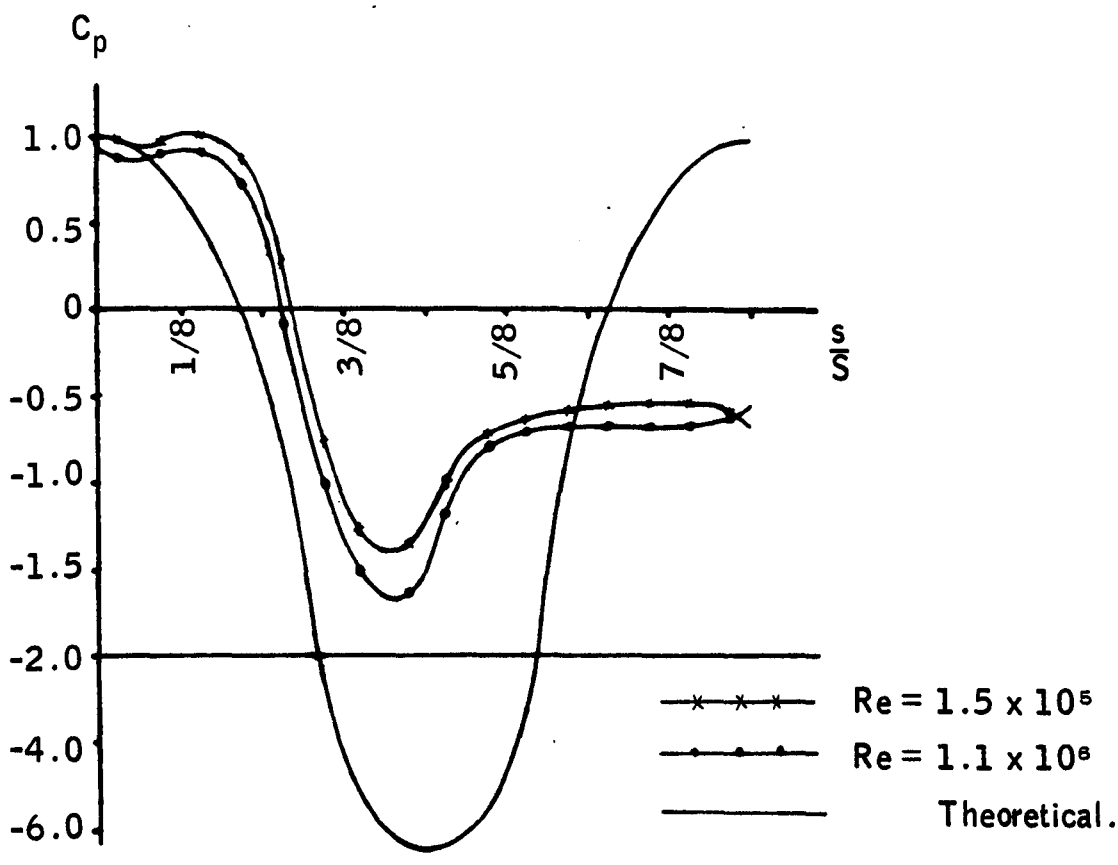

Graph 3.5a - Distribution of pressure coefficient on a semi-elliptical cylinder.

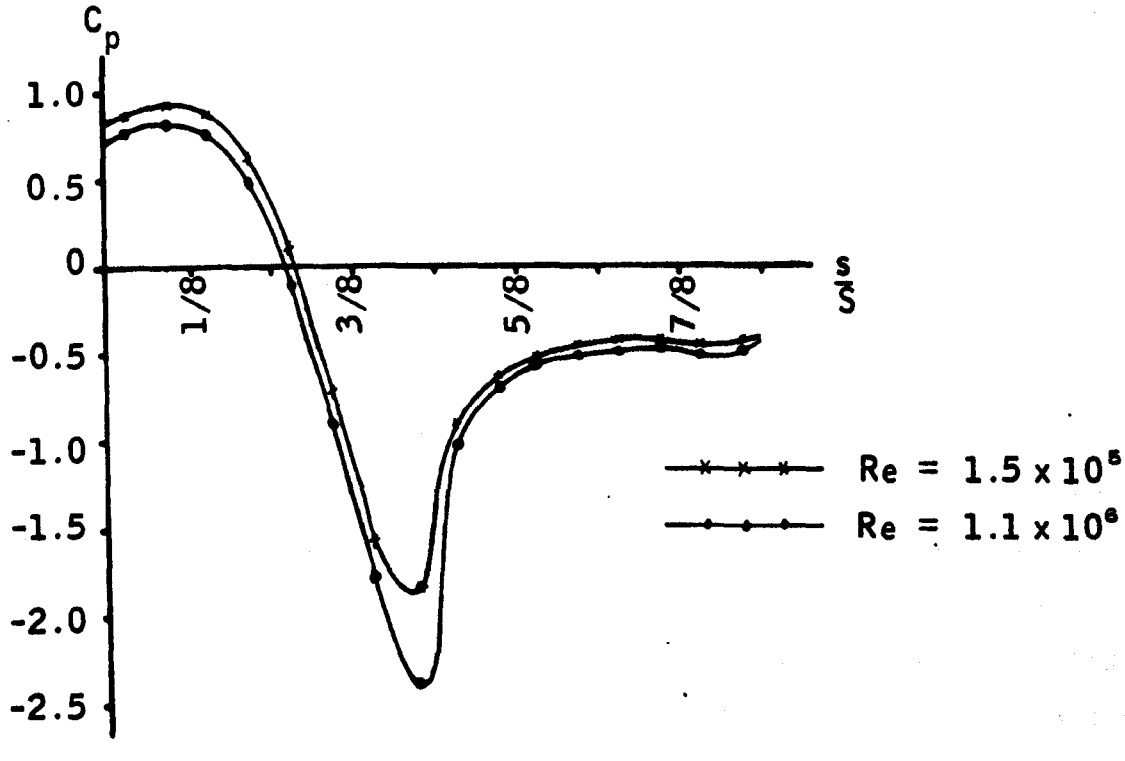

Graph 3.5b - Distribution of pressure coefficient on the model of the proposed structure.

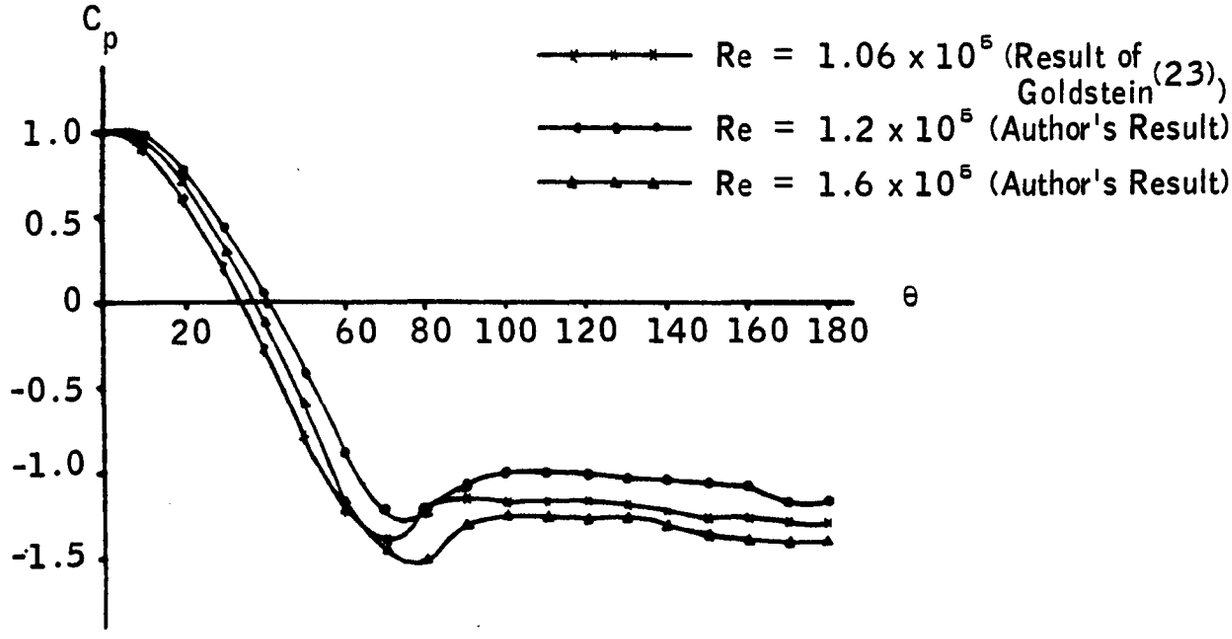

Graph 3.6 - Distribution of pressure coefficient on a circular cylinder.

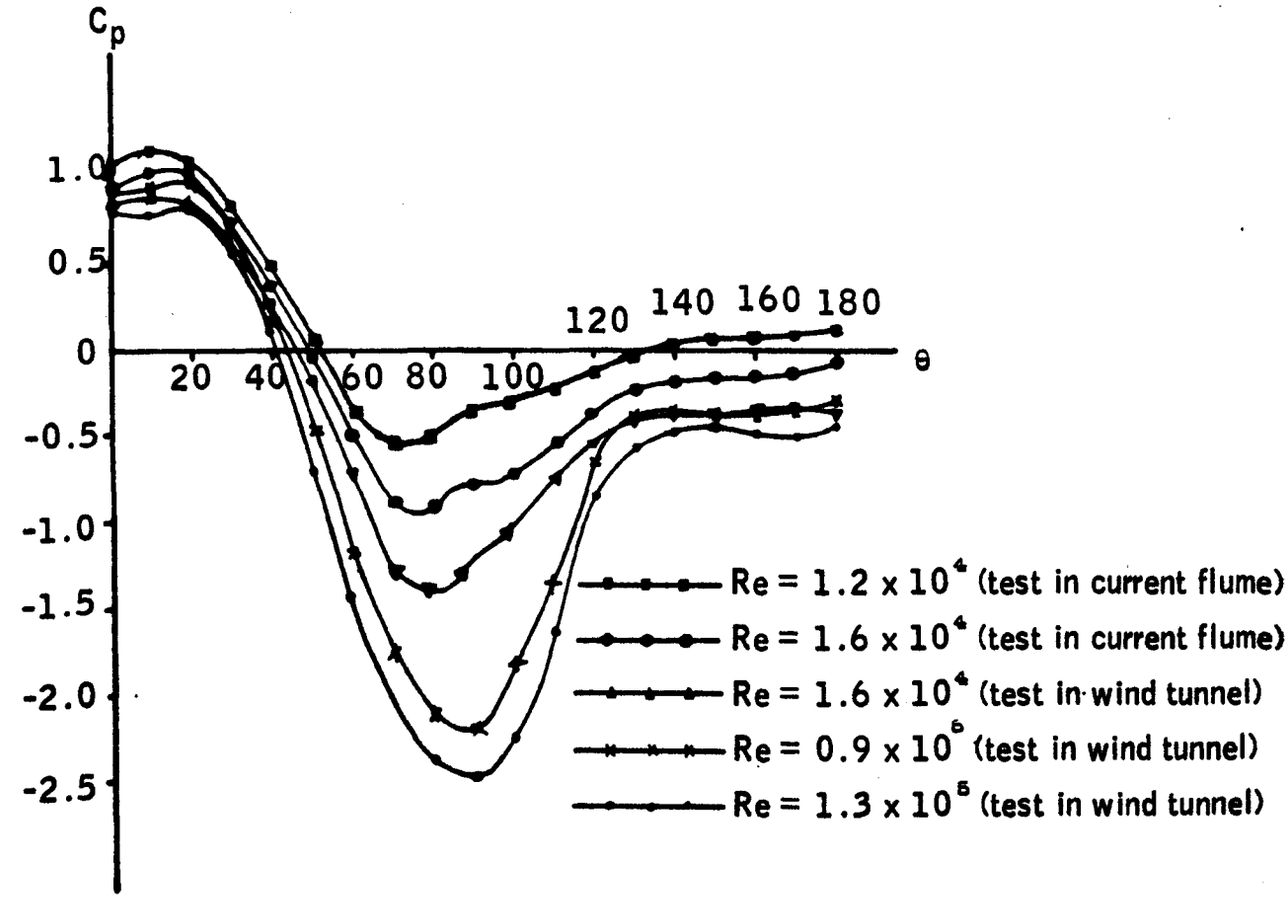

Graph 3.7 - Distribution of pressure coefficient on a semi-circular cylinder.

CHAPTER FOUR

CONCLUSIONS AND SUGGESTIONS FOR FURTHER WORK

4.1 Conclusions.

In recent years, considerable attention has been given to the development of inflatable membrane structures because of their numerous advantages such as speed of erection, portability and low capital cost. One potential area of application of inflatable structures is in the underwater environment where the water pressure counterbalances some of the internal gas pressure and thus the load on the structure is considerably reduced. It may therefore be possible to use underwater inflatable structures as an economical means for the storage of large quantities of gases. The feasibility of this method of storing gas has to be carefully investigated. The main areas of investigation are as follows:

- Structural analysis of a flexible membrane gas container for use in the underwater environment.
- Hydrodynamic analysis of the above structure.
- Study of the physical and chemical properties of the flexible membrane material, particularly its strength, elasticity and its gas permeability properties.
- Comparative study of the various anchorage systems.
- Examination of the techniques of construction and installation of the flexible structure.
- Study of the operating procedures for the structure.
- Comparative cost analysis of the proposed gas storage scheme with regards to other alternative methods.

The present study has been mainly concerned with the first two areas of investigation listed above, namely the structural and the hydrodynamic analysis of a gas-filled membrane structure in the underwater environment. However, some of the other aspects of the proposed structure have been briefly discussed. It

is suggested that the proposed gas-storage container can be used for the storage of hydrogen gas produced from the electroysis of water using surplus electricity. It can also be used for the storage of associated petroleum gas from offshore oil wells.

The structural analysis of the proposed flexible container involves the determination of its equilibrium configuration and the computation of the associated tension in the membrane. It is assumed that the container consists of a long cylindrical membrane which is fixed along its base. The shape of the cross-section of the container has to be obtained by solving the differential equations of equilibrium. A theoretical method has been developed for the solution of the equilibrium equations for the case of idealized weightless membrane.

By generating numerical results, the effect of different design parameters on the profile and the tension in the membrane are investigated. It is found that:

- Many configurations are possible for a certain cross-sectional area or perimeter, with different base widths which in turn produce different tensions in the membrane.
- A physical configuration is not possible for base angles greater than 130^{0}.
- If the base width is kept constant, any increase in the base angle will cause the tension in the membrane, the cross-sectional area and the perimeter of the structure profile to increase.
- For any constant value of cross-sectional area above a minimum practical value of 5 m^{2}, an increase in the design base width beyond 1 m, causes a decrease in the perimeter and the tension in the membrane down to a minimum value, after which any further increase in the base width, increases the perimeter and the tension in the membrane. However, the minimum tension in the membrane does not occur at the same value of the base width as the minimum perimeter occurs.

The validity of the theoretical solution is confirmed by model experiments. It is found that the shape taken up by the membrane models, under the same resultant

pressure distribution as the prototype is in very close agreement with the results of the theoretical analysis.

An optimum configuration based on minimum tension profile is obtained for a prototype structure which has a cross-sectional area of 40 m^2. The profile obtained, has a base width of 7.5 m, a maximum height of about 6.4 m and a base angle of 90.7°. The tension in the membrane is found to be 201 kN/m.

In order to provide additional strength in the structure, a two-way set of reinforcing cables is incorporated in the membrane. In the analysis of the cable-reinforced membrane structure, the action of the membrane is neglected except for transmitting the pressure load to the cables. A general computer program is developed for the analysis of cable networks. A number of different gas-filled, cable-reinforced membrane structures submerged in water are analysed by the computer. The effects of changing the overall length of the structures and changing the spacing of the cables are examined. Some of the results obtained, are summarized in Table 4.1. It is observed that:

- The change of the overall length of the structure does not have a significant effect on the shape of the cross-sectional profile of the structure.
- An increase in the overall length of the structure causes reductions in the magnitudes of the forces in some of the cable elements of the structure but the rate of reduction of the cable forces is not simply related to the rate of increase in the length of the structure. The changes in the circumferential cable forces due to the change of the overall length of the structure are very slight.
- The effect of reducing the spacing of the cables is a reduction in the magnitudes of the cable forces. The forces in the circumferential cables usually reduce by approximately the same ratio as the shortening of the cable spacing.
- The forces in the circumferential cables are always higher than those in the longitudinal cables.

The comparison of the structural analyses on the reinforced and the non-reinforced membrane structures shows that the reinforced structure has an

Table 4.1a - The maximum cable forces in cylindrical reinforced membrane structures which have flat ends.

cable spacing (m)			2			1		
height of water in the structure (m)			0	2	4	0	2	4
Total length of the structure (m)	8	maximum circumferential cable force (kN)	431	268	149	206	129	71
		Maximum longitudinal cable force (kN)	123	105	160	28	55	107
	16	maximum circumferential cable force (kN)	409		119			
		maximum longitudinal cable force (kN)	19		98			
	32	maximum circumferential cable force (kN)	408		112			
		maximum longitudinal cable force (kN)	2		60			

Table 4.1b - The maximum cable forces in cylindrical reinforced membrane structures which have curved ends.

	cable spacing (m)		2			1		
	height of water in the structure (m)		0	2	4	0	2	4
Total length of the structure (m)	15.5	maximum circumferential cable force (kN)	412	241	107	206	123	57
		maximum longitudinal cable force (kN)	185	159	93	108	97	72
	23.5	maximum circumferential cable force (kN)	412	242	109			
		maximum longitudinal cable force (kN)	179	146	90			
	39.5	maximum circumferential cable force (kN)	412	242	109			
		maximum longitudinal cable force (kN)	172	135	83			

Table 4.1c - The maximum cable forces in dome-shaped reinforced membrane structures.

Cable spacing (m)	2.0			1.0			0.6	
Height of water in the structure (m)	0.	2.0	4.0	0.0	2.0	4.0	0.	2.0
Maximum circumferential cable force (kN)	244	139	58	157	94	40	118	72
Maximum horizontal cable force (kN)	148	66	16	82	48	25	74	47

advantage over the non-reinforced one in that it allows larger structures to be constructed, without having to increase the strength of the membrane or the cables, requiring only the shortening of the spacing of the reinforcements.

In the process of discharging the gas-storage container, the container is kept in equilibrium by replacing the removed gas by an equivalent amount of water so that the internal gas pressure remains unaltered. The non-reinforced membrane and the reinforced membrane structures are analysed for the case when they have been partially discharged. The results show that as water enters the structure, the height of the structure increases and the profile of its cross-section narrows, while the tensile forces decrease. In the case of the non-reinforced membrane structure, the force in the membrane reduces from 201 kN/m to 87 kN/m when the water level inside the structure rises to about 3.0 m. The results of the changes in the maximum cable forces in the reinforced membrane structures due to the discharge of gas are shown in Table 4.1. It is concluded that the structure experiences its maximum tensile forces when it is completely filled with gas. In the case of the non-reinforced membrane container, the theoretical results are confirmed by experimental studies. It is shown that the profiles of the partially discharged models are in good agreement with the corresponding profiles obtained theoretically.

Since the quantity of the gas which can be stored in the container increases with the depth of water, the container is more suitable for deep water locations. The main factors of the fluid environment which should be considered in the design of the proposed structure for deep water conditions are water pressure, current, waves, earthquake and the reactive forces of the foundation medium. The effect of water pressure which is one of the main determinant factors in obtaining an equilibrium configuration for the membrane container, has been considered in the structural analysis. In the hydrodynamic analysis of the proposed structure, the effects of currents and waves are discussed.

The effect of a uniform current on the reinforced membrane gas-storage container is investigated. The investigation is based on the assumption that the forces due to currents on the proposed flexible structure are the same as those on an identical rigid structure. The pressure distribution on the structure due to the action of a

uniform current is obtained theoretically and experimentally. The theoretical analysis is based on the potential flow theory. It is found that the theoretical analysis cannot accurately predict the effect of current on the proposed structure. A better estimation can be obtained by experimental studies. The experiment is carried out in a wind-tunnel, using a rigid model. The pressure around the model due to uniform wind velocities is measured and the distribution of the pressure coefficient at Reynolds numbers of 1.5×10^5 and 1.1×10^6 is found. The results show that the minimum pressure coefficients are -1.9 and -2.4 for the two cases respectively and they occur at about 0.44 and 0.46 of the perimeter from the leading edge. The results also show that the separation point occurs around 0.55 of the perimeter from the leading edge. This is in agreement with the theoretical value of 0.535 obtained by the boundary layer calculation.

The results of the theoretical and the experimental investigations are used to estimate the effects of a typical prototype current of 1 m/s velocity on the proposed reinforced membrane structure. It is observed that where the theoretical results of the effect of current are used, the maximum displacement of cable joints is less than 6 percent of the original positions of the joints and it is found that there is a reduction of about 3 percent in the tension of the circumferential cables. In the case where the experimental results of the effect of current are used, the corresponding change in the displacement of cables is about 2 percent and there is a reduction of around 1 percent in the tension of the circumferential cables. It is therefore concluded that the static effects of uniform currents on the proposed structure are relatively small.

The scouring action of currents is studied experimentally. The results provide a qualitative indication of the pattern of erosion and deposition in the prototype case. It is found that the depth of scour increases with increasing Reynolds number.

The effect of sinusoidal waves on the proposed structure is investigated experimentally for the case when the size of the object is small compared to the wavelength. The coefficient of inertia for the model of the proposed structure is found to be about 3.6 for the horizontal force and about 2.8 for the vertical

force. These experimental results correspond to a prototype case where the prototype is located in 28 m deep water and is subjected to a sinusoidal wave of 88 m wavelength and 4 m wave height. The horizontal and the vertical wave forces produced on a unit length of the structure will then be 55 kN and 9 kN respectively. Since the structure is designed for water depths of about 100 m and because the effects of wave disturbances decrease exponentially with the depth of water, the magnitude of the wave forces on the prototype will be considerably less than the above values. It is therefore concluded that the static equilibrium of the proposed structure is not likely to be seriously affected by the action of the waves. However, detailed model study is desirable before arriving at final design.

The main aspects of the structural and the hydraulic analysis of the submerged gas-filled membrane structure are examined in this study. It is concluded that the proposed method of using flexible containers for storing gas under the sea is feasible, using available material at present time. However, further investigation is required, particularly on the dynamic behaviour of the structure and its construction prooedures, before the proposed method can be put into practice.

4.2 Suggestions for Further Work.

The use of underwater flexible containers for the storage of pressurized gas has been investigated from the structural and the hydraulics points of view. It is shown that the proposed method enables large quantities of gases to be efficiently stored in flexible membrane structures. The present study is however, only a small part of the extensive investigations required for the complete development of the proposed gas storage concept. Further research is needed to be carried out mainly in the following areas:

(a) Dynamic Analysis - Although for structures of small size, a quasi-static analysis may suffice, in order to determine the structural behaviour with reasonable accuracy, a full dynamic analysis is also required. The stiffness, damping and the virtual mass of the structure have to be determined for the appropriate design conditions in order to investigate the dynamic response of the structure particularly under the action of waves and currents. The dynamic behaviour of the structure can be best studied experimentally using large scale models.

(b) Material Properties - The selection of suitable materials for the construction of the proposed structure is vitally important and needs thorough research. The materials should possess the required mechanical properties including strength, elasticity and fatigue life. The diffusion of gas through the material has to be investigated, taking into account the effects of the environment especially high pressure and sea water. Also, the effect of the temperature variations on the membrane, in the process of charging and discharging of gas should be studied.

(c) Anchorage - The hydraulics and structural problems relating to the anchoring of the container must be examined and a comparative study of the various anchorage systems has to be carried out. The choice of a suitable way of anchoring the structure can then be made.

(d) Construction, Installation and Storage Process System - The details of the construction procedures of the container should be carefully investigated using large scale models. The effects of waves and currents on the stability of the structure during the towing and installation operations have to be examined. A suitable system for the charging and discharging process of the proposed gas-storage container must be designed and tested. The structure should be fitted with appropriate inlet and outlet. Care must be taken that there is no leakage of gas through any point on the container.

(e) Cost Analysis - It is of utmost importance that a detailed cost analysis is carried out on the proposed gas-storage system. The cost of collection and treatment of the gas must be included in the cost analysis. The proposed scheme should then be economically assessed against the existing alternative methods.

APPENDICES

List of Notations in the Appendices.

A	cross-sectional area
B	base width
d_{ij}	length of member i-j before deformation
d'_{ij}	length of member i-j after deformation
e_{mnl}	permutation symbol
E	Young's modulus
$E(k,\phi)$	elliptic integral of second kind
$F(k,\phi)$	elliptic integral of first kind
H	total height of the structure
K_{ij}	elasticity of member i-j
L	unstretched length of the membrane
M	total number of joints
N	total number of unrestrained joints
N_{ij}	force in member i-j
N^*_{ij}	initial force in member i-j
p	resultant pressure
Q_{ij}	generalized force in member i-j
s	distance along unstretched perimeter
S^*	distance along stretched perimeter
t	thickness of the membrane
t_{ij}	unit vector along member i-j
T	tensile force per unit length
T_o	initial tension per unit length
${}_k u_i$	displacement of joint i in direction k

x	co-ordinate
X_j	external force acting on joint j
y	co-ordinate
γ	specific weight of water
δ_{ij}	Kronecker's delta
ϵ_{ij}	generalized elongation of member i-j
ρ	radius of curvature
σ	stress
ϕ	inclination to horizontal
ω	weight per unit area of the membrane.

APPENDIX I

ANALYSIS OF AN INFLATABLE STRUCTURE SUBMERGED IN WATER

APPENDIX I.

ANALYSIS OF AN INFLATABLE STRUCTURE SUBMERGED IN WATER.

AI .1 - Derivation of the Differential Equations of Equilibrium for the Membrane.

The co-ordinate system and the pressure distribution on the membrane is shown in Figure 2.1. The forces acting on an elemental strip of until width are shown in Figure AI.1.

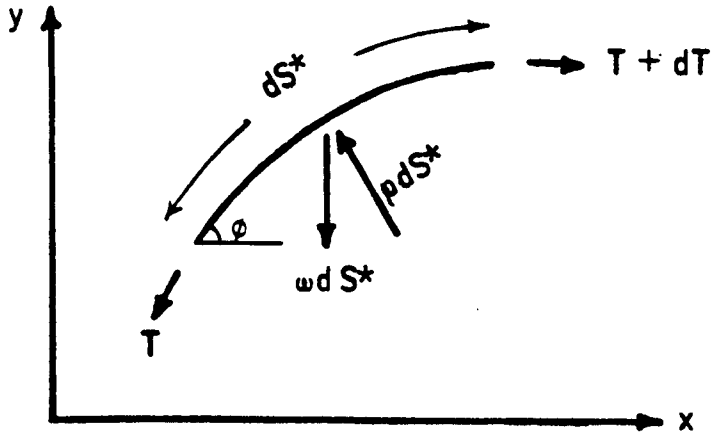

Figure AI.1 - Forces on an elemental strip.

Summing the forces in the tangential direction and taking the limit $dS^* \to 0$, gives

$$\frac{dT}{dS^*} = \omega \sin \phi \qquad (I.1)$$

Similarly in the normal direction it gives

$$-T\, d\phi/dS^* = p - \omega \cos \phi \qquad (I.2)$$

The radius of curvature ρ is given by

$$\frac{1}{\rho} = -\frac{d\phi}{dS^*} \qquad (I.3)$$

Equation (I.3) is substituted into equation (I.2) to give

$$\frac{1}{\rho} = \frac{1}{T}(p - \omega \cos \phi) \qquad (I.4)$$

By geometry

$$dx/dS^* = \cos\phi \tag{I.5}$$

$$dy/dS^* = \sin\phi \tag{I.6}$$

If the membrane obeys an elastic relation of the form $\epsilon = g(\sigma)$ where $\sigma = T/t$, then the ratio dS^*/ds can be written as

$$\frac{dS^*}{ds} = f(\sigma) \tag{I.7}$$

Substituting equation (I.6) into equation (I.1) and integrating gives

$$T = T_0 + \omega y \tag{I.8}$$

where $T_0 = T(0)$. Substituting equation (I.8) into equations (I.2),(I.5) and (I.6) gives

$$\frac{d\phi}{ds} = -\frac{f}{T_0 + \omega y}(p - \omega \cos\phi) \tag{I.9}$$

$$\frac{dx}{ds} = f\cos\phi \tag{I.10}$$

$$\frac{dy}{ds} = f\sin\phi \tag{I.11}$$

Equations (I.9) to (I.11) together with the boundary conditions

$$x(0) = -B/2,\ y(0) = 0 \tag{I.12}$$

$$x(L) = B/2,\ y(L) = 0 \tag{I.13}$$

define the equilibrium shape of the inflated membrane.

A1.2 - Solution of the Differential Equations of Equilibrium.

Due to nonlinearity of the differential equations of equilibrium, an iterative method of solution is required. However, Parbery[53] has found that for practical values of the membrane self-weight, the effect of this parameter is negligible. If the weight ω is zero, then from equation (1.8) the tension and the strain are constant around the perimeter. A theoretical solution can then be developed for the proposed inflated structure. Putting $\omega = 0$ and $f = 1$ in equations(1.9) to (1.11) and letting $p = \gamma y$ (from figure 2.1), the differential equations of equilibrium reduce to:

$$\frac{d\phi}{ds} = \frac{-\gamma y}{T} \tag{1.14}$$

$$\frac{dx}{ds} = \cos\phi \tag{1.15}$$

$$\frac{dy}{ds} = \sin\phi \tag{1.16}$$

Differentiating equation (1.14) and substituting from equation (1.16) gives:

$$\frac{d^2\phi}{ds^2} = -\frac{\gamma}{T}\sin\phi \tag{1.17}$$

This equation can be integrated after multiplying by $\frac{d\phi}{ds}$ to give

$$\frac{1}{2}\left(\frac{d\phi}{ds}\right)^2 = \frac{1}{T}\gamma\cos\phi + C \tag{1.18}$$

C is found by putting $y = 0$ in equation (1.14) and substituting into equation (1.18)

$$\left(\frac{d\phi}{ds}\right)^2 = \frac{2}{T}\gamma(\cos\phi - \cos\phi_0) \tag{1.19}$$

Hence

$$\frac{d\phi}{ds} = \pm a\sqrt{\left(1 - k^2\sin^2\frac{\phi}{2}\right)} \tag{1.20}$$

where

$$a^2 = \frac{2\gamma}{T}(1 - \cos\phi_0) \tag{1.21}$$

and

$$k^2 = \frac{4\gamma}{a^2 T} = \frac{2}{(1 - \cos\phi_0)} \tag{1.22}$$

Since the net pressure on the membrane is outward, the negative root of equation (I.20) applies. The relationship of the co-ordinates x and y to the inclination ϕ is found from equations (I.15), (I.16) and (I.20) to be

$$\frac{dx}{d\phi} = -\frac{1 - 2\,\mathrm{Sin}^2\frac{\phi}{2}}{a\sqrt{(1 - k^2\,\mathrm{Sin}^2\frac{\phi}{2})}}$$

so that

$$x = \frac{2}{ak^2}\left\{2\left[E(k,\tfrac{\phi_0}{2}) - E(k,\tfrac{\phi}{2})\right] + (k^2-2)\left[F(k,\tfrac{\phi_0}{2}) - F(k,\tfrac{\phi}{2})\right]\right\} - B/2 \qquad (I.23)$$

where E and F are elliptic integrals of the second and first orders respectively. And

$$\frac{d\phi}{dy} = \frac{-\gamma y}{T\,\mathrm{Sin}\phi}$$

so that

$$y = \sqrt{\frac{2T}{\gamma}(\mathrm{Cos}\,\phi - \mathrm{Cos}\,\phi_0)} \qquad (I.24)$$

The distance along the perimeter and the tension in the membrane can be computed from the two following equations:

$$s = \frac{2}{a}\left[F(k,\tfrac{\phi_0}{2}) - F(k,\tfrac{\phi}{2})\right] \qquad (I.25)$$

$$T = \frac{\gamma H^2}{2(1 - \mathrm{Cos}\,\phi_0)} \qquad (I.26)$$

AI.3 - The Computer Program Flow Chart.

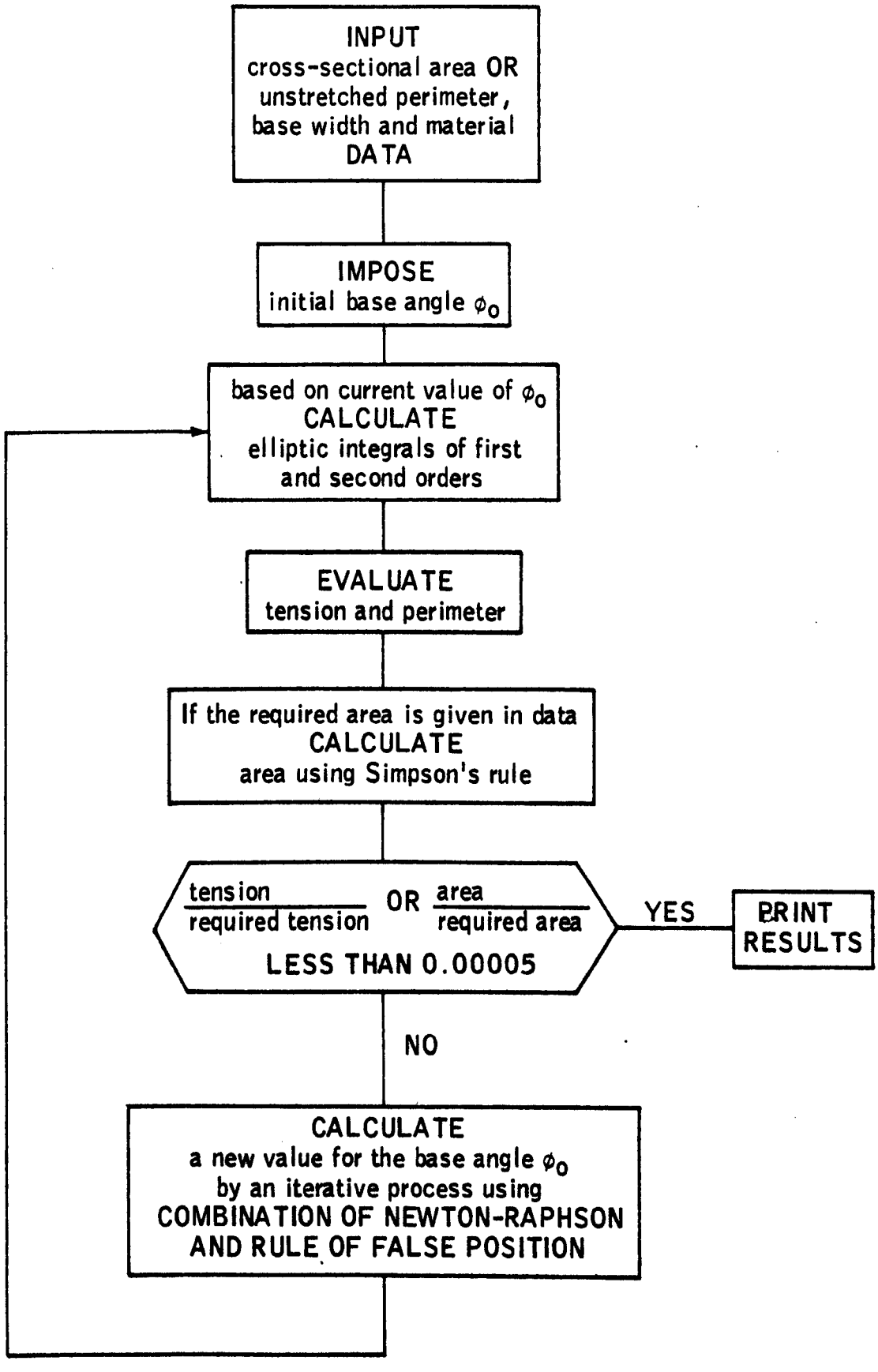

APPENDIX II

CABLE NETWORK ANALYSIS

APPENDIX II.

CABLE NETWORK ANALYSIS.

AII.1. Derivation of the Equilibrium Equations.

The equilibrium equation is derived for a structure with a total of M nodes of which N are entirely unrestrained. By the principle of virtual work

$$\sum_{j>i}^{M}\sum_{i=1}^{N}(Q_{ij}+N^{*}_{ij})\,\delta\epsilon_{ij}-\sum_{j=1}^{N}\vec{X}_j\cdot\delta\vec{u}_j=0 \qquad (II.1)$$

in which Q_{ij} and ϵ_{ij} are the generalized force and the generalized extension respectively, N^{*}_{ij} is the initial prestress force in the member and $\vec{X}_j$ and $\vec{u}_j$ are the vectors of external force and displacement at node j respectively. The generalized extension is given by

$$\epsilon_{ij}=\vec{t}_{ij}\cdot(\vec{u}_j-\vec{u}_i)+\frac{1}{2d_{ij}}(\vec{u}_j-\vec{u}_i)\cdot(\vec{u}_j-\vec{u}_i) \qquad (II.2)$$

where d_{ij} is the initial length of the member connecting nodes i and j and $\vec{t}_{ij}$ is a unit vector in the direction of that member before deformation. The variation of the generalized extension in the scalar form is given by

$$\delta\epsilon_{ij}=\sum_{k=1}^{3}\left[{}_k t_{ij}+\frac{1}{d_{ij}}({}_k u_j-{}_k u_i)\right](\delta_k u_j-\delta_k u_i) \qquad (II.3)$$

in which k denotes the cartesian component of the corresponding vector. Substitution of equation (II.3) into equation (II.1) yields

$$\sum_{j>i}^{M}\sum_{i=1}^{N}(Q_{ij}+N^{*}_{ij})\sum_{k=1}^{3}\left[{}_k t_{ij}+\frac{1}{d_{ij}}({}_k u_j-{}_k u_i)\right](\delta_k u_j-\delta_k u_i)=$$

$$\sum_{j=1}^{N}\sum_{k=1}^{3}{}_k X_j\,\delta_k u_j \qquad (II.4)$$

Given a variation of the form

$$\delta_k u_j = \delta_{kh} \delta_{jl} \tag{II.5}$$

in which δ_{ij} is the Kronecker's delta ($= 1$ if $i = j$, but $= 0$ if $i \neq j$), the right-hand side of equation (II.4) becomes ${}_hX_l$ and the equilibrium equation in direction h for joint l can be written as

$$\sum_{\substack{i=1 \\ i \neq l}}^{M} (Q_{il} + N^*_{il}) \left[{}_ht_{il} + \frac{1}{d_{il}} ({}_hu_l - {}_hu_i) \right] = {}_hX_l \tag{II.6}$$

If N_{il} is the actual force in the member then the generalized force Q_{il} may be defined as

$$Q_{il} = \frac{N_{il} - N^*_{il} \frac{e_{il}}{d_{il}}}{1 + \frac{e_{il}}{d_{il}}} \tag{II.7}$$

in which e_{il} is the actual elongation of the bar. The relation between the generalized elongations and the generalized force can be represented by the generalized constitutive equation

$$Q_{ij} = g(\epsilon_{ij}) \tag{II.8}$$

This functional relation between Q and ϵ can be approximated by a polynomial. The simplest form of this relation is given by the linear function

$$Q_{ij} = K_{ij} \epsilon_{ij} \tag{II.9}$$

in which K_{ij} is a constant for each member of the structure. For small strains equation (II.9) tends to be Hook's law in which case $K = EA$ is equal to the elasticity of the member. Substituting equation (II.2) into equation (II.9)

$$Q_{ij} = K_{ij} \left[\vec{t}_{ij} \cdot (\vec{u}_j - \vec{u}_i) + \frac{1}{2d_{ij}} (\vec{u}_j - \vec{u}_i) \cdot (\vec{u}_j - \vec{u}_i) \right] \tag{II.10}$$

Using equations (II.6) and (II.10), equilibrium equations in terms of the components of the displacements are obtained as follows:

$$\sum_{\substack{i=1 \\ i\neq l}}^{M} \left[{}_h t_{il} + \frac{1}{d_{il}} ({}_h u_l - {}_h u_i) \right] \left\{ N^*_{il} + K_{il} \left[\sum_{k=1}^{3} \left[{}_k t_{il} + \frac{1}{2d_{il}} ({}_k u_l - {}_k u_i) \right] \right. \right.$$

$$\left. \left. ({}_k u_l - {}_k u_i) \right] \right\} = {}_h X_l \quad \begin{matrix} h = 1,2,3 \\ l = 1, \ldots, N \end{matrix} \qquad \text{(II.11)}$$

In the case of the proposed structure, the external loading X_l has to be replaced by the force produced by the resultant pressure on the area between the cables. A unit vector normal to the plane described by the displaced positions of the nodes l, j and k is defined as (Figure II.1)

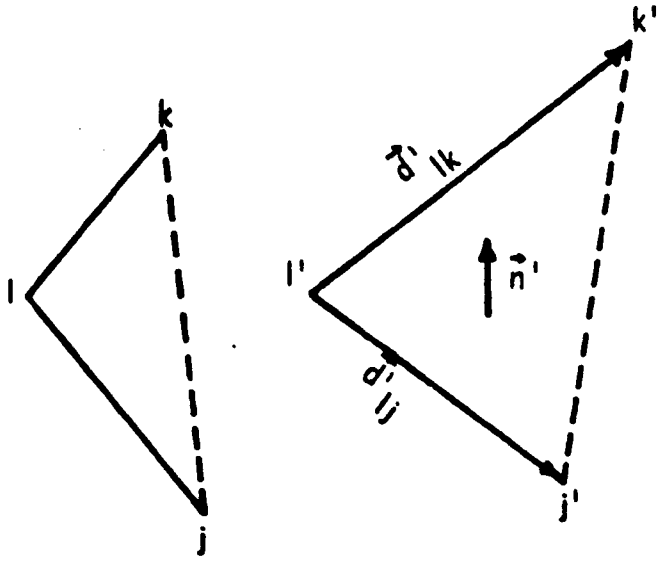

Figure II.1 - Triangular Element

$$\vec{n}' = \frac{1}{2A} \vec{d}'_{lj} \times \vec{d}'_{lk} \qquad \text{(II.12)}$$

in which A is the area of the triangle l' j' k'. The h-direction component of the total force on this triangle due to a normal pressure p, is then

$${}_h X = \frac{p}{2} \; {}_m d'_{lj} \; {}_n d'_{lk} \; e_{mnh} \qquad \text{(II.13)}$$

in which e_{mnh} is the permutation symbol. In terms of the initial length and components of the nodal displacements, equation (II.13) becomes

$$ {}_hX = \frac{p}{2} ({}_m d_{lj} + {}_m u_j - {}_m u_l)({}_n d_{lk} + {}_n u_k - {}_n u_l)\, e_{mnh} $$

which force may be divided equally among nodes l, j and k. In the case of a set of orthogonal cables such as that of figure II.2, the resultant external force at

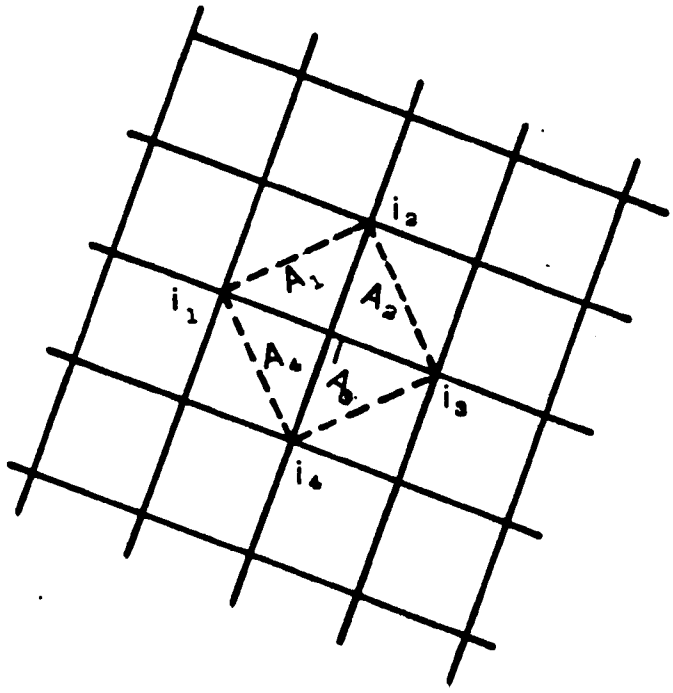

Figure II.2 - Orthogonal Cables.

joint l is the sum of the forces at l due to the pressure on the four triangular areas A_1, A_2, A_3 and A_4. The pressure on each of these areas is assumed to be equal to one third of the sum of the pressures at each of the three nodes surrounding that area. The total external force at node l is then given by

$$
{}_h X_l = \frac{1}{2}\Big\{ \frac{p_1}{2}({}_m d_{li_1} + {}_m u_{i_1} - {}_m u_l)({}_n d_{li_2} + {}_n u_{i_2} - {}_n u_l)\, e_{mnh}
$$

$$
+ \frac{p_2}{2}({}_m d_{li_2} + {}_m u_{i_2} - {}_m u_l)({}_n d_{li_3} + {}_n u_{i_3} - {}_n u_l)\, e_{mnh}
$$

$$
+ \frac{p_3}{2}({}_m d_{li_3} + {}_m u_{i_3} - {}_m u_l)({}_n d_{li_4} + {}_n u_{i_4} - {}_n u_l)\, e_{mnh}
$$

$$
+ \frac{p_4}{2}({}_m d_{i_4} + {}_m u_{i_4} - {}_m u_l)({}_n d_{li_1} + {}_n u_{i_1} - {}_n u_l)\, e_{mnh}\Big\} \qquad \text{(II.14)}
$$

where p_1, p_2, p_3 and p_4 are the average pressures on areas A_1, A_2, A_3 and A_4 respectively.

In order to solve the system of equations (II.11) the Newton-Raphson algorithm is used. The general term of the Jacobian matrix is given by

$$
\frac{\partial_h F_l}{\partial_p u_q} = \sum_{\substack{i=1 \\ i\neq l}}^{M} \frac{1}{d_{il}} \delta_{hp}(\delta_{lq} - \delta_{iq})\Big[N^*_{il} + K_{il}\Big\{\sum_{k=1}^{3}\Big[{}_k t_{il} + \frac{1}{2d_{il}}({}_k u_l - {}_k u_i)\Big]
$$

$$
({}_k u_l - {}_k u_i)\Big\}\Big] + \sum_{\substack{i=1 \\ i\neq l}}^{M}\Big[{}_h t_{il} + \frac{1}{d_{il}}({}_h u_l - {}_h u_i)\Big]K_{il}(\delta_{lq} - \delta_{iq})\Big[{}_p t_{il} + \frac{1}{d_{il}}
$$

$$
({}_p u_l - {}_p u_i)\Big] - \frac{\partial_h X_l}{\partial_p u_q} \qquad \text{(II.15)}
$$

For the force given by equation (II.14), the differentiation of the external force with respect to displacement is given by:

$$\frac{\partial_h X_l}{\partial_p u_q} = (1 - \delta_{hp})(1 - \delta_{hk})(1 - \delta_{pk}) \left\{ \delta_{lq} \left[\frac{p_1}{4} ({}_k d_{li_1} - {}_k d_{li_2} + {}_k u_{i_1} - {}_k u_{i_2}) \right.\right.$$

$$+ \frac{p_2}{4} ({}_k d_{li_2} - {}_k d_{li_3} + {}_k u_{i_2} - {}_k u_{i_3}) + \frac{p_3}{4} ({}_k d_{li_3} - {}_k d_{li_4} + {}_k u_{i_3} - {}_k u_{i_4})$$

$$\left. + \frac{p_4}{4} ({}_k d_{il_4} - {}_k d_{il_1} + {}_k u_{i_4} - {}_k u_{i_1}) \right] + (1 - \delta_{lq}) \left[\frac{p_s}{4} ({}_k d_{lj_1} + {}_k u_{j_1} - {}_k u_l) \right.$$

$$\left.\left. - \frac{p_t}{4} ({}_k d_{lj_2} + {}_k u_{j_2} - {}_k u_l) \right] \right\} \qquad (II.16)$$

in which δ_{lq} is the Kronecker delta, j_1 and j_2 are the nodes connected to l which are on the two sides of the node q; and p_s and p_t are the pressure values acting on the area enclosed by l, q, j_1 and l, q, j_2 respectively. The differentiation of the force with respect to displacement as given by equation (II.16) is based on the assumption that the value of the pressure p does not change significantly with changes of displacement.

If the change in the external force with the changes of displacements is small, the $\frac{\partial_h X_l}{\partial_p u_q}$ term can be omitted from equation II.15.

AII.2 - Computer Program Flow Chart.

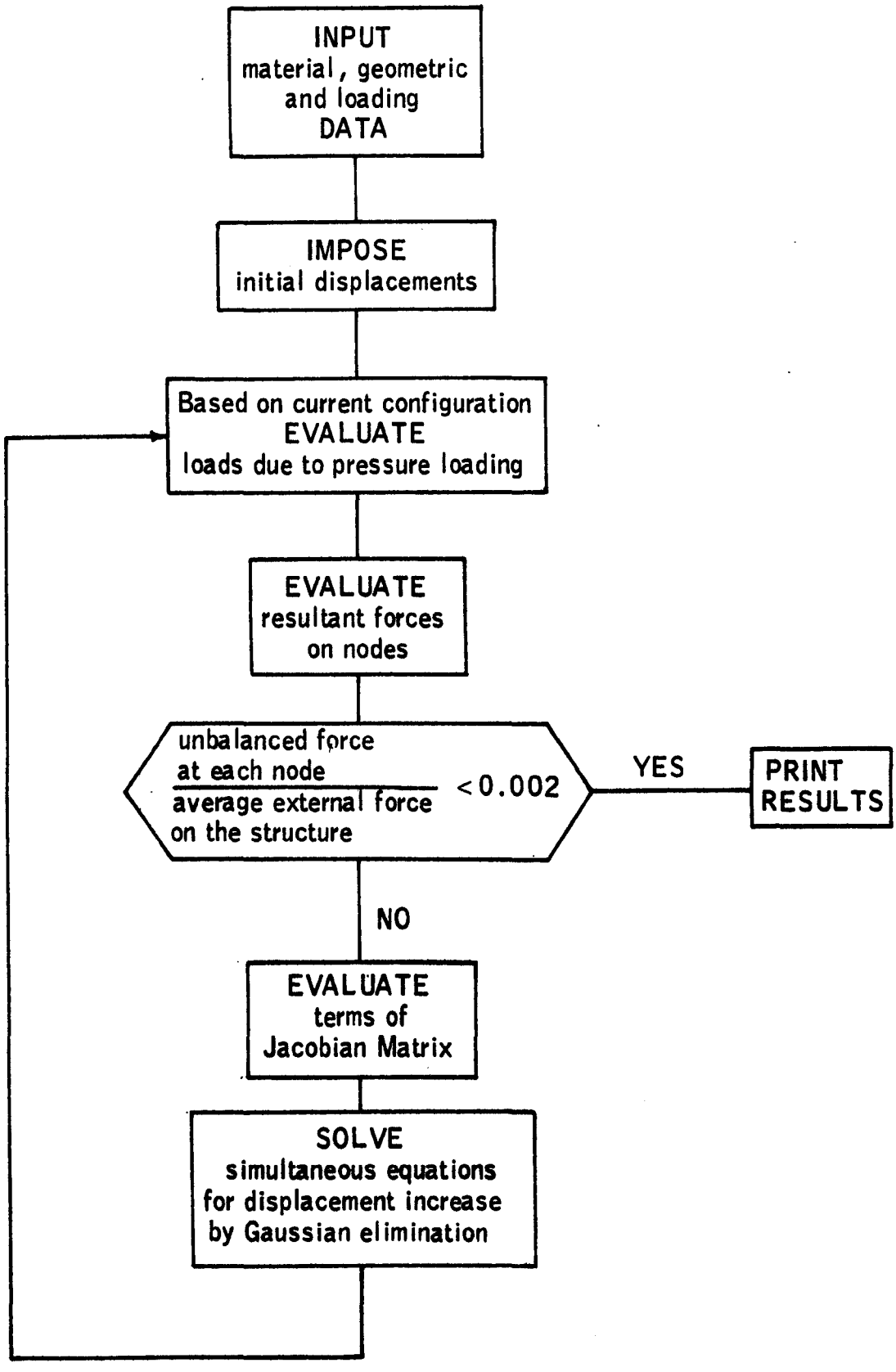

APPENDIX III

EXPERIMENTAL STUDY ON THE EFFECT OF WAVES

APPENDIX III.

EXPERIMENTAL STUDY ON THE EFFECT OF WAVES.

AIII.1. Introduction.

The prediction of the effects of ocean waves on the proposed structure presents numerous problems and can be hardly dealt with completely in this study. Due to the unavailability of accurate theoretical methods for the evaluation of wave forces on submerged structures, these forces can only be estimated experimentally. Laboratory facilities are limited and it is not possible to carry out the experiments under the same ratio of water depth to object size as in the prototype. It is also impossible in wave tanks, to achieve values of Reynolds numbers as large as those which occur in the real situation. Moreover, ocean waves are very irregular and have a complicated nature whereas laboratory waves are generally regular sinusoidal waves which run in a certain direction relative to the model, at any one time. In addition to the above mentioned problems, the study of wave effects on the proposed structure is faced by an extra important problem, namely, modelling the flexible structure. It is not practical to measure the wave forces on a flexible model and with a rigid model, it is not possible to predict the behaviour of a flexible structure under the action of waves. Considering the uncertainties and limitations involved in the study of the effect of waves on the proposed structure using small scale laboratory tests, it is suggested that this investigation has to be carried out by large-scale tests in the ocean. This task is obviously beyond the scope of this study. However, it is decided to carry out a brief investigation into the effect of waves on the proposed structure.

Since the size of the structure is small compared to the wavelength of the incident wave, Morison's equation can be used for the estimation of the wave forces on the structure. The application of Morison's equation requires the knowledge of the two force coefficients; namely drag and inertia. Due to the unavailability of theoretical methods, the values of these force coefficients have to be determined empirically. This appendix is devoted to the experimental investigation into the effect of waves on the proposed structure for the purpose

of determination of the coefficient of inertia.

Although the proposed structure is of flexible type, the model used in the wave experiment is rigid so that the forces can be measured more accuractely. Two different models are used in this study. The first model is similar to the proposed structure and the second model is simply a circular cylinder. Since some published experimental results are available on the effect of waves on horizontal circular cylinders, the results of the experiment on the second model is used for checking the accuracy of the experimental method adopted. The details of the two models are explained in section AIII.2. The wave tank in which the experiments are conducted is described in section AIII.3 followed by a description of the supporting system of the model in the tank and the measuring apparatus in section AIII.4.

AIII.2. The Models for the Wave Experiment.

Laboratory experiments are carried out in order to study the effect of waves on the proposed structure. The experiments are conducted on the model of the proposed structure and on a circular cylinder model. The length of each model is 0.56 m. This length is chosen such that each model spans the total width of the wave tank, allowing 5 mm from each side wall of the tank. The models are made of perspex and they are hollow. Small holes in the models ensure that the models completely fill with water on immersion. This prevents any abrupt change in the distribution of water in the models. Further details of the models are as follows:

Model 1 - Scaled model of the proposed structure (Photo 8). In order that the model is tested under deep water conditions in the wave tank available, and on the other hand wave forces on the model are detectable by the measuring instruments, it is found that the most suitable model to prototype scale factor is about 1:67 . The model is made up of sixteen identical strips of 6 mm thick perspex. The strips are glued to each other along their length to form the appropriate cylindrical shape. They are then mounted on a rectangular 12 mm thick perspex base. Five pieces of perspex in the shape of the required model cross-section are used as stiffening webs inside the model. Holes are drilled in

all the webs for the free passage of water in and out of the model. The outer surface of the model is smoothed and varnished. The method of supporting the model in the tank is explained in section 3.4.2.3.

Model 2 - Circular Cylinder (Photo 8). In order to check the experimental technique used for the study of wave forces on model 1, the same technique is used in the measurement of wave forces on a horizontal circular cylinder for which published results are available. A 0.09 m diameter cylinder is chosen for this purpose. The results obtained are then compared with the results in the literature for horizontal circular cylinders.

AIII.3 The Wave Tank.

The experiments are carried out in a wave tank 9.75 m long, 0.57 m wide and 0.64 m deep. The floor of the tank is covered by sheets of perspex to ensure the smoothness of the tank bottom. Since the model is held close to the base of the tank, any large non-uniformity in the tank floor would reduce the accuracy of the results significantly. The wave-maker consists of a 0.56 m wide flap paddle. The paddle is made of waterproof plywood and is coated with water resistant varnish. A butyl rubber cover round the bearing reduces leakage under the base of the paddle. The drive mechanism enables both the frequency and the amplitude of the flap paddle to be varied. The wave generator is powered with a variable speed motor. An efficient absorbing beach is installed at the other extremity of the tank to prevent reflected waves from interfering with the generated incident waves. The beach is inclined at 15° to the tank floor and is composed of shingle covered with aluminium honeycomb.

The waves generated in the tank are very close to sinusoidal waves. The frequency of the waves generated can be varied between 1.0 Hz and 1.7 Hz but there is no independent control over the wavelength.

AIII.4 The Measuring Apparatus for the Wave Experiment.

In order to measure the forces due to the action of waves on each model, the model has to be held in the wave field on a supporting system in such a way that the entire wave force on the model is transmitted to the measuring apparatus. In this experiment, the model is suspended vertically by means of two fine wires. The upper ends of the wires are supported from small cantilever beams with strain gauges attached. The model is suspended with a clearance of approximately 5.0 mm off the floor of the tank so that the beams provide the sole support of the model. The weight of the model prevents the vertical wires going slack during testing. Horizontal restraint of the model is provided by four fine wires; two wires on the upstream and two on the downstream side of the model. The wires run horizontally along the bottom of the tank and in the direction away from the model. At a distance of 1.6 m from the model, each wire passes under a 40 mm diameter pulley and emerges from the water vertically. The wires are then attached above the free surface to cantilever beams equipped with strain gauges. The horizontal wires are pretensioned so that they do not go slack. It is checked that the natural frequency of the whole system, with the model submerged, is considerably higher than the frequencies of the waves so that resonance does not occur.

The horizontal and the vertical wave forces on the model are transmitted via the fine wires to the cantilever with the strain gauges attached. The strain gauges are connected into Wheatstone bridge circuits, the outputs of which are amplified and then fed into separate channels of a multi-channel U-V recorder. Before starting the actual experiment, the force measuring apparatus is calibrated against known weights.

The wave height and wave profiles are measured by a resistance type wave probe. The signals from the probe are fed into one of the channels of the U-V recorder. The probe is positioned directly above the model so that the passing of each wave crest past the model would be marked on the recorder and the phase angle between the wave crest and the maximum wave forces can be measured. Prior to the experiment, the wave probe is calibrated using a depth gauge.

The details of the experimental procedures are given in section AIII.5.

AIII.5 The Experimental Technique.

The model is suspended in the wave tank by the supporting system as shown in Photo 9. The horizontal and the vertical force measuring apparatus is calibrated before and after each experiment. A wave probe is positioned directly above the model in order to measure the wave height. The probe is calibrated prior to each experiment.

Waves of different frequencies are generated in the wave tank. Traces of horizontal and vertical forces and traces of the waves are recorded for each wave frequency. The wave heights and the maximum wave forces are measured from the traces. Linear wave theory is used to calculate the horizontal and the vertical components of water particle velocities and accelerations. The Reynolds numbers, the Keulegan-Carpenter numbers and the coefficients of inertia are then calculated using the values of the wave heights and the maximum forces corresponding to each wave frequency.

AIII.6 Discussion of the Experimental Results.

The effect of waves is studied on a circular cylinder model and the model of the proposed structure. The Reynolds numbers obtainable in the wave tank for both models are in the range of 1×10^3 to 6×10^3. The values of the Keulegan-Carpenter numbers for the two models are in the range of 0.08 to 0.6. Since the values of the Keulegan-Carpenter numbers are less than 4, the drag effects are neglected and the wave forces are assumed to be inertia dominated. The results for the coefficients of inertia are shown in table AIII.1. It is observed that the inertia coefficients obtained for the circular cylinder model are in the range of 1.7 and 2.8. Keulegan and Carpenter[34] have reported that for horizontal cylinders, the inertia coefficients are in the range 0.6 to 2.6 for Reynolds numbers between 4×10^3 and 3×10^4. The present results are therefore in agreement with those of Keulegan and Carpenter[34]. The present results are also in good agreement with other published results such as those reviewed by Hogben et al[29] for horizontal cylinders.

Table AIII.1 - The results of the experimental study on the effect of waves.

	Wavelength (m)	Wave period (s)	Wave height (m)	Reynolds number x 10^{-3}	Keulegan-Carpenter number	Max. horizontal force (N)	Max. vertical force (N)	Coeff. of inertia for the horizontal force.	Coeff of inertia for the vertical force
Circular cylinder model	0.58	0.61	0.083	1.26	0.09	1.33	0.47	2.79	2.00
	0.62	0.63	0.087	1.65	0.12	1.64	0.59	2.71	2.06
	0.72	0.68	0.081	2.42	0.19	2.17	0.70	2.63	2.08
	0.94	0.78	0.073	4.16	0.37	3.18	0.83	2.56	2.09
	1.15	0.87	0.061	5.03	0.50	2.92	0.75	2.17	2.10
	1.39	0.97	0.042	4.74	0.53	1.86	0.47	1.71	1.95
Model of the proposed structure	0.58	0.61	0.083	1.40	0.08	2.74	0.87	4.05	2.80
	0.62	0.63	0.087	1.83	0.11	3.84	1.05	4.45	2.82
	0.72	0.68	0.081	2.58	0.16	5.16	1.29	4.38	2.86
	0.94	0.78	0.073	4.52	0.33	6.45	1.52	3.62	2.88
	1.15	0.87	0.061	5.59	0.45	4.36	1.33	2.26	2.83
	1.39	0.97	0.042	5.16	0.47	4.17	0.89	2.67	2.78

The agreement of the experimental results of the cylinder model, with the results of published work, ensures that the method of experimentation is correct and the results obtained are reliable. It is observed that the inertia coefficients for horizontal forces on the model of the proposed structure are in the range 2.2 to 4.5, with an average value of 3.6. The inertia coefficient for vertical forces is about 2.8 and is almost unaffected by the variation of wavelength. The results of the experiments on the two models show that the inertia coefficient for the model of the proposed structure is slightly higher than that for a circular cylinder.

The pressure distribution around the model of the proposed structure due to the action of waves has also been measured. The measured pressure distribution due to a sinusoidal wave of 1.15 m wavelength, 0.061 m wave height and 0.87 s wave period is shown in figure AIII.1. The maximum horizontal force evaluated from this pressure distribution, namely 3.75 N is found to be in reasonable agreement with the directly measured value of 4.36 N.

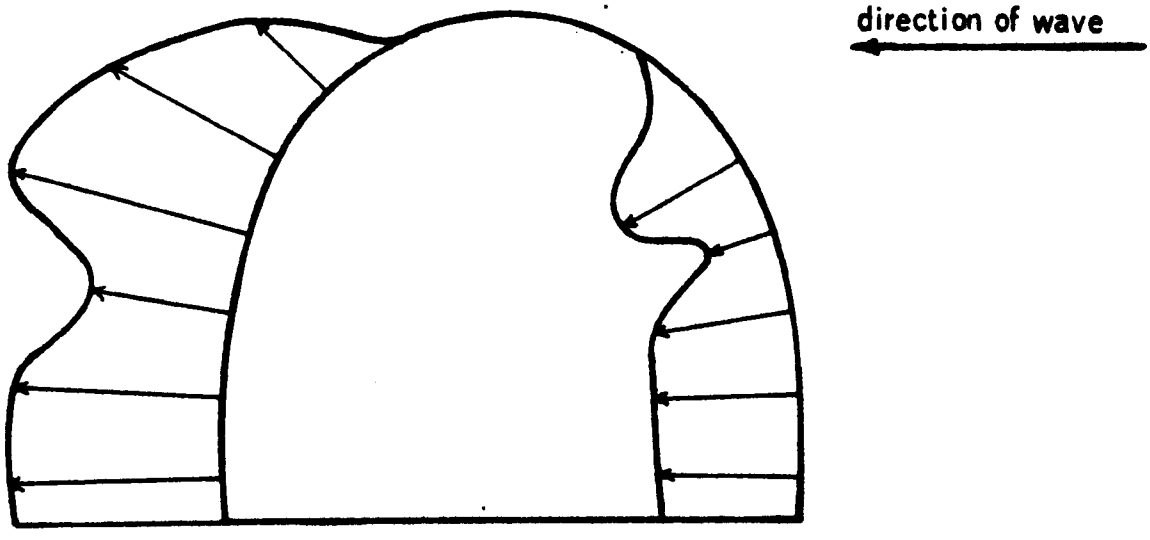

Figure AIII.1. - Pressure distribution due to a sinusoidal wave, around the model of the proposed structure.

Wavelength = 1.15 m

Wave period = 0.87 s

Wave height = 0.061 m.

PAGE
MISSING
IN
ORIGINAL

PHOTOGRAPHS

Photo 1. The semi-elliptical cylinder model (A) and the scaled model of the proposed structure (B) for the current experiment.

Photo 2 - Position of the model in the wind tunnel.

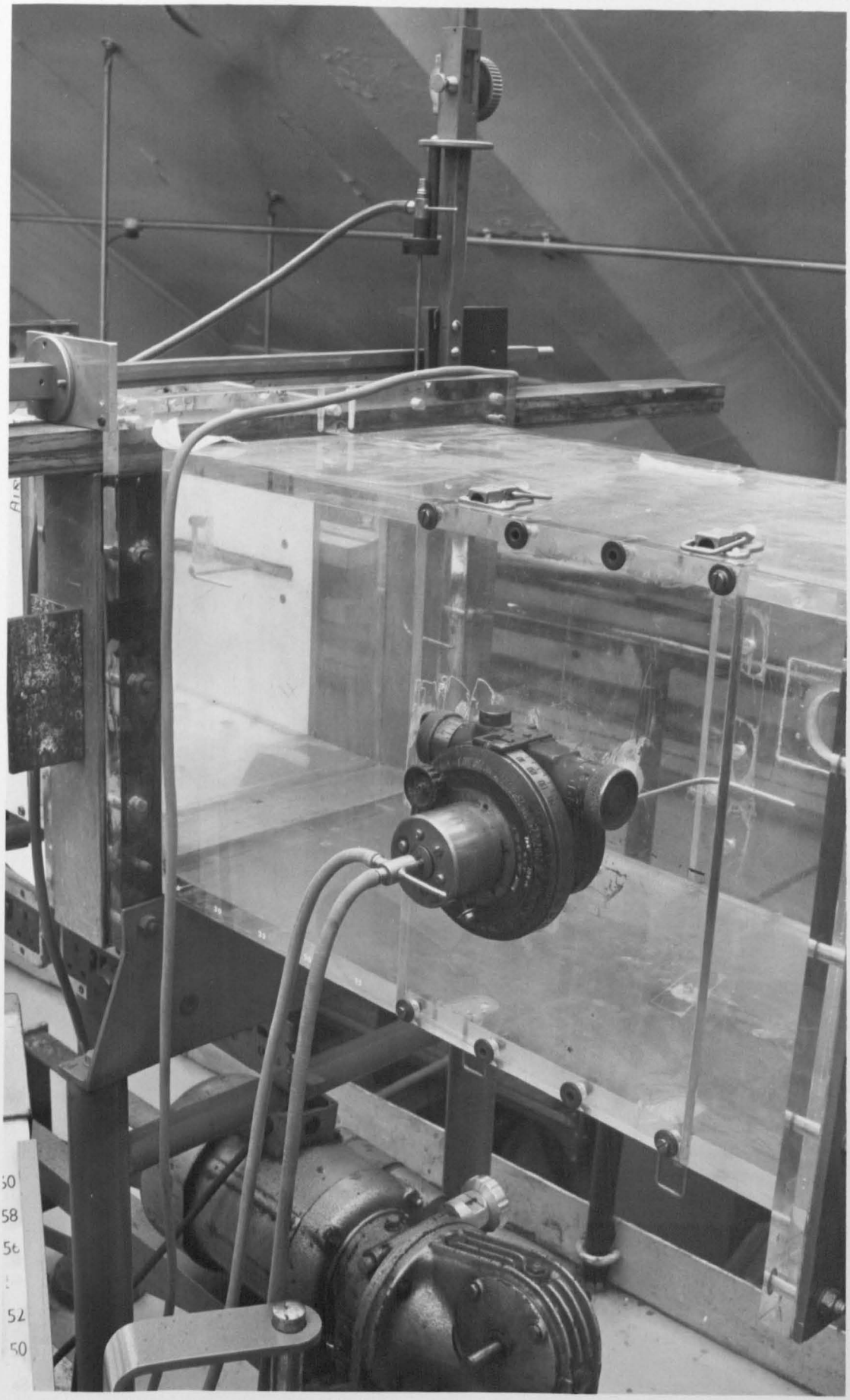

Photo 3 - The rotating disc of the wind tunnel.

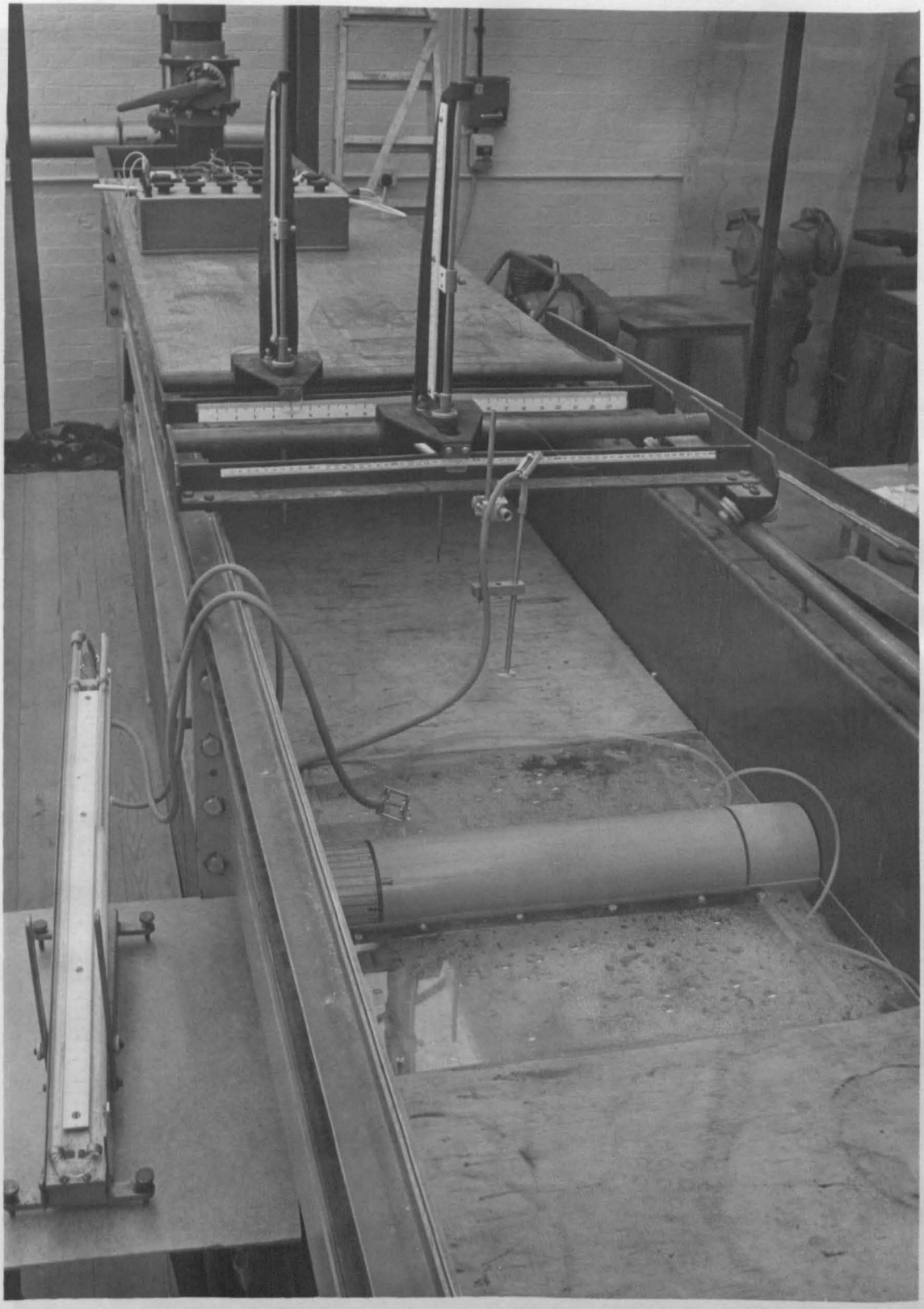

Photo 4 - Semi-circular cylinder model in the flume.

Photo 5 - The wind tunnel.

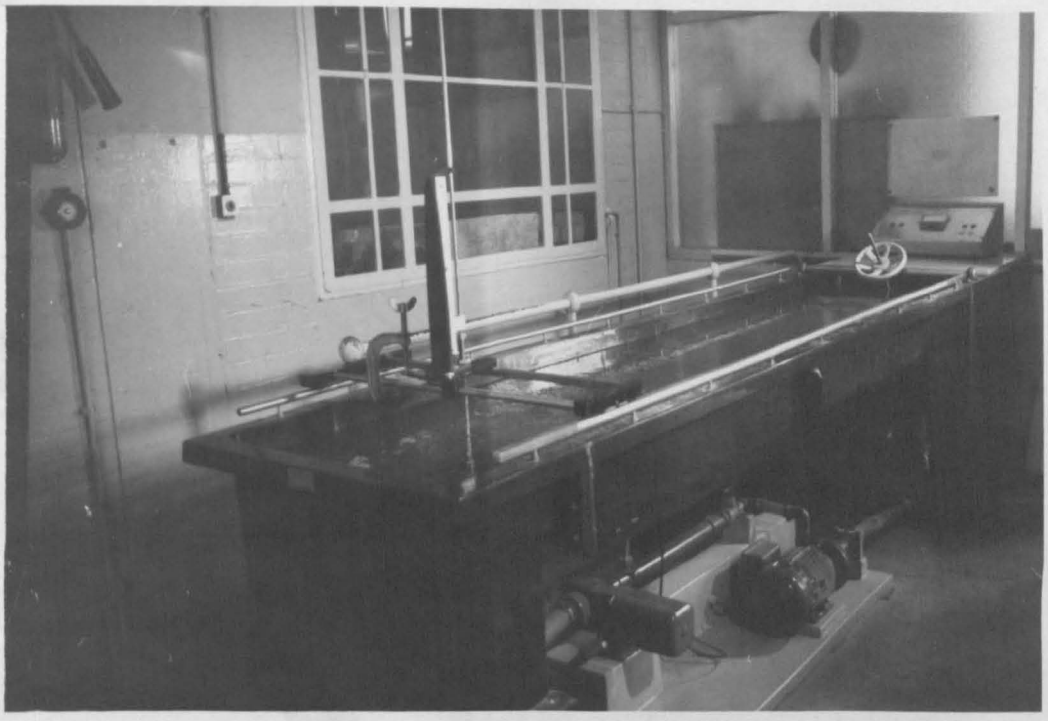

Photo 6 - The flow tank for the study of scour patterns.

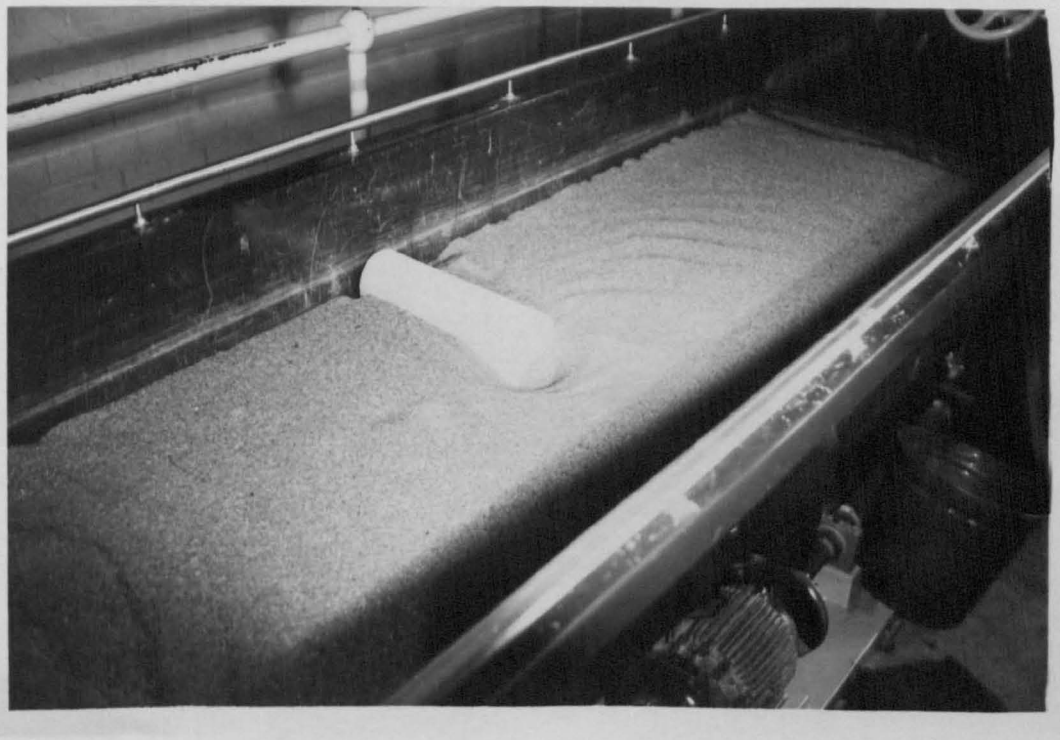

Photo 7 - An example of scour contours around the model.

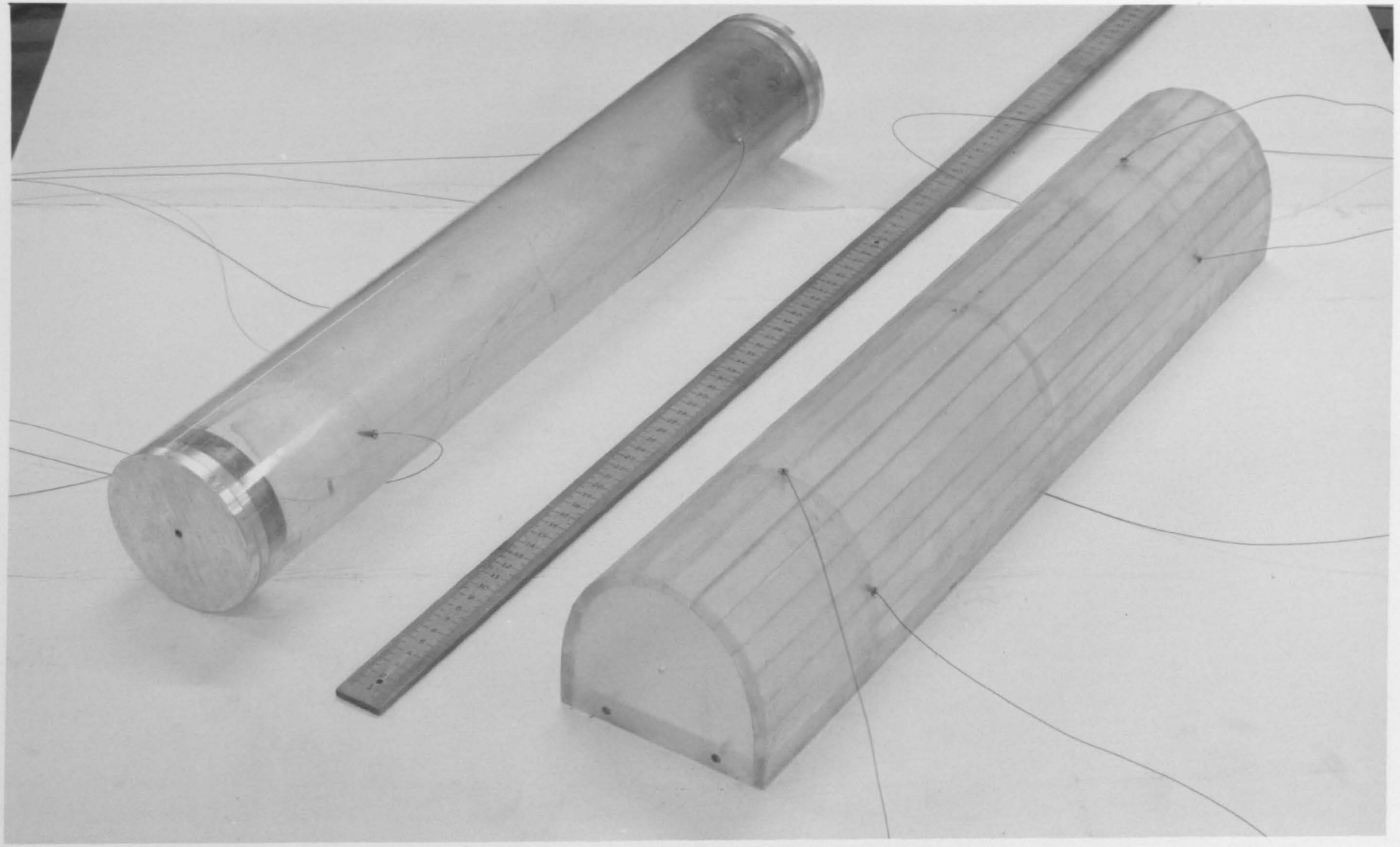

Photo 8. The circular cylinder model and the model of the proposed structure for the wave experiment.

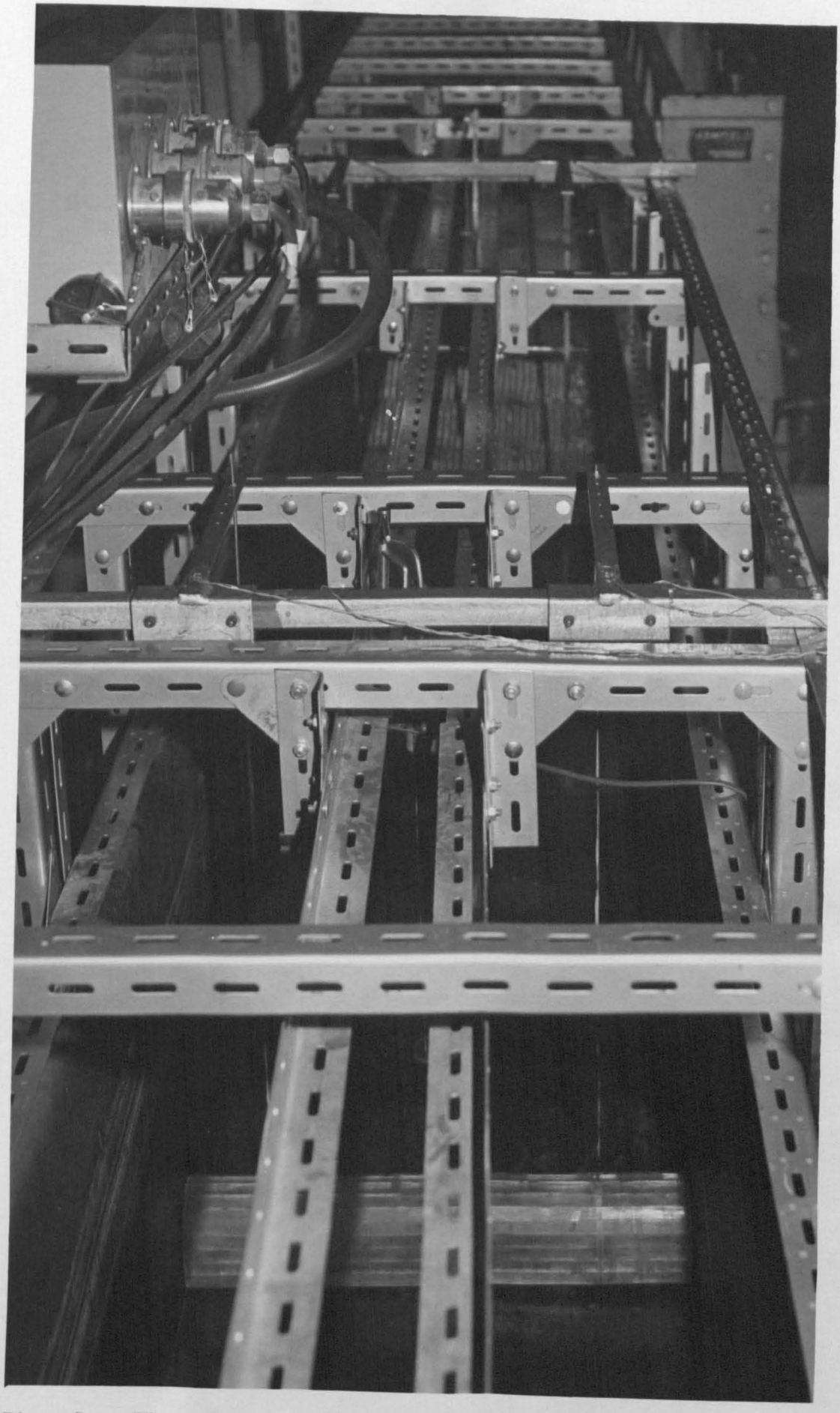

Photo 9 - The model of the proposed structure suspended in the wave tank.

REFERENCES

REFERENCES

1. Altinisik D., Karadeniz H. and Severn R.T.
Theoretical and experimental studies on dynamic structure-fluid coupling, Proc. Instn. Civ. Engrs., Part 2, 1981, 71, pp.675-704.

2. Anwar H.O.
Inflatable dams, Journal of the Hydraulics Division, Proc. ASCE, Vol. 93, HY 3, May 1967, pp. 99-119.

3. Avula X.J.R. and Ural O.
Large elastic deformations of a closed axisymmetric membrane simultaneously inflated by a gas and a liquid, Shell structures and climatic influences, Int. Assoc. for Shell Struct., IASS, Calgary Symp. Proc., July 3-6, 1972.

4. Avula X.J.R. and Ural O.
Underwater stabilization of a gas-filled membrane shell, Proc. 4th. Canadian Congress of Applied Mechanics, Montreal, May 28-June 1st 1973, pp.203-204.

5. Baffico R., Di Lucrezia S., Bozzo G.M. and Faso D.
The use of rubberized sheeting as partitions for submerged tanks utilized for offshore oil fields, International Rubber Conference, Venice, Oct. 1979, pp.408-426.

6. Batham J.P.
Pressure distributions on circular cylinders at critical Reynolds numbers, J. Fluid Mech. 1973, vol. 57, part 2, pp.209-228.

7. Binnie A.M.
The theory of flexible dams inflated by water pressure, J. Hydraul. Res. 1973, Vol.11, No.1, pp.61-68.

8. Blaisdell F.W., Anderson C.L. and Hebaus G.G.
Ultimate dimensions of local scour, Journal of the Hydraulics Division, Proc. ASCE, Vol.107, HY3, March 1981, pp.327-337.

9. Bozzo G.M., Cannavaciuolo A., Faso D. and Zanchettin F.
Design of a new concept of underwater oil storage tank in 300 m water depth with rubberized diaphragm, OTC 3471, 11th Annual OTC in Houston, Tex., April 30-May 3, 1979, pp.989-1001.

10. Budiansky B.
Remarks on theories of solid and structural mechanics, Harvard University, Cambridge, Mass., 1967.

11. Chakrabarti S.K., Naftzger R.A.
Nonlinear wave forces on half cylinder and hemisphere, Journal of the Waterways, Harbours and Coastal Engineering Division, Proc. ASCE, vol. 100, WW3, Aug. 1974, pp.189-204.

12. Chan H.C., Tseung A.C.C. and Cheng K.B.
A novel method of gas storage under the sea, 3rd World Hydrogen Energy Conference, June 23-26 1980, Tokyo, Japan.

13. Chandrasekaran A.R., Saini S.S. and Malhotra M.M.
Virtual mass of submerged structures, Journal of the Hydraulics Division, Proc. ASCE, Vol.98, HY5, May 1972, pp.887-896.

14. Cowan H.J. and Gero J.S.
Pneumatic structures constrained by networks, Shell structures and climatic influences, Int. Assoc. for Shell Struct., IASS, Calgary Symp. Proc., July 3-6, 1972.

15. Dean R.G.
Relative validities of water wave theories, Journal of the Waterways, Harbours and Coastal Engineering Division, Proc. ASCE, Vol.96, WW1, Feb. 1970, pp.105-119.

16. Department of Energy.
Offshore installations: Guidance on design and construction, 5th edition 1983, London HMSO.

17. Department of Energy.
Development of the oil and gas resources of the United Kingdom 1983, (The Brown Book), April 1983, London HMSO.

18. Efthymiou M. and Narayanan R.
Wave forces on unburied pipelines, J. Hydraul. Res., 1980, Vol.18, No.3, pp.197-211.

19. Efthymiou M. and Narayanan R.
Wave forces on submarine pipelines, Proc. Instn. Civ. Engrs., Part 2, 1981, 71, pp.773-787.

20. Epstein M. and Tene Y.
Nonlinear analysis of pin-jointed space trusses, Journal of the Structural Division, Proc. ASCE, Vol.97, ST9, Sept. 1971, pp.2189-2202.

21. Garrison C.J. and Seetharama R.
Interaction of waves with submerged objects, Journal of the Waterways, Harbours and Coastal Engineering Division, Proc. ASCE. Vol.97, WW2, May 1971, pp.259-277.

22. Garrison C.J. and Chow P.Y.
Forces exerted on a submerged oil storage tank by surface waves, OTC 1555, 4th Annual OTC in Houston, Tex., May 1-3 1972, pp.443-452.

23. Goldstein S.
Modern developments in fluid dynamics, Vol.2, Dover Publications, New York, 1965.

24. Harrison H.B.
The analysis and behaviour of inflatable membrane dams under static loading, Proc. Instn. Civ. Engrs., 1970, 45, pp.661-676.

25. Hart-Smith J.J. and Crisp J.D.C.
Large elastic deformations of thin rubber membranes, Int. Journal of Engineering Science, Vol.5, No.1, Jan. 1967.

26. Herzog T.
Pneumatic structure, Crosby Lockwood Staples Publication, London, 1977.

27. Hill, M.N.
The Sea, Wiley and Sons, New York, 1966.

28. Hix C.M.
A systems approach to design of an offshore oil storage reservoir, Proc. of the 1971 Symp. of the Int. Assoc. for Shell Structures, Pacific Symp., Part 1, edited by Rudolph Sziland, University Press of Hawaii, Honolulu, pp.100-114.

29. Hogben N., Miller B.L., Searle J.W. and Ward G.
Estimation of fluid loading on offshore structure, Proc. Instn. Civ. Engrs., Part 2, 1977, 63, pp.515-562.

30. Howard J.L. and Anderson P.G.
A barge-mounted gas liquifaction and storage plant, Chemical Engineering Progress, Vol.75, No.10, Oct. 1979, pp.76-81.

31. International Association for Shell Structures.
Proc. of the First International Colloquim on Pneumatic Structures, University of Stuttgart, West Germany, 1967.

32. Ippen A.T.
Estuary and coastline hydrodynamics, McGraw-Hill, New York, 1966.

33. Itokawa H., Ohira T., Hirose T. and Sakuta M.
Undersea oil storage system, Models I and II, Proc. of the 1971 Symp. of the Int. Assoc. for Shell Structures, Pacific Symp., Part I, edited by Rudolph Szilard, University Press of Hawaii, Honolulu, pp. 150-179.

34. Keulegan G.H. and Carpenter L.H.
Forces on cylinders and plates in an oscillating fluid, J. Res. Natn. Bur. Stand., 1958, 60, No.5, pp.423-440.

35. Lamb H.
Hydrodynamics, 5th edition, Cambridge University Press, 1924.

36. Lanchester F.W.
"Patent 119339", London, 1917.

37. Laursen E.M.
Observations on the nature of scour, Proc. of the 5th Hydraulic Conference, Bulletin 34, University of Iowa, Iowa City, Iowa, June 9-11, 1952, pp.179-197.

38. Leonard J.W.
Inflatable shells: Pressurization phase, Journal of the Engineering Mechanics Division, Proc. ASCE, vol.93, EM2, 1967.

39. Leonard J.W.
Inflatable shells: In-service phase, Journal of the Engineering Mechanics Division, Proc. ASCE, vol.93, EM6, 1967.

40. Leonard J.W.
Inflatable shells for underwater use, OTC 1404, 3rd Annual OTC in Houston, Tex., April 19-21, 1971, pp.789-806.

41. Leonard J.W.
Inflatable shells in the fluid environment, Proc. of the 1971 Symp. of the Int. Assoc. for Shell Structures, Pacific Symp., Part I, edited by Rudolph Sziland, University Press of Hawaii, Honolulu, pp.124-139.

42. Leonard J.W., Garrison C.J. and Hudspeth R.T.
Deterministic fluid forces on structures: A review, Journal of the Structural Division, Proc. ASCE, vol.107, ST6, June 1981, pp.1041-1057.

43. Malcolm D.J. and Glockner P.G.
Optimum cable configuration for air-supported structures, Journal of the Structural Division, Proc. ASCE, vol.105, ST2, Feb.1979, pp.421-435.

44. McCormick M.E.
Anchoring Systems, Oxford, Pergamon, 1979.

45. Milne-Thomson L.M.
Theoretical Hydrodynamics, Macmillan and Co., London, 1949.

46. Misra A.K. and Modi V.J.
Flexural study of a neutrally buoyant inflated viscoelastic-structural member, J. Hydronautics, vol.10, No.1, Jan.1976, pp.18-25.

47. Modi V.J. and Wiland E.
Unsteady aerodynamics of stationary elliptic cylinders in subcritical flow, AIAA journal, Vol.8, No.10, Oct. 1970, pp.1814-1821.

48. Morison J.R. et al.
The forces exerted by surface waves on piles, Trans. Am. Inst. Min. Metall. Engrs, Petroleum Branch, 1950, 189, pp.149-154.

49. Myers J.J., Holm C.H. and McAllister R.F.
Handbook of ocean and underwater engineering, McGraw-Hill, New York, 1969.

50. OdenJ.T. and Kubitza W.K.
Numerical analysis of nonlinear pneumatic structures, Proc. 1st International Colloquium on Pneumatic Structures, IASS, Stuttgart, 1967.

51. Otto F.
Tensile structures, MIT Press, Cambridge, Mass., USA, 1962.

52. Parbery R.D.
A continuous method of analysis for the inflatable dam, Proc. Instn. Civ. Engrs., Part 2, 1976, 61, pp.725-736.

53. Parbery R.D.
Factors affecting the membrane dam inflated by air pressure, Proc. Instn. Civ. Engrs., Part 2, 1978, 65, pp.645-654.

54. Pohlhausen K.
Zur näherungsweisen Integration der Differentialgleichung der laminaren Reibungsschicht. ZAMM1, 1921, pp.252-268.

55. Price C.
Air Structures, London HMSO, 1971.

56. QMC Anchor Technology Ltd.,
The development of an embedded anchor to provide multi-directional restraint.

57. Roshko A.
Experiments on the flow past a circular cylinder at very high Reynolds number, J.Fluid Mech. 1961, vol.10, pp.345-356.

58. Schlichting H.
Boundary layer theory, McGraw-Hill, New York, 1960.

59. Selna L. and Cho D.
Resonant response of offshore structure, Journal of the Waterways, Harbours and Coastal Engineering Division, Proc. ASCE, vol.98, WW1, Feb. 1972, pp.15-24.

60. Shen H.W., Schnieider V.R. and Karaki S.
Local scour around bridge piers, Journal of the Hydraulics Division, Proc. ASCE, vol.95, HY6, Nov. 1969, pp.1919-1940.

61. Shrivastava N.K., Handa V.K. and Critchley S.
Failures of air-supported structures, International Symposium on Air-Supported Structures, IASS, Venice, Italy, June 1977, pp.302-313.

62. Vance W.G.
New methods of laying sea-bed tubes, PhD. Thesis submitted to Queens University of Belfast, March 1968.

63. Ven Te Chow
Handbook of applied hydrology, McGraw-Hill, New York, 1964.

64. Verma V.K. and Leonard J.W.
Nonlinear behaviour of cable-reinforced membranes, Journal of the Engineering Mechanics Division, Proc. ASCE, vol.104, EM4, Aug. 1978, pp.735-750.

65. Vinogradov O.G., Malcolm D.J. and Glockner P.G.
Vibrations of cable-reinforced inflatable structures, Journal of the Structural Division, Proc. ASCE, vol.107, ST 10, Oct. 1981, pp. 1985-1999.

66. Wiegel R.L.
Oceanographical engineering, Prentice-Hall, Englewood Cliffs, N.J., 1964.

67. Wilson Q. and Sahota B.S.
Suction anchors, European Offshore Petroleum Conference and Exhibition in London, Oct. 24-27, 1978.

68. Wright J.C. and Yamamoto T.
Wave forces on cylinders near plane boundaries, Journal of the Waterway, Port, Coastal and Ocean Division, Proc. ASCE, vol.105, WW1, Feb. 1979, pp.1-13.